



Université
de Toulouse

THESE

En vue de l'obtention du

DOCTORAT DE L'UNIVERSITÉ DE TOULOUSE

Délivré par *l'Université Toulouse III - Paul Sabatier*
Discipline ou spécialité : *Géochimie marine et Modélisation*

Présentée et soutenue par *Thomas ARSOUZE*
Le 03 Décembre 2008

Titre : *Modélisation du cycle océanique du néodyme*

JURY

Monsieur Christophe Colin, Rapporteur ; Monsieur Jean-Claude Dutay, Directeur de thèse
Monsieur Yves Godderis, Examinateur ; Monsieur Nick Hall, Président
Monsieur Bruno Hamelin, Rapporteur
Madame Catherine Jeandel, Directeur de thèse
Monsieur Bernhard Peucker-Ehrenbrink, Invité
Madame Kazuyo Tachikawa, Examinateur
Madame Anne-Marie Tréguier, Examinateur

Ecole doctorale : *Sciente De l'Univers de l'Environnement et de l'Espace*
Unité de recherche : *Laboratoire d'Etude en Géophysique et Océanographie Spatiale(UMR 5566)*
Laboratoire en Sciences du Climat et de L'environnement (UMR 1572)
Directeur(s) de Thèse : *Madame Catherine Jeandel et Monsieur Jean-Claude Dutay*
Rapporteurs : *Monsieur Christophe Colin et Monsieur Bruno Hamelin*

Table des matières

Résumé	7
Abstract	9
Remerciements	11
1 Introduction	13
1.1 L'océan et la géochimie marine	15
1.1.1 L'océan dans le système climatique	15
1.1.2 La géochimie marine	17
1.1.2.1 Les enjeux	17
1.1.2.2 Les traceurs géochimiques	18
1.1.2.3 Vers la modélisation	20
1.2 Le traceur ε_{Nd} océanique	21
1.2.1 L'élément chimique Nd et le rapport isotopique ε_{Nd}	21
1.2.1.1 Le Nd	21
1.2.1.2 La composition isotopique du Nd	21
1.2.1.3 Hétérogénéité de la distribution de ε_{Nd}	22
1.2.2 Les propriétés du traceur ε_{Nd}	25
1.2.2.1 ε_{Nd} comme traceur de masses d'eau	25
1.2.2.2 ε_{Nd} comme traceur de flux d'apport de matière	26
1.2.2.3 ε_{Nd} comme traceur paléo	26
1.2.3 Les termes sources-puits du Nd océanique	27
1.2.3.1 Le paradoxe de la CI et de la concentration	28
1.2.3.2 Les premières modélisations du cycle du Nd océanique . .	29
1.2.3.3 Les observations	29
1.2.3.4 Le "Boundary Exchange" comme source et puits de l'élément	30
1.3 Plan et objectifs de la thèse	32

2 Le modèle de circulation océanique	35
2.1 Introduction	37
2.2 Présentation du modèle	38
2.2.1 Approximations et équations primitives	38
2.2.2 Les fermetures turbulentes du modèle	40
2.2.3 Les grilles ORCA	40
2.3 Configuration globale	41
2.3.1 La grille ORCA2	41
2.3.2 Configurations	41
2.3.2.1 Runs forcés	41
2.3.2.2 Runs couplés	42
2.4 Configuration régionale	43
2.4.1 Grille NATL4	43
2.4.2 Conditions initiales et forçages	44
2.5 Le modèle de traceurs passifs de NEMO	44
3 Impact du Boundary Exchange sur le cycle océanique du ε_{Nd}	47
3.1 Introduction	49
3.2 Compilation de données de Nd sur la marge continentale	50
3.2.1 Résumé	50
3.2.2 <i>Isotopic Nd compositions and concentrations of the lithogenic inputs into the ocean : a compilation, with an emphasis on the margins.</i> . . .	52
3.3 Modélisation de la composition isotopique du Nd à l'échelle globale	62
3.3.1 Résumé	62
3.3.2 <i>Modeling the neodymium isotopic composition with a global ocean circulation model</i>	63
4 Modélisation de la composition isotopique du Nd au Dernier Maximum Glaciaire	79
4.1 Contexte et configuration du modèle	81
4.1.1 Le Dernier Maximum Glaciaire	81
4.1.2 Le projet PMIP	81
4.2 Résumé	81
4.3 <i>Influence of the Atlantic meridional overturning circulation on neodymium isotopic composition at the Last Glacial Maximum, a modelling sensitivity study.</i>	83

5 Modélisation de la composition isotopique en Atlantique nord	99
5.1 Résumé	101
5.2 <i>Modeling the Nd isotopic composition in the North Atlantic basin using an eddy-permitting model</i>	101
6 Modélisation couplée de la concentration et de la composition isotopique du Nd	117
6.1 Résumé	119
6.2 <i>Reconstructing the Nd oceanic cycle using a coupled dynamical - biogeochemical model</i>	121
6.3 Compléments sur la description du modèle PISCES	140
7 Conclusion	145
7.1 Problématique	147
7.2 Principaux résultats	147
7.3 Perspectives	149
A Compilation de données	155

Table des figures

1.1	Schéma simplifié de la circulation thermohaline selon le modèle de <i>conveyor belt</i> établit par Broecker.	16
1.2	Définition isotopique du Nd lors de la formation du manteau et de la croûte continentale.	23
1.3	Variabilité mondiale de la composition isotopique en Nd des terrains cotiers	23
1.4	Disparité des mesures de ε_{Nd} entre chaque bassin océanique	24
1.5	Section méridienne de salinité et ε_{Nd} en Atlantique	25
1.6	Carte des échanges observés entre une masse d'eau et les marges continentales.	30
1.7	Sources et puits de Nd océanique	31
2.1	Maillage de la grille ORCA2	42
2.2	Maillage de la grille ORCA025 dont est extrait le domaine NATL4	43
3.1	Carte géologique mondiale en zone cotière	51
4.1	Schéma récapitulatif de la circulation proposée au DMG par les simulations de ε_{Nd} , en comparaison avec la situation moderne, dans le bassin Atlantique	83
6.1	Schéma récapitulatif du fonctionnement du modèle biogéochimique PISCES	140
6.2	Schéma des sources de nutriments et des interactions entre les différentes phases dans le modèle PISCES	141
6.3	Concentration en particules zonale moyenne globale (en g/l), pour chaque type de particules modélisé	142
6.4	Carte en surface de concentration particulaire (en g/l), pour chaque type de particules modélisé	143

Résumé

La composition isotopique du néodyme (CI de Nd, aussi notée ε_{Nd}) est un traceur de la circulation océanique et des apports lithogéniques. Dans le cadre de cette thèse, nous avons inséré les isotopes du Nd dans un modèle de circulation océanique général, afin de valider par la modélisation l'hypothèse de “Boundary Exchange” (BE, Boundary Scavenging associé à un apport de matière à l'océan le long de la marge continentale) comme principal source et puits de l'élément au réservoir océanique, et de simuler son cycle océanique.

Dans un premier temps, en considérant le seul BE comme terme source/puits, nous avons pu reproduire les principales caractéristiques de la distribution océanique en ε_{Nd} (signature des principales masses d'eau, augmentation vers des valeurs radiogéniques le long de la circulation thermohaline) à la fois au niveau global et régional. Ce résultat confirme le BE comme processus primordial dans le cycle océanique de l'élément.

Cette même paramétrisation du BE dans une configuration du modèle au Dernier Maximum Glaciaire nous a permis de constater que cet apport est sensible à la fois aux changements de forçages et aux changements de circulation océanique. La comparaison avec les données suggère un scénario dans le bassin Atlantique de prédominance d'eaux profondes en provenance du Sud avec une cellule méridienne vigoureuse en surface et jusqu'à 2000m de profondeur.

Enfin, nous avons mis en place un modèle couplé dynamique/biogéochimique permettant de modéliser à la fois la CI et la concentration en Nd, afin de résoudre le “Paradoxe du Nd” (qui résulte d'un découplage de comportement entre ces deux paramètres) et quantifier les sources de Nd à l'océan. Les résultats montrent que les interactions dissous/particulaires sont nécessaires pour réconcilier la distribution des deux paramètres, et que la remobilisation sédimentaire (source du processus de BE) est la source principale de Nd à l'océan ($1.1.10^{10}$ g(Nd)/an), avec des flux jusqu'à 25 fois plus fort que les autres flux externes (décharges fluviales sous forme dissoute et poussières atmosphériques).

Abstract

Neodymium isotopic composition (Nd IC, currently noted as ε_{Nd}) is a tracer of oceanic circulation and lithogenic inputs to the ocean. The current work aims to validate the "Boundary Exchange" hypothesis (BE, Boundary Scavenging associated with important inputs along the continental margin) as the main source/sink term of Nd to the oceanic reservoir, using an oceanic global circulation model.

First, considering the only BE term for Nd IC sources/sinks, we successfully simulated the main distribution's characteristics (inter basin gradient, isotopic signature of the main water masses) both at global and regional scale. This result confirms BE as an important process in the element's oceanic cycle.

The same parameterization of BE has been used at Last Glacial Maximum. Results show that this input varies both with a change in forcings, and a change in circulation. Comparison with data suggest a circulation scenario in the Atlantic with a predominance of southern deep waters and a vigorous meridional cell from surface to 2000m depth.

In a second place, we used a coupled dynamical/biogeochemical model to explicitly represent Nd IC and Nd concentrations, for studying the "Nd Paradox" (resulting from the decoupling of both parameters) and quantify the Nd sources to the ocean. Results suggest that dissolve/particulate interactions must be invoked to conciliate both distributions, and that oceanic margins are the main sources of Nd to the ocean ($1.1 \cdot 10^{10} \text{ g(Nd)/year}$), representing inputs up to 25 times higher than other external sources (dissolved river discharge and atmospheric dusts).

Remerciements

Même si le travail réalisé au cours d'une thèse peut parfois s'apparenter à un exercice solitaire, il s'agit avant tout d'un projet qui s'inscrit dans une démarche scientifique d'équipe. A ce titre, je tiens à souligner le travail de préparation effectué par mes encadrants qui m'ont permis d'avoir un sujet parfaitement défini, avec tous les outils nécessaires afin de mener à bien mon projet de thèse. Je tiens donc à les remercier pour cela, mais aussi pour m'avoir fait partager sans retenue leurs connaissances scientifiques ou encore pour avoir su s'adapter à mon rythme et à ma façon de travailler, en particulier au moment délicat de la rédaction du manuscrit de thèse. Ainsi je souhaite remercier Catherine Jeandel, qui est une source d'idées et d'informations inestimable, et surtout car elle a réussi à me donner goût à la géochimie marine en m'inondant de données dès mon arrivée... félicitations, ce n'était vraiment pas gagné d'avance ! Je remercie Jean-Claude Dutay pour son suivi minutieux dans l'avancement de mon travail et pour m'avoir aidé à retrouver mon chemin quand je pouvais m'égarer. Je remercie Anne-Marie Tréguier pour sa volonté et son enthousiasme à se lancer dans un travail de modélisation de traceur "exotique". Enfin, même s'il n'a pas été officiellement impliqué dans mon travail, je remercie François Lacan pour sa partition active et pour les nombreuses discussions passionnées que l'on a pu avoir. Je crois que je ne soulignerai jamais assez le plaisir que j'ai pu avoir à travailler quotidiennement avec des personnes aussi stimulantes intellectuellement, et attachantes humainement.

Je souhaite remercier l'ensemble de mon jury de thèse pour avoir répondu positivement à mon invitation. Merci à Christophe Colin et Bruno Hamelin pour leurs commentaires sur le manuscrit. Merci à Kazuyo Tachikawa, Yves Godderis, Bernhard Peucker-Ehrenbrink et Nick Hall pour leur présence le jour de la soutenance et leur implication dans cette thèse.

Enfin je tiens bien sur à remercier toutes les personnes que j'ai pu rencontrer, autant au LEGOS, qu'au LSCE ou encore au LPO, et qui m'ont permis de travailler dans des conditions que l'on peut qu'espérer retrouver ailleurs. Je pense en particulier au personnel administratif, qui a, a de nombreuses reprises, du faire face à mon incompétence notoire dès qu'il me faut remplir un quelconque formulaire ; au personnel informatique qui a toujours répondu le plus efficacement possible à mes demandes ; aux ingénieurs de l'IPSL, qui m'ont débloqué bon nombre de situations et n'ont pas hésité à développer certains outils spécialement pour moi ; aux autres chercheurs ; et enfin (last but not least) aux autres thésards, stagiaires, post-docs, ingénieurs avec qui j'ai partagé beaucoup de temps, et dont bon nombre sont devenus des amis proches.

Chapitre 1

Introduction

Sommaire

1.1 L'océan et la géochimie marine	15
1.1.1 L'océan dans le système climatique	15
1.1.2 La géochimie marine	17
1.1.2.1 Les enjeux	17
1.1.2.2 Les traceurs géochimiques	18
1.1.2.3 Vers la modélisation	20
1.2 Le traceur ε_{Nd} océanique	21
1.2.1 L'élément chimique Nd et le rapport isotopique ε_{Nd}	21
1.2.1.1 Le Nd	21
1.2.1.2 La composition isotopique du Nd	21
1.2.1.3 Hétérogénéité de la distribution de ε_{Nd}	22
1.2.2 Les propriétés du traceur ε_{Nd}	25
1.2.2.1 ε_{Nd} comme traceur de masses d'eau	25
1.2.2.2 ε_{Nd} comme traceur de flux d'apport de matière	26
1.2.2.3 ε_{Nd} comme traceur paléo	26
1.2.3 Les termes sources-puits du Nd océanique	27
1.2.3.1 Le paradoxe de la CI et de la concentration	28
1.2.3.2 Les premières modélisations du cycle du Nd océanique	29
1.2.3.3 Les observations	29
1.2.3.4 Le "Boundary Exchange" comme source et puits de l'élément	30
1.3 Plan et objectifs de la thèse	32

L'objectif de cette thèse est de modéliser pour la première fois le cycle océanique du néodyme (Nd) dans un modèle de circulation océanique générale (Oceanic General Circulation Model - OGCM)¹). Plus particulièrement, le but est de comprendre quels sont les sources et les puits² de cet élément chimique, et par extension des Terre Rares, et quels sont les processus qui contrôlent sa distribution au sein de l'océan. L'intérêt de l'étude de la géochimie marine en général, ainsi que de la distribution des éléments traces et du rôle qu'ils jouent au sein de l'océan en particulier, sont décrits au sein de la première partie de cette introduction. On s'attache ensuite, au sein d'une seconde partie, à saisir les objectifs de cette thèse et décrire les propriétés du Nd en tant que traceur océanique.

1.1 L'océan et la géochimie marine

Il est tout d'abord opportun de commencer par évoquer le rôle que joue l'océan dans l'évolution du climat pour comprendre l'intérêt que peut fournir l'étude de la géochimie marine en général et du traceur Nd en particulier dans la compréhension du fonctionnement de l'océan.

1.1.1 L'océan dans le système climatique

L'océan joue un rôle essentiel dans le système climatique de la Terre. Plusieurs études ont révélé le rôle majeur qu'a pu jouer la circulation thermohaline lors des changements climatiques dans le passé (Duplessy et al., 1984; Broecker et Denton, 1989; Rahmstorf, 2002).

Broecker (1991) a établi un modèle schématique très simplifié de circulation océanique globale, appelé *conveyor belt*, représenté ici sur la figure 1.1. Les eaux de surface et subsurface sont chauffées aux basses latitudes dans les différents bassins avant d'être transportées aux hautes latitudes en Atlantique nord où elles sont refroidies au cours de leur trajet. Ainsi, en mer d'Irminger et du Labrador, ces eaux deviennent assez froides et donc denses pour plonger en profondeur et se diriger vers le sud en longeant le continent américain au sein d'une masse d'eau appelée North Atlantic Deep Water (NADW). Cette masse d'eau atteint l'océan austral où elle rejoint l'Antarctic Circumpolar Current (ACC), où elle est alors entraînée jusqu'aux secteurs Indien puis Pacifique de l'océan Austral. Les eaux pénètrent alors dans ces bassins, toujours en profondeur, mais sous l'effet du mélange vertical "remontent" vers la surface tout au long de leur trajet, de façon plus privilégiée dans les zones d'upwelling (Robinson et Stommel, 1959). Le temps moyen pour qu'une eau qui subducte en profondeur en Atlantique nord remonte à la surface dans le Pacifique nord est estimé à 1 000 ans (Broecker, 1991). Le retour des eaux de surface et intermédiaires dans le Pacifique vers le lieu de formation de la NADW est sujet à débat. Deux chemins préférentiels ont été historiquement considérés : le transport par les Eaux Antarctiques Intermédiaires (AAIW) en passant par le passage de Drake (la route froide,

¹modèles numériques résolvant les équations primitives de la physique océanique dans un océan discrétréisé

²termes d'apport et de soustraction au réservoir océanique

(Rintoul, 1991)), ou bien le transport par les eaux de surface en passant par les détroits indonésiens (la route chaude, (Gordon, 1986)). Il existe vraisemblablement une troisième route, appelée *Tasman leakage* par les auteurs (Speich et al., 2002), et le retour des eaux en Atlantique Nord se fait par une contribution équivalente de ces routes (Ganachaud et Wunsch, 2000; Speich et al., 2001).

Plus récemment, certains auteurs (Toggweiler et Samuels, 1995; Gnanadesikan, 1999) ont suggéré une remontée des eaux profondes non plus dans les bassins Pacifique et Indien, mais plutôt dans l'océan austral par un upwelling. Cette remontée est due à un transport d'Ekman important vers le nord, provoqué par les forts vents d'ouest dans la région. Ce sont alors les eaux intermédiaires de l'ACC qui rejoignent l'intérieur des bassins avant d'éventuellement rallier le bassin Atlantique par la surface.

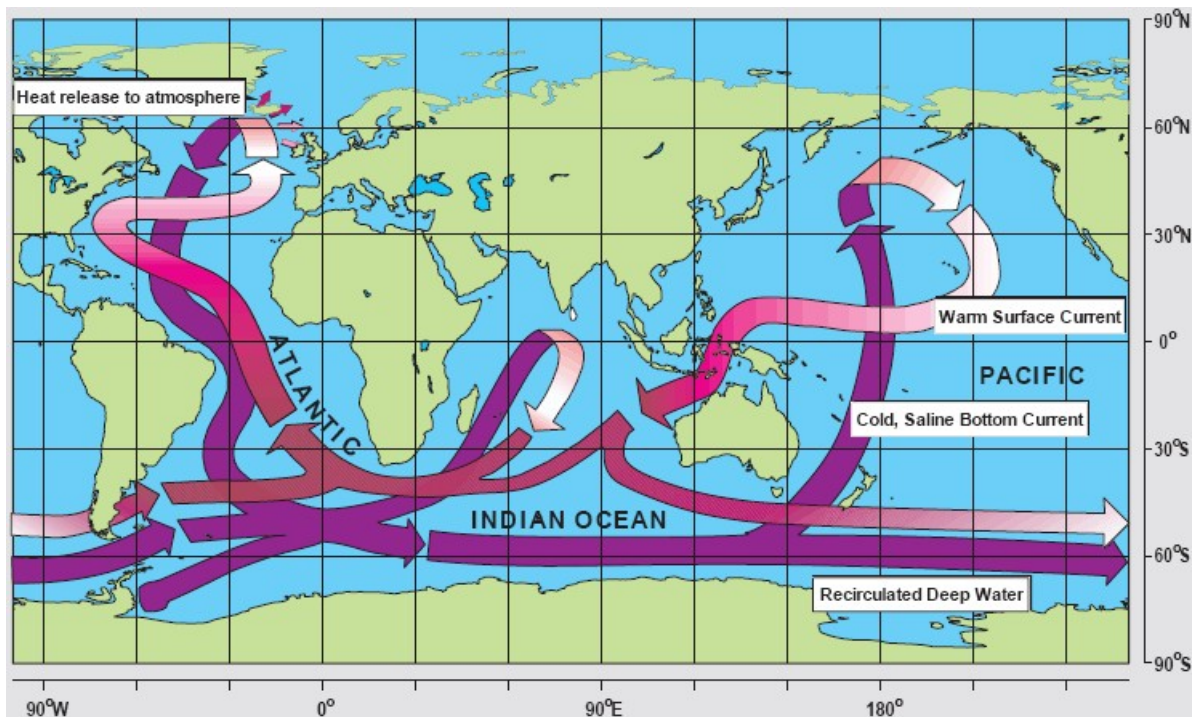


FIG. 1.1 – Schéma simplifié de la circulation thermohaline selon le modèle de *conveyor belt* établit par Broecker (1991). Les flèches mauves représentent la circulation des eaux froides et profondes, les flèches rouges les eaux chaudes de surface.

Ces différentes visions de la circulation océanique méridienne suggèrent une redistribution de la chaleur aux différentes latitudes : des eaux chaudes des tropiques vers les hautes latitudes en surface et des eaux froides des zones polaires vers les basses latitudes en passant par le fond de l'océan. L'océan joue ainsi un rôle majeur direct dans la régulation thermique de la Terre.

De plus il intervient de façon majeure dans la distribution globale des éléments chimiques, ce qui influe là encore sur la stabilité du climat, comme nous allons l'illustrer en ayant recours à quelques exemples.

1.1.2 La géochimie marine

La discipline de géochimie marine consiste en l'étude de la composition chimique de l'océan et de ses échanges de matière avec les différentes géosphères environnantes : atmosphère, sédiments ou surfaces continentales. En d'autres termes, il s'agit de comprendre et contraindre le rôle de l'océan dans les grands cycles géochimiques. Pour cela, il faut connaître et quantifier à la fois les sources et puits des éléments dans l'océan, mais aussi les processus biologiques (consommation biologique, reminéralisation), chimiques (échanges gazeux) et physiques (advection, diffusion, aggrégation, désaggrégation) au sein de la colonne d'eau.

1.1.2.1 Les enjeux

Les principales voies permettant d'acheminer le matériel continental dans l'océan sont les poussières atmosphériques, les fleuves, les eaux souterraines ou encore les calottes glaciaires. Cependant, l'influence relative de ces différents types d'apports varie grandement autant spatialement que temporellement. Ainsi, les calottes glaciaires transportent vers l'océan voisin des quantités de matière très importantes, mais dont les effets sont très locaux (principalement en Arctique et Antarctique). Cependant qu'en était-t-il au cours des périodes glaciaires, lorsque de grosses calottes de glace recouvriraient des zones jusqu'à 40° de latitude ?

Le carbone, en tant que gaz à effet de serre, tient une place particulière dans l'étude des cycles biogéochimiques. En effet, la relation entre le CO_2 atmosphérique et la température moyenne sur Terre est clairement établie (Sigman et Boyle, 2000). Néanmoins, il existe encore des incertitudes concernant les processus qui mènent aux changements de distribution globale de CO_2 atmosphérique au cours du temps. En particulier, on n'identifie pas aujourd'hui si ces variations sont des causes ou des conséquences des variations climatiques (e.g. les cycles glaciaire-interglaciaire). Tout particulièrement, l'absorption de carbone par l'océan est encore mal contrainte.

Par exemple, les changements importants de CO_2 atmosphérique peuvent refléter une variation d'apport de matériel à l'océan. Par exemple, l'océan Austral est une région "High Nutrients Low Chlorophyl" (HNLC, forte concentration en nutriment, faible teneur en chlorophylle), où le fer est un élément limitant de la production primaire (Martin et al., 1990). L'augmentation observée de concentration de poussières atmosphériques lors des périodes glaciaires (Petit et al., 1999) a induit une augmentation d'apports de fer dans cette région. Cela aurait engendré une augmentation de la production primaire, qui aurait accru la pompe biologique et l'enfouissement de carbone vers le sédiment, et ainsi réduit la concentration en CO_2 atmosphérique de 15 ppm (Bopp et al., 2003) à 40 ppm (Watson et al., 2000) selon les études.

Par ailleurs, les données de ^{230}Th et ^{232}Th montrent que les apports de matière en provenance de l'Atlantique Sud-Ouest par l'ACC dans la région Atlantique de l'océan Austral ont été jusqu'à sept (7) fois plus importants au Dernier Maximum Glaciare (DMG) qu'au présent, résultant d'une augmentation de sédiments glaciaires de Patagonie et d'Antarctique, et d'un ACC plus vigoureux (Franzese et al., 2006). Ce flux de matière est potentiel-

lement une source de fer importante pour permettre une augmentation de la production primaire, et en conséquence une baisse du CO_2 atmosphérique. De même, l'activité tectonique dans la région de Papouasie Nouvelle-Guinée a probablement engendré une variation d'apport de fer dans le Pacifique Equatorial (via le Sous Courant Equatorial, EUC), ayant pour conséquence un changement de production primaire dans cette autre région HNLC (Wells et al., 1999).

Plus généralement, la façon dont sont distribués les nutriments et les éléments chimiques dans l'océan est un point essentiel dans l'étude globale de la production primaire et de l'export de carbone. Sarmiento et al., Sarmiento et al. (2004) ont par exemple établi que l'Océan Austral fournit, via les Eaux Modales Sub Antarctiques (SAMW), les nutriments de 75% de la production biologique au nord de 30°S.

Comme on peut le voir à travers ces trois exemples, le transport de matière dans/vers l'océan joue un rôle important dans l'absorption du CO_2 atmosphérique en influant sur la production primaire. On comprend en effet l'intérêt d'étudier les liens entre les sources d'éléments chimiques, leur intensité, et la composition chimique de l'océan. Or, on connaît encore actuellement mal ces flux, leurs variabilités autant géographique que temporelle, ou encore leurs influences sur la production primaire. Les éléments ont des temps de résidence dans l'océan variant de quelques jours à plusieurs millions d'années. Ils sont donc soumis au transport par les masses d'eau et aux processus de "transformation" entre les phases dissoutes, colloïdales et particulières liées notamment au cycle du matériel biologique (consommation en surface et reminéralisation en profondeur lors de la chute des particules). Des éléments apportés à l'océan peuvent être transportés sur de longues distances, et sous différentes phases, susceptibles d'évoluer au cours de ce transport. La distribution océanique des éléments se fait donc à la fois par les apports/soustractions extérieurs au réservoir océanique (sources et puits) et par le cycle interne (transport et "transformation" entre les différentes phases). Ces processus sont déterminants dans les variations climatiques.

Afin de décrire et quantifier ces processus, on se base sur l'utilisation d'outils permettant d'obtenir des informations à la fois sur les sources et puits, ainsi que sur les facteurs agissant sur le cycle interne des éléments. Parmis ces outils : les traceurs océaniques.

1.1.2.2 Les traceurs géochimiques

On appelle traceurs géochimiques des éléments chimiques et/ou leurs isotopes dont l'étude permet d'obtenir des informations sur le fonctionnement des processus chimiques, biologiques ou physiques. Il existe de nombreux traceurs dont les cycles répondent à des processus propres à chaque traceur, ce qui permet l'approche d'une grande diversité de mécanismes. Ces traceurs peuvent être d'origine anthropique³ ($CFCs$, $\delta^{14}C$ des bombes, 3H , ^{210}Pb , uranium nucléaire, etc...), et présentent des intérêts particuliers liés notamment à la date précise de leur introduction, ou bien naturelle (éléments traces comme le Mn ,

³de source humaine

l' Al , le Fe , $\delta^{14}C$ naturel, et les éléments radiogéniques), qui ont eux l'avantage de pouvoir être utilisés pour étudier les variations d'état de l'océan dans le passé.

Ainsi, les traceurs biogéochimiques océaniques permettent d'obtenir des informations sur :

- **la circulation océanique (traceurs conservatifs)** : Une grande partie de la connaissance actuelle sur la circulation physique provient de l'étude de la température, de la salinité et des macro-nutriments (NO_3^- , PO_4^{3-} et SiO_4^{2-}) soit directement à partir des observations, soit par l'utilisation d'OGCMs. Certains traceurs, une fois éloignés de leurs sources et puits se comportent de manière conservative dans l'océan, c'est à dire qu'ils n'évoluent que par mélange entre différentes masses d'eau. Ainsi, ces traceurs permettent d'obtenir des informations sur le mélange des masses d'eau, sur les temps de ventilation, ou encore sur la circulation (traceurs transitoires : SF_6 , $CFCs$, $\delta^{14}C$ des bombes ; ou bien traceurs radiogéniques : ε_{Nd} , ε_{Hf} , Ra). Ils apportent des informations complémentaires et indépendantes aux traceurs classiques (température et salinité) de la circulation océanique (Moore, 1996).
- **les échanges dissous-particulaires (traceurs non conservatifs)** : Certains traceurs peu solubles et facilement adsorbés sur les particules, sont scavengés⁴ dans la colonne d'eau, alors que d'autres sont insensibles au scavenging. Ces différences de comportements permettent d'étudier les flux de matière solide, les vitesses de chute des particules et les interactions entre phase dissoute et phase particulaire. Ces informations sont nécessaires pour comprendre quels sont les processus qui contrôlent la distribution des éléments dans la colonne d'eau ou encore quels sont les flux de carbone exportés ($^{231}Pa/^{230}Th$, ^{10}Be , ^{234}Th , Ba_{Ex} , REE).
- **les flux entre les différents réservoirs**. Les traceurs dont les sources sont originaires de réservoirs différents permettent de quantifier soit l'influence de ces réservoirs spécifiques sur l'océan, soit les échanges entre ces différents réservoirs. Par exemple, l' 3He , le ^{228}Ra ou encore les $CFCs$ permettent de quantifier respectivement les apports à l'océan des sources hydrothermales, des eaux souterraines et de l'atmosphère par échange gazeux à la surface. Aussi, la grande majorité des éléments sortent du réservoir océanique au sein des particules qui chutent dans la colonne d'eau. Certains traceurs (^{230}Th , Ra) permettent de calculer précisément les taux d'accumulation sédimentaire et ainsi de façon subséquente la quantification des taux de sédimentation d'un grand nombre d'éléments.
- **l'état passé de l'océan (paléo-proxy)**. Les outils classiques des océanographes comme la température et la salinité, qui sont des traceurs actifs, ou les concentrations en nutriments comme les phosphates ou les nitrates, qui ont des valeurs caractéristiques pour certaines masses d'eau, ne sont pas conservés au cours du temps. Au contraire, l'accumulation de matière dans certaines phases (sédiments, croutes de Mn , particules biogéniques) au fond de l'océan permet l'utilisation de certains proxies comme archives de l'état de l'océan au cours du temps. Il est ainsi possible par carottage d'accéder aux informations enregistrées par les traceurs, telles que les changements de circulation (Cd/Ca , ε_{Nd} , $\delta^{13}C$, $^{231}Pa/^{230}Th$, etc...), les varia-

⁴/adsorption/aggrégation de l'élément autour d'une particule, et soustraction par chute de ces particules

tions de flux d'érosion des continents (^{230}Th , ε_{Nd} , etc....), les taux de sédimentation ($^{231}Pa/^{230}Th$) au cours du temps. La principale difficulté dans ces études réside dans la déconvolution des processus qui affectent le proxy (circulation, biologie, etc...)

Une approche multi-traceurs permet d'apporter des informations complémentaires. En effet, chaque traceur a un comportement différent en fonction des processus biogéochimiques ou des forçages physiques. C'est justement en comprenant la façon dont leurs réactions diffèrent en fonction d'un processus qui permettra d'étudier le-dit processus.

1.1.2.3 Vers la modélisation

Afin de comprendre le rôle de l'océan dans le système climatique, l'utilisation d'OGCMs s'est développée pour prédire et essayer de mieux comprendre les courants océaniques, ainsi que la température et la salinité (cf. review par McWilliams, 1996) .

En revanche, pendant longtemps, les modèles en boîtes ont été le principal outil de modélisation des géochimistes pour l'étude de la distribution des éléments chimiques dans un milieu donné. Ceci à cause des moyens de calcul limités, du besoin de simulations physiques réalistes, mais aussi et surtout à cause du faible nombre de données de traceurs disponibles. L'intérêt de ces modèles est qu'ils permettent de déterminer et quantifier l'impact de différents processus sur la distribution en concentration ou en rapport isotopique d'un élément. Encore aujourd'hui, le faible coût de calcul numérique, la possibilité d'effectuer des tests de sensibilité et la facilité d'implémentation font de ces modèles des outils privilégiés pour l'étude et la quantification de processus.

Cependant, depuis peu, l'amélioration des techniques analytiques a permis une augmentation du nombre d'observations. Parallèlement, la communauté scientifique a vu les moyens de calcul augmenter, et a été dotée de moyens propres aux problématiques de modélisation de traceurs (Ethé et al., 2006; Khatiwala et al., 2005; Aumont et al., 1998), permettant un essor de travaux de modélisation numérique. L'utilisation d'OGCMs pour la modélisation de traceurs s'est développée entre autre avec des études sur les radiocarbones ($\Delta^{14}C$), l' 3He , le tritium (3H), et les chlorofluorocarbones (*CFCs*), qui sont des traceurs ayant bénéficié d'une bonne couverture spatiale de données grâce au programme WOCE et GEOSECS (Maier-Reimer et Hasselmann, 1987; Sarmiento, 1983; England et Garçon, 1994). Depuis, d'autres traceurs ont aussi bénéficié de l'amélioration des moyens et du nombre de mesures et leur modélisation à l'aide d'OGCMs a été développée, notamment au cours du programme OCMIP ($\delta^{13}C$, Pa , Th , Pb , Fe , 3He , ^{32}Si , etc...) (e.g. Peng et al., 1993; Tagliabue et Bopp, 2008; Henderson et al., 1999; Siddall et al., 2005; Henderson et Maier-Reimer, 2002; Dutay et al., 2004, 2002; Matsumoto et al., 2004; Aumont et Bopp, 2006).

Les modèles sont importants car ils fournissent un cadre d'étude unique pour l'interprétation des données. Les OGCMs sont des outils adaptés pour évaluer, permettre de séparer et quantifier les différents processus qui contrôlent la distribution des traceurs : processus physiques (transport), biogéochimiques (interactions dissous-particulaires et cycle vertical), flux de sources-puits. Par exemple, la modélisation de traceurs tels que les isotopes du carbone, le tritium, l'oxygène, l'hélium, l'argon ou encore les *CFCs* peut contraindre

la circulation océanique (e.g. Matsumoto et al., 2004; England et Rahmstorf, 1999; Sarmiento, 1983) ou reconstituer une circulation passée dans le cas des modèles pronostiques.

Plus récemment la mise en place de modèles inverses a permis d'estimer le flux de carbone organique exporté vers les sédiments (Schlitzer, 2004) ou encore les taux de reminéralisation des particules (Usbeck et al., 2003). A terme, ces modèles vont devenir essentiels pour aider à remonter aux informations (origine et quantification) des sources, puits, transport et flux verticaux des éléments traces.

Pour la modélisation du cycle océanique du Nd, après une présentation succincte de l'élément et de ses propriétés, je montrerai qu'après plusieurs modélisations en boîtes, et des études basées sur des données, l'utilisation d'un OGCM pour simuler l'introduction du traceur, et sa distribution dans l'océan, va justement permettre de tester une hypothèse sur les processus qui contrôlent la distribution océanique de Nd.

1.2 Le traceur ε_{Nd} océanique

1.2.1 L'élément chimique Nd et le rapport isotopique ε_{Nd}

1.2.1.1 Le Nd

Le néodyme est un élément chimique (numéro atomique : 60, symbole : Nd) qui fait partie du groupe des terres rares (*Rare Earth Element, REE*, ou lanthanides).

Comme tous les éléments de sa famille, il se trouve à l'état de trace dans l'océan (concentration de l'ordre de 10^{-9} gramme par litre d'eau), préférentiellement sous forme dissoute (seulement 5 à 10% sous phase particulaire (Jeandel et al., 1995)). Son profil dans la colonne d'eau est appauvri dans les eaux de surface et abondant en eaux profondes. Son cycle océanique est donc partiellement contrôlé par le scavenging en surface, et par la reminéralisation en profondeur.

1.2.1.2 La composition isotopique du Nd

Le Nd possède 7 isotopes (tous stables), dont un est radiogénique : le ^{143}Nd produit par désintégration active du ^{147}Sm . L'abondance relative de ^{143}Nd par rapport aux autres isotopes du Nd varie dans les différents réservoirs terrestres. On définit le rapport isotopique $^{143}Nd/^{144}Nd$, que l'on appellera par la suite "composition isotopique" (CI). Cette CI augmente au cours du temps, par production de ^{143}Nd . Cependant, la période de désintégration du ^{147}Sm en ^{143}Nd est suffisamment longue ($6.54 \cdot 10^{12}$ ans) pour que l'augmentation de ^{143}Nd soit négligeable à l'échelle du fonctionnement actuel de l'océan (de l'ordre du millier d'années).

On exprime couramment la CI. en Nd par la grandeur ε_{Nd} , qui représente en parties par 10 000, l'écart du rapport $^{143}Nd/^{144}Nd$ mesuré dans un échantillon par rapport à une

valeur de référence, $(^{143}\text{Nd}/^{144}\text{Nd})_{CHUR} = 0.512638$, qui représente la valeur moyenne du rapport $^{143}\text{Nd}/^{144}\text{Nd}$ de la planète Terre à ce jour :

$$\varepsilon_{Nd} = \left[\frac{(^{143}\text{Nd}/^{144}\text{Nd})_{\text{echantillon}}}{(^{143}\text{Nd}/^{144}\text{Nd})_{CHUR}} - 1 \right] \cdot 10^4 \quad (1.1)$$

Ce sont les variations de composition isotopique de ε_{Nd} en phase dissoute dans l'océan qui permettent d'utiliser le Nd comme traceur océanique.

1.2.1.3 Hétérogénéité de la distribution de ε_{Nd}

On observe une grande variabilité de la composition isotopique dans les océans, tant verticale que géographique. Comme le Nd dans l'océan est lithogénique, ces variations reflètent les variations de CI des continents ainsi que la redistribution du Nd par la circulation océanique.

Variabilité de ε_{Nd} à la surface terrestre Le rapport isotopique ε_{Nd} d'un échantillon est déterminé par :

- l'abondance relative en Sm par rapport au Nd : lors de la formation des continents, le Nd est préférentiellement inséré dans la croûte terrestre plutôt que dans le magma, contrairement au Sm. Il en résulte un rapport Sm/Nd plus petit dans les terrains granitiques (e.g. roches continentales crustales) que dans les formations basaltiques (issues du magma, e.g. arcs volcaniques et ridges mid-océaniques).
- l'âge du matériel échantillonné : d'après le point précédent, une formation continentale récente aura une CI proche de la valeur moyenne, alors que plus le continent est ancien, plus le rapport ε_{Nd} sera négatif. À l'opposé, toutes les formations basaltiques récentes ont un rapport ε_{Nd} positif.

Ces processus sont représentés Fig. 1.2.

On trouve à la surface de la terre des valeurs allant de $-60 \varepsilon_{Nd}$ (Moorbath et al., 1997) (on parle alors de valeurs non radiogéniques) jusqu'à $+10 \varepsilon_{Nd}$ (Zhuravlev et al., 1987) (valeurs radiogéniques).

La carte Fig. 1.3, réalisée au cours de cette thèse ((Jeandel et al., 2007) ; cf. section 3.2) illustre l'hétérogénéité de la CI de Nd à l'échelle globale, avec des valeurs très négatives sur les terrains bordant l'Atlantique nord (vieux terrains granitiques au Canada et Groenland) jusqu'à des valeurs plus radiogéniques autour du Pacifique (arcs volcaniques récents en Papouasie Nouvelle-Guinée, îles Kuriles, etc...).

Variabilité océanique On observe des disparités entre les différents bassins océaniques qui ont pour origine les contributions relatives de terrains d'âge et de composition isotopique différents. Le temps de résidence du néodyme dans l'eau mer (estimé entre 500 et 1 000 ans ; (Tachikawa et al., 2003)) inférieur au temps de mélange des eaux océaniques à l'échelle globale (entre 1 000 et 1 500 ans (Broecker et Peng, 1982)) ce qui préserve les hétérogénéités entre chaque bassin océanique. Ceci est illustré sur la Fig. 1.4.

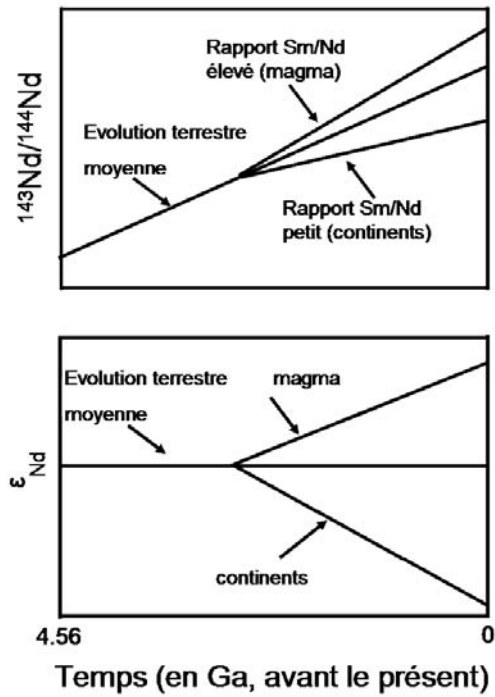


FIG. 1.2 – Différenciation isotopique du Nd lors de la formation du manteau et de la croute continentale. (Goldstein et Hemming, 2003).

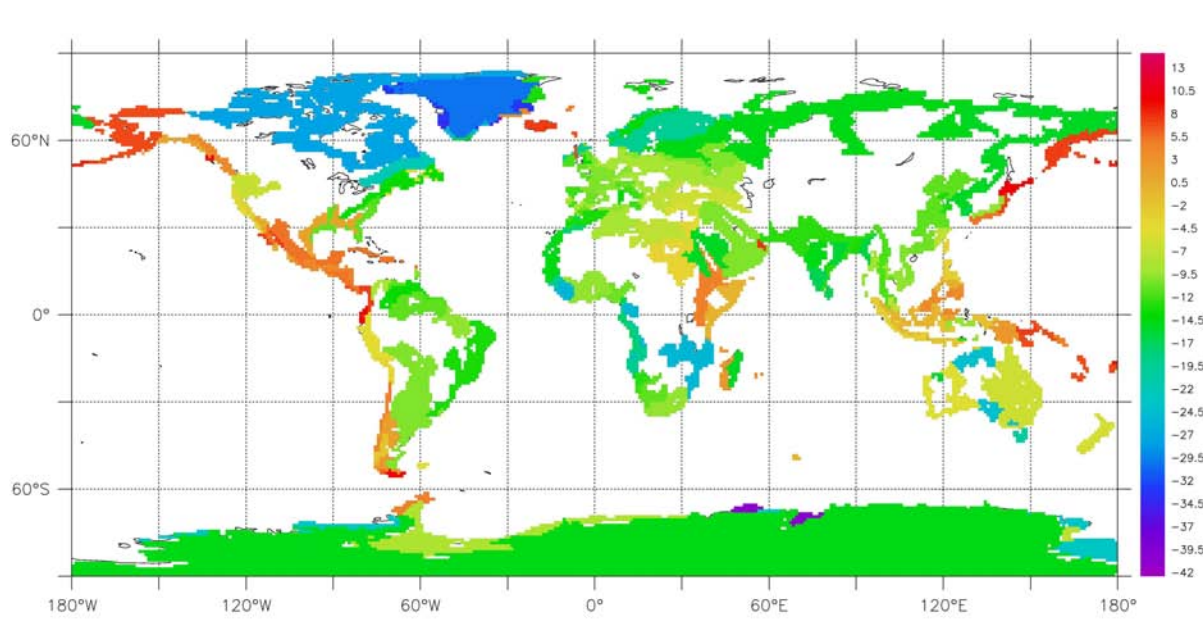


FIG. 1.3 – Variabilité mondiale de la composition isotopique en Nd des terrains cotiers, (Jeandel et al., 2007) ; cf. section 3.2.

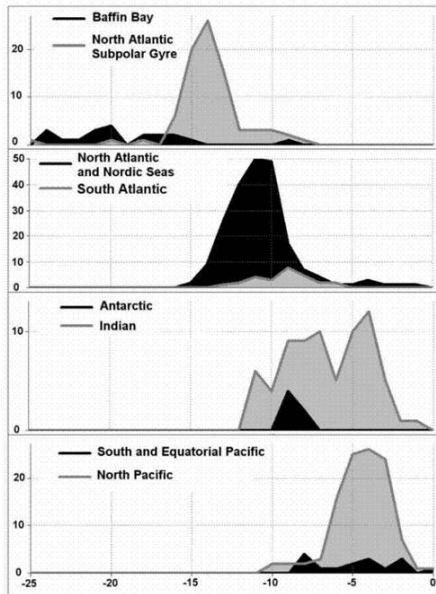


FIG. 1.4 – Nombre de mesures entre chaque bassin océanique en fonction de ε_{Nd} . On remarque clairement une disparité entre chaque bassin avec un gradient positif de ε_{Nd} qui suit la circulation thermohaline globale. (Lacan et Jeandel, 2005b).

Il est établi depuis longtemps que les apports de Nd à l'océan sont de source lithogénique (O'Nions et al., 1978) et que les flux hydrothermaux sont négligeables (Michard et al., 1983; Piepgras et Wasserburg, 1985). L'hétérogénéité isotopique des continents est ainsi redistribuée dans l'océan. Les apports à la fois dissous et particulaires par les rivières et les poussières atmosphériques ont longtemps été les termes sources privilégiés (Goldstein et Jacobsen, 1987; Elderfield, 1988; Bertram et Elderfield, 1992; Jeandel et al., 1995). Des études récentes semblent cependant privilégier l'apport des sédiments déposés sur la marge continentale comme principale source de Nd à l'océan (Jeandel et al., 1998; Tachikawa et al., 2003; Lacan et Jeandel, 2001, 2005b; Arsouze et al., 2007).

Les bassins océaniques ont des valeurs moyennes d' ε_{Nd} distinctes. Les valeurs les moins radiogéniques sont dans l'océan Atlantique (moyenne de $\varepsilon_{Nd} \approx -12$), les plus radiogéniques dans l'océan Pacifique (moyenne de $\varepsilon_{Nd} \approx -5$) alors que l'océan Indien a des valeurs intermédiaires (moyenne de $\varepsilon_{Nd} \approx -8$).

Une synthèse d'un travail sur une compilation globale de l'hétérogénéité de la CI en Nd sur les zones cotières des continents et de ses répercussions sur la CI océanique est présenté section 3.2, (Jeandel et al., 2007).

1.2.2 Les propriétés du traceur ε_{Nd}

Outre le fait que chaque bassin possède une CI moyenne distincte, des hétérogénéités sont aussi observées verticalement dans la colonne d'eau. Comprendre la cause de ces variations, autant au milieu d'un bassin océanique, loin d'apports lithogéniques, qu'en surface ou près de la marge continentale, près des sources, permet d'obtenir des informations sur la dynamique océanique (trajectoires, mélanges) et sur les flux de matière d'origine continentale.

1.2.2.1 ε_{Nd} comme traceur de masses d'eau

Les données de ε_{Nd} dissout montrent une bonne corrélation avec la salinité et les silicates, qui sont deux traceurs connus de la circulation océanique (Elderfield et Greaves, 1982; Goldstein et Hemming, 2003). Par exemple, la coupe verticale du bassin Atlantique Ouest (Fig. 1.5) montre un maximum de salinité représentatif de la NADW à 2 500 mètres de profondeur avec une valeur ε_{Nd} comprise entre -13 et -14, constante le long de son trajet et qui est acquise dans sa zone de formation près du bassin du Labrador (Lacan et Jeandel, 2005a).

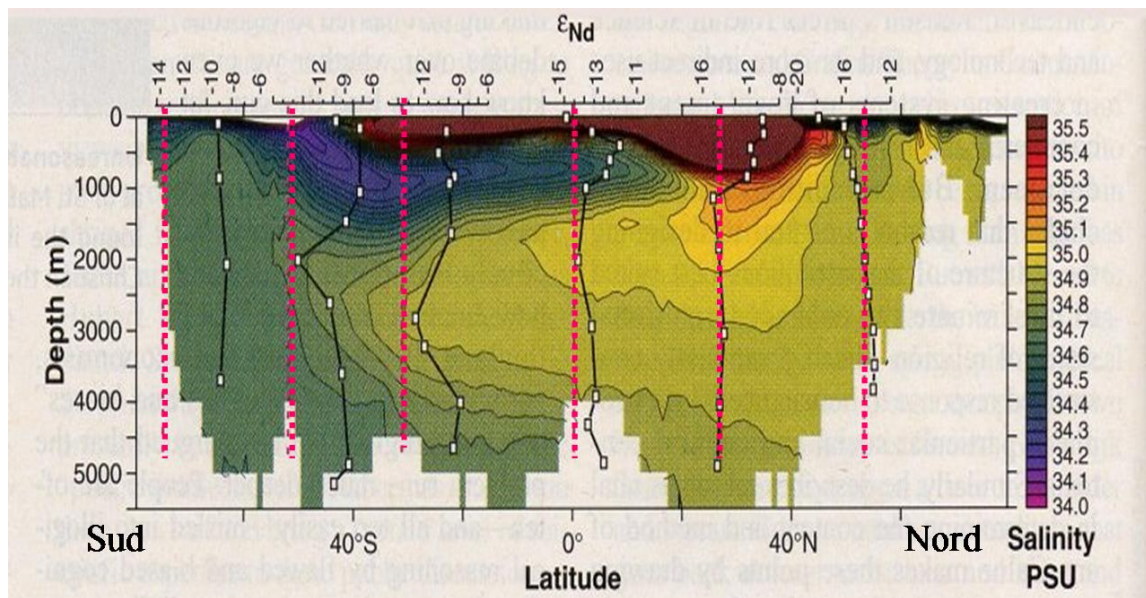


FIG. 1.5 – Section mérienne de l'océan Atlantique où sont reportées la salinité et la composition isotopique du Nd. On constate que le ε_{Nd} est un traceur conservatif puisque ses isovaleurs suivent les isovaleurs de salinité. von Blanckenburg (1999).

La CI de Nd ne dépend pas de l'activité biologique ou de la soustraction par les particules (ces processus n'induisent pas de fractionnement isotopique entre les deux isotopes ^{143}Nd et ^{144}Nd). La seule façon de modifier la CI d'une masse d'eau est d'y apporter du Nd avec une CI différente : soit par apport de Nd lithogénique avec une Nd différente (le

long des marges continentales, ou en surface, soumis à l'influence des poussières atmosphériques et des décharges fluviales) - dans ces cas là, ε_{Nd} n'est pas un traceur conservatif -, soit par mélange avec une masse d'eau de CI différente - ε_{Nd} est conservatif loin des ses sources, il est alors un traceur de trajectoires et de mélange des masses d'eau.

L'avantage de ce traceur par rapport aux traceurs classiques de la circulation (température, salinité, nutriments) est que l'hétérogénéité des sources (Jeandel et al., 2007) permet de marquer les masses d'eau et de comprendre l'origine de leurs formations (Lacan et Jeandel, 2005a).

Cette propriété de traceur de masses d'eau dans l'océan ouvert et été largement utilisée par la communauté scientifique (Piepgras et Wasserburg, 1982; Piepgras et Jacobsen, 1988; Jeandel, 1993; Jeandel et al., 1998; Amakawa et al., 2000; Lacan et Jeandel, 2001, 2005a).

1.2.2.2 ε_{Nd} comme traceur de flux d'apport de matière

Les apports de Nd à l'océan sont lithogéniques. Comme on l'a vu précédemment, il est important de pouvoir quantifier ces flux (que cela soit les poussières atmosphériques, les rivières ou bien les sédiments), non seulement pour l'étude même du cycle de l'élément, mais aussi de manière plus globale dans un cadre d'étude de variation climatique.

Il est possible de quantifier dans un modèle en boîte les apports d'une source de Nd lithogénique par l'étude conjointe de la concentration en Nd et de la CI (Lacan et Jeandel, 2005b). En mesurant ces deux paramètres dans la source, ainsi que dans une masse d'eau en amont puis en aval de la source, il suffit alors d'équilibrer les bilans de CI et de concentration en Nd pour déterminer les flux nécessaires de Nd à apporter à la masse d'eau, puis en déduire une quantité de matière globale apportée par la source (cf. un exemple dans Lacan et Jeandel, 2001).

1.2.2.3 ε_{Nd} comme traceur paléo

La sédimentation des particules marines au fond de l'océan au cours du temps permet un archivage naturel des propriétés de l'océan. Ainsi, le Nd accumulé dans différentes phases permet d'étudier les variations de circulation à différentes profondeurs et différentes échelles de temps. Par exemple, les croûtes et oxyhydroxydes de ferro-manganèse (Fe-Mn), ainsi que les foraminifères benthiques enregistrent la CI des eaux de fond (Albarède et Goldstein, 1992; Foster et al., 2007; Klevenz et al., 2008). La CI de Nd dans les fossiles de dents de poissons est caractéristique de la profondeur où vivent ces espèces (généralement les couches de surface ou subsurface) (Scher et Martin, 2008; Martin et Scher, 2006; Pucéat et al., 2005). De même, les tests de foraminifères planctoniques enregistrent eux aussi la CI des eaux dans lesquelles ils vivent (Vance et Burton, 1999; Burton et Vance, 2000).

Couplé avec d'autres proxies paléo ($\delta^{13}C$, $^{87}Sr/^{86}Sr$ ou encore $^{231}Pa/^{230}Th$ par exemple), l'objectif est alors de reconstruire l'état chimique et dynamique de l'océan dans le passé en contraignant et dissociant les variations de sources et de circulation, et d'établir ainsi un lien avec les changements climatiques.

Cependant, les flux de sédimentation sont très variables, autant spatialement que temporellement, ce qui rend généralement très difficile l'accès à un échantillonage temporel supérieur à un ordre du millier d'années (ce qui est limitatif pour l'étude des stades glaciaires-interglaciaires), et qui constraint le nombre de données disponibles.

Pour le Nd, une problématique importante est de savoir si les sources et la signature isotopique en Nd des "end-members" sont transposables à l'étude des variations de la circulation océanique ou du transport de matière de la marge continentale vers le large sous différentes contraintes climatiques : modification des apports lithogéniques (variations de flux de poussières atmosphériques, de décharges sédimentaires sur la marge continentale, etc...) et modification de la circulation. Par exemple, la CI en Nd de la *NADW* a-t-elle toujours été de $\varepsilon_{Nd} = -13.5$ au cours des différents épisodes climatiques ? Etant donné le nombre de processus impliqués, et la complexité de l'acquisition de la signature isotopique des masses d'eau (Lacan et Jeandel, 2005a), il serait surprenant d'observer une invariance de tous ces processus au cours du temps. Si les flux d'érosion ont changé globalement au cours du temps, il ne semble pas que cela impacte la distribution du ε_{Nd} (Tachikawa et al., 2003). En revanche, des changements dans les contributions relatives des flux d'érosion peuvent influer sur l'acquisition de la CI d'une masse d'eau. De même, un changement de circulation océanique peut induire un changement dans la remobilisation des sédiments et dans les apports des sources. Enfin, il est établi que la distribution en ε_{Nd} dépend à la fois de l'advection latérale (propriété de traceur de masses d'eau) et de processus d'interactions particulières verticalement (scavenging en surface et reminéralisation en profondeur) (Jeandel et al., 1995; Siddall et al., 2008). Des changements sur ce cycle vertical de l'élément au cours du temps, liés aux variations de production primaire et du flux de particules généré, sont donc susceptibles d'affecter la distribution en ε_{Nd} .

Un des objectifs de cette thèse est donc de comprendre quel peut être le rôle du ε_{Nd} en temps que proxy paléo.

1.2.3 Les termes sources-puits du Nd océanique

Afin de contraindre le cycle océanique du Nd, il est nécessaire de connaître et de quantifier les flux de l'élément au réservoir océanique.

Il est établi que les sources hydrothermales jouent un rôle négligeable au niveau global dans les apports de Nd, puisqu'il est immédiatement soustrait de l'eau sur le site (Piegras et Wasserburg, 1985), comme toutes les terres rares (Michard et al., 1983). Cependant, la connaissance actuelle sur ces sources ne permet pas de négliger un impact local si les flux sont importants, permettant un échange dissout-particulaire avant que tout le Nd ne soit retiré de la colonne d'eau. Ceci incite à ne pas systématiquement négliger ce type de sources. De même, s'il semble clair que les sources de Nd sont lithogéniques, des incertitudes restent sur les contributions relatives des décharges fluviales et poussières atmosphériques (Goldstein et al., 1984; Grousset et al., 1998; Nakai et al., 1993), des sources souterraines (Johannesson et Burdige, 2007), ou encore des apports par remobilisation sur la marge continentale (Lacan et Jeandel, 2001, 2005b). Ces ambiguïtés sont principalement dues à la mauvaise connaissance des processus se déroulant aux in-

terfaces continent-océan et atmosphère-océan (taux de dissolution et de remobilisation), ainsi qu'aux interactions dissout-particulaires (formation de particules authigéniques de Nd puis reminéralisation dans la colonne d'eau) (Frank, 2002). Mieux contraindre tous ces processus est un des objectifs du programme international *GEOTRACES* (Geotraces, 2005).

L'étude conjointe de la CI et de la concentration en Nd va permettre d'apporter des informations complémentaires sur les sources de l'élément.

1.2.3.1 Le paradoxe de la CI et de la concentration

Les variations de CI observées dans une même colonne d'eau (pouvant aller jusqu'à $8 \varepsilon_{Nd}$) sont corrélées avec les variations de propriétés fondamentales des différentes masses d'eau. Ceci indique que ε_{Nd} est conservatif loin de ses sources (on dit alors "quasi-conservatif") et n'évolue que par mélange des masses d'eau (Goldstein et Hemming, 2003). De plus, on a vu que la CI du Nd diffère selon les bassins océaniques, ce qui implique un temps de résidence de l'élément inférieur au temps de mélange des océans (soit $\sim 1\ 500$ ans (Broecker et Peng, 1982)).

En revanche, les profils en concentration en Nd dissout montrent une augmentation légère avec la profondeur, couplée à une tendance à l'augmentation le long de la circulation thermohaline (de $15\ pmol.kg^{-1}$ en Atlantique Nord à $45\ pmol.kg^{-1}$ dans le Pacifique Nord). Ceci montre que du Nd est ajouté aux masses d'eau qui se propagent en profondeur, et suggère un rôle du cycle vertical d'interactions dissout-particulaire pour expliquer cet apport (scavenging en surface et desorption/désaggrégation/dissous en profondeur, (Nozaki et Alibo, 2003)). Jeandel et al. (1995), ont estimé à partir de ces flux verticaux un temps de résidence de cet élément de 2 000 ans. De même, un inventaire des sources fluviates et de poussières atmosphériques au niveau global montre (Goldstein et Jacobsen, 1987; Duce et al., 1991; Grousset et al., 1998) un temps de résidence de l'ordre de 5 000 ans.

Le comportement du Nd océanique apparaît donc contradictoire selon que l'on se base sur l'étude de la CI, qui propose des variations par mélange des masses d'eau, ou de la concentration, qui suggère une influence de processus dans la colonne d'eau, ce que les données de CI excluent. De plus, les temps de résidence calculés par la CI et par la concentration diffèrent. Ce découplage du comportement a par la suite été appelé "paradoxe du Nd" (cf. (Goldstein et Hemming, 2003) pour un résumé sur cette problématique).

La résolution de ce paradoxe passe par une meilleure quantification des termes sources ou puits pour réduire le temps de résidence estimé par la concentration, et par la compréhension du cycle vertical de l'élément permettant de rejoindre le profil vertical de concentration et la propriété de traceur de circulation de la CI.

1.2.3.2 Les premières modélisations du cycle du Nd océanique

Ce “Nd paradox” a été mis en évidence notamment lors des premières tentatives de modélisation du cycle océanique du Nd.

Bertram et Elderfield (1992), utilisant un modèle à sept boîtes et considérant comme inputs des flux de rivières, ont calculé un temps de résidence du Nd de l’ordre de 5 000 ans, incompatible avec le gradient inter-bassin de ε_{Nd} observé. De plus, le flux de particules calculé par les auteurs pour équilibrer le bilan de CI est un ordre de grandeur plus important que pour équilibrer celui de la concentration, i.e. les flux de sources/puits nécessaires pour reproduire les variations observées en concentration en Nd sont donc dix fois moins importants que pour la CI. Afin de résoudre ce problème et d’équilibrer à la fois la CI et la concentration en Nd, ils envisagèrent un important échange dissout-particulaire, soit au sein même de la colonne d’eau, soit à l’interface avec les sédiments profonds.

Tachikawa et al. (2003), en considérant un modèle en boîtes global et des apports fluviaux et atmosphériques en Nd à l’océan, montrent qu’il est impossible d’équilibrer la CI et la concentration. Des processus d’échange déjà signalés aux marges (permettant de changer la CI sans influer sur la concentration), impliquant des apports jusqu’à dix fois plus importants que par les poussières atmosphériques et les décharges fluviales envisagés, sont requis pour fermer à la fois le bilan en concentration et la CI.

Enfin, Van de Flierdt et al. (2004), dans un modèle en boîte dans le Pacifique Nord ont eux aussi considéré une source de Nd environnante avec une préférence pour des échanges dissout-particulaire pour équilibrer la concentration tout en maintenant le budget isotopique, et en réconciliant le profil de concentration qui augmente avec la profondeur.

Il est nécessaire d’envisager un **échange** pour équilibrer à la fois la concentration et la CI en Nd. Ces conclusions mettent en évidence l’influence d’apports extérieurs et d’interactions dissout-particulaire pour permettre d’expliquer ce “paradoxe du Nd”.

1.2.3.3 Les observations

Parallèlement à ces travaux de modélisation, des études de terrains ont pu mettre en évidence la nécessité d’apports locaux en provenance des continents pour pouvoir expliquer les variations de ε_{Nd} dissout (Jeandel et al., 1995; Tachikawa et al., 1997; Jeandel et al., 1998; Tachikawa et al., 1999; Lacan et Jeandel, 2001; Amakawa et al., 2004; Lacan et Jeandel, 2004a).

Plusieurs observations de concentration de Nd et de CI dans des masses d’eau en amont, au contact, et en aval d’une marge continentale montrent un changement significatif de la CI, sans un changement de concentration associé. Et ceci, aussi bien pour des terrains basaltiques que granitiques, et à des profondeurs allant de 200 m jusqu’à 2 700 m, (cf. Fig.1.6 Lacan et Jeandel, 2005b). Cela semble bien montrer à la fois une perte de Nd dissous de la masse d’eau par “Boundary Scavenging”⁵ compensée par un apport de Nd

⁵scavenging important qui a lieu à l’interface continent-océan (e.g. Bacon, 1988)

(permettant de rééquilibrer la concentration) mais avec une CI différente (probablement sous forme de dissolution de sédiments remobilisés) venant de la marge.

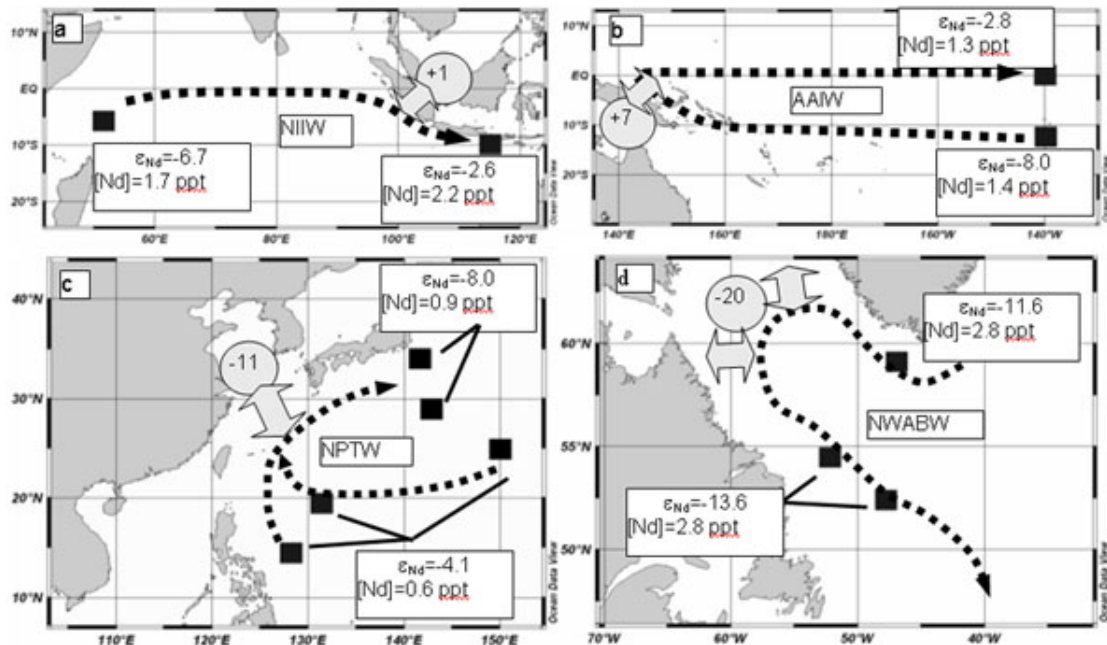


FIG. 1.6 – Carte des échanges observés entre une masse d'eau et les marges continentales. Les carrés représentent les lieux d'observation de Nd dissous, la concentration et la composition isotopique étant indiquées pour chaque donnée ; les pointillés représentent le chemin symbolique de la masse d'eau ; et la double flèche symbolise l'échange entre la masse d'eau et la marge continentale avec une CI indiquée à l'intérieur des ronds (Lacan et Jeandel, 2005b).

1.2.3.4 Le "Boundary Exchange" comme source et puits de l'élément

Les conclusions obtenues suite aux observations des données *in-situ* semblent confirmer les hypothèses suggérées par les modèles en boîte (Bertram et Elderfield, 1992; Tachikawa et al., 2003) : un processus d'échange de Nd dissous/particulaire est mis en évidence entre la marge continentale et les masses d'eau qui passent au contact de celle-ci. Cet échange est potentiellement le terme sources-puits dominant du cycle océanique du Nd. Lacan et Jeandel (2005b) ont nommé cet échange aux marges "Boundary Exchange" (BE).

La figure 1.7 résume tous les processus sources et puits en jeu dans le cycle océanique du Nd.

On a pu voir que l'enregistrement du signal isotopique dans les hydroxydes de manganèse permet de quantifier les flux de matière de source lithogénique dans le temps. De même, on a vu que les différentes sources d'apport de matière ont varié au cours du temps. Comprendre quelle est la source principale de Nd à l'océan est donc primordial pour comprendre l'origine des variations passées d'apport de matière.

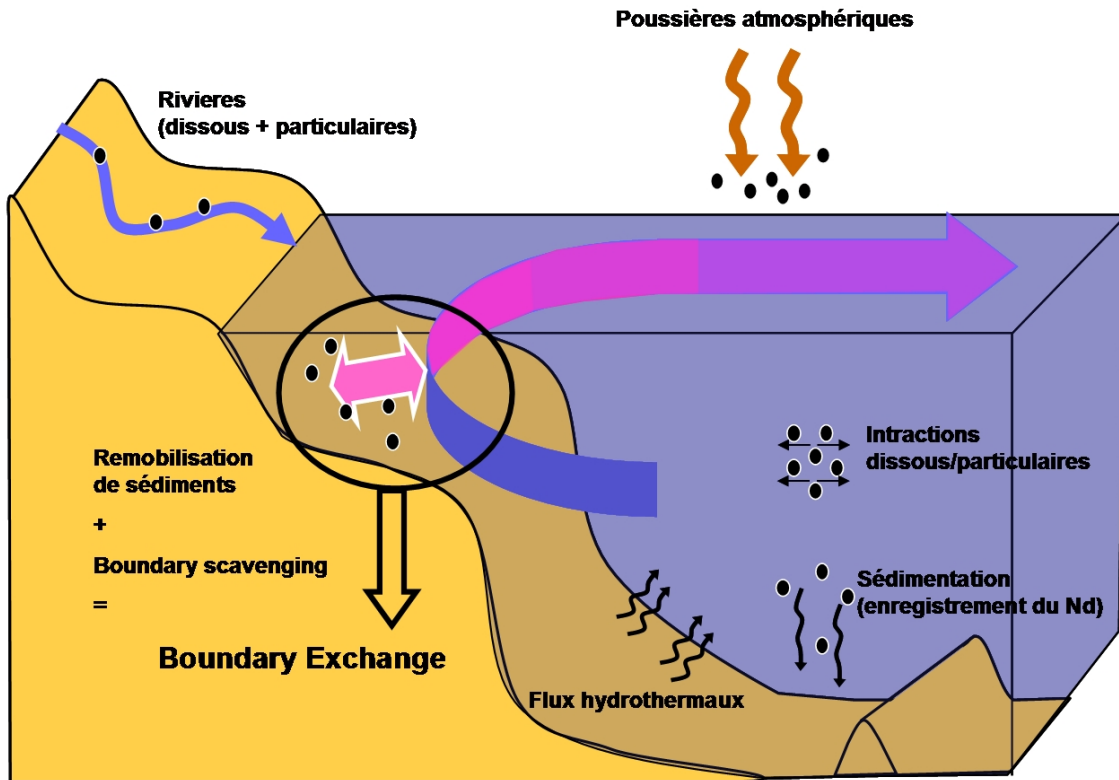


FIG. 1.7 – Sources et puits de Nd océanique. La masse d'eau qui vient au contact de la marge continentale est symbolisée par la flèche de couleur. Les sources lithogéniques de Nd sont les poussières atmosphériques, les flux hydrothermaux, les décharges fluviales (sous forme dissoute et particulaire), et la remobilisation des sédiments sur la marge continentale. Le Nd sort du réservoir océanique par sédimentation, au contact avec la marge continentale par Boundary Scavenging, ou au sein de l'océan ouvert. Dans l'hypothèse de Lacan et Jeandel (2005b), le phénomène de Boundary Scavenging associé à une importante remobilisation des sédiments sur la marge continentale, permettant un apport conséquent de Nd dissous à la masse d'eau est nommé "Boundary Exchange" (BE). Au sein de la colonne d'eau, les échanges dissout-particulaire font évoluer la concentration et la CI en Nd.

L'hypothèse du BE comme processus important dans le cycle océanique du Nd permet une quantification des apports de matière sur toute la marge continentale vers l'océan ouvert. Aussi, la variabilité de signature isotopique des continents (cf. Figure 1.3 p. 23) permet de déterminer l'origine de la source de cette matière. Ceci est donc particulièrement important d'un point de vue géochimique pour contrôler les flux lithogéniques, en particulier dans le cadre de l'étude du fer en tant qu'élément limitant de la production, dont les apports le long de la marge continentale comptent aussi parmi ses sources (Fantle et DePaolo, 2004; Laes et al., 2003). Le BE permet alors la quantification des apports de matière par les marges continentales au cours du temps.

Ces flux de matière sont ensuite à mettre en relation avec les flux d'érosion du continent

et de décharge sédimentaire associée sur la marge, afin d'estimer la proportion de matériel qui va transiter par l'océan avant d'être enfouie dans les sédiments profonds. A terme, il est donc envisageable d'utiliser le Nd comme élément pour mettre en relation les variations d'érosion des continents avec la production primaire dans certaines zones affectées en aval par les apports de matière induits.

1.3 Plan et objectifs de la thèse

Cette thèse s'inscrit dans la continuité des travaux effectués par Jeandel, Tachikawa et Lacan (Tachikawa et al., 2003; Jeandel et al., 1998; Lacan et Jeandel, 2005b) sur les sources et puits de l'élément.

Comme on a pu le voir, le cycle océanique du Nd reste encore partiellement incompris. Les études menées jusqu'à présent permettent d'établir des hypothèses au niveau local, grâce aux données *in situ*, et au niveau global par des valeurs moyennées, grâce aux modèles en boîtes. La modélisation par un modèle de circulation numérique permettra d'obtenir des informations complémentaires par rapport à ces deux approches, en permettant une approche avec une distribution dynamique plus réaliste des masses d'eau.

L'objectif de cette thèse est d'utiliser l'outil de modélisation numérique pour mieux contraindre le cycle global du Nd, tant au niveau des sources et puits de l'élément (validation du postulat de BE comme principal composant), que de son comportement dans la colonne d'eau (résolution du paradoxe du Nd).

J'ai choisi de présenter les travaux de cette thèse selon leur progression chronologique, qui correspond à une réflexion logique dans l'approche et la compréhension du cycle océanique du Nd.

Dans un premier temps, (chapitre 2) le modèle utilisé au cours de cette thèse est présenté avec les différentes configurations mises en place selon les études.

Quel est le poids du BE en tant que source et puits du Nd océanique ? Est-il réellement un terme prépondérant ? Ce sont à ces questions que je m'attacherai de répondre dans le chapitre 3. Pour cela, j'ai mis en place une paramétrisation du BE dans un modèle globale à basse résolution ($2^\circ \times 2^\circ$). Le traceur ε_{Nd} est considéré comme conservatif et dans cette première approche, il est le seul modélisé (la concentration en Nd est considérée comme uniforme). Afin de déterminer l'influence du BE sur le cycle du Nd océanique, seul ce terme sources-puits est représenté et couplé à la circulation océanique. On regarde alors si la simulation de la distribution de la CI est réaliste. L'échelle de temps des processus d'échange entre la marge continentale et la masse d'eau est évaluée par différents tests de sensibilité.

Dans le chapitre 4, je m'intéresse au ε_{Nd} en tant que traceur paléo-océanographique. Quel est son comportement dans une configuration climatique passée comme le DMG ? Dans quelle mesure ce traceur reste-t-il un traceur de la circulation océanique, soumis à différents scénarios de circulation ? Alors que l'acquisition de la signature isotopique en Nd de la NADW relève d'un processus complexe (Lacan et Jeandel, 2005a), de façon assez surprenante, certaines données semblent montrer que celle-ci n'aurait pas évolué au

cours du temps (Van de Flierdt et al., 2006; Foster et al., 2007). En se basant sur cette hypothèse, Piotrowski et al. (2004) expliquent les changements de ε_{Nd} observés dans un enregistrement sédimentaire uniquement par des changements de distribution de masses d'eau. La modélisation du traceur au DMG nous permet de progresser sur cette question en donnant des indications concernant l'influence relative du processus de BE par rapport à la circulation océanique. Qui des changements de signature isotopique des "end-members" sous l'influence de leur contact aux marges ou des changements de circulation dans la distribution passée du ε_{Nd} sont responsables des variations temporelles de ε_{Nd} ?

Le chapitre 5 aborde la modélisation du ε_{Nd} avec un modèle régional NATL4 eddy-permitting ($1/4^\circ \times 1/4^\circ$) dans l'Atlantique Nord. Cette étude fait suite aux travaux effectués par F. Lacan au cours de sa thèse (Lacan, 2002) qui avait mesuré près de 200 échantillons d'eau de mer dans la région de l'Atlantique Nord et des mers Arctiques. L'objectif est d'utiliser une version plus réaliste du modèle de circulation pour voir comment cela affecte notre compréhension du BE, et ainsi de confirmer si la paramétrisation mise en place au chapitre 3 permet une simulation à plus petite échelle de la distribution de la CI du Nd. La densité des observations sur la zone, plus importante que n'importe où ailleurs, ainsi que la qualité de la dynamique du modèle, permettent aussi d'effectuer des tests de sensibilité sur la paramétrisation du BE et ainsi de tester les facteurs (type de roche, dynamique) qui influent sur cet échange.

Quels sont les flux de matière entre les continents et l'océan qui permettent d'équilibrer à la fois le cycle de la concentration et la CI en Nd ?, au sein de la colonne d'eau entre les particules et la phase dissoute ? Quels sont les flux de sédimentation ? En d'autres termes, quels sont les processus intra et extra océaniques qui permettent d'expliquer la distribution de la concentration et de la CI du Nd, et ainsi d'expliquer le paradoxe du Nd ? Je m'attacherai dans le chapitre 6 à proposer une réponse, en utilisant un modèle couplé dynamique, biogéochimique, ainsi qu'un modèle de scavenging reversible. Ici, la concentration en Nd et la CI sont tous deux modélisés, ce qui permet une simulation complète du cycle du Nd.

Enfin, on récapitulera les principaux résultats obtenus lors de cette étude dans une conclusion où l'on s'attachera à déterminer les perspectives de travail à venir.

Chapitre 2

Le modèle de circulation océanique

Sommaire

2.1	Introduction	37
2.2	Présentation du modèle	38
2.2.1	Approximations et équations primitives	38
2.2.2	Les fermetures turbulentes du modèle	40
2.2.3	Les grilles ORCA	40
2.3	Configuration globale	41
2.3.1	La grille ORCA2	41
2.3.2	Configurations	41
2.3.2.1	Runs forcés	41
2.3.2.2	Runs couplés	42
2.4	Configuration régionale	43
2.4.1	Grille NATL4	43
2.4.2	Conditions initiales et forçages	44
2.5	Le modèle de traceurs passifs de NEMO	44

2.1 Introduction

Le choix du modèle ainsi que la configuration d'utilisation sont déterminants pour cibler les objectifs d'une étude et l'interprétation des résultats. Le modèle de dynamique océanique utilisé pour forcer les simulations de traceur géochimique réalisées au cours de cette thèse est le modèle NEMO. Contrairement aux modélisations dynamiques dites "classiques" de température et salinité, où les observations sont nombreuses autant temporellement que géographiquement, une des principales difficultés de la modélisation des éléments traces est la validation des résultats, en raison du faible nombre de données disponibles. De plus, la modélisation océanique du Nd est une étude à caractère exploratoire de par la connaissance encore incertaine de ses sources et de son comportement au sein de la colonne d'eau.

Ainsi, les configurations d'utilisation du modèle ont été établies en fonction des besoins et des objectifs qui ont évolués au cours de cette thèse.

Toutes les simulations effectuées au cours de cette thèse sont intégrées jusqu'à l'obtention d'une distribution à l'équilibre. Ceci implique des coûts élevés de simulation. Or, dans le cadre de la nature exploratoire de la première étude sur le rôle du BE en tant que source-puit du Nd océanique, il est nécessaire d'utiliser le modèle dans une configuration globale, et de pouvoir effectuer de nombreux tests de sensibilité (sur le temps d'échange entre la marge continentale et la masse d'eau, cf. Chapitre 3). Le choix d'une configuration globale basse résolution (grille de $2^\circ \times 2^\circ$, ORCA2) s'est donc imposé afin de limiter les problèmes liés au coût de calcul. De plus, cette version a déjà été largement testée pour d'autres traceurs ($CFCs$, 3He , ^{14}C) et la circulation est suffisamment réaliste pour la simulation de traceurs biogéochimiques. De plus, la base de données actuelle de Nd océanique (environ 600 points, disponible sur http://www.legos.obs-mip.fr/fr/equipes/geomar/results/database_may06.xls) ne justifie pas une résolution spatiale plus élevée. Utilisé en mode forcé (flux de chaleur, d'eau et de quantité de mouvement prescrits à la surface de l'océan), cette version est la configuration standard du modèle. Même si la simulation des courants de bords par le modèle est inexacte (ce qui peut sembler problamétique au regard de l'hypothèse de BE que l'on veut tester), cette configuration est adaptée pour permettre une modélisation globale à coût numérique raisonnable, et déterminer l'influence du BE au premier ordre.

Lors de l'étude de l'évolution de la composition isotopique du Nd au Dernier Maximum Glaciaire (LGM, cf. Chapitre 4), le modèle a été utilisé dans une configuration couplée, c'est à dire que le modèle océanique a été couplé avec un modèle de circulation atmosphérique général (AGCM) et un modèle de surface continentale (les flux de chaleur, eau et quantité de mouvement sont alors prescrits par le modèle atmosphérique). Le coût d'intégration de ces systèmes couplés est prohibitif, et l'objectif de ces simulations est de dégager de grandes tendances d'interactions entre les différentes composantes du système afin de comprendre les évolutions climatiques. La même résolution de grille du modèle océanique ($2^\circ \times 2^\circ$) que celle utilisée précédemment a donc été imposée.

L'étude régionale en Atlantique Nord (cf. Chapitre 5) intervient à la suite des travaux de thèse de F. Lacan sur des données *in-situ* dans cette zone (Lacan, 2002), mettant ainsi

à disposition une base de données importante pour comparer les sorties du modèle, et de l'étude de modélisation globale du ε_{Nd} (cf. Chapitre 3). Le même modèle a été utilisé dans une configuration eddy-permitting (grille au quart de degré), afin de profiter d'une dynamique plus réaliste (meilleure reproduction des courants de bord et de la formation des eaux profondes entre autres), dans le but de confirmer et affiner la paramétrisation du BE.

Enfin, l'étude couplée de la CI et de la concentration en Nd (cf. Chapitre 6) est de nouveau une étude exploratoire visant à déterminer les processus qui contrôlent le cycle du Nd, avec une autre paramétrisation des termes sources-puits, ce qui implique de nombreux tests de sensibilité. C'est pourquoi on a réutilisé la même configuration ORCA2 dont le coût de calcul a permis de réaliser plusieurs simulations..

Dans ce chapitre, je présente tout d'abord de manière générique le modèle NEMO, avant de décrire et préciser les différentes configurations d'utilisation. Enfin, le néodyme étant un traceur passif dans l'océan, le modèle de traceur passif a été utilisé et une brève présentation de ce modèle est proposée.

2.2 Présentation du modèle

NEMO (Nucleus for European Modelling of the Ocean), a été développé au “Laboratoire d’Océanographie et du Climat : Expérimentations et Approches Numériques” (*LOCEAN – IPSL*) à Jussieu (Paris). C'est un modèle numérique permettant de mettre en relation la dynamique océanique et la thermodynamique (grâce à OPA - Océan Parallelisé) avec la glace de mer (module LIM - Louvain-la-Neuve Ice Model) et les traceurs passifs biogéochimiques (module TOP - Tracer in Ocean Paradigm, comprenant le transport et les termes sources et puits). Il permet l'étude des interactions de l'océan avec les autres éléments du système climatique, comme l'atmosphère ou les surfaces continentales, grâce au coupleur OASIS. Son développement est réalisé dans le but d'être adaptable à différents problèmes aux dimensions spatiales et temporelles variables. Dans le cadre de cette thèse, on décrit dans un premier temps le modèle physique avant de s'intéresser au formalisme mathématique et numérique qui permet de résoudre ces équations. Les détails concernant le fonctionnement du modèle et les schémas numériques utilisés sont disponibles dans le manuel d'utilisation de *NEMO* (Madec (2008)). Une présentation rapide des principales caractéristiques de chaque configuration est faite.

2.2.1 Approximations et équations primitives

L'océan est un fluide dont la circulation à grande échelle peut être décrite avec une bonne approximation par les équations primitives, qui sont les équations de Navier-Stokes avec une équation d'état non-linéaire qui couple les deux traceurs actifs (salinité et température) à la vitesse du fluide, et les différentes hypothèses simplificatrices liées à des considérations d'échelle :

- *approximation de couche mince* : on suppose que la profondeur de l'océan est négligeable devant le rayon de la terre.
- *approximation de sphéricité de la terre* : on suppose que les surfaces géopotentielles sont des sphères. Ainsi, la gravité est parallèle aux rayons de la terre.
- *hypothèse d'incompressibilité* : l'équation de conservation de la masse se réduit à la nullité de la divergence du vecteur vitesse tridimensionnel. Cette hypothèse permet de filtrer les ondes qui n'ont pas d'influence sur les mouvements à grande échelle.
- *approximation hydrostatique* : on néglige dans l'équation de conservation de la quantité de mouvement verticale tous les termes autres que la gravité et le gradient vertical de pression. Cette équation s'écrit alors :

$$\partial_z P = -\rho g.$$

Cette hypothèse est valide si l'échelle caractéristique verticale H est petite devant l'échelle caractéristique horizontale L . Le plus petit pas de grille horizontal étant de 30 kilomètres, les plus petites longueurs d'ondes résolues sont de 60 kilomètres. La profondeur de l'océan dans le modèle étant de 5000 mètres au plus, on obtient un rapport $\frac{H}{L} < 0.1$, ce qui valide l'hypothèse.

- *approximation de Boussinesq* : on néglige les variations de densité (qui ne sont de l'ordre que de quelques pour cent - de $1022 \text{ à } 1036 \text{ kg/m}^3$) dans l'équation de conservation de la quantité de mouvement horizontale due à l'accélération du fluide.
- *hypothèse de fermeture turbulente* : les flux turbulents représentent les effets des mouvements à petite échelle sur les mouvements à grande échelle. Ces interactions entre les différentes échelles sont induites par les termes non linéaires et sont représentées dans le modèle par des termes diffusifs.

Considérons un ensemble de vecteurs unitaires orthogonaux $(\mathbf{i}, \mathbf{j}, \mathbf{k})$ tels que \mathbf{k} est le vecteur unitaire sortant et (\mathbf{i}, \mathbf{j}) sont tangents aux surfaces géopotentielles. Soit \mathbf{U} le vecteur vitesse, $\mathbf{U} = \mathbf{U}_h + w\mathbf{k}$ (h exprime le plan horizontal (\mathbf{i}, \mathbf{j})), T la température potentielle (température de l'eau portée à la surface adiabatiquement, c'est à dire sans échange de chaleur), S la salinité et ρ la densité *in-situ*. Les hypothèses précédentes appliquées aux équations de Navier-Stokes (conservation de la quantité de mouvement), d'équilibre hydrostatique, de continuité (conservation de la masse), de conservation de chaleur et de sel, nous donnent le système simplifié d'équations suivant :

$$\frac{\partial \mathbf{U}_h}{\partial t} = - \left[(\nabla \times \mathbf{U}) \times \mathbf{U} + \frac{1}{2} \nabla(\mathbf{U}^2) \right]_h - f\mathbf{k} \times \mathbf{U} - \frac{1}{\rho_0} \nabla_h p + D^{\mathbf{U}} \quad (2.1)$$

$$\frac{\partial p}{\partial z} = -\rho g \quad (2.2)$$

$$\nabla \cdot \mathbf{U} = 0 \quad (2.3)$$

$$\frac{\partial T}{\partial t} = -\nabla \cdot (T\mathbf{U}) + D^T \quad (2.4)$$

$$\frac{\partial S}{\partial t} = -\nabla \cdot (S\mathbf{U}) + D^S \quad (2.5)$$

$$\rho = \rho(T, S, p) \quad (2.6)$$

où ρ_0 est la densité de référence, p la pression, f le terme de Coriolis ($f = 2\Omega \sin \Theta$ avec Ω vitesse de rotation angulaire de la terre et Θ latitude du point considéré) et D^U , D^T et D^S sont les termes de paramétrisation à petite échelle pour la quantité de mouvement, la température et la salinité, aussi appelé termes de fermeture turbulente.

2.2.2 Les fermetures turbulentes du modèle

Les équations primitives décrivent des phénomènes à une échelle d'ordre trop petit pour pouvoir être résolus sur les grilles et avec les pas de temps utilisés par le modèle. Ces effets de petite échelle, générés par les termes advecifs des équations de Navier-Stokes doivent être paramétrisés à grande échelle pour fermer les bilans des variables pronostiques. Les termes de fermetures turbulentes se décomposent en composantes horizontales et verticales.

$$\begin{aligned} D^U &= D^{vU} + D^{hU} \\ &= \frac{\partial}{\partial z} \left(A^{vm} \frac{\partial U^h}{\partial z} \right) + \nabla_h \cdot (A_h^u \nabla_h U^h) - \nabla_h \times (A_h^u \nabla_h \times \mathbf{U}^h) \\ D^T &= D^{vT} + D^{hT} \\ &= \frac{\partial}{\partial z} \left(A^{vT} \frac{\partial T}{\partial z} \right) + \nabla_h \cdot (A_h^t \nabla_h T) \\ D^S &= D^{vS} + D^{hS} \\ &= \frac{\partial}{\partial z} \left(A^{vS} \frac{\partial S}{\partial z} \right) + \nabla_h \cdot (A_h^t \nabla_h S) \end{aligned}$$

ou A^{vm} et A^{hm} sont les coefficients de viscosité turbulente verticale et horizontale respectivement, A^{vT} et A^{hT} sont les coefficients de diffusivité turbulente verticale et horizontale.

Les coefficients verticaux sont prescrits suivant le modèle TKE (Turbulent Closure Scheme) proposé par Gaspar et al. (1990) puis adapté au modèle par Blanke et Delecluse (1993), permettant une représentation explicite de la couche mélangée ainsi qu'un minimum de diffusion dans la thermocline. Les coefficients horizontaux sont eux linéairement dépendants du gradient latéral grande échelle. Cependant, afin d'améliorer la diffusion turbulente latérale, Gent et McWilliams (1990) ont établi une paramétrisation qui relie une vitesse induite à la pente des isopycnies. Ce schéma est utilisé dans toutes les configurations du modèle présentées lors de cette thèse.

2.2.3 Les grilles ORCA

Les modèles d'océan sont souvent écrits en différences finies. Cette méthode a l'avantage d'être évolutive et peut traiter des conditions aux limites complexes formées par la géométrie des lignes de côte et des fonds sous-marins. Cependant, ce type de schéma est aussi soumis à des contraintes numériques.

Le code *NEMO - ORCA* est un modèle en différences finies. Les schémas explicites utilisés imposent une condition de stabilité CFL ((Courant et al., 1928)) sur les pas de

discrétisation temporelle Δt et spatial Δx :

$$\frac{c \cdot \Delta t}{\Delta x} < 1$$

où c est la vitesse de propagation du phénomène modélisé le plus rapide.

Un problème important à prendre en compte pour modéliser l'océan global est la présence d'un point singulier du système de coordonnées géographiques (longitude-latitude) sur la sphère : le pôle nord (le pôle sud n'étant pas un point de l'océan, il ne pose pas de problème). Dans le cas d'une grille de discrétisation liée au système géographique, le pas de grille méridien tend vers zéro au voisinage du pôle nord. Le critère de stabilité CFL impose alors d'importantes contraintes sur le pas de temps, voir théoriquement un pas de temps infiniment petit, ce qui entraîne une augmentation considérable des coûts informatiques.

La solution envisagée par Madec (2008) a été de déformer la grille géographique de façon à placer les points singuliers dans les terres, c'est-à-dire concrètement en Amérique du Nord et en Europe, hors du domaine de calcul. Ainsi, les zones de la grille où le pas spatial est très petit ne sont pas traitées par le modèle et on s'affranchit des contraintes les plus fortes imposées par les conditions CFL. En revanche, le positionnement des deux points singuliers dans l'hémisphère Nord oblige à déformer la grille.

2.3 Configuration globale

2.3.1 La grille ORCA2

La résolution de la grille dans la configuration *ORCA2* est de deux degrés en latitude par un degré et demi en longitude, lorsque la grille est régulière, dans l'hémisphère Sud. Au niveau de l'équateur, la résolution est accrue en latitude (jusqu'à un dixième de degré) pour bien simuler la dynamique particulière de cette région (caractérisée par des courants très fins parallèles aux latitudes) induite par les termes non linéaires plus importants que la force de Coriolis qui s'annule (cf. Fig. 2.1). Au final, la grille horizontale se compose de 182 par 149 points, et comporte 31 niveaux verticaux (dix dans les 100 premiers mètres, augmentant jusqu'à une résolution de 500 mètres au fond). Le domaine d'intégration est donc défini par environ 840 000 points.

2.3.2 Configurations

Deux configurations différentes du modèle *NEMO – ORCA2* sont utilisées au cours de cette thèse.

2.3.2.1 Runs forcés

Pour les premières simulations (cf. section 3), le modèle est utilisé dans sa configuration couplée avec le modèle de glace de mer *LIM* (Goosse et Fichefet, 1999). Le mélange

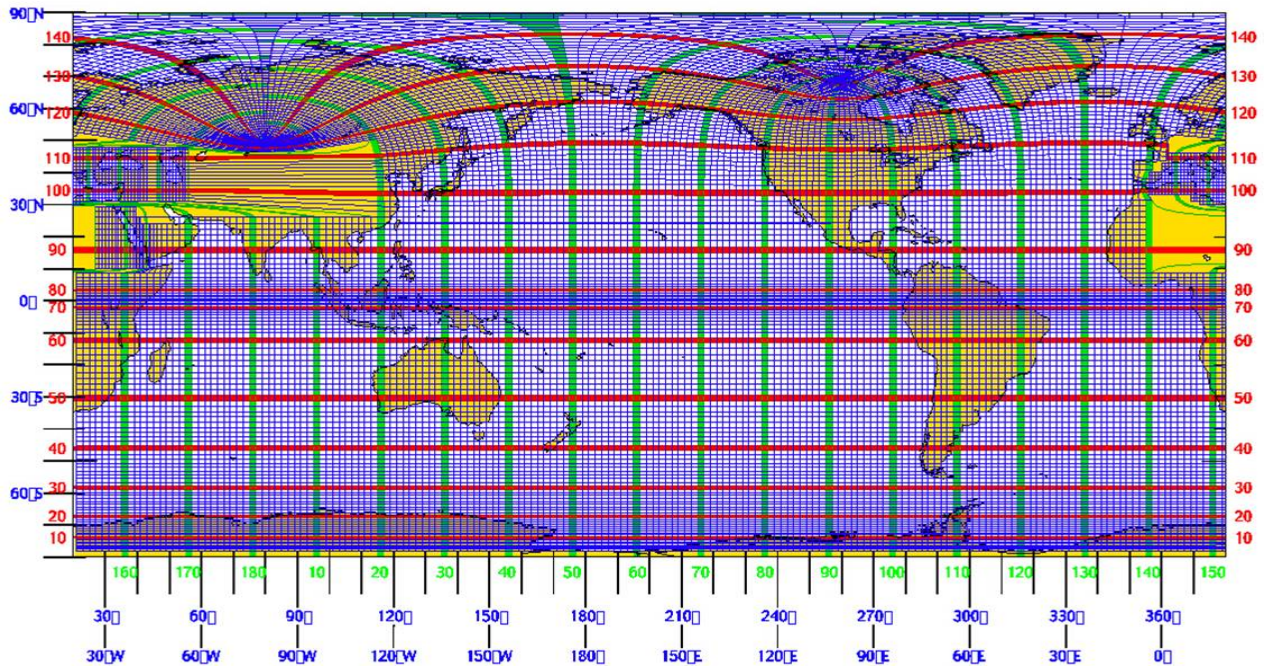


FIG. 2.1 – Maillage de la grille ORCA2. Les nombres verts et rouges représentent les indices horizontaux et verticaux de la grille.

latéral est appliqué le long des isopycnies, et la paramétrisation sous-maille de Gent et McWilliams (1990) est implémentée. Un schéma de fermeture turbulente pour le mélange vertical (Blanke et Delecluse, 1993), ainsi que la paramétrisation d'une couche de diffusion au fond de l'océan (Beckmann et Scher, 1997) sont inclus.

Le modèle est forcé à la surface de l'océan. Flux de chaleur et d'eau douce, et forçage par le vent sont prescrits par les climatologies mensuelles ERS1/2 aux tropiques et NCEP/NCAR aux latitudes supérieures à 50°.

2.3.2.2 Runs couplés

Lors de la modélisation du Nd au Dernier Maximum Glaciaire (DMG) (cf. section 4), la simulation océanique est extraite d'une configuration de modèle couplé IPSLCM4 v2 incluant un modèle de dynamique atmosphérique *LMDZ3.3* (Hourdin et al., 2006) qui prescrit les flux à la surface océanique. Les mêmes modèles *NEMO* – *ORCA2* et *LIM* sont utilisés pour la composante océanique. Les interactions entre chaque modèles sont prises en compte via le coupleur *OASIS* (CERFACS, (Valcke, 2006)).

2.4 Configuration régionale

La configuration NATL4 du modèle NEMO est une configuration régionale haute résolution en Atlantique Nord et dans les Mers Nordiques extraite de la configuration globale. Les études menées avec cette configuration font partie intégrante du programme international DRAKKAR (projet de modélisation de l'océan à haute résolution des variations océaniques en Atlantique Nord et dans l'océan Austral). Une description détaillée de cette configuration et du projet DRAKKAR en général se trouvent sur le site web <http://www.ifremer.fr/lpo/drakkar/index.htm>.

Comme dans la configuration *ORCA2*, le modèle utilisé est NEMO, couplé avec le modèle de glace LIM2.0 développé à Louvain La Neuve.

2.4.1 Grille NATL4

La grille utilisée est une grille Mercator au $1/4^\circ$ à l'équateur, qui s'étend du 20°S à 80°N (correspondant au détroit de FRAM). La limite Est en Méditerranée est fixée à 23°E . Cette grille de 486×529 points est extraite de la grille au $1/4^\circ$ globale ORCA025 (indices 757 à 1242 et 370 à 943 pour les dimensions i et j respectivement).

Verticalement, la grille possède 46 niveaux définis en coordonnées z espacés de 6 m en surface jusqu'à 250 m au fond, pour un total de 12 000 000 points de grille. Les partial-steps sont utilisés pour déterminer la hauteur du dernier niveau.

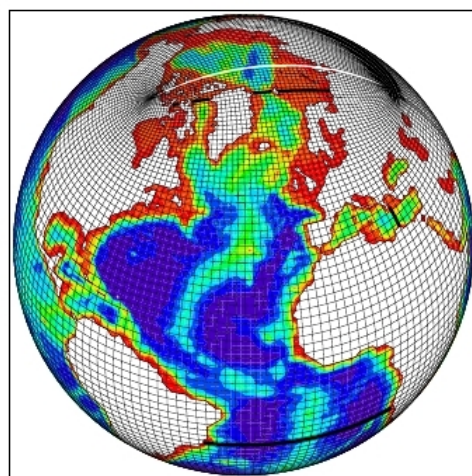


FIG. 2.2 – Maillage de la grille ORCA025 dont est extrait le domaine NATL4 (délimité par les traits épais noirs). Un point de grille sur 10 est représenté.

2.4.2 Conditions initiales et forçages

Le temps d'intégration du modèle est de 5 ans, initialisé à partir des climatologies Levitus98-PH2.1 et Medatlas, interpolées sur tous les points de grille.

Les flux de surface sont calculés par une formulation “bulk”.

- Couverture nuageuse et humidité : données CLIO mensuelles.
- Tension de vitesse du vent : données ERS/NCEP sur la période 1992-2000 journalières.
- Précipitations : données CMAP sur la période 1992-2000 mensuelles.
- Température de l'air : données NCEP sur la période 1992-2000 journalières.

2.5 Le modèle de traceurs passifs de NEMO

Pour modéliser la propagation d' ε_{Nd} dans l'océan, on utilise un modèle de transport de traceurs passifs NEMO (Ethé et al., 2006). ε_{Nd} est considéré ici comme un traceur passif car il n'affecte pas la circulation océanique (par opposition aux traceurs actifs comme la température et la salinité). Le modèle peut donc calculer l'évolution du traceur en *off-line*, c'est à dire en utilisant des sorties de champs dynamique (vitesse des courants, coefficients de diffusion), de température et de salinité préalablement calculées. Ceci ne permet pas en revanche d'effectuer des tests de sensibilité sur la dynamique du modèle général, mais le coût de calcul bien plus faible permet de faire des tests de sensibilité sur la géochimie.

Le modèle de transport résoud une équation de transport, forcée par un terme «source et puits» spécifique pour chaque traceur passif C :

$$\frac{\partial C}{\partial t} = S(C) - \mathbf{U} \cdot \nabla C + \nabla \cdot (K \nabla C) \quad (2.7)$$

où :

- $S(C)$, premier terme du membre de droite, est le terme source- puits inhérent au traceur.
- le second terme représente l'advection du traceur dans les trois directions.
- le troisième terme représente la diffusion latérale et verticale.

Les conditions aux limites de l'équation sont déterminées par des conditions de flux de traceurs sur le bord du domaine.

Ce modèle a déjà été utilisé dans des configurations proches de la nôtre pour la modélisation de tritium-hélium-3 et CFCs par exemple (Dutay et al., 2002, 2004). La principale différence dans la modélisation d'un traceur par rapport à un autre réside dans la formulation de son terme sources-puits.

Chapitre 3

Impact du Boundary Exchange sur le cycle océanique du ε_{Nd}

Sommaire

3.1	Introduction	49
3.2	Compilation de données de Nd sur la marge continentale	50
3.2.1	Résumé	50
3.2.2	<i>Isotopic Nd compositions and concentrations of the lithogenic inputs into the ocean : a compilation, with an emphasis on the margins.</i>	52
3.3	Modélisation de la composition isotopique du Nd à l'échelle globale	62
3.3.1	Résumé	62
3.3.2	<i>Modeling the neodymium isotopic composition with a global ocean circulation model</i>	63

3.1 Introduction

Afin de déterminer quels sont les processus contrôlant la distribution océanique du Nd, il est essentiel de comprendre quels sont ses apports au sein du réservoir océanique. Cette première étape dans la modélisation du cycle océanique du Nd s'inscrit dans la continuité des travaux de Tachikawa et al. (2003) et Lacan et Jeandel (2001, 2005b) concernant l'étude des termes sources-puits du Nd dans l'océan. Ces études ont suggéré que le BE est un terme important des sources-puits de l'élément (cf. Introduction générale). Le premier objectif est donc de s'appliquer à tester cette hypothèse, et de voir s'il est possible de retrouver par une première approche volontairement simplifiée de modélisation avec un OGCM, les principales caractéristiques de la distribution globale de ε_{Nd} ainsi que les résultats obtenus par les observations et les premières études de modèles en boîtes. Volontairement, dans un premier temps, les autres termes sources (poussières atmosphériques, apports fluviaux dissous et particulaires, eaux souterraines) et puits (sédimentation) de l'élément sont négligés : on ne modélise que le BE. Ceci permet d'appréhender directement le rôle qu'il joue sur la distribution océanique du ε_{Nd} , sans avoir à le découpler des autres termes d'apport ou de soustraction.

De plus, dans le cadre d'une première approche exploratoire, on considère le traceur ε_{Nd} comme conservatif (hypothèse réaliste selon ce qui a été présenté section 1.2.2.1, p.25), ce qui nous permet de ne prendre en compte et de ne modéliser que la composition isotopique du Nd, sans simuler la concentration dans un premier temps. Si cette décision ne permet pas d'appréhender complètement le “paradoxe du Nd” (défini suite à l'observation du découplage de comportement de la concentration et de la composition isotopique, cf. section 1.2.3.1, p.28), elle est néanmoins cohérente sur la volonté de tester les sources et puits de l'élément. En effet, reproduire une distribution cohérente du traceur, à l'échelle globale (par la reproduction du gradient inter-bassin de ε_{Nd}) et à l'échelle du bassin, voir même locale (composition des principales masses d'eau, changement de composition isotopique au contact de la marge (Lacan et Jeandel, 2005b)) est suffisant pour conclure sur l'importance du rôle du BE dans le cadre de cette étude. De plus, l'approche proposée permet d'obtenir une estimation sur le temps d'échange entre la marge continentale et l'océan ouvert permettant à la masse d'eau de changer de CI.

En revanche, l'inconvénient d'une telle approche est que l'on ne peut ni étudier, ni quantifier les processus en jeu (dissolution, scavenging, reminéralisation, chute des particules, remobilisation des sédiments sur la marge continentale). Ainsi, si cette étude a pour but de déterminer au premier ordre le rôle du BE dans le cycle océanique du Nd, elle ne peut en aucun cas permettre de le quantifier. Cela sera l'objectif de l'étude du chapitre 6, p.119

Le terme de BE est paramétré au sein du modèle par une équation de rappel de la valeur ε_{Nd} de l'eau en contact avec la marge continentale à la valeur ε_{Nd} du sédiment sur la marge continentale :

$$S(\varepsilon_{Nd}) = \gamma (\varepsilon_{Nd_{marge}} - \varepsilon_{Nd}) \times pmarge \quad (3.1)$$

avec :

- $\varepsilon_{Nd_{marge}}$ est la valeur de ε_{Nd} sur la marge continentale.
- $\gamma = \frac{1}{\tau}$ où τ représente le temps d'échange entre l'océan et la marge continentale.
- p_{marge} est le pourcentage de surface de marge dans chaque cellule du modèle (déterminé à partir d'une bathymétrie à haute résolution : gebco-1min, disponible sur http://www.bodc.ac.uk/data/online_delivery/gebco/).

La modélisation de la composition isotopique de Nd océanique se déroule donc en deux étapes :

- détermination de composition isotopique de la marge continentale $\varepsilon_{Nd_{marge}}$.
- détermination du temps de rappel τ .

Ces deux étapes sont l'objet des deux sections suivantes qui composent ce chapitre. Chacune comprend un résumé et un article publié.

3.2 Compilation de données de Nd sur la marge continentale

3.2.1 Résumé

Afin d'évaluer la signature isotopique que les échanges marge / océan sont susceptibles d'imprégnier aux masses d'eau, la composition isotopique de la marge continentale a été déterminée à partir d'une compilation de données de la littérature. Cette base de données contient près de 250 valeurs issues de plus de 80 références bibliographiques, et est disponible en annexe A, p.155. Plusieurs types de données ont été répertoriés :

- les sédiments de surface le long des marges. Ce sont les données les plus importantes puisque les plus représentatives du matériel en contact avec les masses d'eau. Il a cependant fallu s'assurer de la représentativité de ces données sur une région géologique alors que le transport de sédiments par les courants de fond peut atteindre plusieurs centaines de kilomètres dans certaines régions. Pour cela, l'utilisation de cartes de topographie sous-marine sur la marge continentale a permis de limiter géographiquement l'influence géologique d'une zone.
- les décharges sédimentaires des rivières. Ces données sont les plus représentatives de la composition isotopique moyenne de tout le bassin versant.
- les roches érodables à proximité des côtes, seulement si elles sont représentatives des caractéristiques géologiques environnantes.
- les poussières atmosphériques. Même si elles ne seront pas explicitement prises en compte plus tard dans la modélisation, nous les avons inventoriées pour des tests futurs. En outre, ces données donnent des informations sur leur région d'origine (ce qui est le cas en Antarctique, dans le Pacifique ou dans l'Atlantique pour des loess provenant de Patagonie, Chine et Sahara respectivement).

On obtient ainsi la carte de compilation Fig. 2 p.55

On a vu précédemment (section 1.2.1.3, .22) que la composition isotopique du Nd varie en fonction de l'âge et la nature du terrain. Ainsi, pour déterminer la valeur de la composition isotopique sur toute la côte océanique, les données ont été interpolées à l'aide d'une carte géologique numérique.

En ne sélectionnant que les terrains en contact avec une côte océanique, on obtient la distribution géologique carte Fig. 3.1, p. 51.

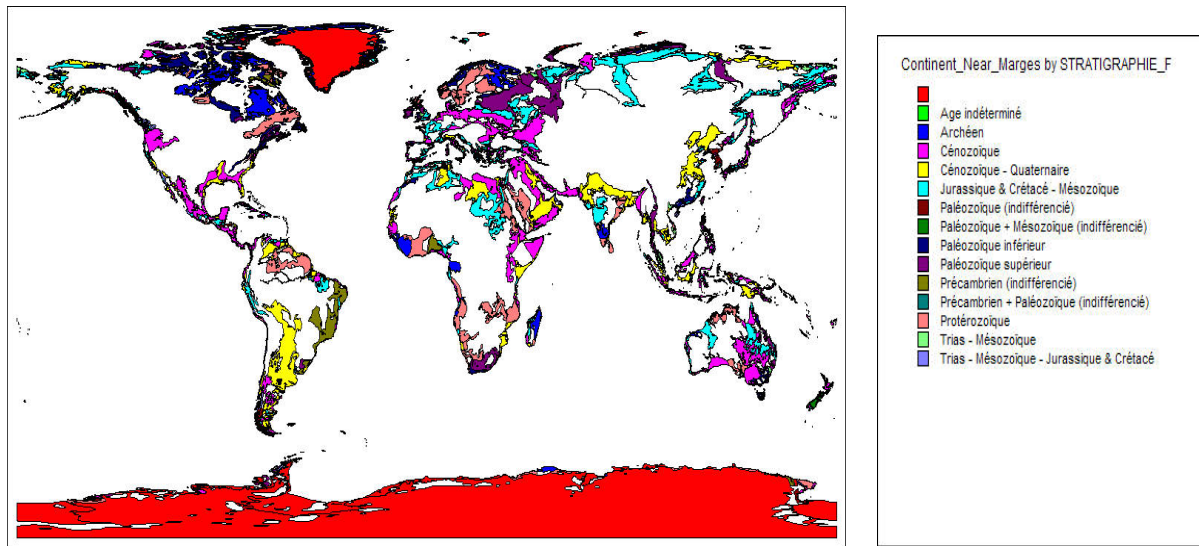


FIG. 3.1 – Carte géologique mondiale en zone cotière.

L'interpolation des données sur cette carte géologique est proposée Fig. 2, p. 58. Les zones hachurées sur cette carte correspondent aux régions ne disposant pas de données de ε_{Nd} . Dans ces rares cas, l'interpolation s'est faite en appliquant la valeur ε_{Nd} des zones ayant une géologie similaire, et dans la mesure du possible, en s'appuyant sur l'histoire géochimique du terrain. Bien que paraissant un peu brusque, la relation entre l'âge d'un terrain et sa valeur en ε_{Nd} est bien établie (Allègre, 2005), et il serait surprenant que cette méthode entraîne une incertitude supérieure à $2 \varepsilon_{Nd}$.

On observe finalement une variation de la composition isotopique des marges continentales, allant de **valeurs très négatives en Atlantique nord, à des valeurs plus radiogéniques dans le Pacifique**. Ces variations sont cohérentes avec les variations de composition isotopiques de Nd dissous au sein des bassins le long de la circulation thermohaline (cf. Fig.1.4, p. 24). Même si le gradient océanique observé est plus faible que sur les marges continentales, cette observation appuie l'idée que les marges peuvent jouer un rôle important dans la distribution de la composition isotopique du Nd. En se servant de la carte Fig. 2, p. 58 comme source de Nd à la marge, la prochaine étape consiste donc à modéliser le ε_{Nd} grâce à un OGCM.

3.2.2 *Isotopic Nd compositions and concentrations of the lithogenic inputs into the ocean : a compilation, with an emphasis on the margins.*

Article publié dans Chemical Geology 239 (2007) 156-164



Isotopic Nd compositions and concentrations of the lithogenic inputs into the ocean: A compilation, with an emphasis on the margins

C. Jeandel ^{a,*}, T. Arsuze ^{a,b}, F. Lacan ^a, P. Téchiné ^a, J.-C. Dutay ^b

^a Laboratoire d'Etudes en Géophysique et Océanographie Spatiale (LEGOS), CNRS/CNES/UPS/IRD,
Observatoire Midi-Pyrénées, 14 av. E. Belin, 31400 Toulouse, France

^b Laboratoire des Sciences du Climat et de l'Environnement (LSCE), CEA/CNRS/UVSQ/IPSL,
Orme des Merisiers, Gif-Sur-Yvette, Bat 712, 91191 Gif sur Yvette Cedex, France

Received 10 April 2006; received in revised form 25 September 2006; accepted 7 November 2006

Editor: S.L. Goldstein

Abstract

An extensive compilation of published Nd isotopic values has been made in order to establish a database and a map of the isotopic composition of Nd of the world coasts. Both the database and the map are set out here, together with the way we interpolated the data to make the map. The margin Nd isotopic signatures vary from non-radiogenic values around the Atlantic Ocean to radiogenic values around the Pacific consistent with the trajectory of the “conveyor belt” global circulation, reinforcing the hypothesis that the exchange of Nd along the margins could play a significant role in driving the oceanic distribution of this tracer.

© 2006 Elsevier B.V. All rights reserved.

Keywords: Nd isotopic composition; Oceanic margins; Lithogenic inputs; Database

1. Introduction

The neodymium isotopic composition (Nd IC) is expressed as ε_{Nd} , defined by:

$$\varepsilon_{\text{Nd}} = \left(\frac{\left(\frac{^{143}\text{Nd}}{^{144}\text{Nd}} \right)_{\text{Sample}}}{\left(\frac{^{143}\text{Nd}}{^{144}\text{Nd}} \right)_{\text{CHUR}}} - 1 \right) \times 10^4 \quad (1)$$

Where CHUR stands for Chondritic Uniform Reservoir and represents a present day average earth value ($^{143}\text{Nd}/^{144}\text{Nd}_{\text{CHUR}} = 0.512638$, Jacobsen and Wasserburg, 1980). The Nd IC of the continents is heterogeneous, with

ε_{Nd} values ranging from -56 in old granitic cratons to $+12$ in recent mid-oceanic ridge basalts (Goldstein and Hemming, 2003; GEOROC database: <http://georoc.mph-mainz.gwdg.de/georoc/>). Nd ICs of marine lithogenic particles are therefore used to follow their pathways. In the ocean, Nd is a trace element of lithogenic origin (concentrations of the order of 10^{-12} g/g), predominantly found in the dissolved form (90 to 95%, Jeandel et al., 1995). Its residence time is around 500 to 1000 years, in other words less than the oceanic mixing time (Tachikawa et al., 2003). The oceanic Nd IC distribution is partly governed by the sources and sinks of this element, partly by its redistribution via thermohaline circulation. It displays heterogeneous ε_{Nd} values, increasing along the global “conveyor belt” circulation from -25 in the extreme North-West Atlantic to 0 in the North Pacific surface

* Corresponding author. Tel.: +33 561 332933; fax: +33 561 253205.
E-mail address: catherine.jeandel@legos.obs-mip.fr (C. Jeandel).

waters (Lacan and Jeandel, 2005), with intermediate values of -8 observed in the Indian Ocean. The ε_{Nd} vertical distribution in a given oceanic basin is also heterogeneous, mostly reflecting the different water masses, as illustrated for the Atlantic by von Blanckenburg (1999). In the absence of lithogenic input, ε_{Nd} behaves conservatively in the ocean; since variations have been observed between the different water masses of the same water column, it is also used as a water mass tracer (Piepgras and Wasserburg, 1982; Jeandel, 1993; von Blanckenburg, 1999; Amakawa et al., 2004; Lacan and Jeandel, 2004). During the last few years, significant progress has been made understanding how different water masses acquire their Nd IC. As demonstrated by Tachikawa et al. (2003), riverine and atmospheric fluxes cannot explain the variations of the Nd isotopic signatures between the Atlantic and Pacific oceans, whereas the concentration budget is easily balanced. This discrepancy between concentration and isotope budgets was called the “Nd paradox” and is extensively described in Goldstein and Hemming (2003). In fact, balancing both concentrations and isotopic signatures required more Nd inputs than those provided by the riverine and atmospheric fluxes in order to significantly modify the Nd isotopic composition along the conveyor belt (i.e.: a source was clearly missing) together with an intra-oceanic Nd subtraction in order to equilibrate the concentrations (a sink was therefore also missing). Tachikawa et al. (2003) suspect that the potential Nd sources may be the continental margins. More recently, Lacan and Jeandel (2005) evidenced that significant dissolved/particulate exchange occurs at the ocean margins and quantified this exchange, at 4 locations in the three oceanic basins and along basaltic as well as granitic margins (Greenland, Java island, Papua New Guinea and South China Sea). Such an exchange (called “Boundary Exchange” — BE — by these authors) modifies the isotopic signature of a water mass without significantly affecting its concentration, thereby resolving the main issue raised by the “Nd paradox”.

Although the processes controlling the sources and sinks of Nd in the ocean have not been clearly identified yet, the following hypothesis can be deduced from the literature. Margin sources of Nd are likely diagenetic, probably increased under reducing conditions but also probably under high hydrodynamic conditions, favoring the resuspension of deposited sediments, hence enhancing their remobilization and dissolution (German and Elderfield, 1989; Sholkovitz and Schneider, 1991; Haley et al., 2004). Conversely, large particle fluxes occurring in margin environments (due to large biogenic and terrigenous fluxes and the re-suspension of deposited material) are effective ways to scavenge the

dissolved elements, acting as a sink for these elements along this interface. This mechanism, called “Boundary scavenging” has been abundantly documented for trace elements like Th, Pa, Be and Pb in many works (e.g: Anderson et al., 1990, 1994; Santschi et al., 1999). Rare Earth Elements (and therefore neodymium) could also be sensitive to this intensified scavenging close to the margins. Mn oxide coating of the sinking particles has been put forward as a scavenging agent (Tachikawa et al., 1999). However, the detailed processes of Nd input/output to the ocean are not clearly understood and the temporal and spatial scales on which water mass Nd IC is modified has not been quantified yet.

Since these results could have further implications for our understanding of margin/ocean interactions and their influence on oceanic chemistry, we propose to investigate more closely the importance of this “exchange term” in the oceanic Nd cycle. For this purpose, we 1) established an exhaustive compilation of the concentrations and isotopic compositions of different materials expected to interact with the water masses when they enter into contact with the margins 2) estimated parameters for this process in an oceanic global circulation model (OPA-ORCA, Madec et al., 1998; Dutay et al., 2002) to explore whether Boundary Exchange could be significant in the control of the global oceanic cycle of the Nd IC (relative to the other fluxes). This paper presents the methods used to characterize the Nd signature of all the margins surrounding the oceans, the data compilation and the resulting map. The model simulations and their results are the subject of a companion paper (Arsouze et al., 2007-this issue).

2. Data compilation and representation

The first step of this work was to define as precisely as possible the Nd concentrations and isotopic signatures of the whole oceanic margins. To this purpose we first delimited the geographic and topographic extension of the oceanic margins at the 3000 m isobath, following the morphological definition proposed by Boillot and Coulon (1998). However, some cores deeper than 3000 m were also considered in this compilation, in two cases: 1) these cores were located close to very steep continental margins (e.g: Peru–Chile and Java Trenches, Table 1) that are suspected to receive the continental weathered material and 2) cores that sample turbidites, whose specific geological and geochemical properties allow them to be used for extrapolation (Bay of Bengal, Biscayne abyssal plain, Newfoundland basin etc., Table 1).

We then compiled the data from three kinds of samples: 1) the large river solid loads which are deposited on

the shelf and slope 2) core tops of sediments collected along a given margin 3) geological material outcropping above or close to an oceanic margin which were expected to be weathered, constituting the lithogenic fraction of the margin sediments; since this fraction comprises the majority of the deposited Nd, our hypothesis is that the average margin signature is similar to that of the weathered fields. Special attention has been paid to ensure that the samples are representative.

Given their origins, we considered that the first two categories of data are directly in contact with the water masses and therefore representative of the signatures of the sediments supposed to “contaminate” the waters flowing along them. Contrastingly, outcropping fields provide indirect data, which is therefore more hypothetical than the river and core tops results; on the other hand, the surfaces covered by these outcrops are definitely larger than those of the core tops and thus the signatures deduced from the weathered fields are more integrative than those of other origins.

Finally, we also included aeolian inputs to our compilation, although these are known to reach remote areas and will not be immediately used in our modeling approach; this allowed us to build the most comprehensive data set.

All the discrete data extracted from the literature are reported in Table 1 and Fig. 1.

2.1. River inputs

Dissolved REE behaviors during estuarine mixing have been largely documented (Sholkowitz and Sym-

zak, 2000 and ref. therein). Although large scale removal of up to 95% of dissolved river REE in the low salinity regions is an ubiquitous feature of estuaries, recent works evidenced small to extensive release in the mid to high salinity regions of some estuaries (Nozaki et al., 2000; Sholkowitz and Symczak, 2000). These authors suggest that estuarine and shelf sediments could be the sources of dissolved Rare Earth to these mid to high salinity waters and therefore could impact the neighbor ocean. In addition, Winter et al. (1997) clearly demonstrated that dissolved load cannot be the primary source of Rare Earth to the Arctic seawater and that ice-rafted detritus (derived from the neighbor shelf) was an important potential source of trace elements to seawater in ice-covered oceans. Therefore our compilation will disregard the dissolved river Nd flux; conversely, the suspended river load, delta, shelf and fan deposits have been considered as significant potential sources of Nd to the ocean.

Goldstein et al. (1984) proposed an extensive pioneer paper describing the ε_{Nd} together with Sm–Nd content values of particulates from major river systems. Their study allowed the documentation of about 30% of the total particulate flux discharged into the ocean. They also showed that ε_{Nd} does not vary with the grain size of the particles. The river systems covered by their study drain about 25% of the exposed continental crust and we have reported their published values in our database.

Since Goldstein's major pioneering work proposing a global approach, little data on river suspended particles and/or shelf mud have been published. However, McDaniel et al. (1997) confirmed that the Amazon fan

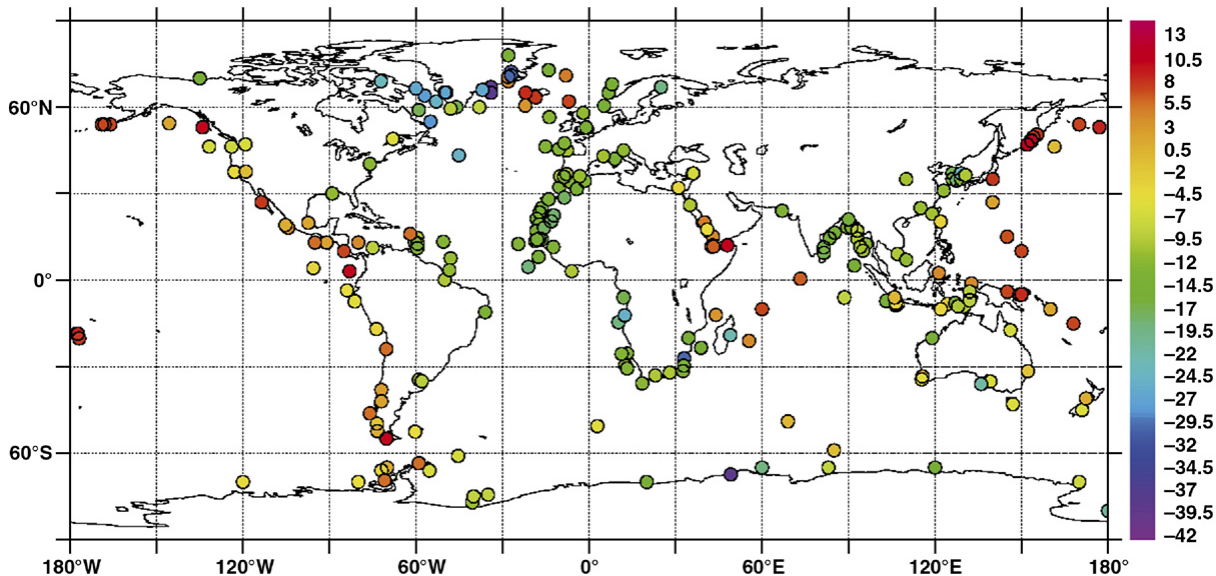


Fig. 1. Location of the discrete data compiled in Table 1 and used to make the extrapolated map.

muds and sediments of the subaqueous delta are derived predominantly from the Andean highlands, displaying homogeneous values which are slightly lower than those observed for the river sediments by Goldstein et al. (1984). Henry et al. (1996) measured the Uruguay River particulate material in addition to that of the Paraná one: although Uruguay's values are more radiogenic than Paraná's, the corresponding Nd flux represents only 10% of that of Paraná River. The weighted average ε_{Nd} value that we attributed to the Río de la Plata sediments is therefore similar to the pure Paraná end-member. Lan et al. (2002) provided values from Taiwan sediments and (Münker, 2000) from a New-Zealand river system. The Congo River sediments isotopic signature is provided by Bayon et al. (2004). McCulloch et al. (2003) documented relatively non-radiogenic ε_{Nd} values of the Johnstone River particles ($\varepsilon_{\text{Nd}} = -8$, Australia) but underlined the fact that these sediments are reworked in the Great Barrier Reef lagoon with fine grained basaltic particles, yielding values of -4 close to the reef: we kept this value for this coastal area, since it is in contact with offshore waters.

River system particles are weathering products, eroded and transported by water, one of the most efficient media for mixing the material. The resulting sediment deposited on the shelf and slope is likely to represent the mean isotopic signature of the average drainage basin, as demonstrated by Goldstein et al. (1984, 1997). In addition, solid discharge ε_{Nd} values have been considered as a good integrator of the average value of the drainage basins (Goldstein et al., 1984; Goldstein and Jacobsen, 1987; Goldstein et al., 1997), which contributed to the extrapolation of the discrete data compiled here. We therefore attributed the data extracted from the above cited works to the whole drainage basin area on the continent side and to the length of coast affected by the river plume on the ocean side.

Solid river inputs are identified by the symbol « s » in Table 1.

2.2. Sediment core tops

Surface sediments collected by coring on the shelf or the slope of any margin provide direct information on the geochemical and isotopic characteristics of the material being in contact with the water masses flowing above or along this margin. Our goal here is not to make a detailed study of the processes yielding sediment/water exchange but to model the effect of this exchange on large temporal and spatial scales. Therefore we assumed that the isotopic composition of sediments

deposited during the recent Holocene was satisfactory for the present work. The most relevant data would have been provided by the analyses of multi-corer samples, since these tools correctly preserve the sediment–water interface, but multi-coring is too rare to provide the required exhaustive data. Another issue related to coring is that it allows the recovery of discrete samples only: for each paper providing isotopic data of surface sediments, we carefully established the extent to which we could extrapolate the measured values to the whole margin. The validity of the extrapolation is based on a) the number of cores collected in a given area, b) the occurrence (or not) of strong bottom currents that could redistribute (but also homogenize) the weathered material on the ocean floor, c) the geochemical characteristics of the analyzed sediments, related to the geology and the geochemistry of the neighbor continent.

The work based on surface sediments cored along margins can be divided into two categories:

On the regional scale, areas of high climatic or geodynamic interest have been extensively cored, yielding a high resolution for the spatial distribution of the cores. This is the case of the northern North Atlantic (a key area for the deep water formation, where sediments are expected to imprint major climatic events) from which about 35 cores have been sampled and well documented by different authors (Revel et al., 1996; Innocent et al., 1997; Farmer et al., 2003; Fagel et al., 2004). The Bay of Bengal off the Ganges/Brahmaputra rivers has also been well documented with 15 cores, allowing the reconstruction of glacial/Holocene variations of the Himalayan and Burman inputs in this area. For geodynamic purposes, White et al. (1985) established the isotopic characteristics of more than 35 surface sediment samples from the Lesser Antilles arc: this allowed proper documentation of the Orinoco margin and Antilles arc values; to a lesser extent, 5 cores collected along the margins of the Angola and Cape basins in the South Atlantic allowed the characterization of their isotopic signatures. Similarly, Walter et al. (2000) characterized surface sediments of the South-East Pacific and South Atlantic in the southern ocean, helping to characterize the Weddell Sea and Drake Passage margins.

Studies performed on the global scale have also revealed a very rich mine of data for our purpose: although the spatial distribution is definitely poorer than for the first category, the cores themselves have been taken to be representative of the geochemistry of a specific margin area. McLennan et al. (1990) established the isotopic characteristics of 32 recent turbidites specifically characterizing different types of margins:

trailing edge margins, continental collision margins, strike slip margins, back arc basins, continental arc basins and fore arc basins. Although some of these samples were collected below 3000 m depth and therefore should not be reported as “direct data” given the depth criteria of our database, the geological and geochemical specificities of the turbidites make them an inestimable source of information for extrapolation purposes. Therefore, we decided to report them in Table 1. Indeed, turbidites are a major component of the sediment which is presently accumulating at the edges of continents. Rare Earths are among the tracers providing an index of the average composition of the sediment provenance, helping to trace the composition of the crust exposed to weathering (McLennan et al., 1990). Taking account of the geochemical and isotopic data for these sediments accumulated in different tectonic settings all around the world and published in McLennan et al. (1990), together with values of erodible material compiled in the following section, helped in attributing isotopic values to poorly documented margins such as those of Peru–Chile, the Bay of Biscaye, and Alaska. In the same manner, Ben Othman et al. (1989) proposed an extensive study of the geochemistry of modern marine sediments from the Pacific, Indian and Atlantic oceans close to subducting areas. Again, we could not directly report all the data here because many samples were taken from depths below 3000 m. However, we used the shallowest samples to document the Sunda arc and some isolated spots in the Atlantic, the remaining data being used as complementary information for the extrapolation task. These works were completed by the surface sediment data published by Dia et al. (1992) who showed that continent-derived material exerts a major control over Nd budgets in marine sediments.

2.3. Erodable material

The third source of data consisted in the geological material outcropping along the coasts of the world ocean and liable to be weathered. The main objective in this approach is to assess if this material is effectively deposited on the nearby margin and if it effectively contributes to the composition of the sediments found on the shelf and slope. Dymond (1981) determined the chemical composition of 425 sediment samples deposited on the Nazca plate. He demonstrated that the lithogenic abundance of these sediments exceeds 80% in the region within 1500 km of the South American continent, this proportion increasing close to the margin, despite a slight dilution by biogenic material under the

upwelling areas. As strongly suggested by Dymond (1981), the bottom nepheloid-layer is a highly active vector for the transport of deposited sediments originating from the South American continent to the open ocean abyss. Another work that confirmed the validity of the link between the deposited sediment at the bottom of the open ocean and the surrounding continents was the extensive study of the chemical composition of subducting sediments proposed by Plank and Langmuir (1998). This work did not provide direct “core top” data for the present compilation, since the cores were collected deep in oceanic trenches and/or on oceanic plates and should represent the average signatures of the areas that have been crossed by the moving tectonic plate. However, these authors observed that the subducting sediment is made up of up to 76% terrigenous material, and emphasized that within a sedimentary province a single drill core can capture the regional characteristics of the sediments. In addition, the comparison of Nd isotopic composition of surface sediments of cores and the nearby outcropping fields, when available, displayed similar values (e.g.: the Aleutian and Alaska fields, McCulloch and Perfit, 1981 and cores DSDP 183 and 178, Plank and Langmuir, 1998). These observations confirmed that the sediments deposited on a given margin have an isotopic composition similar to (or very close to) the surrounding fields exposed to weathering. These studies hold for relatively large scales.

On more regional scales, several studies are based on Pb and Nd isotopic composition and grain size of the fine fraction of the sediment in order to reconstruct changes in the deep oceanic circulation in the North Atlantic (Revel et al., 1996; Innocent et al., 1997; Fagel et al., 2004). Indeed, it is suspected that bottom currents transport fine grain size deposited sediments to sites located relatively distant from their sources. This observation is in apparent contradiction with our hypothesis directly linking the isotopic composition of coastal erodible material and that of the nearby deposited sediment. Conversely, the extensive study of Farmer et al. (2003) shows that the composition of the layers of sediment deposited at a given site and time in the North Atlantic reflect the Sr, Nd and Pb isotopic compositions of the neighboring Greenland and North American fields. Our purpose here is not to reconcile these different uses of isotopic composition imprinted in the sediment in these areas subjected to energetic bottom currents. Although we are aware of the fact that local bottom transports could move the fine fraction of the sediment from one place to the other, we considered this effect to be negligible on the global scale on which the present study is conducted.

There are more than 30 geological studies based on Nd isotopic data in coastal areas, mostly for geodynamic purposes: for the sake of conciseness, we chose not to report all the references that we selected for our goal in this text, although they are exhaustively documented in Table 1 and the database captions. Our main purpose when considering this literature was to identify (and to retain) the Nd signatures characterizing the whole geological province under consideration and not the specific intrusion (widely studied by our geologist colleagues and certainly of major geodynamic interest), which is not relevant to the present case.

Using selected examples, the following section illustrates our approach to the extrapolation of the discrete data extracted from the three main sources of information detailed above.

2.4. Extrapolation

After collecting all this information, we were confronted with a set of more than 200 discrete data (Table 1), represented in Fig. 1. Our main task was then to extrapolate them, in order to continuously characterize the Nd isotopic composition of the margin. In other words, we had to attribute an isotopic signature to any part of a field liable to be in contact with a given oceanic water mass.

To this end, the tools and approaches described below were used.

Digital geological map: since the Nd isotopic composition of any field is closely related to its geological

nature and to its age (e.g.: old granitic continental crust vs recent volcanic MORB in extreme cases), we used a digital geological map from MapInfo (<http://extranet.mapinfo.com/products/Overview.cfm?ProductID=1868> and productcategoryid=0). This map allowed us to establish the geographical coverage of any outcropping field.

Solid river inputs: Goldstein et al. (1984, 1997) and more recently Peucker-Ehrenbrink (personal communication) have shown that the Nd (and also Sr, which is not our purpose here) isotopic compositions of river solid discharges, measured at the river mouth, average the isotopic signatures of the weathered fields making up the drainage basin. We therefore combined the following information: solid river discharge data (references given in Section 2.1), the geographical extension of drainage basins (digital geological map referenced above, Vörösmarty et al., 2000; Amiotte-Suchet et al., 2003), satellite information on the extension of the large river plumes in the neighbour coastal ocean (see details hereafter) and topographical/sedimentologic information provided by McLennan et al. (1990) on the one hand, and a close examination of the bathymetry (<http://www.ngdc.noaa.gov/mgg/gebco/gebco.html>) on the other hand. The river plume extensions were established by studying maps and satellite images from several data banks including www.earthobservatory.nasa.gov, www.pubs.usgs.gov, www.oceanexplorer.noaa.gov, www.gesource.ac.uk and www.asiaoceania.org. This combination of information allowed us to attribute data for many outcropping fields along the coast, represented in the map proposed in Fig. 2.

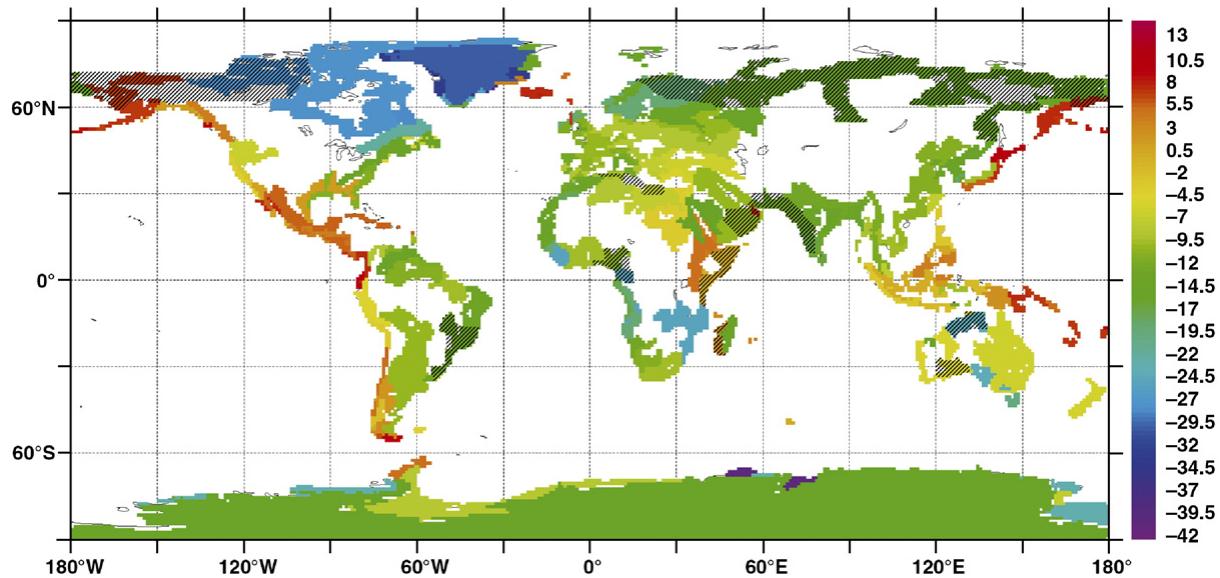


Fig. 2. Extrapolated map providing a picture of the Nd signature of all the margins surrounding the ocean. Same colour coding as in Fig. 1. Hatched areas correspond to those for which Nd signature was estimated because they were uncharacterized in the published literature, to our knowledge.

Relating core top data to the neighbour coastal area: As underlined in Sections 2.2 and 2.3, the consistency between the signatures of a core top collected on a margin and that of the fields which follow the contours of the nearby coast, was one of our means of assessing the representativity of these core tops. The issue raised by the extrapolation was how to establish the size of the coastal segment that could provide material with Nd signature close to that of the studied core top. This was done using the digital geological map providing the contours of the fields of a given age and nature (i.e. granitic, volcanic and — if sediment — the kind of sediments) on the one hand, and on the other hand the model–age theory based on the Nd isotope signature of the rocks (O’Nions et al., 1979; Goldstein et al., 1984, 1997; Allegre, 2005).

Attributing a signature to any potentially erodable material: for some coastal areas no information was available (e.g.: the east African or parts of the Brazilian and Argentinian coasts, see the hatched coastlines in Fig. 2); we therefore had to “arbitrarily” attribute a ε_{Nd} value to the material outcropping along these coasts. This approach rests on studies showing that the Sm–Nd model–age of the sediments deposited in the lower parts of a weathering basin reflects average crustal-residence ages of the sediment sources, as for example demonstrated by Goldstein et al. (1984, 1997). As above, we first considered the age and geochemical nature of the field. Then: 1) we compared it to similar fields of the same age that outcrop at another previously documented site for Nd and/or 2) we used the Nd model–age relationships to check the consistency of the attributed ε_{Nd} value. By doing that, we had to ensure that we considered the crustal residence age of the sediment, and not — for example — its depositional age. This was done by checking the geology, geochemistry and Nd signatures of the fields identified as the source of deposited material. These sources are located in the inner part of the continents. Following the river trajectories on the atlas helped to link a mountain and its adjacent plain. In other words, these delicate extrapolations are based on several convergent observations and a thorough use of the model–age relationship. We are aware that this approach assigns noteworthy uncertainties to the deduced Nd signatures. However, the number and size of the concerned fields, identified by the hatched area in Fig. 2, are relatively small.

3. Result: map of the outcropping Nd values and comments

All the discrete values are compiled in Table 1, together with the associated list of references.

The map represented in Fig. 2 provides a visualization of the patchwork of the fields to which we attributed an isotopic signature. Cold colors represent the old non-radiogenic rocks whereas the warm colors correspond to the recent radiogenic ones. The fields outcropping inside the continents have not been documented since our interest was focused on the material entering in contact with the oceans, either directly or through river inputs (drainage basins).

Not surprisingly, the Proterozoic fields surrounding the Arctic Seas and northern part of the Atlantic are the most negative, together with parts of the Antarctic coast. The documentation concerning this continent recently significantly improved, thanks to the exhaustive work of Roy et al. (in revision). The oldest rocks on Antarctica are found around Prydz Bay with negative values as low as −42. On the opposite side, the Antarctic Peninsula is characterized by radiogenic values (+5). Caledonian and Hercynian rocks cover most of the European, East-American and West African continents, yielding ε_{Nd} values ranging from −16 to −10. The same ranges of values characterize the Asian continent, down to the coasts of India, China, Korea and Vietnam, although some Precambrian basements have been identified in South Korea. Australia displays a relatively homogeneous east coast (ε_{Nd} around −6 to −4) whereas the south and west coasts are more heterogeneous: Precambrian rocks have been reworked and invaded by cretaceous volcanism, yielding contrasting isotopic signatures.

Radiogenic rocks surround the Pacific Ocean and characterize the west coasts of the American continents (the mountains of the Rockies and the Andes) as well as the east coast of Africa, although this part of the world is probably the least documented so far: A few papers provided an explanation of the geodynamical and geochemical origins of these fields, and therefore made it possible to attribute an ε_{Nd} value (Cohen et al., 1984; Baker et al., 1996; Harmer et al., 1998; Table 1). Recent volcanic intrusions and/or plate subduction have caused volcanic activity in Iceland, Greenland, Kourile Islands, The Antilles and all the arcs along the west Pacific and on the Antarctic Peninsula, which explains the radiogenic values observed for these areas. Finally, intra-plate volcanism is at the origin of islands like Reunion Island, The Seychelles, Tahiti, Kerguelen or Hawaii characterized by radiogenic values too.

At this stage of our compilation which was prepared manually, field by field, with a thorough check of the geological contour of the outcropping material, we suggest that the present map is not far from the truth,

although we are aware of the uncertainties surrounding some areas.

Note that this compilation provides a global picture of the Nd isotopic composition of the continents close to the coasts which could interest other earth science fields than oceanography only (e.g. weathering, tectonic, solid earth, etc). In any case, our database is available as supplementary material, and any contributions from colleagues who have either not been mentioned in this study or who are holding unpublished values, will be welcome. In other words, the authors invite the community to make the presented database truly complete.

As a whole, the coasts surrounding the world oceans display varied Nd isotopic compositions but the general trend is that the margin signatures are non-radiogenic around the Atlantic Ocean and radiogenic around the Pacific, a picture which is not so clear when considering the other sources of this element: as an example, Chinese rivers and dusts display values of *ca* – 11. Although the gradient is less pronounced, seawater (and seafloor) Nd isotopic signatures also vary from non-radiogenic to radiogenic values between the Atlantic and Pacific Oceans, with intermediate values in the Indian Basin. This observation — together with regional ones presented in detail in [Lacan and Jeandel \(2005\)](#) — are at the root of the “boundary exchange” hypothesis and its potential impact on the oceanic distribution of Nd isotopes. Our next step was therefore to use this interpolated map as a continuous source of Nd to make a link between an ocean circulation model and the tracer inputs from the margins, which is proposed in the companion paper ([Arsouze et al., 2007](#)-this issue).

Acknowledgements

The authors wish to acknowledge Anne Briais, Georges Ceuleneer, Valerie Chavagnac, Michel Grégoire and Mireille Polvé who nicely answered our sometimes naive questions on geological features, which greatly helped for the interpolation. Special and affectionate thanks to the late Henriette Lapierre who always enthusiastically answered our requests. Lucas Panin is acknowledged for his contribution at the early beginning of this compilation as well as Alexei Kouraiev, who nicely initiated T.A. to the use of MAPINFO. Victoria McBride considerably helped to correct the English of this manuscript. Finally, the authors warmly thank Tina van der Flierdt (reviewer) and Steve Goldstein (associate editor) for their constructive remarks.

This work was partly supported by the national program INSU/PNEDC/TIP2000.

Appendix A. Supplementary data

Supplementary data associated with this article can be found, in the online version, at [doi:10.1016/j.chemgeo.2006.11.013](https://doi.org/10.1016/j.chemgeo.2006.11.013).

References

- Allegre, C.J., 2005. Géologie Isotopique. Belin ed. Paris.
- Amakawa, H., Alibo, D.S., Nozaki, Y., 2004. Nd abundance and isotopic composition distributions of surface seawaters of the Northwest Pacific Ocean and its adjacent seas. *Geochem. J.* 38 (6), 493–504.
- Amiotte-Suchet, P., Probst, J.-L., Ludwig, W., 2003. Worldwide distribution of continental rock lithology: implications for the atmospheric/soil CO₂ uptake by continental weathering and alkalinity river transport to the oceans. *Glob. Biogeochem. Cycles* 17, 1038. [doi:10.1029/2002GB001891](https://doi.org/10.1029/2002GB001891).
- Anderson, R.F., et al., 1990. Boundary scavenging in the Pacific ocean: A comparison of ¹⁰Be and ²³¹Pa. *Earth Planet. Sci. Lett.* 90, 237–304.
- Anderson, R.F., et al., 1994. Anomalous boundary scavenging in the Middle Atlantic Bight: evidence from ²³⁰Th, ²³¹Pa, ¹⁰Be and ²¹⁰Pb. *Deep-Sea Res I* 41, 537–561.
- Arsouze, T., Dutay, J.-C., Lacan, T., Jeandel, C., 2007. Modeling the neodymium isotopic composition with an ocean global circulation model. *Chem. Geol.* 239, 165–177 (this issue). [doi:10.1016/j.chemgeo.2006.12.006](https://doi.org/10.1016/j.chemgeo.2006.12.006).
- Baker, J.A., Thirlwall, M.F., Menzies, M.A., 1996. Sr–Nd–Pb isotopic and trace element evidence for crustal contamination of plume-derived flood basalts: oligocene flood volcanism in western Yemen. *Geochim. Cosmochim. Acta* 60, 2559–2581.
- Bayon, G.R., German, C.R., Burton, K.W., Nesbitt, R.W., Rogers, N., 2004. Sedimentary Fe–Mn oxyhydroxides as paleoceanographic archives and the role of aeolian flux in regulating oceanic dissolved REE. *Earth Planet. Sci. Lett.* 224, 477–492.
- Ben Othman, D., White, W.M., Patchett, J., 1989. The isotopic and trace element composition of sediments: constraints on the genesis of island arc volcanoes and crust–mantle recycling. *Earth Planet. Sci. Lett.* 94, 1–21.
- Boillot, G., Coulon, C., 1998. La déchirure continentale et l’ouverture océanique. *Géologie des marges passives*. Gordon and Breach Science Publishers, Amsterdam. 208 pp.
- Cohen, R.S., O’Nions, R.K., Dawson, J.B., 1984. Isotope Geochemistry of xenoliths from East Africa: implications for development of mantle reservoirs and their interaction. *Earth Planet. Sci. Lett.* 68, 209–220.
- Dia, A., Dupré, B., Allègre, C.J., 1992. Nd isotopes in Indian Ocean sediments used as a tracer of supply to the ocean and circulation paths. *Mar. Geol.* 103, 349–359.
- Dutay, J.C., et al., 2002. Evaluation of ocean model ventilation with CFC-11: comparison of 13 global ocean models. *Ocean Model.* 4, 120.
- Dymond, J., 1981. Geochemistry of Nazca Plate surface sediments: an evaluation of hydrothermal, biogenic, detrital and hydrogenous sources. In: America, G.S.O. (Ed.), *Memoir*, vol. 154, pp. 133–173.
- Fagel, N., Hillaire-Marcel, C., Humbert, M., Brasseur, R., Weis, D., Stevenson, R., 2004. Nd and Pb isotopic signatures of the clay-size fraction of Labrador Sea sediments during the Holocene: implications for the inception of the modern deep circulation pattern. *Paleoceanography* 19. [doi:10.1029/2003PA000993: PA3002](https://doi.org/10.1029/2003PA000993).

- Farmer, G.L., Barber, D., Andrews, J., 2003. Provenance of Late Quaternary ice-proximal sediments in the North-Atlantic: Nd, Sr and Pb isotopic evidence. *Earth Planet. Sci. Lett.* 209, 227–243.
- German, C.R., Elderfield, H., 1989. Rare earth elements in Saanich Inlet, British Columbia, a seasonally anoxic basin. *Geochim. Cosmochim. Acta* 53, 2561–2571.
- Goldstein, S., Hemming, S.R., 2003. Long Lived isotopic tracers in oceanography, paleoceanography and ice-sheet dynamics. Treatise on Geochemistry, ch 6.17, vol. 6. Elsevier, New-York, pp. 453–489.
- Goldstein, S.L., Jacobsen, S.B., 1987. The Nd and Sr isotopic systematics of river-water dissolved material: implications for the sources of Nd and Sr in the seawater. *Chem. Geol. (Isotope Geosc. Section)* 66, 245–272.
- Goldstein, S.L., O’Nions, R.K., Hamilton, P.J., 1984. A Sm–Nd study of atmospheric dusts and particulates from major river systems. *Earth Planet. Sci. Lett.* 70, 221–236.
- Goldstein, S.L., Arndt, N.T., Stallard, R.F., 1997. The history of a continent from U–Pb ages of zircons from Orinoco River sand and Sm–Nd isotopes in Orinoco basin river sediments. *Chem. Geol.* 139, 271–286.
- Haley, B.A., Klinkhammer, G.P., J.M., 2004. Rare earth elements in pore waters of marine sediments. *Geochim. Cosmochim. Acta* 68, 1265–1279.
- Harmer, R.E., Lee, C.A., Eglington, B.M., 1998. A deep mantle source for carbonatite magmatism: evidence from the nephelinites and carbonatites of the Buhera district, SE Zimbabwe. *Earth Planet. Sci. Lett.* 158, 131–142.
- Henry, F., Probst, J.-L., Thouron, D., Depetris, P., Garçon, V., 1996. Nd–Sr isotopic compositions of dissolved and particulate material transported by the Parana and Uruguay rivers during high 5 December 1993) and low (September 1994) water periods. *Sci. Géol. Bull.* 49, 89–100 (Strasbourg).
- Innocent, C., Fagel, N., Stevenson, R.K., Hillaire-Marcel, C., 1997. Sm–Nd signature of modern and late Quaternary sediments from the northwest North Atlantic: implications for deep current changes since the Last Glacial Maximum. *Earth Planet. Sci. Lett.* 146, 607–625.
- Jacobsen, S.B., Wasserburg, G.J., 1980. Sm–Nd isotopic evolution of chondrites. *Earth Plan. Sci. Lett.* 50, 139–155.
- Jeandel, C., 1993. Concentration and isotopic composition of neodymium in the South Atlantic Ocean. *Earth Planet. Sci. Lett.* 117, 581–591.
- Jeandel, C., Bishop, J.K., Zindler, A., 1995. Exchange of Nd and its isotopes between seawater small and large particles in the Sargasso Sea. *Geochim. Cosmochim. Acta* 59, 535–547.
- Lacan, F., Jeandel, C., 2004. Subpolar Mode Water formation traced by neodymium isotopic composition. *Geophys. Res. Lett.* 31, L14306'. doi:10.1029/2004GL019747.
- Lacan, F., Jeandel, C., 2005. Neodymium isotopes as a new tool for quantifying exchange fluxes at the continent–ocean interface. *Earth Planet. Sci. Lett.* 232, 245–257.
- Lan, C.-Y., et al., 2002. Nd–Sr Isotopic composition and geochemistry of sediments from AIWAN and their implications. *West Pacif. Earth Sci.* 2, 205–222.
- Madec, G., Delecluse, P., Imbard, M. and Levy, C., n°11., 1998. OPA8.1 Ocean general circulation model reference manual. 11.
- McCulloch, M.T., Perfit, M.R., 1981. $^{143}\text{Nd}/^{144}\text{Nd}$, $^{87}\text{Sr}/^{86}\text{Sr}$ and trace element constraints on the petrogenesis of Aleutian island arc magmas. *Earth Plan. Sci. Lett.* 56, 167–179.
- McCulloch, M., Pailles, C., Moody, P., Martin, C.E., 2003. Tracing the source of sediment and phosphorus into the Great Barrier Reef lagoon. *Earth Plan. Sci. Lett.* 210, 249–258.
- McDaniel, D.K., McLennan, S.M., Hanson, G.N., 1997. Provenance of Amazon fan muds: constraints from Nd and Pb isotopes. In: Flood, R.D., Piper, D.J.W., Klaus, A., Peterson, L.C. (Eds.), Proceedings of the Ocean Drilling Program, Scientific Results, pp. 169–176.
- McLennan, S.M., Taylor, S.R., McCulloch, M.T., Maynard, J.B., 1990. Geochemical and Nd–Sr isotopic composition of deep-sea turbidites: crustal evolution and plate tectonic associations. *Geochim. Cosmochim. Acta* 54, 2015–2050.
- Münker, C., 2000. The isotope and Trace element budget of the Cambrian Devil River Arc System, New Zealand: identification of four source components. *J. Petrol.* 41, 759–788.
- Nozaki, Y., Lerche, D., Alibo, D.S., Snidvongs, A., 2000. The estuarine geochemistry of rare earth elements and indium in the Chao Phraya River, Thailand. *Geochim. Cosmochim. Acta* 64, 3983–3994.
- O’Nions, R.K., Carter, S.R., Evensen, N.M., Hamilton, P.J., 1979. Geochemical and cosmochemical applications of Nd isotope analysis. *Annu. Rev. Earth Planet. Sci.* 7, 11–38.
- Piepraga, D.J., Wasserburg, G.J., 1982. Isotopic composition of neodymium in waters from the Drake Passage. *Science* 217, 207–217.
- Plank, T., Langmuir, C.H., 1998. The chemical composition of subducting sediment and its consequences for the crust and mantle. *Chem. Geol.* 145, 325–394.
- Revel, M., Sinko, J.A., Grousset, F.E., Biscaye, P.E., 1996. Sr and Nd isotopes as tracers of North Atlantic lithic particles: paleoclimatic implications. *Paleoceanography* 11, 95–113.
- Roy, M., van de Flierdt, T., Hemming, S.R., Goldstein, S.L.: Sm–Nd isotopes and 40Ar/39Ar Ages of Proximal Circum-Antarctic Marine Sediments: Insights into the Geological History of an Ice-Covered Continent. In revision to *Chem. Geology*.
- Santschi, P.H., Guo, L., Walsh, I.D., Quigley, M.S., Baskaran, M., 1999. *Cont. Shelf Res.* 609–636.
- Sholkovitz, E.R., Schneider, D.L., 1991. Cerium redox cycles and rare earth elements in the Sargasso Sea. *Geochim. Cosmochim. Acta* 55, 2737–2743.
- Sholkovitz, E., Symczak, R., 2000. The estuarine chemistry of rare earth elements: comparison of the Amazon, Fly, Sepik and the Gulf of Papua system. *Earth Planet. Sci. Lett.* 179, 299–309.
- Tachikawa, K., Jeandel, C., Roy-Barman, M., 1999. A new approach to the Nd residence time in the ocean: the role of atmospheric inputs. *Earth Planet. Sci. Lett.* 170, 433–446.
- Tachikawa, K., Athias, V., Jeandel, C., 2003. Neodymium budget in the ocean and paleoceanographic implications. *J. Geophys. Res.* 108, 3254. doi:10.1029/1999JC000285.
- von Blanckenburg, F., 1999. Tracing past ocean circulation? *Science* 286, 1862b–1863b.
- Vörösmarty, C.J., Fekete, B.M., Meybeck, M., Lammers, R.B., 2000. Global systems of rivers: Its role in organizing continental land mass and defining land-to-ocean linkages. *Glob. Biogeochem. Cycles* 14, 599–621.
- Walter, H.J., Hegner, E., Diekmann, B., Kuhn, G., Rutgers van der Loeff, M.M., 2000. Provenance and transport of terrigenous sediment in the South Atlantic Ocean and their relations to glacial and interglacial cycles: Nd and Sr isotopic evidence. *Geochim. Cosmochim. Acta* 64, 3813–3827.
- White, W.M., Dupré, B., Vidal, P., 1985. Isotope and trace elements geochemistry of sediments from the Barbados Ridge–Demera Plain region, Atlantic Ocean. *Geochim. Cosmochim. Acta* 49, 1875–1886.
- Winter, B.L., Johnson, C.M., Clark, D.L., 1997. Strontium, neodymium, and lead isotope variations of authigenic and silicate sediment components from the Late Cenozoic Arctic Ocean: implications for sediment provenance and the source of trace metals in seawater. *Geochim. Cosmochim. Acta* 61, 4181–4200.

3.3 Modélisation de la composition isotopique du Nd à l'échelle globale

3.3.1 Résumé

La section précédente nous a permis d'obtenir une carte globale de $\varepsilon_{Nd_{marge}}$ qui va servir pour paramétriser les sources de Nd de la marge continentale vers l'océan, conformément à l'hypothèse de BE. Au regard de la figure 2, p. 58, on peut voir l'océan comme un réservoir dans lequel va circuler et se mélanger du colorant apporté par les marges, et dont la couleur varie en fonction de $\varepsilon_{Nd_{marge}}$. L'équation de paramétrisation du BE (3.1) p.49 montre qu'une fois déterminée cette valeur $\varepsilon_{Nd_{marge}}$, il reste à évaluer le temps de rappel τ d'échange entre la marge continentale et l'océan. Ce dernier est déterminé de façon empirique par des tests de sensibilité.

Les bilans locaux établis à partir de données de terrain montrent que les masses d'eau, lorsqu'elles viennent au contact d'une marge continentale changent significativement de composition isotopique en un temps estimé entre 1 et 10 ans (Lacan et Jeandel, 2005a).

Ainsi, plusieurs tests sont effectués avec des temps de rappel de 1 an, 10 ans, 50 ans et un temps variant verticalement de 6 mois en surface à 10 ans en profondeur. Cette dernière simulation est motivée par le fait que les échanges sont supposés plus importants en surface qu'en profondeur (principalement dus à des courants plus forts en surface, entraînant ainsi une remobilisation des sédiments sur la marge plus importante et finalement une augmentation des échanges dissous/particulaire ; mais aussi car les zones de surface reçoivent en général beaucoup d'apports biogéniques, entraînant une dégradation et une consommation importante d' O_2 par diagénèse, favorisant ainsi le relargage des terres rares).

Les résultats de ces quatre simulations se trouvent Fig 3. p.69 et Fig. 4 p.70.

On constate que pour $\tau = 1$ an, on retrouve le gradient inter-bassin vu par les données, mais on observe localement des effets de patchs, dus à un échange surestimé par rapport au transport dynamique. De plus, des valeurs très positives sont simulées dans le Pacifique (jusqu'à $+10\varepsilon_{Nd}$) alors que les données ne montrent pas de valeurs supérieures à 0.

Au contraire, pour $\tau = 50$ ans et dans une moindre mesure pour $\tau = 10$ ans, les valeurs simulées sont beaucoup trop homogènes, ne reproduisant pas le gradient inter-bassin. L'échange n'est pas assez important et la circulation homogénéise ainsi tout l'océan.

C'est finalement la simulation avec le temps de rappel variant verticalement qui donne les résultats les plus concluants, reproduisant un gradient inter-bassin correct, et caractérisant les principales masses d'eau (cf. Fig.5 p.72). Cependant, des valeurs légèrement trop radiogéniques (jusqu'à $+3\varepsilon_{Nd}$) sont simulées en Atlantique, dues à une mauvaise reproduction de la formation de la NADW et d'une diffusion trop élevée du courant de bord ouest dans le modèle, mais aussi à la paramétrisation du BE qui accorde une influence surestimée aux marges basaltiques de l'Arc Ecosse-Islande-Groënland dans la région.

La paramétrisation simplifiée du BE proposée permet de reproduire de façon très satisfaisante au premier ordre la distribution océanique de la CI du

Nd en ne prenant en compte que ce seul terme. Ce résultat suggère qu'il sagit d'un terme source-puits important dans le cycle océanique du Nd. De plus, les différentes paramétrisations montrent que ce temps d'échange caractéristique entre la marge continentale et la masse d'eau est de l'ordre de l'année, augmentant en profondeur.

3.3.2 *Modeling the neodymium isotopic composition with a global ocean circulation model*

Article publié dans Chemical Geology 239 (2007) 165-177



ELSEVIER

Chemical Geology 239 (2007) 165–177

**CHEMICAL
GEOLOGY**
INCLUDING
ISOTOPE GEOSCIENCE

www.elsevier.com/locate/chemgeo

Modeling the neodymium isotopic composition with a global ocean circulation model

T. Arsouze^{a,b,*}, J.-C. Dutay^a, F. Lacan^b, C. Jeandel^b

^a Laboratoire des Sciences du Climat et de l'Environnement (LSCE), CEA/CNRS/UVSQ/IPSL, Orme des Merisiers, Gif-Sur-Yvette, Bat 712, 91191 Gif sur Yvette cedex, France

^b Laboratoire d'Etudes en Géophysique et Océanographie Spatiale (LEGOS), CNES/CNRS/UPS/IRD, Observatoire Midi-Pyrénées, 14 av. E. Belin, 31400 Toulouse, France

Received 10 April 2006; received in revised form 4 December 2006; accepted 10 December 2006

Editor: S.L. Goldstein

Abstract

For the first time, modeling of the neodymium (Nd) isotopic composition (expressed as ε_{Nd}) is performed in an Ocean Global Circulation Model (OPA-ORCA2.0 model). In the interest of simplicity, Nd concentration is not explicitly included and ε_{Nd} is modeled as a passive tracer. Recent studies suggest that dissolved/particulate exchanges between continental margin sediments and seawater (termed boundary exchange, BE), could be the dominant source-sink terms that determine the distribution of neodymium isotopes in the global ocean. To test this hypothesis, we only included this BE source-sink term in the model. BE was parameterized as a relaxing term that forces ε_{Nd} of seawater to the isotopic composition of the continental margin over a characteristic exchange time. Sensitivity tests were made using different exchange times and parameterizations. The model reproduces most of the general trends of ε_{Nd} composition in seawater at global scale (inter-basin gradient, composition of some of the main water masses). These results suggest that BE process may account for the major sources and sinks of oceanic Nd, while indicating that the characteristic time of interaction between seawater and margins varies from about half a year in surface waters to several years at depth. The disparities between the model and observations might reflect the typical shortcomings of utilizing a coarse resolution ocean model circulation fields or neglected sources of neodymium such as dissolution of aeolian inputs or dissolved river loads.

© 2006 Elsevier B.V. All rights reserved.

Keywords: Numerical modeling; Neodymium isotopic composition; Boundary exchange; Continent ocean interactions

1. Introduction

The Nd isotopic composition (ε_{Nd}) is commonly expressed as:

$$\varepsilon_{\text{Nd}} = \left(\frac{(^{143}\text{Nd} / ^{144}\text{Nd})_{\text{sample}}}{(^{143}\text{Nd} / ^{144}\text{Nd})_{\text{CHUR}}} - 1 \right) \cdot 10^4$$

(where CHUR is the Chondritic Uniform Reservoir, representing an average earth value, presently 0.512638

* Corresponding author. Laboratoire d'Etudes en Géophysique et Océanographie Spatiale (LEGOS), CNES/CNRS/UPS/IRD, Observatoire Midi-Pyrénées, 14 av. E. Belin, 31400 Toulouse, France. Tel.: +33 5 61 33 30 03, +33 1 69 08 31 03; fax: +33 1 69 08 77 16.

E-mail address: arsouze@cea.fr (T. Arsouze).

(Jacobsen and Wasserburg, 1980)). ε_{Nd} composition is heterogeneous in the continent, and these variations are redistributed into the ocean via lithogenic inputs (Goldstein and Hemming, 2003). The properties of Nd as a oceanic water mass tracer have been extensively studied during the last 20 years (Jeandel et al., 2007-this issue, and references therein). The oceanic ε_{Nd} distribution is governed by sources and sinks alongside ocean circulation. These terms must be weighed in order to understand the processes that control the ε_{Nd} oceanic cycle. Modeling the distribution of ε_{Nd} in the ocean is one way of achieving this goal.

At present, very few studies have been focused on modeling Nd oceanic cycle. Bertram and Elderfield (1993) used a global box model to balance Nd concentrations but were unable to generate regional variability in the Nd isotopic composition. These authors suggested that some exchange process must be operating, either by reversible exchange of Nd between dissolved and particulate form in the water column, or by significant sediment-water exchange. Subsequently, Albarede et al. (1997) derived a global ocean Nd budget, identifying the potential for substantial sources of dissolved Nd to the ocean from desorption of suspended particles and diagenetic fluxes. In another global ocean Nd budget that considered dissolved river loads and dissolution of aeolian particles as the only sources terms, Tachikawa et al. (2003) were unable to balance both Nd concentration and isotopic composition simultaneously. Their budget required a “missing term”, such as an exchange of Nd along the continental margin, as this was the only way to modify the Nd isotopic composition without changing Nd concentration significantly. The same process was invoked in a simple box model study by Van De Flierdt et al. (2004) in order to achieve adequate exchange between seawater and the continent as a source of Nd to the North Pacific.

Utilizing field data from different locations in the ocean, Lacan and Jeandel (2001, 2004, 2005b) illustrated the importance of Nd exchange on different margin-ocean contact areas, reinforcing the hypothesis of local exchange process. These authors observed important changes in ε_{Nd} composition associated with small variations in Nd concentration within water masses flowing along different continental margins. These observations required the co-occurrence of both neodymium fluxes from the sediment to seawater and from seawater to the sediment (by substantial dissolved-particulate exchange, termed Boundary Exchange, BE, by these authors). All these studies suggest BE is important in the global Nd oceanic cycle. However, the importance of BE compared to other processes, as well

as the characteristic time of this exchange and the mechanisms involved, are still poorly understood. Here we aim to assess if BE could be the dominant mechanism that controls the ocean Nd cycle.

Ocean general circulation models (OGCMs) provide the opportunity to study processes that control large scale distribution of conservative tracers such as ^3He , ^{14}C or CFCs (England and Maier-Reimer, 2001). However modeling trace elements like Nd, Pa, Th, Be or Pb requires an OGCM coupled to a biogeochemistry model to produce the non-conservative process associated with particle export (Maier-Reimer and Henderson, 1998; Henderson et al., 1999; Siddall et al., 2005). ε_{Nd} being considered as a conservative tracer, we have simulated the distribution of ε_{Nd} in the global-scale OGCM OPA-ORCA2.0 developed at IPSL (Madec et al., 1998). To evaluate if BE is a substantial contributor to the oceanic distribution of ε_{Nd} as well as the isotopic signature of water masses, BE is the only source and sink term included (other sources, such as dust or rivers have been neglected). Unlike previous studies, we simulate ε_{Nd} in an OGCM that accounts for ocean circulation as well as sources and sinks of Nd. This work is presented in two stages: Jeandel et al. (2007-this issue) first determine the ε_{Nd} signature of the continental margins in order to constrain the isotopic composition that can exchange with seawater. Then, herein we used this global ε_{Nd} data set for the continental margins to set boundary conditions in the OGCM and the importance of BE to global Nd budget was determined. Subsequently, we used dissolved ε_{Nd} data compiled by Lacan and Jeandel (2005b) to evaluate the global characteristics of the modeled ε_{Nd} distribution.

2. Description of the model

We used the Ocean General Circulation Model OPA8.2, developed at IPSL/LOCEAN (Madec et al., 1998), in its global coarse resolution configuration ORCA2.0. The mesh is based on a regular 2° by 2° mercator grid. However, to overcome singularities near the North Pole, the mesh is modified by including two inland poles on the northern hemisphere. Meridional grid spacing ranges from $2^\circ \times \cos(\text{lat})$ in the Southern hemisphere, to 0.5° near the equator, to improve regional dynamics. In the vertical, the 30 depth layers range in thickness from 10 m at the surface to 500 m at the bottom. The model is coupled with the dynamic — thermodynamic sea ice model LIM (Fichefet and Maqueda, 1997).

Free surface formulation is applied at the upper boundary. The model is dynamically forced by monthly climatological fluxes (ERS1/2 for the Tropics and

NCEP/NCAR near the poles) of heat, freshwater, and wind stress. Surface salinity is readjusted to a climatology, with significant effects at high latitude. The mixed layer component of the ocean model relies on the turbulent kinetic energy (TKE) closure scheme (Blanke and Delecluse, 1993). Lateral diffusion follows local isopycnal surfaces, also including the eddy induced velocity parameterization of Gent and McWilliams (1990). In order to account for increased mixing in the bottom layer and stratification in the upper layer, the vertical diffusivity coefficient increases linearly with depth from 0.12 cm²/s at surface to 1 cm²/s at the bottom. A detailed description of the model, including numerical schemes, can be found in the OPA8.1 reference manual (<http://www.lodyc.jussieu.fr/opa/>).

3. Modeling the Nd isotopic composition

The range of variation in ε_{Nd} shows a high degree of heterogeneity both in the continents and open ocean. On the contrary, oceanic Nd concentrations are more homogeneous. Data compiled by Lacan and Jeandel (2005b) from 800 m depth to the seafloor reveal concentrations that range between 15 and 35 pmol/kg for more than 90% of the samples. The few samples that have significantly higher Nd concentrations are located near the continental margins. To include the Nd concentration as a separate tracer would require the specification and quantification of Nd fluxes (and thus material fluxes) from continents to the margins. Therefore, as a first approach, we have adopted a simple relaxation parameterization and let this important question for future work. This approach should be adequate as at the different locations where BE has been documented and its effect modeled, it appears to have little effect on Nd concentration (relative to large ε_{Nd} changes, Lacan and Jeandel, 2001; Lacan, 2002). The purpose of this study is not to determine and quantify the physical, chemical or biological processes that characterize BE, but rather to estimate if this mechanism represents the major source-sink term controlling the oceanic ε_{Nd} cycle. Thus, we included only the ε_{Nd} tracer in our OGCM simulations. Despite our simplistic working hypothesis, it is a practical, and necessary first step to assess the role and the characteristic time of BE in the oceanic Nd cycle. The results presented therein demonstrate that this simplified approach leads to reasonable results, justifying a posteriori such a choice.

3.1. The tracer model

The ε_{Nd} tracer is implemented in the model as a passive conservative tracer. It is transported in the ocean by a classical advection-diffusion equation, plus the

sources minus the sinks (SMS) (1). The rate of change of oceanic Nd isotopic composition (noted $\dot{\varepsilon}_{\text{Nd}}$) is:

$$\frac{\partial \varepsilon_{\text{Nd}}}{\partial t} = S(\varepsilon_{\text{Nd}}) - U \cdot \nabla \varepsilon_{\text{Nd}} + \nabla \cdot (K \nabla \varepsilon_{\text{Nd}}) \quad (1)$$

where $S(\varepsilon_{\text{Nd}})$ is the ε_{Nd} SMS term, $-U \cdot \nabla \varepsilon_{\text{Nd}}$ is the three-dimensional advection and $\nabla \cdot (K \nabla \varepsilon_{\text{Nd}})$ is both lateral and vertical diffusion of ε_{Nd} . Since ε_{Nd} is a passive tracer, we performed “off-line” simulations in a tracer transport model that relies on precomputed advective and diffusive fields (U, K) from the dynamic ocean model (Ludicone et al., submitted for publication-a-b). This “off-line” method is less expensive computationally, thereby allowing for sensitivity tests on the SMS term parameterization.

3.2. The SMS term

According to our hypothesis, the only SMS term taken into account is BE. It is parameterized by a relaxing equation that restores the initial ε_{Nd} signature of a water mass entering in contact with any margin towards the value of this particular margin such that:

$$S(\varepsilon_{\text{Nd}}) = 1/\tau \cdot (\varepsilon_{\text{Nd}_{\text{margin}}} - \varepsilon_{\text{Nd}}) \cdot \text{mask}_{\text{margin}} \quad (2)$$

where τ is the characteristic relaxing time, $\varepsilon_{\text{Nd}_{\text{margin}}}$ is the relaxing value, ε_{Nd} is the isotopic composition of seawater, and $\text{mask}_{\text{margin}}$ is the fraction of margin in the grid box.

More specially, τ represents the characteristic time of BE for ε_{Nd} .

$\text{mask}_{\text{margin}}$ represents the percentage of continental margin (in other words, the shelf and the slope located below this coastline) in a grid cell of the model. It denotes the proportion of the surface in the grid where the BE process occurs. It has been estimated from the high-resolution bathymetry ETOPO-2 (Aumont, personal communication). The value of $\text{mask}_{\text{margin}}$ ranges between 0 and 1. The depth limit of the margin has been chosen to the 3000 m (Boillot and Coulon, 1998). We did not account for volcanic fluxes of Nd as oceanic ridges do not affect the global budget of rare-earth elements (Michard et al., 1983) and hydrothermal solutions cannot maintain isotopic balance.

The $\varepsilon_{\text{Nd}_{\text{margin}}}$ term represents the Nd isotopic composition of the continental margin. Its spatial distribution is estimated using the compilation of Jeandel et al. (2007-this issue). This data set provides ε_{Nd} along global ocean coastline, via an interpolation of data collected from core top sediments, river material, and rocks that outcrop in

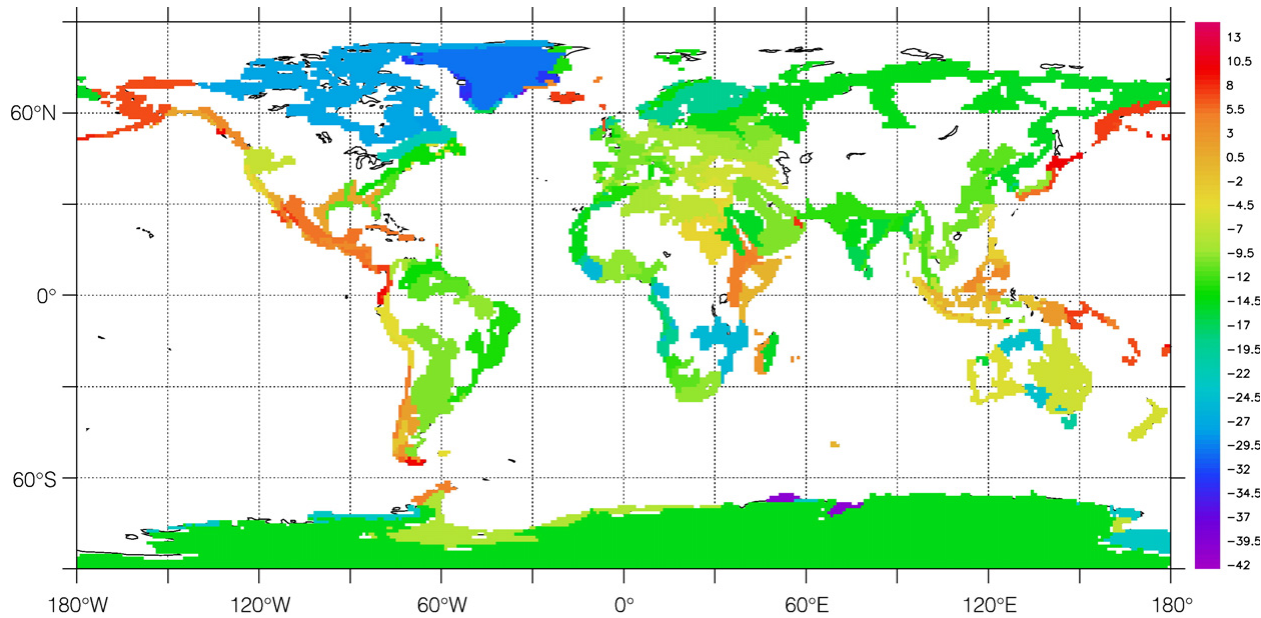


Fig. 1. Global map of the ε_{Nd} on the continents elaborated by interpolation of data in the literature (Jeandel et al., 2007-this issue).

the close vicinity of the continental margin. This coastal signature characterizes the material that is in contact with the surface coastal waters around the world (Fig. 1). To

extrapolate to the deepest layers of the global continental margin (i.e., down to 3000 m), we assumed that the sediment covering the margin of interest for this work

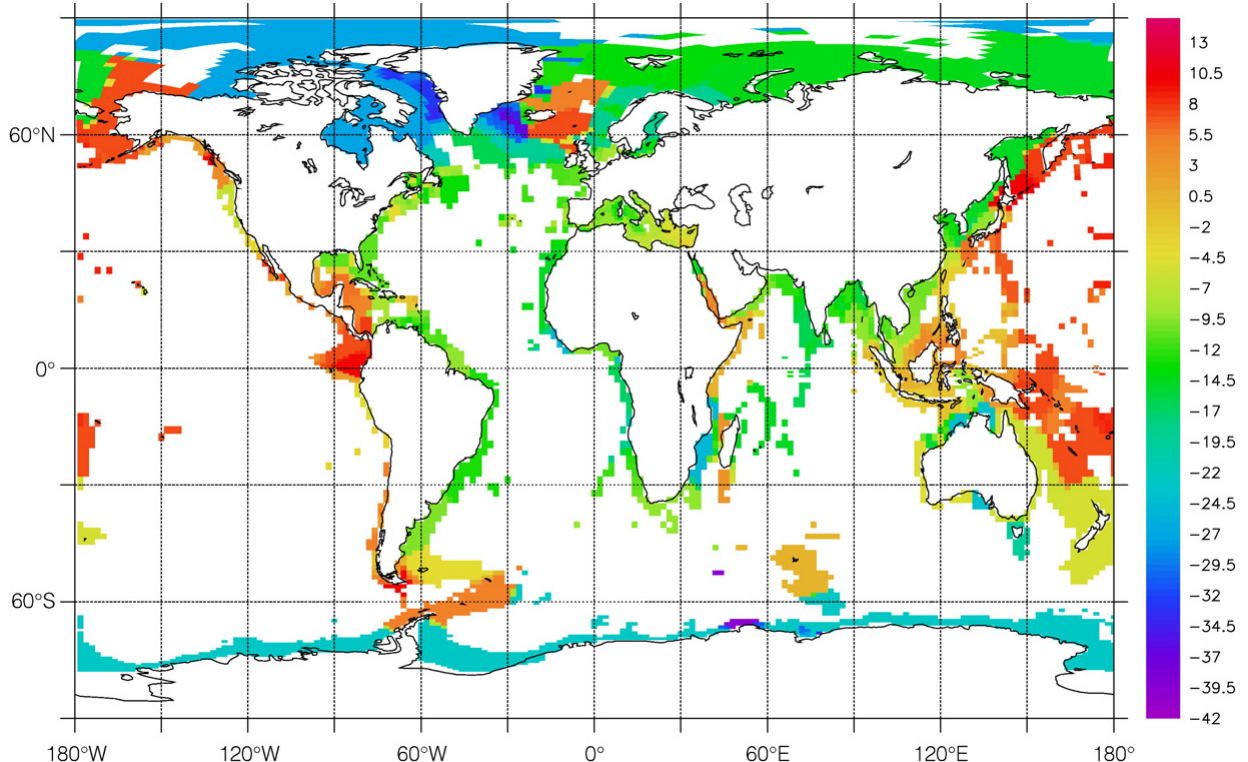


Fig. 2. Global map of the $\varepsilon_{\text{Nd}_{\text{margin}}}$ used in the model, done by interpolation of Fig. 1. Discrepancies with Fig. 1 concerning Antarctic isotopic composition can be observed. Therefore, the main values available in this region, recently provided by Roy et al. (submitted for publication), have been added in the database and interpolated after the runs were made. For computational cost purpose, runs could not have been performed with a $\varepsilon_{\text{Nd}_{\text{margin}}}$ map in agreement with Fig. 1 Antarctic isotopic composition.

was deposited during the Holocene and that it originates from the nearest coastline (even for the deepest part of the slope). This assumption is corroborated by many synthesis efforts (e.g. Dymond and Lyle, 1994; Boillot and Coulon, 1998). Thus, we have linearly extrapolated the continental data to the point representing the margin in the ORCA grid, at each model layer depth. Therefore, $\varepsilon_{Nd,margin}$ is constant with depth for a given margin location (Fig. 2). Particular attention has to be paid to the characterization of the Antarctic. Fig. 2 shows a relatively homogeneous value of ε_{Nd} around the Antarctic continent of -23 . This value was determined before most of the local data, recently provided by Roy et al. (submitted for publication), had been included in the database used to generate Fig. 1 (Jeandel et al., 2007–this issue). Therefore, the Antarctic margin is characterized by an average $\varepsilon_{Nd} \approx -13$, not reported in Fig. 2 thus far. Indeed, for computational cost purpose, the simulations presented here have not been rerun with this more complete database. The fact that most of the Antarctic characterization is under evaluated by 10 epsilon units ($\varepsilon_{Nd} \approx -23$ instead of $\varepsilon_{Nd} \approx -13$) will be taken in account, in a cautious discussion of the result.

This simple parameterization of the SMS term tends to drive the ε_{Nd} of water flowing along the coast toward the local ε_{Nd} continental signature. Therefore it adequately represents BE as far as it is currently understood. A motionless water mass would exponentially converge to $\varepsilon_{Nd,margin}$ in a characteristic time τ . This SMS term parameterizes together the different BE processes (such as sediment remobilization, early diagenesis, dissolution, as well as scavenging and local dynamical features along the margins that are not resolved in the OGCM). The resulting characteristic exchange time τ also provides an average rate, for all processes. Degrouping these processes will eventually require more detailed simulations to be performed.

3.3. Sensitivity tests

To investigate the characteristic exchange rate τ between seawater and the continental margins, we performed sensitivity tests that varied τ , but used the same circulation dynamics.

As a first step, we used field data to help constrain the range of τ that would be geochemically consistent to the test. Observations show that variations in the ε_{Nd} composition affects different water masses flowing along different continental margins, characterized by different sediment composition and depths (from surface to 2600 m depth, (Lacan and Jeandel, 2005b)). In each case, the transit time of the water masses affected by BE was estimated to

be on the order of a few years. Such a time scale allows for substantial modification of the seawater ε_{Nd} signature. As a first estimate, we assumed that the exchange rate of ε_{Nd} between the margin and the water masses was of roughly the same order. Nonetheless, data remain sparse and transit times of waters flowing along margins have not been compiled from all the literature. All of which means there must be a large uncertainty in estimates of τ . For simplicity, we tested 3 different values of τ : 1, 10 and 50 years and these simulations are referred as experiments a), b) and c) respectively. Moreover, given the difficulties of Tachikawa et al. (2003) to equilibrate both Nd isotopic composition and Nd concentration in global budget with the Pandora box model, they suggested that the intensity of exchange should vary with depth and propose that BE should be more intense in surface and intermediate layers than in the deepest one. Finally, ocean currents generally have higher velocities at surface than at depth. This enhances sediment remobilization, and probably the consequent exchange of Nd via dissolved-particulates interactions. The potential for the intensity of BE to vary with depth motivated us to make an additional simulation wherein τ varies exponentially with depth from half a year at the surface to 10 years at 1500 m (thus $\tau=200$ years at 3000 m). This ultimate simulation is referred as experiment d). The simulations are summarized in Table 1.

The four simulations were initialized with a uniform Nd isotopic composition of $\varepsilon_{Nd} = -20$ and integrated to steady state, i.e. the global averaged drift was less than $10^{-3} \varepsilon_{Nd}$ per thousand years. This criterion is reached after different time of integration depending on the value of τ . It ranges from 5500 years of integration for $\tau=1$ year, to 16,000 years for $\tau=50$ years. Unfortunately, these long, computationally expensive simulations, do not permit to exhaustive sensitivity tests.

4. Results and comparison with the data

The results of the simulations are compared with a compilation of seawater data collected by Lacan and Jeandel (2005b). More than 550 individual measurements are available so far, from the three oceanic basins.

Table 1
Relaxing time associated with the four different simulations

Experiment reference	Relaxing time
a)	$\tau=1$ year
b)	$\tau=10$ years
c)	$\tau=50$ years
d)	$\tau=0.5$ year in surface to $\tau=10$ years at 1500 m

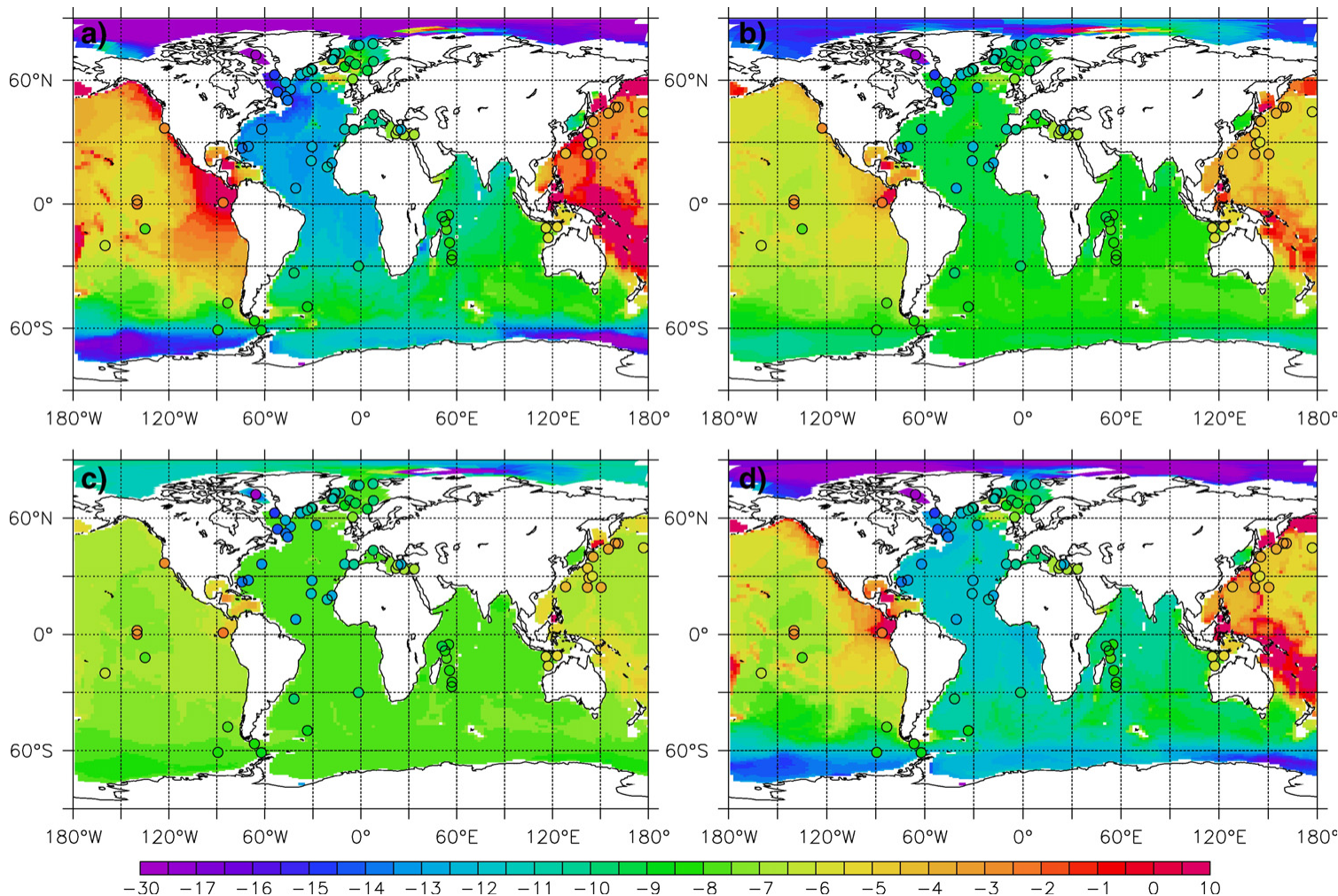


Fig. 3. Global ε_{Nd} map averaged between 800 and 5000 m for simulations a), b), c) and d), i.e. for $\tau = 1$ year, 10 years, 50 years and τ varying vertically respectively (cf. Table 1). Superimposed to these maps are filled circles with the same color scheme for the ε_{Nd} data from the compilation done by Lacan and Jeandel (2005b) averaged between the same depths. The color scale is non-linear.

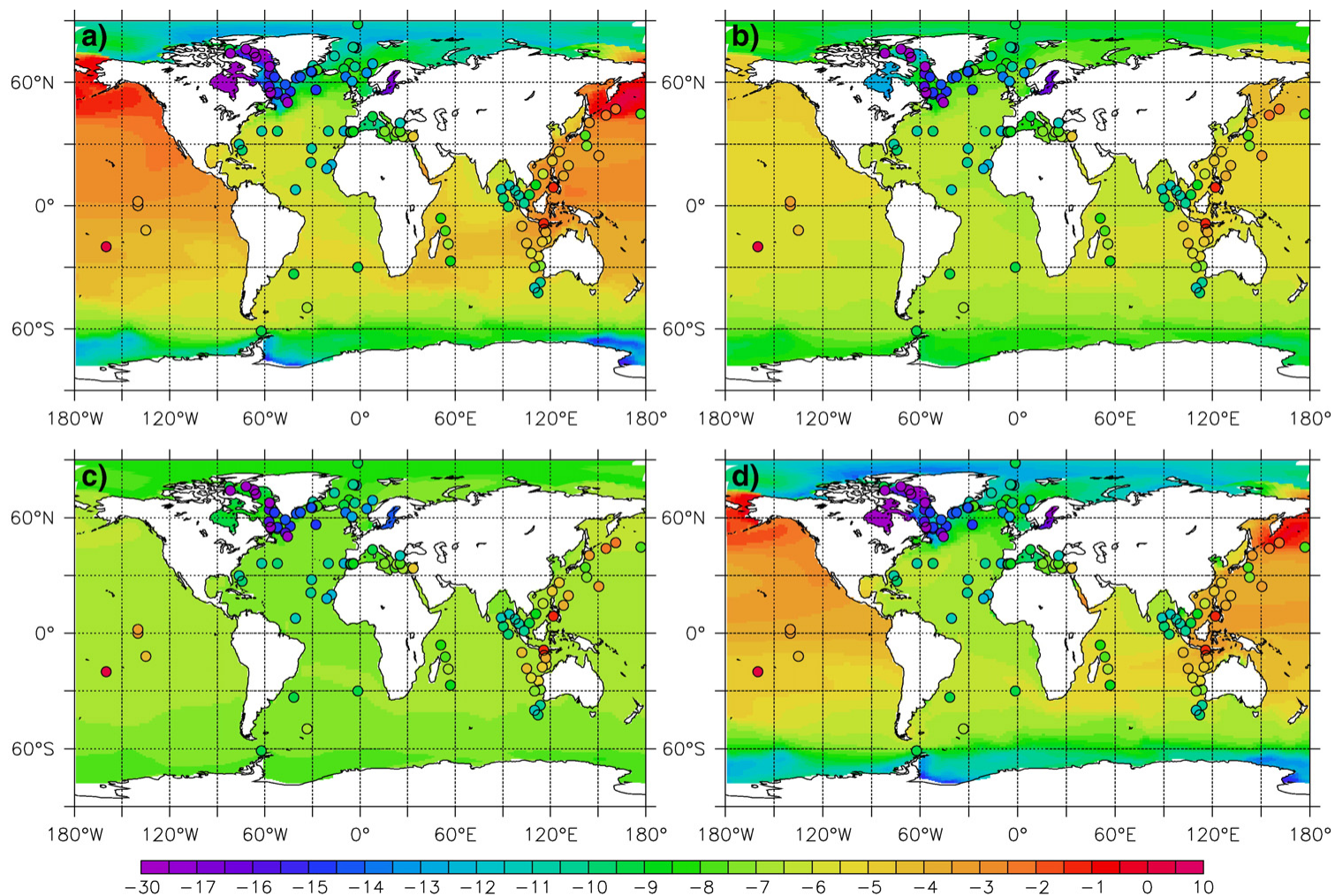


Fig. 4. Global ε_{Nd} map averaged between 0 and 400 m for simulations a), b), c) and d). Data and model results are provided as in Fig. 3. The color scale is non-linear.

However, data are not homogeneously distributed spatially (Figs. 3 and 4) and are concentrated in areas of interest for local studies, such as East Japan, the Nordic seas, the Labrador Sea, the East Indian basin, the Bay of Bengal and East of Madagascar. These areas may not always be representative of the whole basin. However, the global ε_{Nd} analyses have been made cautiously, by taking the large standard deviation into account (Table 2) when calculating mean basin values for each simulation.

4.1. Global maps

Firstly, we compare the simulated results to the dataset by analyzing global horizontal maps and basin averages from the data and the four simulations (Figs. 3, 4, Table 2).

4.1.1. ε_{Nd} in deep ocean

We averaged ε_{Nd} values between 800 m and the bottom to evaluate the simulated inter-basin variation of ε_{Nd} along the conveyor belt in intermediate and deep waters (Fig. 3). Examination of the averaged ε_{Nd} data reveals a clear gradient along the path of the deep conveyor belt. Values increase from $\varepsilon_{\text{Nd}} = -12$ in the Atlantic to $\varepsilon_{\text{Nd}} = -4.5$ in the Pacific, with intermediate values of $\varepsilon_{\text{Nd}} = -7.2$ and $\varepsilon_{\text{Nd}} = -8.5$ in the Indian and Antarctic respectively.

Turning to the model results, an inter-basin gradient is found in each simulation, although its range varies between simulations. The smallest gradient between Atlantic and Pacific is found in simulation c) ($\tau = 50$ years), whereas the highest is found in simulation a) ($\tau = 1$ year) (Table 2). Thus, it appears that BE intensity drives inter-basin contrast, such that the shorter the relaxing time, the more accentuated the BE. Therefore, we can ignore simulations b) ($\tau = 10$ years) and c) ($\tau = 50$ years), as they yield distributions that are globally homogeneous. In each of these simulations, the Atlantic is too positive and the Pacific is too negative. Local extremes such as the strong

negative signal characterizing the North Atlantic data are not reproduced, and the inter-basin gradient is too weak and not represented in the data (Fig. 3).

Although simulations a) ($\tau = 1$ year) and d) (τ varies vertically) yield more realistic inter-basin gradients, they are also too weak. This is likely due to the too positive values modeled in the Atlantic ocean (Fig. 3). Otherwise, global tendencies are consistent with the data, especially for simulation d). Aside from in the Atlantic, mean basin values are correct in simulation d). Moreover, the ε_{Nd} distribution in North Atlantic Gyre and Labrador Basin have realistic values ($\varepsilon_{\text{Nd}} \approx -10$ and -14 , respectively) and East Indian and North West Pacific also have ε_{Nd} signatures consistent with the data. Simulation a) shows features that are comparable to simulation d), although the Pacific is too radiogenic (e.g. enriched in ^{143}Nd): values as high as +5 ε_{Nd} units are simulated (e.g. in Papua New Guinea or Panama areas), whereas no such positive ε_{Nd} values have been measured in Pacific seawater. Furthermore, simulated Antarctic basin values agree with the data, even though a strong non-radiogenic signal ($\varepsilon_{\text{Nd}} \approx -20$) is simulated near the Antarctic continent. This feature is very different from the mean signal over the basin, but the lack of data near the continent does not allow us to conclude as to its cause.

4.1.2. ε_{Nd} in surface

Fig. 4 displays the global simulated ε_{Nd} distribution averaged between surface and 400 m depth. The characteristics of this upper layer are similar to those for the deep ocean. Simulations b) and c) are globally too homogeneous and do not reveal the signature of local sources well. Pacific ocean ε_{Nd} , as well as Indian ocean, are adequately simulated in simulation d), but Atlantic and Antarctic are too radiogenic values compared to the data. Even if some trends are correctly simulated (e.g. in the Indian and Pacific oceans), the simulated surface water distribution is less realistic than the deep ocean. Overall,

Table 2

Mean ε_{Nd} for the Atlantic, Indian, Pacific and Antarctic basins, for each simulation and for the data

Experiment reference	Mean ε_{Nd} between 0–400 m					Mean ε_{Nd} between 800–5000 m					
	Atlantic	Indian	Pacific	Antarctic	Global	Atlantic	Indian	Pacific	Antarctic	Global	
Data	Mean	-13	-6.6	-4.4	-9.4	-9.9	-12	-7.2	-4.5	-8.5	-8.8
	Std	4	2.7	2.5	1.6	4.8	2.4	1.9	1.3	1.4	3.8
a)		-6.7	-4.8	-3.3	-6.6	-5.1	-12.1	-9.3	-3.4	-9.6	-7.5
b)		-6.7	-6.0	-5.5	-6.9	-6.2	-8.4	-8.4	-5.5	-8.2	-7.2
c)		-7.2	-6.9	-6.8	-7.2	-7.0	-7.6	-7.7	-6.7	-7.6	-7.3
d)		-7.3	-5.5	-4.0	-7.4	-5.8	-11.3	-9.8	-5.2	-10.2	-8.3

Average values are calculated between 0 and 400 m, and between 800 and 5000 m. The Antarctic is defined south of 36°S. Note the heterogeneous distribution of the data while considering the averaged ε_{Nd} value.

results are too radiogenic in all basins (Table 2). In particular, the inter-basin gradient is weaker than for the deep ocean circulation and is underestimated relative to the data. However, as the distribution of data is heterogeneous in the Atlantic ocean, the simulated average ε_{Nd} might be shifted to non-radiogenic North Atlantic values, and result in the underestimation of the influence of less radiogenic values in the South Atlantic. Local patterns such as radiogenic waters from Pacific Ocean entering Indian Ocean via the Banda and Java Seas or non-radiogenic waters in the Labrador Basin are consistent with the data. Simulation a) presents features that are comparable to simulation d) but shifted globally by +0.7 ε_{Nd} units (i.e. even more radiogenic than simulation d).

4.2. Zonal sections

Globally, simulations a) and d) produce realistic results, both in the surface and the deep ocean. Zonal ε_{Nd} sections in Pacific and Atlantic basins for experiment d) are now discussed in order to better evaluate the vertical structure, and compare that with known ε_{Nd} water masses signatures.

4.2.1. Pacific section

Fig. 5a shows the modeled ε_{Nd} distribution along a zonal section averaged between 120°W and 160°W in the Pacific Ocean, for experiment d), versus observations. Three main water masses are found in this region:

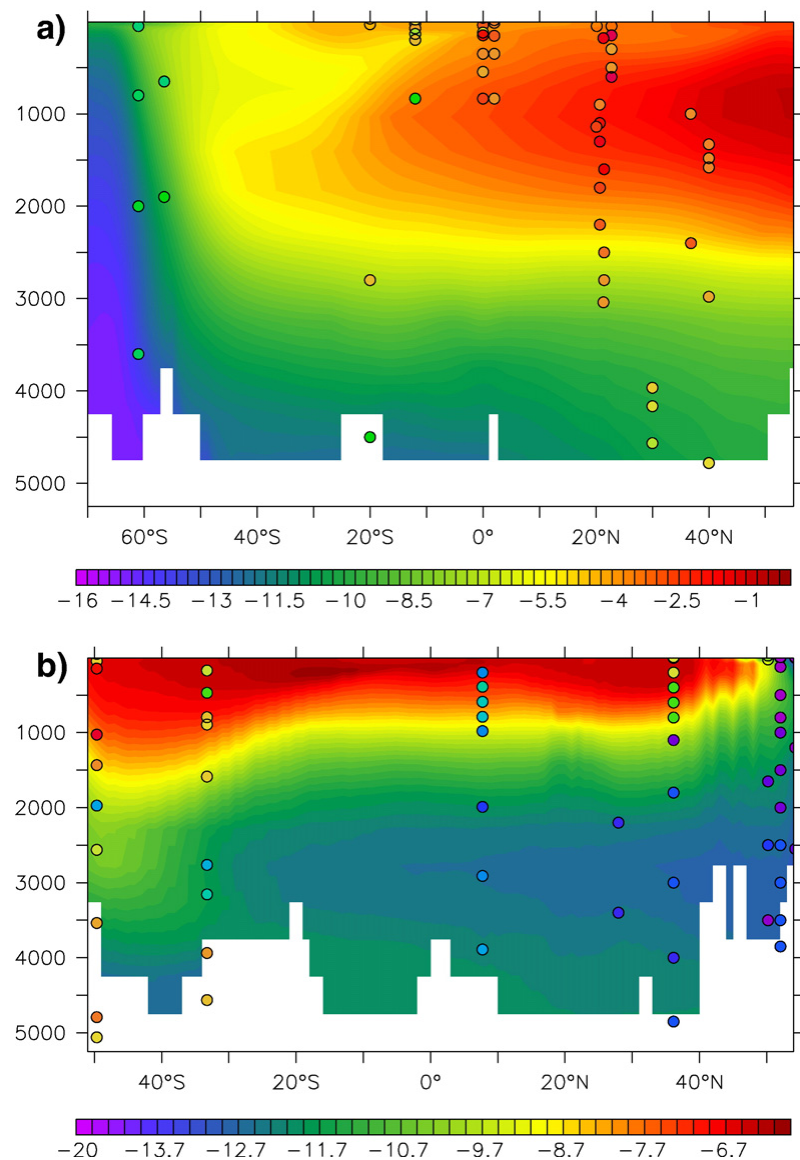


Fig. 5. Modeled ε_{Nd} from simulation d) for (a) the Pacific section averaged between 120°W and 160°W, and for (b) the Atlantic section following the West side of the basin. Data are superimposed to both profiles.

two flowing northward, Antarctic Bottom Water (AABW, below 3000 m) and Antarctic Intermediate Water (AAIW, between 500 m and 1000 m); the North Pacific Intermediate Water (NPIW) flows in southward direction at a depth centered around 1500 m. Observed ε_{Nd} values for AABW, AAIW and NPIW are approximately -8.5 , -8 and -3 , respectively (Pieprag and Wasserburg, 1982; Pieprag and Jacobsen, 1988; Jeandel et al., 1998; Amakawa et al., 2000; Lacan and Jeandel, 2001; Lacan and Jeandel, 2005b).

Simulation d) suggests deep water originating from the Southern Ocean that is characterized by the most negative ε_{Nd} is present through the entire deep Pacific Basin. The transport of these low ε_{Nd} (-8 to -10) waters northward at depths >3000 m is evident, in agreement with existing ε_{Nd} measurements from AABW. The ε_{Nd} signature of AAIW is represented in the model by a tongue of less radiogenic values at approximately 800 m depth from 40°S to 20°S (values close to -6) and are slightly too radiogenic relative to observations. Finally, the signature of a large water mass with a strong positive ε_{Nd} acquired in North Pacific, flowing southward and identified as the NPIW, displays ε_{Nd} values around -3 , in good agreement with the data.

4.2.2. Atlantic section

Fig. 5b represents a zonal section of modeled ε_{Nd} for experiment d) at 40°W in the Atlantic Ocean. We compare those results with the data from the Atlantic zonal section provided by Pieprag and Wasserburg (1987). In experiment d), the model does a good job at producing the main feature observed along this section. The signal of the North Atlantic Deep Water (NADW) that flows southward with an ε_{Nd} of around -12.5 , is in good agreement with the data ($\varepsilon_{\text{Nd}} = -13$). However, the Nd isotopic signal representing the deep convection of non-radiogenic surface waters ($\varepsilon_{\text{Nd}} = -17$) from Labrador Current and Baffin Bay observed in the data is not correctly simulated, and the ε_{Nd} signature of NADW is acquired at depth. Furthermore, ε_{Nd} values as high as -6.5 are simulated in surface waters in the tropical zone whereas no data more radiogenic than $\varepsilon_{\text{Nd}} = -9$ in this region has been measured yet. Finally, AABW is not well represented with ε_{Nd} values much too low ($\varepsilon_{\text{Nd}} = -11$), relative to the data ($\varepsilon_{\text{Nd}} = -8$).

5. Discussion

Simulations b) and c) ($\tau = 10$ and 50 years respectively) display homogenous range of values globally and do not reproduce characteristics features for each basin, neither at the surface nor at depth. On the other

hand, simulation a), with a relaxing time of 1 year, generates a realistic inter-basin gradient reproduction, although values tend to be too radiogenic globally.

The distribution of ε_{Nd} in simulation d), with a relaxing time varying vertically, displays general trends similar to simulation a). The trends between and within the different basins are correctly simulated, and the distribution observed along the thermohaline circulation is adequately captured by the model. Model-data comparison reveals that results are more realistic in the deep ocean than in the surface ocean. The inter-basin gradient is too weak at the surface, suggesting that the exchange is underestimated in the upper layers of the model. Thus, BE should be increased in the surface layers by reducing the relaxing time for the SMS term. This vertical function was implemented because strong surface dynamics might enhance the exchange process. Our present results suggest that the variation of the BE rate between the deep and surface waters is likely underestimated.

Simulation d) adequately represents the ε_{Nd} signature of the Nordic seas. The main artifacts of this simulation concern the Atlantic Ocean, which is 3 to 4 ε_{Nd} units more radiogenic than observed. This may result from either: 1) overestimated exchange with radiogenic margins in the South east Atlantic that imprint positively lower intermediate and mode waters, or 2) underestimated exchange in areas of intense exchange, e.g. in the Denmark Strait or in the Labrador Sea, before deep water forms in the North Atlantic, which is a key region that influences the entire basin. Ocean dynamics in this area are complex. The induced Deep Western Boundary Current (DWBC) is only crudely represented in coarse resolution models (England and Holloway, 1998; Dutay et al., 2002). The surrounding margins in this region are characterized by low ε_{Nd} , with strong exchange occurring in narrow straits, where currents are intense. It is likely that these processes are underestimated. It is noteworthy that despite this underestimation, deep Atlantic waters are more negative than deep Indian or Pacific waters and the simulation reproduces the ε_{Nd} gradient observed along the path of the deep conveyor belt. Simulating this gradient when the ε_{Nd} distribution is only forced with BE is important since its occurrence is the base of past reconstructions of the thermohaline circulation (Goldstein and Hemming, 2003). In this study, the relaxing time was kept geographically constant. Investigating the spatial variation of this term between the different basins, and imposing a greater exchange in the North Atlantic could improve our simulations. The underlying causes of the variations in relaxing time are numerous (one could cite, for instance: high local hydrodynamic conditions like

vertical mixing, internal waves, turbulences, etc...; lithology and geochemical nature of the margin surface sediments; bathymetry and surface of contact between the margin and the water mass; influence of the local oxygen minima (Sholkovitz et al., 1989; Sholkovitz et al., 1992); importance of the weathering fluxes). Basaltic derived material that composes most of the Pacific Basin margins are known to be more rapidly weathered than granitic material and gneisses on margins that surround the Atlantic (Amiotte Suchet et al., 2003). Thus, sediments on the Atlantic margin may be less efficient in modifying the isotopic composition of a given water mass than in the Pacific. Lithologic characteristics alone cannot explain why exchange is underestimated in North Atlantic. Therefore, other processes can play a significant role in driving this exchange.

When considering the ε_{Nd} section of the Atlantic, Piepras and Wasserburg (1987) assumed that the NADW isotopic signature resulted from the deep convection of unradiogenic surface waters. However, this study suggests that NADW acquires its signal in deep waters, which agrees with more recent studies that suggest that NADW originates mainly from deep water mass mixing, with an additional BE acting in the deepest waters (Lacan and Jeandel, 2005a). Therefore, a better reproduction of mixing in this area together with a local enhancement of the BE in the Labrador Sea (which is the main unradiogenic end-member of the region) would create 1) a better parameterization of processes that are prevalent in the northern part of the Atlantic and 2) a less radiogenic composition in the Atlantic Basin. The non-radiogenic value of the simulated AABW can be explained by the too negative isotopic composition assigned to the Antarctic continent compared to the data (Figs. 1, 2), that is subsequently reflected in the formation zone of AABW.

The influence of important dusts like Asian dust, Patagonian dust, Australian dust or Saharian dust, as well as river inputs, is not modeled here. All these sources must have non negligible influence in the global Nd isotopic balance. For example, Saharan dusts are likely to influence the ε_{Nd} signal of the Atlantic surface and subsurface waters and their inclusion could lower the modeled signal (too radiogenic yet). The influence of river loads is implicitly taken into account via the relaxing term, as it contributes to the sediment discharge on the continental margin that is exchanged with seawater. However, an increase in the relaxing term near a river mouth, or an explicit parameterization, would integrate the influence of this discharge and locally enhance the exchange. Such a hypothesis could be tested in the Atlantic ocean, where river inputs such

as the Amazon, the Parana or the Congo, have a negative ε_{Nd} ranging between -9 to -13 . Together with the Saharan dust effect, increasing the exchange in the river mouth area could help to lower the modeled radiogenic ($\varepsilon_{\text{Nd}} = -6$) surface values to get more realistic negative ε_{Nd} ($\varepsilon_{\text{Nd}} = -9$).

Although for computational cost reasons, sensitivity tests on $\varepsilon_{\text{Nd}_{\text{margin}}}$ distribution could not be performed, we are aware that uncertainties resulting from data extrapolation on the margins can be important in several regions (Jeandel et al., 2007-this issue). For example, the ε_{Nd} signature of the East Africa margin is relatively unconstrained and the signature of the south-west Indian Ocean water masses can influence the modeled southern Atlantic values. Because Africa is an old craton, better constraining the east African margin could lower the signature of the Indian slope waters and consequently the south Atlantic surface and intermediate waters. Nevertheless, poorly constrained regions such as south-east Africa are very rare. Moreover, we do not expect that modifying the ε_{Nd} (constrained by local geology (Jeandel et al., 2007-this issue)) at random, will have a strong influence on the resulting average ε_{Nd} that characterizes the surrounding continents of each oceanic basin and thus significantly affect the modeled global seawater distribution.

The modeled composition of the Pacific waters is globally comparable to the data, although some discrepancies are observed. The data suggests that simulated ε_{Nd} values are generally too low. In the South Pacific (50°S), the model simulates strong non-radiogenic values that are not reflected by the data. These values correspond to the AABW signal and propagate northward (up to 30°N). This likely reflects the low ε_{Nd} of the Antarctic used in our simulations, that is lower than suggested by the recent data set of Roy et al (Figs. 1 and 2). As AABW upwells in the northern part of the Pacific basin, the non-radiogenic signal associated likely lowers the signal of Pacific Deep Water. Another possibility that could yield such low values is that exchange may be underestimated in the deep North Pacific. Our parameterization of BE does not take into account regional weathering differences and local gradients observed near Papua New Guinea or Japan by Lacan and Jeandel (2001) and Amakawa et al. (2004) are only partially reproduced. Unfortunately the coarse resolution of our model does not allow the representation of such detailed features. The evaluation in the Indian basin is more difficult due to the paucity of data, but simulated values of ε_{Nd} are in reasonable agreement with available observations. As mentioned above, the low modeled Antarctic water signatures likely reflect the too low margin isotopic composition of this continent.

Overall, the satisfactory results obtained when only BE is a SMS term (neglecting other sources) indicates that BE plays a major role in controlling the ε_{Nd} oceanic distribution. Comparison of the results of the different experiments allows us to estimate that the characteristic time for BE ranges from half a year in surface waters to 10 years at depth.

6. Conclusions

This study proposed to parameterize boundary exchange by a relaxing toward the isotopic composition of the margin. This simple approach provides an approximation of the rate of exchange that is compatible with the dynamics of our model. Our modeling results suggest that 1) boundary exchange plays a major role in the oceanic Nd cycle, 2) the characteristic exchange time ranges between half a year in surface waters to 10 years at 1500 m, then rapidly decreasing with depth. Some features cannot be explained by our simple horizontally constant relaxing time and this unique BE source-sink term. Therefore, further work will focus on:

- A dynamical dependant parameterization of the relaxing time to enhance exchange in surface, straits or western boundary current zones.
- An explicit parameterization of the others source like dust inputs (Saharan in Atlantic and Chinese in Pacific), or river inputs.

These new approaches will also take in account the recently updated data base, mostly concerning the Antarctic margin.

Our modeling via a relaxing term was suitable for testing the hypotheses that BE represents the main mechanism of transfer of Nd in the ocean. Determining such an average relaxing time is an essential first step, as it provides for a framework for conducting further field and model studies that aim to distinguish the physical, chemical and biological processes that drive this exchange. Two different approaches, 1) focused process studies along a margin and 2) simulations that include not only isotopic composition but also Nd concentration while taking into account the particle flux, will provide key quantitative information about the sources and sinks of Nd. Therefore, ongoing works are 1) field projects coupling key margins studies to open ocean section as proposed in the framework of **GEOTRACES** program (2005) and 2) the development of coupling the dynamical model OPA with the biogeochemistry model PISCES (Pelagic Interaction Scheme for Carbon and Ecosystem Studies) (Aumont and Bopp, 2006) for Nd. Resulting

improvements in the knowledge of Nd and its isotope cycles should help quantify fluxes of solid material that are exchanged between the continental margin and the open ocean, which still remains an important and unconstrained question.

Acknowledgments

We thank P. Brockman for his help with technical aspects, J. Orr and A. Tagliabue for the linguistic advice. We also thank S. Goldstein, T. van de Flierdt and an anonymous reviewer for their careful reading of the manuscript and helpful remarks.

References

- Albarede, F., Goldstein, S.L., Dautel, D., 1997. The neodymium isotopic composition in Mn nodules from the Southern and Indian Oceans, the global oceanic neodymium budget and their bearing on deep ocean circulation. *Geochimica et Cosmochimica Acta* 61 (6), 1277–1291.
- Amakawa, H., Alibo, D.S., Nozaki, Y., 2000. Nd isotopic and REE pattern in the surface waters of the eastern Indian Ocean and its adjacent seas. *Geochimica et Cosmochimica Acta* 64, 1715–1727.
- Amakawa, H., et al., 2004. Neodymium isotopic variations in Northwest Pacific waters. *Geochimica et Cosmochimica Acta* 68, 715–727.
- Amiotte Suchet, P., Probst, J.-L., Ludwig, W., 2003. Worldwide distribution of continental rock lithology: implications for the atmospheric/soil CO₂ uptake by continental weathering and alkalinity river transport to the oceans. *Global Biogeochemical Cycles* 17, 1038. doi:10.1029/2002GB001891.
- Aumont, O., Bopp, L., 2006. Globalizing results from ocean *in situ* iron fertilization studies. *Global Biogeochemical Cycles* 20 (2).
- Bertram, C.J., Elderfield, H., 1993. The geochemical balance of the rare earth elements and Nd isotopes in the oceans. *Geochimica et Cosmochimica Acta* 57, 1957–1986.
- Blanke, B., Delecluse, P., 1993. Variability of the tropical Atlantic-Ocean simulated by a general circulation model with 2 different mixed-layer physics. *Journal of Physical Oceanography* 23 (7), 1363–1388.
- Boillot, G., Coulon, C., 1998. La déchirure continentale et l'ouverture océanique — Géologie des marges passives. Gordon and Breach Science Publishers ed.
- Dutay, J.C., et al., 2002. Evaluation of ocean model ventilation with CFC-11: comparison of 13 global ocean models. *Ocean Modelling* 4 (2), 120.
- Dymond, J., Lyle, M., 1994. Particle fluxes in the ocean and implications for sources and preservation of ocean sediment, material fluxes on the surface of the earth. National Research Council, Washington D. C., pp. 125–142.
- England, M.H., Holloway, G., 1998. Simulations of CFC content and water mass age in the deep North Atlantic. *Journal of Geophysical Research [Oceans]* 103 (C8), 15885–15901.
- England, M., Maier-Reimer, E., 2001. Using chemical tracers to assess ocean models. *Reviews of Geophysics* 39, 29–70.
- Fichefet, T., Maqueda, M.A.M., 1997. Sensitivity of a global sea ice model to the treatment of ice thermodynamics and dynamics. *Journal of Geophysical Research [Oceans]* 102 (C6), 12609–12646.

- Gent, P.R., McWilliams, J.C., 1990. Isopycnal mixing in ocean circulation models. *Journal of Physical Oceanography* 20 (1), 150–155.
- Geotrades, G., 2005. An International Study of the Marine Biogeochemical Cycles of Trace Elements and Isotopes. <http://www.geotrades.org/>.
- Goldstein, S.L., Hemming, S.R., 2003. Long lived isotopic tracers in oceanography, paleoceanography, and ice sheet dynamics. In: Elderfield, H. (Ed.), *Treatise on Geochemistry*. Elsevier Pergamon press, Amsterdam. chapter 6.17.
- Henderson, G.M., Heinze, C., Anderson, R.F., Winguth, A.M.E., 1999. Global distribution of the Th-230 flux to ocean sediments constrained by GCM modelling. *Deep-Sea Research Part I-Oceanographic Research Papers* 46 (11), 1861–1893.
- Iudicone, D., Madec, G., Blanke, B., Speich, S., submitted for publication-a. The role of Southern Ocean surface forcings and mixing in the global conveyor. *Journal of Physical Oceanography*.
- Iudicone, D., Madec, G., Speich, S., Blanke, B., submitted for publication-b. The global Conveyor Belt in a Southern Ocean perspective. *Journal of Physical Oceanography*.
- Jacobsen, S.B., Wasserburg, G.J., 1980. Sm-Nd isotopic evolution of chondrites. *Earth and Planetary Science Letters* 50, 139–155.
- Jeandel, C., Thouron, D., Fieux, M., 1998. Concentrations and isotopic compositions of Nd in the Eastern Indian Ocean and Indonesian Straits. *Geochimica et Cosmochimica Acta* 62, 2597–2607.
- Jeandel, C., et al., 2007. Nd isotopic compositions and concentrations of the lithogenic inputs into the ocean: a compilation, with an emphasis on the margins. *Chemical Geology* 239, 156–164 (this issue). doi:[10.1016/j.chemgeo.2006.11.013](https://doi.org/10.1016/j.chemgeo.2006.11.013).
- Lacan, F., 2002. Masses d'eau des Mers Nordiques et de l'Atlantique Subarctique tracées par les isotopes du néodyme. PhD thesis Thesis, Toulouse III University, France. Available at <http://francois.lacan.free.fr/job.htm>, 293 pp.
- Lacan, F., Jeandel, C., 2001. Tracing Papua New Guinea imprint on the central equatorial Pacific Ocean using neodymium isotopic compositions and rare earth element patterns. *Earth and Planetary Science Letters* 186, 497–512.
- Lacan, F., Jeandel, C., 2004. Neodymium isotopic composition and rare earth element concentrations in the deep and intermediate Nordic Seas: constraints on the Iceland Scotland Overflow Water signature. *Geochemistry Geophysics Geosystems* 5, Q11006. doi:[10.1029/2004GC000742](https://doi.org/10.1029/2004GC000742).
- Lacan, F., Jeandel, C., 2005a. Acquisition of the neodymium isotopic composition of the North Atlantic Deep Water. *Geochemistry Geophysics Geosystems* 6.
- Lacan, F., Jeandel, C., 2005b. Neodymium isotopes as a new tool for quantifying exchange fluxes at the continent — ocean interface. *Earth and Planetary Science Letters* 232 (3–4), 245–257.
- Madec, G., Delecluse, P., Imbard, M., Levy, C., 1998. OPA8.1 ocean general circulation model reference manual. Notes du Pole de Modélisation 11.
- Maier-Reimer, E., Henderson, G., 1998. Pb-210 in the ocean: a pilot tracer for modeling particle reactive elements. *Proceedings of the Indian Academy of Sciences. A Earth and Planetary Sciences* 107 (4), 351–357.
- Michard, A., Albarede, F., Michard, G., Minster, J.F., Charlou, J.L., 1983. Rare-earth elements and uranium in high-temperature solutions from east pacific rise hydrothermal vent field (13-degrees-N). *Nature* 303 (5920), 795–797.
- Piepragis, D.J., Jacobsen, S.B., 1988. The isotopic composition of neodymium in the North Pacific. *Geochimica et Cosmochimica Acta* 52, 1373–1381.
- Piepragis, D.J., Wasserburg, G.J., 1982. Isotopic composition of neodymium in waters from the Drake Passage. *Science* 217, 207–217.
- Piepragis, D.J., Wasserburg, G.J., 1987. Rare earth element transport in the western North Atlantic inferred from isotopic observations. *Geochimica et Cosmochimica Acta* 51, 1257–1271.
- Roy, M., Van de Flierdt, T., Hemming, S.R., Goldstein, S.L., submitted for publication. Sm-Nd isotopes and 40Ar/39Ar Ages of Proximal Circum-Antarctic Sediments: Reflections of Antarctica's Geological History. *Chemical Geology*.
- Sholkovitz, E.R., Piepragis, D.J., Jacobsen, S.B., 1989. The pore water chemistry of rare earth elements in Buzzards Bay sediments. *Geochimica et Cosmochimica Acta* 53, 2847–2856.
- Sholkovitz, E.R., Shaw, T.J., Schneider, D.L., 1992. The geochemistry of rare earth elements in the seasonally anoxic water column and porewaters of Chesapeake Bay. *Geochimica et Cosmochimica Acta* 56, 3389–3402.
- Siddall, M., et al., 2005. Pa-231/Th-210 fractionation by ocean transport, biogenic particle flux and particle type. *Earth and Planetary Science Letters* 237 (1–2), 135–155.
- Tachikawa, K., Athias, V., Jeandel, C., 2003. Neodymium budget in the ocean and paleoceanographic implications. *Journal of Geophysical Research* 108, 3254. doi:[10.1029/1999JC000285](https://doi.org/10.1029/1999JC000285).
- Van De Flierdt, T., et al., 2004. New constraints on the sources and behavior of neodymium and hafnium in seawater from Pacific Ocean ferromanganese crusts. *Geochimica et Cosmochimica Acta* 68 (19), 3827–3843.

Chapitre 4

Modélisation de la composition isotopique du Nd au Dernier Maximum Glaciaire

Sommaire

4.1	Contexte et configuration du modèle	81
4.1.1	Le Dernier Maximum Glaciaire	81
4.1.2	Le projet PMIP	81
4.2	Résumé	81
4.3	<i>Influence of the Atlantic meridional overturning circulation on neodymium isotopic composition at the Last Glacial Maximum, a modelling sensitivity study.</i>	83

4.1 Contexte et configuration du modèle

4.1.1 Le Dernier Maximum Glaciaire

Le Dernier Maximum Glaciaire (DMG) est une période climatique extrême et stable durant quelques millénaires. Il est important de comprendre les processus qui ont mené à un tel climat et qui ont permis sa stabilisation sur une période assez importante, afin de mieux comprendre les variations climatiques futures.

Le fait que cette période soit encore relativement récente (de 23 à 19 ka Before Present), avec un climat très contrasté en regard au climat actuel (l'Holocène) et sur une durée relativement longue en font une fenêtre d'étude paléoclimatique privilégiée. Ainsi, de nombreux enregistrements sont disponibles, autant au niveau océanique, atmosphérique que de végétation (Cd/Ca , Mg/Ca , $\delta^{13}C$, ^{14}C , $^{231}Pa/^{230}Th$, Nd , $\delta^{18}O$), permettant une approche multi-traceurs de l'étude des variations climatiques.

4.1.2 Le projet PMIP

Le projet Paleoclimate Modelling Intercomparison Project (PMIP, <http://pmip2.lsce.ipsl.fr/>) a pour but d'étudier les rétroactions entre les différents réservoirs climatiques (atmosphère, océan, surfaces continentales, glace de mer et calottes de glace terrestres - *ice sheets*) et d'observer la capacité des modèles couplés climatiques à reproduire des conditions climatiques différentes de l'Holocène (comme le DMG par exemple).

Ainsi, dans les simulations présentées dans ce chapitre nous avons utilisé les sorties océaniques du modèle couplé pronostique IPSLCM4 v2 (http://forge.ipsl.jussieu.fr/igcmg/wiki/IPSLCM4_v2_PAR). Le run de control à l'Holocène correspond à la simulation effectuée pour l'IPCC 2007 (<http://ipcc-wg1.ucar.edu/wg1/wg1-report.html>). Pour le DMG, un routage réaliste des rivières a été mis en place (Alkama et al., 2006) et les paramètres orbitaux, les forçages atmosphériques, la topographie ainsi que l'extension de la glace de mer sont prescrits par le protocole PMIP.

La modélisation de proxies océaniques dans ce projet (ε_{Nd} , $^{231}Pa/^{230}Th$, ^{13}C , ^{14}C) permet de comprendre l'information climatique enregistrée en découplant les processus agissant sur ces éléments.

4.2 Résumé

On a vu précédemment (section 3.3) que la paramétrisation du BE mis en place permet une simulation réaliste de la distribution globale de la composition isotopique du Nd à l'Holocène (gradient inter-bassin, caractérisation des principales masses d'eau).

Il est alors tentant d'appliquer cette paramétrisation au DMG afin d'étudier le comportement du traceur ε_{Nd} sous différentes conditions climatiques et soumis à différents scénarios de circulation océanique. Plus précisément, dans le cadre de l'étude du traceur ε_{Nd}

en tant que paleo-proxy, il est important de savoir quelles sont les causes des variations observées dans les données au cours du temps :

- changement dans la distribution des masses d'eau,
- évolution temporelle des CI des principales masses d'eau, due à un changement de sources, e.g. variations de flux de poussières atmosphériques ou de décharges fluviales, ou dans le cadre de cette étude un changement de matériel apporté par les marges continentales suite à une évolution de la bathymétrie et/ou de la dynamique entraînant un déplacement de la zone d'échange avec les masses d'eau,
- une combinaison des deux.

Les observations sont encore contradictoires à ce sujet (Van de Flierdt et al., 2006; Foster et al., 2007; Gutjahr et al., 2008).

Dans le cadre de cet article, l'analyse de la simulation globale est réduite au bassin Atlantique et son secteur Antarctique. Il s'agit en effet du seul endroit où il existe des données de ε_{Nd} au DMG (Rutberg et al., 2000; Piotrowski et al., 2004; Foster et al., 2007; Gutjahr et al., 2008), ainsi que du bassin de formation de la NADW (qui est l'élément moteur de la circulation méridienne, et donc des redistributions de chaleur aux différentes latitudes).

Trois scénarii de circulation océaniques distinctes au DMG ont été générés grâce à différents forçages de décharge des rivières dans l'océan (cf les sections méridiennes de circulation dans le bassin Atlantique Fig.2 p.88). De même, les forçages (atmosphériques, paramètres orbitaux) et la bathymétrie (baisse du niveau de la mer, présence de calottes glaciaires) du modèle couplé ont été adaptés aux conditions du DMG.

Une quatrième simulation “test” a été effectuée avec les forçages modernes mais avec une bathymétrie et une configuration de glace continentale propres au DMG. Il en résulte un changement de sources induit par cette configuration de mask terre/océan, qui réduit le temps de résidence des eaux dans les régions nordiques, et inhibe ou réduit considérablement l'échange avec les marges peu radiogéniques de la zone. La composition isotopique moyenne du bassin, ainsi que la signature isotopique des masses d'eau qui se forment en Atlantique Nord s'en retrouveront donc affectée.

La comparaison des simulations au DMG avec les données (cf. Fig.3, Fig. 4 et Fig. 5 p. 90, 91 et 92 respectivement) montre que seule la simulation simulant une Antarctic Bottom Water (AABW) dominante dans le bassin, reproduit une tendance en ε_{Nd} DMG-moderne correcte pour les eaux de fond à l'ouest du bassin. Les autres simulations simulant une prédominance des eaux formées en Atlantique Nord rendent une tendance inverse aux observations. En revanche, ces dernières simulent une cellule de circulation très vigoureuse permettant aux eaux radiogéniques de surface venant du sud de propager leur influence jusqu'au lieu de formation de la NADW, affectant ainsi la signature isotopique de la masse d'eau, ce qui est aussi suggéré par les données (Gutjahr et al., 2008). Aucun des trois scénarii de circulation proposés n'est donc privilégié pour simuler la distribution de ε_{Nd} .

Ces résultats proposent donc comme schéma le plus probable une présence importante en profondeur des masses d'eau en provenance du sud, et une cellule de circulation méridienne vigoureuse en surface et sub-surface, comme

représenté sur la figure Fig. 4.1. Ce scénario de circulation est en accord avec les récents résultats de Gherardi et al. (2005) obtenus à partir de données de $^{231}Pa/^{230}Th$ et de $\delta^{13}C$. Le modèle suggère un changement de signature des masses d'eau, en accord avec Foster et al. (2007) et suggéré par Lacan et Jeandel (2005a), et souligne aussi le besoin de données supplémentaires notamment dans le courant de bord ouest en Atlantique nord, afin de contraindre clairement l'évolution de la composition isotopique de la masse d'eau récemment formée en Atlantique Nord, et de déterminer l'amplitude de la pénétration des masses d'eau venant du sud dans le bassin.

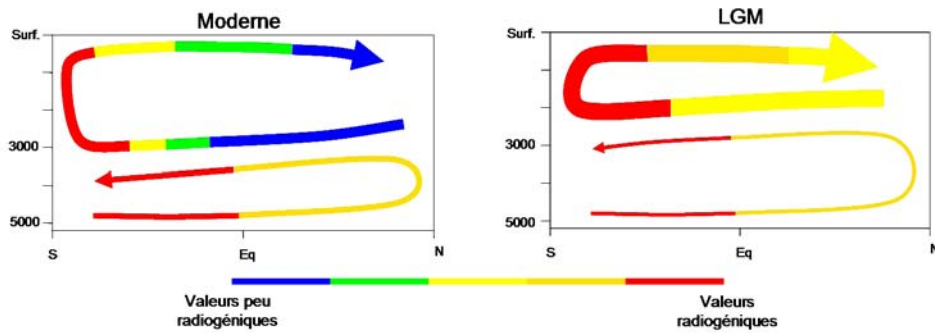


FIG. 4.1 – Schéma récapitulatif de la circulation proposée au DMG par les simulations de ε_{Nd} , en comparaison avec la situation moderne, dans le bassin Atlantique. Sont représentées de manière simplifiée les masses d'eau en provenance du nord (NADW actuelle, Glacial North Atlantic Intermediate Water - GNAIW - au DMG) et du sud (AABW). L'épaisseur du trait symbolise l'intensité du flux d'eau, et le code couleur représente sa signature isotopique. Les simulations suggèrent une augmentation de l'intensité de cellule de circulation de surface et intermédiaire au DMG par rapport à l'Holocène, permettant aux eaux radiogéniques du sud de transporter leur signal jusqu'au lieu de formation de la GNAIW (présente jusqu'à 2000 m de profondeur) dans le nord. La CI de cette dernière s'en retrouve ainsi affectée avec des valeurs jusqu'à $3\varepsilon_{Nd}$ plus radiogéniques au DMG qu'à l'Holocène Gutjahr et al. (2008). En profondeur, la prédominance des eaux en provenance du sud dans le bassin au DMG permet d'expliquer les données de ε_{Nd} plus radiogéniques au DMG qu'au présent Gutjahr et al. (2008).

4.3 *Influence of the Atlantic meridional overturning circulation on neodymium isotopic composition at the Last Glacial Maximum, a modelling sensitivity study.*

A modeling sensitivity study of the influence of the Atlantic meridional overturning circulation on neodymium isotopic composition at the Last Glacial Maximum

T. Arsouze^{1,2}, J.-C. Dutay¹, M. Kageyama¹, F. Lacan², R. Alkama¹, O. Martí¹, and C. Jeandel²

¹Laboratoire des Sciences du Climat et de l'Environnement (LSCE), CEA/CNRS/UVSQ/IPSL, Orme des Merisiers, Gif-Sur-Yvette, Bat 712, 91191 Gif sur Yvette cedex, France

²Laboratoire d'Etudes en Géophysique et Océanographie Spatiale (LEGOS), CNES/CNRS/UPS/IRD, Observatoire Midi-Pyrénées, 14 av. E. Belin, 31400 Toulouse, France

Received: 6 February 2008 – Published in Clim. Past Discuss.: 18 March 2008

Revised: 2 June 2008 – Accepted: 7 August 2008 – Published: 4 September 2008

Abstract. Using a simple parameterisation that resolves the first order global Nd isotopic composition (hereafter expressed as ε_{Nd}) in an Ocean Global Circulation Model, we have tested the impact of different circulation scenarios on the ε_{Nd} in the Atlantic for the Last Glacial Maximum (LGM), relative to a modern control run. Three different LGM freshwater forcing experiments are performed to test for variability in the ε_{Nd} oceanic distribution as a function of ocean circulation. Highly distinct representations of the ocean circulation are generated in the three simulations, which drive significant differences in ε_{Nd} , particularly in deep waters of the western part of the basin. However, at the LGM, the Atlantic is more radiogenic than in the modern control run, particularly in the Labrador basin and in the Southern Ocean. A fourth experiment shows that changes in Nd sources and bathymetry drive a shift in the ε_{Nd} signature of the basin that is sufficient to explain the changes in the ε_{Nd} signature of the northern end-member (NADW or GNAIW glacial equivalent) in our LGM simulations. All three of our LGM circulation scenarios show good agreement with the existing intermediate depth ε_{Nd} paleo-data. This study cannot indicate the likelihood of a given LGM oceanic circulation scenario, even if simulations with a prominent water mass of southern origin provide the most conclusive results. Instead, our modeling results highlight the need for more data from deep and bottom waters from western Atlantic, where the ε_{Nd} change in the three LGM scenarios is the most important (up to 3 ε_{Nd}). This would also aid more precise conclusions concern-

ing the evolution of the northern end-member ε_{Nd} signature, and thus the potential use of ε_{Nd} as a tracer of past oceanic circulation.

1 Introduction

Ocean circulation plays an important role in climate change as it is suspected to be an amplifier, or even a trigger, of shifts between glacial and interglacial periods (Broecker and Denton, 1989; Charles and Fairbanks, 1992; Rahmstorf, 2002). The meridional circulation structure (Meridional Overturning Circulation – MOC) of the North Atlantic Basin plays a key role in transferring heat to the high latitudes of this basin. The southward transport of cold water at depth, as the North Atlantic Deep Water (NADW), towards the Antarctic circumpolar current is compensated by the northward transport of heat from the south in surface and thermocline waters. This Atlantic overturning cell is a dynamic element of the oceanic thermohaline circulation (THC) and acts on the atmospheric circulation and chemistry (CO_2 in particular), which are directly involved in governing climate. An ongoing problem for climatologists is to determine if the MOC will persist in the future and therefore to determine what controls its strength and variability. Studying different climate scenarios can assist in understanding the factors controlling the MOC and permits the evaluation of different forcings.

The climate during the Last Glacial Maximum (LGM) was drastically different to today and lasted a few millennia (from 23 to 19 ky BP). Assessing how changes in the different components of the climate system (atmosphere, ice, land, and



Correspondence to: J.-C. Dutay
(dutay@lsce.ipsl.fr)

in this present study, MOC) control the overall climate requires the determination of the distinct processes which result in different climatic conditions. However, understanding the behaviour of past oceanic circulation, water-mass composition and flow patterns, remains problematic due to the multiple factors that force the ocean system, as well as controlling the distribution of relevant paleo-proxies. Different geochemical and isotopic paleo-proxies often give contradictory results (Lynch-Stieglitz et al., 2007) and up to three possible MOC scenarios are considered at LGM:

1. A highly stratified basin with a water mass at a maximum depth of 2200 m (with characteristics comparable to modern NADW; often referred to as Glacial North Atlantic Intermediate Water, GNAIW), overlying a large volume of water that originates from the Antarctic (which can be viewed as a more northward version of modern Antarctic Bottom Water, AABW). This view was first suggested by cadmium to calcium ratios (Cd/Ca) and carbon isotopes ($\delta^{13}\text{C}$) preserved in the fossilised shells of benthic foraminifera, which are used as proxies of the paleo nutrient distribution (Marchitto and Broecker, 2006; Duplessy et al., 1988; Curry and Lohmann, 1983; Charles and Fairbanks, 1992). Measurements of radiocarbon (^{14}C) from benthic foraminifera suggest an older age for GNAIW at the LGM (Keigwin, 2004), which implies a slower circulation, with deep water ventilation times as great as 2000 years (compared to 500 years for Holocene, Keigwin and Schlegel, 2002).
2. On the other hand, carbon isotope data (Curry and Oppo, 2005) and Cd/Ca data (Oppo and Rosenthal, 1994) has also suggested that vigorous overturning was maintained. Protactinium and thorium isotopes (231Pa/230Th) initially indicated that there was no significant change in the MOC at the LGM (Yu et al., 1996), while more recent data indicate a slowdown by almost 30% of the MOC associated with shorter residence times for waters in the Atlantic basin. This suggests that a shallower more vigorous overturning down to intermediate depths was associated with a weakened deep water ventilation (Marchal et al., 2000; McManus et al., 2004; Gherardi et al., 2005).
3. Oxygen isotopes ($\delta^{18}\text{O}$) from benthic foraminifera permit the reconstruction of water density at a given depth and suggest that during the LGM, the east-west $\delta^{18}\text{O}$ gradient was at least reduced or even reversed at the LGM (Lynch-Stieglitz et al., 2006). These observations are consistent with a very weak GNAIW cell, contradicting the circulation scenarios that are based on the above mentioned other proxies (Lynch-Stieglitz et al., 1999). On the other hand, alternative Cd/Ca data support a strong slowdown in the LGM MOC (Oppo

and Fairbanks, 1987; Charles and Fairbanks, 1992; Broecker, 2002).

Each of these hypotheses have to be taken cautiously due to the scarcity of the data characterizing the LGM and the fact that the behaviour of these proxies in the past is not completely understood (Lynch-Stieglitz et al., 2007). Overall, there is currently no consensus on the structure of the LGM ocean circulation. Apart from the necessary acquisition of more field observations, a better knowledge of the processes forcing glacial circulation would be aided by the representation of different circulatory proxies in numerical models. This has motivated the recent modeling of proxies at LGM (Henderson et al., 1999; Marchal et al., 2000), in order to better constrain the processes that drive the observed variability in the temporal distribution of such proxies.

Nd isotopic composition (Nd IC, hereafter expressed as

$$\varepsilon_{\text{Nd}} = \left((\text{Nd}^{143}/\text{Nd}^{144})_{\text{sample}} / (\text{Nd}^{143}/\text{Nd}^{144})_{\text{CHUR}} - 1 \right) \times 10000,$$

where CHUR is the CHondritic Uniform Reservoir, which represents the present day average value for the Earth surface, $(\text{Nd}^{143}/\text{Nd}^{144})_{\text{CHUR}} = 0.512638$; Jacobsen and Wasserburg, 1980), behaves quasi-conservatively in the open ocean, apart from any lithogenic inputs. Although surface scavenging and deep remineralization affects the Nd concentration profiles, ε_{Nd} data suggest that ε_{Nd} is relatively unaffected by biological cycles. Variations in ε_{Nd} have been measured in different water masses of the same water column, and this parameter has been used as a water mass tracer (Piepragras and Wasserburg, 1982; Jeandel, 1993; von Blanckenburg, 1999; Lacan and Jeandel, 2004; Amakawa et al., 2004; Goldstein and Hemming, 2003).

The modern Atlantic basin is characterized by two well-identified end-members: specifically, a negative signature ($-13.5 \pm 0.5 \varepsilon_{\text{Nd}}$; Piepragras and Wasserburg, 1980, 1987; Lacan and Jeandel, 2005a) of NADW acquired in the Nordic and Labrador seas and a less negative signal from the southern water masses (AAIW and AABW, $\varepsilon_{\text{Nd}} = -8 \pm 1$; Piepragras and Wasserburg, 1982; Jeandel, 1993) that originates from mixing of non radiogenic Atlantic waters and radiogenic Pacific waters. The evolution in ε_{Nd} along the modern day THC, from negative values in the north Atlantic, to positive values in the Pacific, makes ε_{Nd} a good candidate as a tracer of paleocirculation, and of the THC in particular. Planktonic or benthic foraminifera, benthic ferromanganese nodules and crusts, as well as iron-manganese oxides coatings are carrier phases that record the variations in ε_{Nd} from surface and bottom water mass signatures over different time scales (Elderfield et al., 1981; Vance and Burton, 1999; Albarede et al., 1997; Abouchami et al., 1999; Rutberg et al., 2000; Bayon et al., 2002; van De Flierdt et al., 2004; Piotrowski et al., 2004). For example, Piotrowski et al. (2004) measured the ε_{Nd} preserved in Fe-Mn oxides from LGM to mid Holocene in the South Atlantic, providing the first determination of circulation variations using Nd isotopic data at LGM. Nd

oceanic cycle is far from being completely constrained and uncertainties remain concerning the ability of ε_{Nd} to trace paleo-circulation. Indeed, Piotrowski et al. (2004) assume no change in the ε_{Nd} in both North Atlantic and North Pacific end-members at the LGM. Accordingly, the temporal variations observed are interpreted as changes in circulation and the relative contribution of the two end members at the core site. However, Lacan and Jeandel (2005a) demonstrated that changes in water mass mixing during the formation of the northern water mass component could directly affect ε_{Nd} of this end-member. These authors further suggested that exchange of Nd between the sediment deposited on continental margins and the seawater occurred. This process, named “Boundary Exchange” (dissolved/particulates interaction along the continental margin, hereafter referred to as BE), is highly likely to modify the signature of water masses flowing along these margins (Jeandel et al., 1998; Lacan and Jeandel, 2005b; Arsouze et al., 2007). Therefore, changes in the continental weathering regime, which will alter sediment fluxes and the type of material deposited along the continental margin, (Vance and Burton, 1999; Reynolds et al., 2004), are likely to affect the ε_{Nd} composition of the end-members. Also, the shifts in the sites of deep water formation to lower latitudes (Ganopolski et al., 1998) may imply a change in the nature of the material exchanged with seawater. Such processes may weaken the hypothesis that Nd end-member signatures are invariant in time and under different climatic conditions. Three recent studies focused on trying to identify if the northern end-member ε_{Nd} varied on glacial-deglacial time scales, based on the analysis of both deep sea corals (van de Flierdt et al., 2006) and ferromanganese crusts (Foster et al., 2007) or oxyhydroxide (Gutjahr et al., 2008) as carrier phases. Unfortunately, their results are still controversial, leaving the problem unresolved (cf. Sect. 5.3). We here suggest that modeling can bring a new perspective to the discussion.

In this study, we use a modeling approach to reconstruct the global scale distribution of ε_{Nd} at the LGM. Our aim is to investigate the extent to which the observed temporal variation in ε_{Nd} data reflects changes in either the MOC, the signatures of the two end-members, or some combination of the two. We therefore test the evolution of ε_{Nd} distribution under different representations of the LGM oceanic circulation generated by the IPSL (Institut Pierre-Simon Laplace) atmosphere-ocean coupled model. Firstly, the characteristics of this model and the dynamical features of the different simulations performed are described. We then present ε_{Nd} distributions for each run, in order to compare the changes in simulated circulation between LGM and modern state. Finally, we compare the output with the available data and evaluate the importance of the different processes that generate the LGM ε_{Nd} distribution.

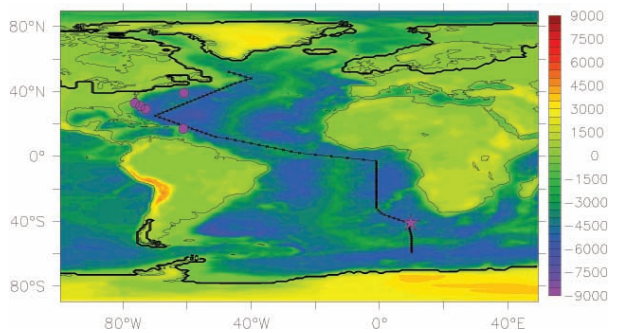


Fig. 1. Bathymetry and topography map at LGM, with modern continent contours. Sea level was 120 m lower at LGM than at Holocene (inducing larger Patagonian or New Foundland Plateau), with present oceanic regions covered by ice sheets (enclosed by thick line) over the Barents Sea, Hudson Bay or Nordic Sea, and the closure of the Bering Strait. The black line represents the trajectory of the vertical section in Figs. 3 and 4. LGM and glacial/interglacial core location are represented by purple star (Piotrowski et al., 2004) and circles (van de Flierdt et al., 2006; Foster et al., 2007; Gutjahr et al., 2008).

2 Description of the numerical experiments

All atmosphere-ocean simulations used in the present study are performed with the IPSL_CM4 model (Ocean Atmosphere Global Circulation Model - OAGCM) developed at Institut Pierre Simon Laplace (Marti et al., 2006). The individual modules of this coupled model are LMDz.3.3 (LMD, Hourdin et al., 2006) in a $3.75^\circ \times 2.5^\circ$ resolution for the atmosphere circulation, ORCHIDEE for the land surface (Krinner et al., 2005), the NEMO model in its coarse resolution version ORCA2, (LOCEAN, Madec, 2006) for the ocean, and the associated sea ice component is represented by the LIM model (developed at UCL-ASTR, Fichefet and Maqueda, 1997; Goosse and Fichefet, 1999). The three constituent parts of the OAGCM (ocean, atmosphere and sea ice) are coupled using the OASIS coupler (CERFACS, Valcke, 2006).

The control simulation (modern run, cf. Table 1 and Fig. 2) is the pre-industrial simulation run for the recent IPCC exercise (IPCC, 2007, <http://ipcc-wg1.ucar.edu/wg1/wg1-report.html>). The MOC in this simulation is relatively weak (≈ 10 Sv) compared to the most recent evaluations (Swingedouw et al., 2007). This shortfall in the modern MOC is partly explained by the lack of convection in the Labrador Sea.

For the LGM simulations, the land-sea mask, topography and ice-sheet extent are prescribed according to the Peltier ICE-5G reconstruction (Peltier, 2004). Consequently, ice sheets cover Hudson Bay, the Baltic Sea, the Bering Strait and the Barents Sea and present shallow areas such as the Patagonian and New Foundland continental shelf become part of the adjacent continent (Fig. 1). All simulations

use reduced atmospheric concentrations of CO₂, CH₄ and N₂O to 185 ppm, 350 ppb and 200 ppb respectively, and the 21 ky BP orbital parameters, according to the PMIP2 protocol (<http://pmip2.lsce.ipsl.fr>). Three runs are been performed that use a river routing scheme adapted for LGM conditions, i.e. addressing the impact of ice-sheets on river basins (Alkama et al., 2006; Alkama et al., 2008). In all three simulations, snow that accumulates on the ice-sheets is redistributed as a fresh water flux to the ocean so that the simulations have a closed fresh water budget. Three latitude bands are defined, with limits at 90° S/50° S/40° N/90° N. The 40° N limit corresponds to the southernmost latitudes reached by icebergs during ice ages. In each latitude band, the excess freshwater, which we define as calving, is integrated and supplied to the ocean in the same latitude band. For the northern band, freshwater fluxes due to calving are delivered to the Atlantic and Arctic Oceans, but not to the Pacific. In all three simulations, there is a remaining imbalance in the fresh water budget due to a slightly non conservative atmospheric convection scheme. In simulations LGMa and LGMb, the fresh water budget is closed using different methods. For LGMa, this bias is compensated for by multiplying global precipitation by 2.1%. This simulation presents in a strong overturning in the Atlantic Ocean, reaching 18 Sv, 8 Sv stronger than the control run). In LGMb, the calving flux is multiplied by 44%. Both LGMa and LGMb have a closed fresh water balance. In LGMc, the calving flux has been multiplied by 100%. The MOC slows down to only 6 Sv. The additional freshwater added to the northern latitude band corresponds to 0.18, 0.25 and 0.35 Sv for LGMa, LGMb and LGMc, respectively (cf. Table 1).

Even though changes in fresh water forcing remain relatively small, they result in a variety of representations of the MOC. LGMb is generally similar to LGMa, where a dominant and vigorous water mass from the north fills the basin, but in contrast to LGMa, bottom water from the south enters to more northerly latitudes during LGMb. The MOC in LGMc can be viewed as a reproduction of one of the proposed LGM circulation scenarios (scenario 1), wherein the influence of southern component water is increased and the northern component water flows south at shallower depth than current NADW (thus corresponding to the GNAIW). In addition, we also performed a simulation with modern boundary conditions but retaining the LGM land-sea distribution. Because a change in sea-level and in the extent of ice-sheets induce a change in the definition of continental margin, and thus a change in Nd inputs, this simulation, hereafter referred as modernM, tests the sensitivity of the ε_{Nd} distribution to changes in land-sea distribution. We note that circulation changes induced by using LGM bathymetry are not significant. AABW is slightly weaker than during the control simulation (≈ 3 Sv compared to 5 Sv), but the main structures and characteristic depths are conserved.

All LGM scenarios of ocean circulation were generated at the “Laboratoire des Sciences du Climat et de l’Environnement” (LSCE). A summary of the simulation characteristics and the overturning sections are provided in Table 1 and Fig. 2.

3 ε_{Nd} modeling

ε_{Nd} is simulated following the approach described in Arsouze et al. (2007). The oceanic ε_{Nd} distribution is generated by a passive tracer model that solves the equation:

$$\frac{\partial \varepsilon_{\text{Nd}}}{\partial t} = S(\varepsilon_{\text{Nd}}) - U \cdot \nabla \varepsilon_{\text{Nd}} + \nabla \cdot (K \nabla \varepsilon_{\text{Nd}}) \quad (1)$$

where $S(\varepsilon_{\text{Nd}})$ is the Source-Sink term of the element, $U \cdot \nabla \varepsilon_{\text{Nd}}$ and $\nabla \cdot (K \nabla \varepsilon_{\text{Nd}})$ are the three dimensional advective and diffusive terms, calculated with pre-computed advection (U) and diffusion (K) fields (off-line method) (Lévy et al., 2006).

The only source/sink term taken into account is BE, which is parameterized as a relaxing term towards the continental margin ε_{Nd} value:

$$S(\varepsilon_{\text{Nd}}) = 1/\tau \cdot (\varepsilon_{\text{Nd}_{\text{mar}}} - \varepsilon_{\text{Nd}}) \cdot \text{mask}_{\text{mar}} \quad (2)$$

where τ is the relaxing time, $\varepsilon_{\text{Nd}_{\text{mar}}}$ is the ε_{Nd} value of the continental margin, ε_{Nd} is the prognostic variable for Nd IC of seawater in the model, and mask_{mar} is a fraction of margin in a numerical grid box.

The relaxing time is set to vary from six months in surface waters to 10 years at 3000 m depth. We have not attempted to account for geographical variations of this profile because it remains a difficult task to parameterize spatial variability, when one considers the current knowledge of the factors acting on BE (e.g. nature of the sediment on the margin, overlying currents, bathymetry, etc...). The parameters chosen for the vertical profiles provide the best results for the modern ocean (Arsouze et al., 2007). This parameterization of BE implies that the short relaxing time at the surface will result in a strong exchange between the water mass and the continental margin, while a longer relaxing time at the at depth results in a weaker exchange between the water mass and the continental margin. We refer to Arsouze et al. (2007) for a more detailed description of this parameterisation used for ε_{Nd} modeling.

Since the decay of the radioactive isotope ^{147}Sm to ^{143}Nd takes much longer (a half life of 106 Gy) than the studied time interval (about 20ky), we assumed there to be no evolution of the isotopic signature of the margin due to natural radioactive decay between LGM and Holocene. In addition, because no major tectonic reorganizations have occurred since the LGM, the overall margin ε_{Nd} distribution was likely very similar to that of today. Therefore, we apply the margin ε_{Nd} composition established by Jeandel et al. (2007) for our LGM simulations. Finally, we assume the

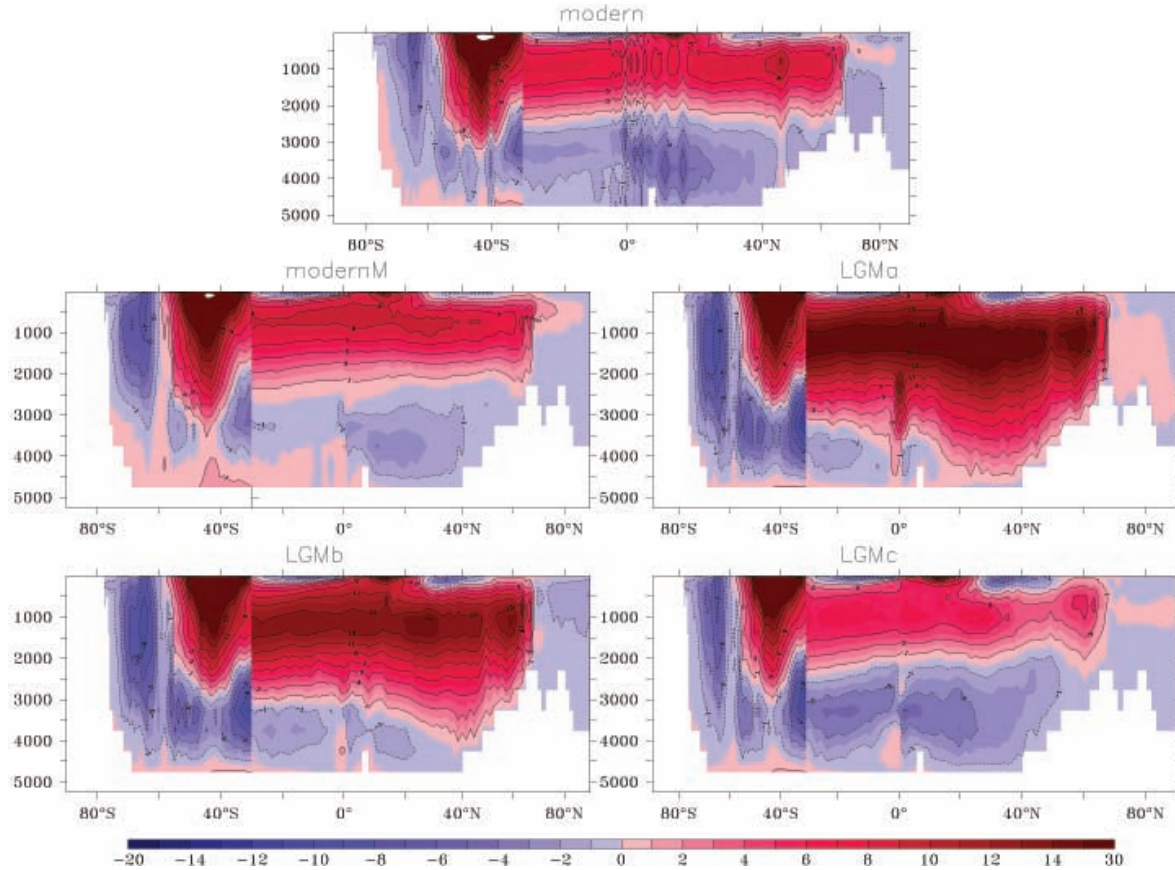


Fig. 2. Meridional overturning streamfunction (in Sv) of the Atlantic basin, north of 30° S, and of global ocean south of 30° S, for all simulations. The vertical line break at 30° S is produced by this change in streamfunction visualisation. modernM simulation produces a circulation somewhat similar to the control run. LGMa, and to a lesser extent LGMb, simulations are characterized by a strong and dominant water mass from the north that fills the basin. However, water masses that originate from the south enter in the basin at northern latitudes in LGMb, which is not the case in LGMa. On the contrary, in LGMc simulation, the influence of southern component water is increased and fulfils the basin at depth, while the northern component water flows south at shallower depth than current NADW.

vertical parameterisation and relaxing time, that characterizes BE, to be unchanged at the LGM. This last hypothesis has to be taken cautiously, because terrigenous fluxes were possibly higher at the LGM (Franzese et al., 2006). However, until the impact of these fluxes on BE can be better constrained, we base our hypothesis on Tachikawa et al.'s results (2003), which found a minor impact of terrigenous flux variations on the ε_{Nd} signatures of deep water masses.

We acknowledge that this simplistic modeling parameterization can only resolve the first order representation of the oceanic ε_{Nd} distribution. Therefore, our ability to determine to which extent changes in circulation drive changes in the ε_{Nd} of end-members is limited by the accuracy of our parameterization of the ε_{Nd} oceanic cycle. In fact, Arsouze et al. (2007) have shown that despite a correct representation of the ε_{Nd} composition of the major ocean water masses of the inter oceanic basin gradient, the modeled values in the At-

lantic are still slightly too radiogenic compared to the available data (Figs. 3 and 5 in Arsouze et al., 2007). In this study, our main objective resides in studying the response of the model to a change in circulation and inputs (in term of ε_{Nd} gradient). Our modeling efforts must be seen as a first step towards reproducing the absolute value of the data provided by paleoceanographers (Piotrowski et al., 2004; Gutjahr et al., 2008). The proposed model must therefore be understood as a tool to further investigate the ε_{Nd} distribution and the end-member signatures in the Atlantic under LGM forcing.

4 Results

A section chosen to fit the classical western basin section in the northern part of the Atlantic, and to compare with the available data in the south (Figs. 3 and 4), as well as a map of

Table 1. Main characteristics of the simulations. ε_{Nd} (Holocene), ε_{Nd} (LGM) and $\Delta\varepsilon_{\text{Nd}}$ are data values. Modern run is the reference run obtained with pre-industrial run forcings. Simulations LGMA, LGMB and LGMC are all produced with LGM forcings and boundary conditions (orbital parameters, ice sheets coverage and subsequent sea ice level drop, realistic river routing, atmosphere chemistry composition). The three LGM simulations are obtained with different calving fluxes (treatment of snow accumulating on the northern mid latitude ice sheets, which excess is redistributed over the ocean to close the freshwater budget). modernM simulation is obtained with modern forcing and LGM land-sea mask.

Experiment Name	Calving (fresh-water from ice sheets melt redistributed north of 40° N)	North component water flow	South component water flow	Mean ε_{Nd} of the basin	ε_{Nd} of the south component water mass (50° S, 30° W) 4000 m	ε_{Nd} of the north component water mass (50° N, 50° W) 2500 m
Modern	—	10 Sv	5 Sv	-9.1	-7.1	-12.5
ModernM	—	9 Sv	3 Sv	-8.7	-6.9	-11.5
LGMA	0.18 Sv	18 Sv	1 Sv	-8.6	-6.5	-10.3
LGMB	0.25 Sv	14 Sv	2 Sv	-8.7	-6.6	-10.2
LGMC	0.35 Sv	6 Sv	4 Sv	-8.7	-6.7	-10.5
Experiment Name	ε_{Nd} , 41° S, 4500 m ε_{Nd} (Holocene) = -9.4 ε_{Nd} (LGM) = -6.5	ε_{Nd} , 30° N, 4500 m ε_{Nd} (Holocene) = -13.6 ε_{Nd} (LGM) = -10.3	ε_{Nd} , 30° N, 2000 m ε_{Nd} (Holocene) = -13.5 ε_{Nd} (LGM) = -9.7	$\Delta\varepsilon_{\text{Nd}}$ (LGM-Hol) 41° S, 4500 m $\Delta\varepsilon_{\text{Nd}}$ (data)= +2.9	$\Delta\varepsilon_{\text{Nd}}$ (LGM-Hol) 30° N, 4500 m $\Delta\varepsilon_{\text{Nd}}$ (data)= +3.3	$\Delta\varepsilon_{\text{Nd}}$ (LGM-Hol) 30° N, 2000 m $\Delta\varepsilon_{\text{Nd}}$ (data)= +3.8
Modern	-7.6	-7.8	-10.9	—	—	—
ModernM	-7.5	-7.8	-10.1	+0.2	+0.1	+0.7
LGMA	-7.1	-9.8	-8.8	+0.4	-1.9	+2.1
LGMB	-7.0	-8.8	-9.4	+0.6	-1.0	+1.5
LGMC	-7.0	-7.6	-9.7	+0.5	+0.3	+1.2

the ε_{Nd} difference between control and other simulations between 3000 and 5000 m depths (Fig. 5) are used to assess the ε_{Nd} distributions in the simulations and to compare them with the data provided by Piotrowski et al. (2004) and Gutjahr et al. (2008). Additionally, mean ε_{Nd} value of the basin and characteristic values of both south and north end-members are used to determine the respective influence of changes in Nd inputs and circulation variations (Table 1).

4.1 Modern simulations

4.1.1 Control simulation

The modern simulation produces a ε_{Nd} distribution that is in broad agreement with the existing data, with a ε_{Nd} composition of -12.5 and -7 for NADW and AABW, respectively (compare to the data values of -13.5 for NADW and -8 and AABW, Table 1, Figs. 3 and 4). Most modeled values fall within 3 ε_{Nd} units of the observed values, even if some important discrepancies are observed. These are mainly in surface and sub-surface waters (above 1000 m), due to the overestimated influence of radiogenic inputs along the Scotland-Iceland-Greenland rise (Fig. 3). Also, as far north as 40° N, unrealistic radiogenic southern waters are observed with val-

ues of -7.5 ε_{Nd} (Fig. 3). The main structure of the ε_{Nd} distribution and its relationship to the main water masses filling the Atlantic basin are however reproduced.

The simulation of realistic first order ε_{Nd} gradients and water masses characteristics in the Atlantic Ocean therefore make the model a tool to consider using it for investigating the impact of the past variations in ocean circulation.

4.1.2 modernM simulation

modernM yields a more radiogenic mean ε_{Nd} distribution than for the control run (+0.4 ε_{Nd} ; Table 1). The largest anomalies are observed in surface waters and at depth for the formation site of the northern end-member (+1; Figs. 4 and 5). This anomaly is subsequently propagated southward via the deep western boundary current. The ε_{Nd} composition of the Atlantic sector of the Southern Ocean remains virtually unaffected by bathymetry and land-sea mask changes (about 0.2 ε_{Nd} more radiogenic).

4.2 LGM simulations

The three LGM simulations produce a ε_{Nd} distribution that is somewhat similar to the modern distribution with very radiogenic surface and bottom waters at all latitudes, and

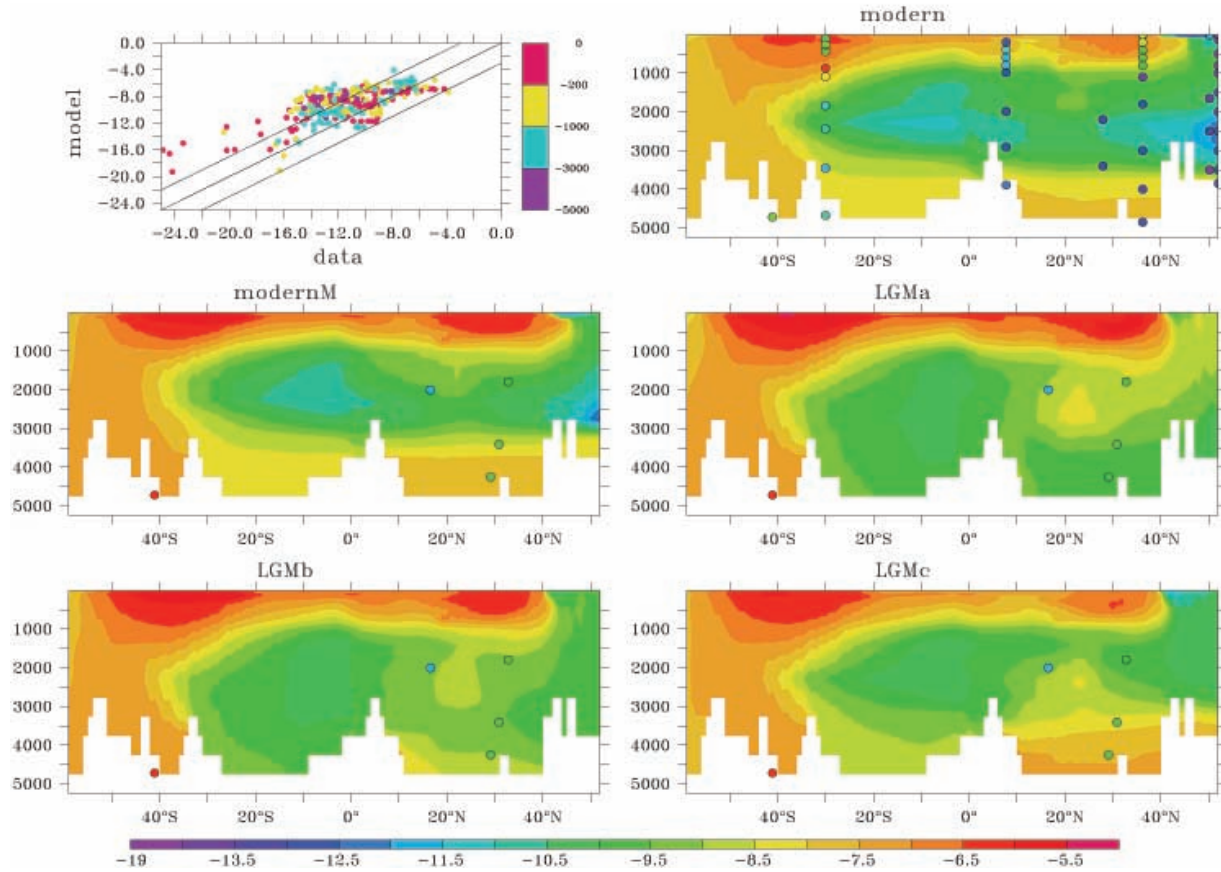


Fig. 3. Top left panel represents modeled ε_{Nd} versus measured ε_{Nd} over the Atlantic basin for reference modern simulation, as function of depth (colour code). Diagonal lines are lines of $\varepsilon_{\text{Nd}}(\text{modeled})=\varepsilon_{\text{Nd}}(\text{data})$, $\varepsilon_{\text{Nd}}(\text{modeled})=\varepsilon_{\text{Nd}}(\text{data})+3\varepsilon_{\text{Nd}}$ and $\varepsilon_{\text{Nd}}(\text{modeled})=\varepsilon_{\text{Nd}}(\text{data})-3\varepsilon_{\text{Nd}}$. Other panels are vertical ε_{Nd} sections along the track represented in black in Fig. 1 for all simulations. Data are superimposed in circles with the same colour code as simulation output. Data are provided by (Lacan and Jeandel, 2005a; Piepraga and Wasserburg, 1987; 1983; Spivack and Wasserburg, 1988; Jeandel, 1993) for modern control run (Foster et al., 2007; Gutjahr et al., 2008; Piotrowski et al., 2004) for LGM runs. The color scale is non linear. Reproduction of ε_{Nd} distribution in the modern control run is in correct agreement with the observation. LGM simulations generate highly distinct ε_{Nd} distribution, particularly at bottom depths.

intermediate waters with high ε_{Nd} values in the southern ocean. In the North, sandwiched between the surface and bottom water masses, there is a more negative ε_{Nd} deep water mass. The northern end-member ε_{Nd} values are however significantly different from the control (from -10.2 to $-10.5 \varepsilon_{\text{Nd}}$ compared to $-12.5 \varepsilon_{\text{Nd}}$ for control run, Table 1, Fig. 3). Despite significant changes in ocean circulation in our scenarios, the global mean ε_{Nd} during the LGM for the three sensitivity tests simulated ε_{Nd} in the Atlantic basin is unaffected by circulation changes and is $0.5 \varepsilon_{\text{Nd}}$ more radiogenic than the modern scenario (Table 1). However, some remarkable changes are observed for different water masses.

4.2.1 LGMa

The MOC in LGMa is so vigorous that it propagates the positive signature from southern surface and intermediate wa-

ters to northerly latitudes ($+1.5 \varepsilon_{\text{Nd}}$, Fig. 4) and further influences the signature of the northern end-member at depth ($2.2 \varepsilon_{\text{Nd}}$ more radiogenic than for the control simulation at 50° N, Table 1). Even further south (20° S), this northern end-member still remains more radiogenic (Fig. 4). The ε_{Nd} composition of the bottom water mass in all LGM simulations is directly related to the relative influence of the northern and southern end-members. Consequently LGMa, which is characterized by a deep and robust NADW cell, has the lowest ε_{Nd} among the three LGM simulations (Fig. 3). Finally, the isotopic composition for the Atlantic sector of the Southern Ocean (south of 30° S) is also more radiogenic (up to $+0.7 \varepsilon_{\text{Nd}}$, Fig. 5) relative to the modern control run. This is due to an increased influence of the more radiogenic south Pacific water masses, since LGMa is typified by a vigorous Antarctic Circumpolar Current (ACC).

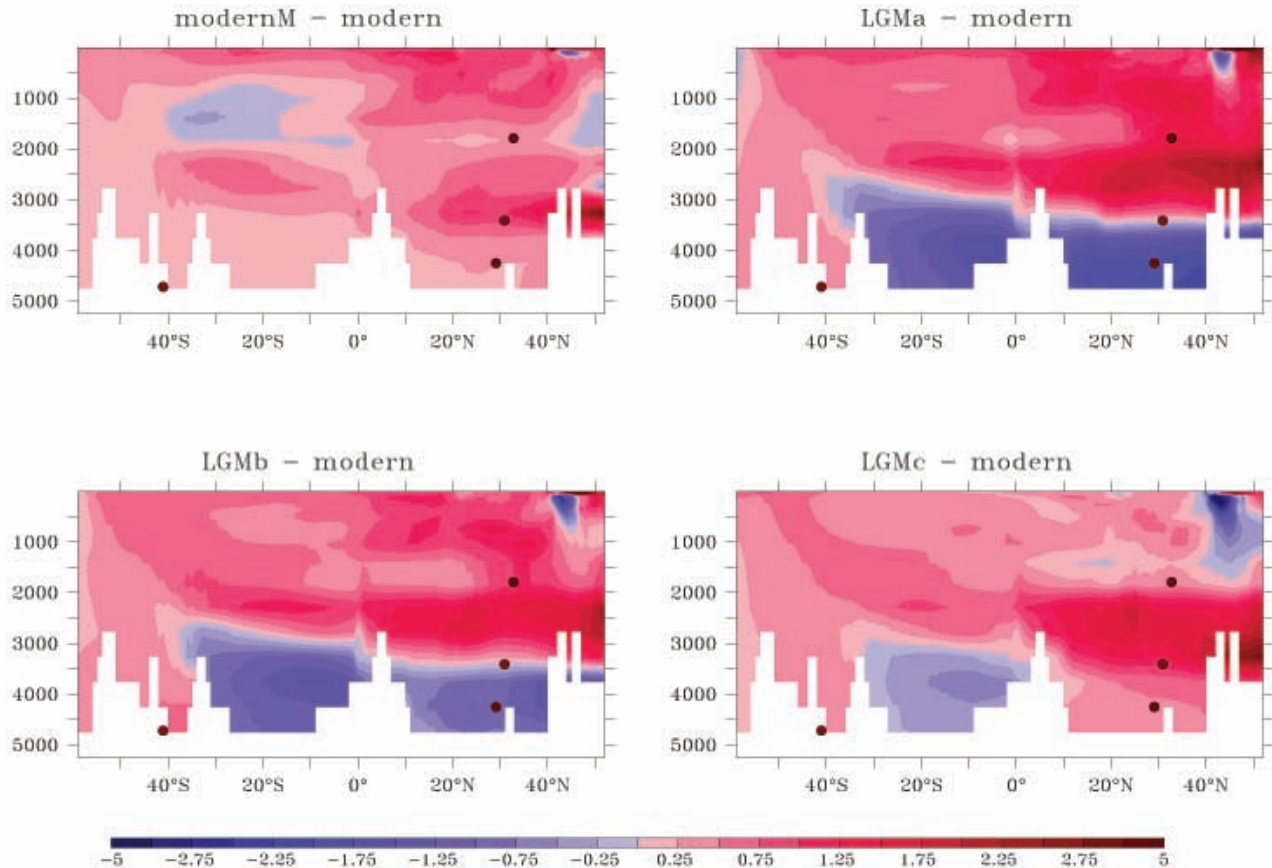


Fig. 4. Vertical ε_{Nd} variations along the track represented in black in Fig. 1 between reference modern run and modernM, LGMA, LGMB and LGMC simulations. Data is superimposed in circles with the same colour code as simulation output. LGM data is provided by (Foster et al., 2007; Gutjahr et al., 2008; Piotrowski et al., 2004). The color scale is non linear. LGMc simulation reproduces a correct tendency at all depths when compared with the available observations. Also, LGMa, with a strong circulation cell, reproduces a correct LGM-modern variation at 2000m, 30° N.

4.2.2 LGMb

The LGMb simulation displays ε_{Nd} distribution similar to that of LGMa. However, the influence of the southern component is greater compared to the LGMa simulation, consistent with the dynamical properties of the simulation. Accordingly, the northern end-member is slightly more radiogenic ($\varepsilon_{\text{Nd}} = -10.2$) than during LGMa, but still influences the bottom water composition ($\varepsilon_{\text{Nd}} = -8.8$ compared to $\varepsilon_{\text{Nd}} = -9.8$ for LGMa and $\varepsilon_{\text{Nd}} = -7.8$ for the control simulation, Fig. 3). As for LGMa, the Atlantic sector of the Southern Ocean is influenced by radiogenic waters from the Pacific (Fig. 5).

4.2.3 LGMc

The northern end-member has a ε_{Nd} value of -10.5 which is slightly higher than our other LGM runs. However, LGMc presents a more dominant radiogenic AABW throughout the basin and consequently produces the highest ε_{Nd} bottom values ($\varepsilon_{\text{Nd}} \approx -7$, Fig. 3). Unsurprisingly, LGMc, which represents the weakest LGM simulated ACC circulation, shows a more moderate influence of radiogenic waters from Pacific (Fig. 5). Also, LGMc simulates large differences in ε_{Nd} between the western and eastern parts of the Atlantic basin (Fig. 5). As AABW preferentially flows in the western part of the Atlantic basin, the negative ε_{Nd} signature of GNAIW for LGMc is reflected only in the eastern part. This east – west gradient in ε_{Nd} is not observed in the other LGM simulations, due to the predominant influence of northern water masses across the entire Atlantic basin.

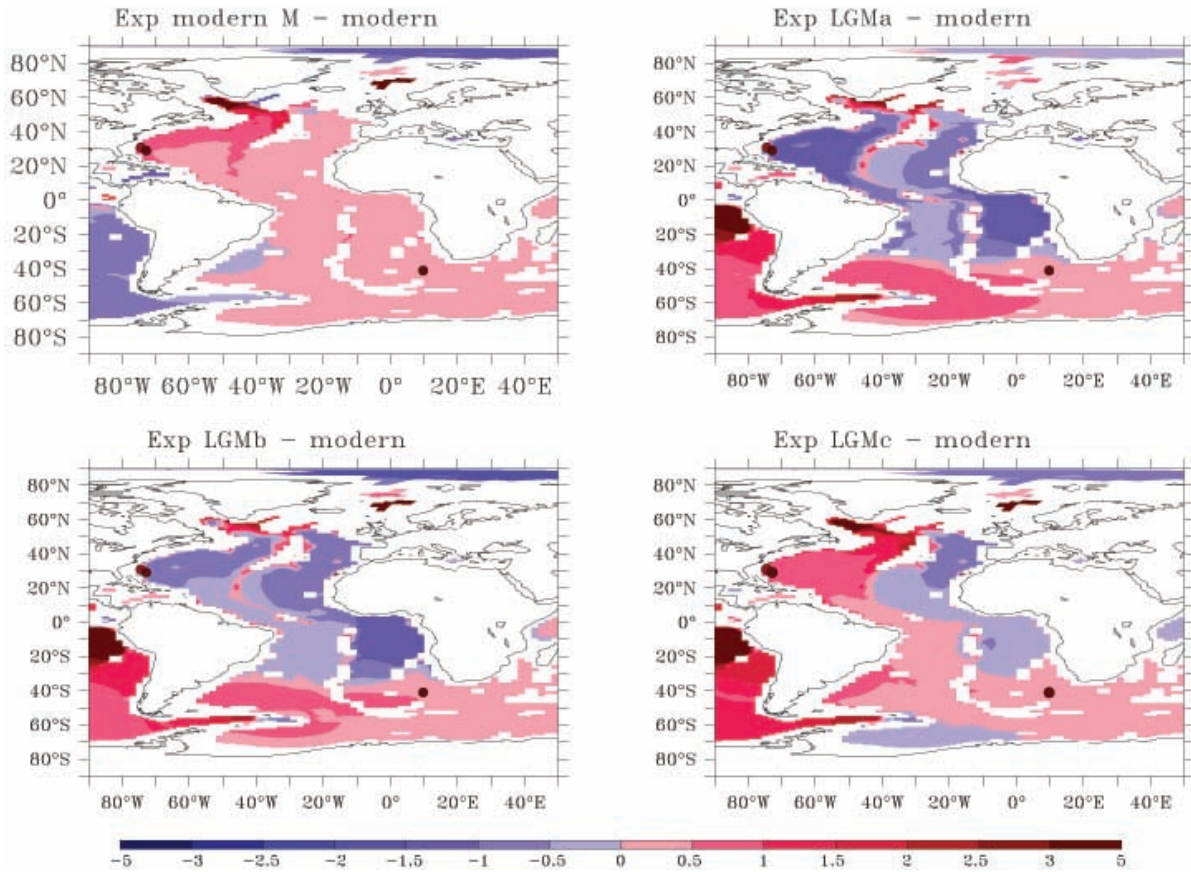


Fig. 5. Map of ε_{Nd} difference between reference run (modern run) and the four other runs (modernM, LGMA, LGMB, LGMC), averaged between 3000 and 5000 m. Data are superimposed in circles with the same colour code as simulation output. LGM data are provided by (Foster et al., 2007; Gutjahr et al., 2008; Piotrowski et al., 2004). The color scale is non linear. LGMc is the only simulation that succeeds in reproducing a positive gradient in the western part of the basin.

5 Discussion

The simulated ε_{Nd} never differs by more than ± 3.2 units between the three LGM simulations. In addition, when ε_{Nd} is averaged over the whole basin, the resulting difference between each set of two simulations never exceeds $+0.1 \varepsilon_{\text{Nd}}$ (Table 1). Thus, the overall isotopic composition of the basin is not drastically influenced by the different circulation schemes with our parameterization scheme. However, circulation redistributes ε_{Nd} properties in different ways.

5.1 Changes induced by bathymetry

Firstly, the isotopic composition of the whole Atlantic basin is $+0.4 \varepsilon_{\text{Nd}}$ more radiogenic for modernM simulation than for the control run. This demonstrates that the ε_{Nd} is likely affected by changes in bathymetry and the subsequent changes in Nd sources. This is due to the presence of ice sheets over the Barents Sea, Hudson Bay and even the Baltic Sea, that prevent BE and reduce contact with very nega-

tive ε_{Nd} margins (respectively -15 , -25 and -18 , Jeandel et al., 2007). The closure of the Bering Strait, which prevents radiogenic waters from the North Pacific from entering the Arctic basin, appears to play a negligible role since the flux involved is important locally only. LGM topography and the presence of northern ice sheets induce variability in the exchange of Nd between water masses and continental margins and therefore drive a change in the ε_{Nd} of the northern end-member. In contrast, the southern end-member remains virtually insensitive to any change in bathymetry (less than $+0.2 \varepsilon_{\text{Nd}}$ variation, during simulation modernM), while the three LGM scenarios result in AABW that is up to $0.7 \varepsilon_{\text{Nd}}$ more radiogenic (Table 1, Figs. 3 and 5). This difference might be explained by changes in circulation, such as the ACC strength, which mixes both the Atlantic and the more radiogenic Indo-Pacific waters to compose the southern end-member signature, as suggested by previous works (Duplessy et al., 1988; Charles and Fairbanks, 1992; Oppo and Rosenthal, 1994).

5.2 Comparison with data in South Atlantic

The measured ε_{Nd} gradient between modern and LGM in the data provided by Piotrowski et al. (2004) (+3 ε_{Nd}) is not fully reproduced by any of our three LGM simulations (only +1 ε_{Nd} at maximum, Fig. 4), despite a good matching of the absolute LGM value of -6.5. The simulation of the correct trend in ε_{Nd} between modern and LGM is encouraging, although the amplitude of the variation remains too low. This deficiency may be ascribed to either 1) the forcing term which may not be adapted to the area, or 2) the poor model resolution, which is therefore unable to reproduce all the processes of AABW propagation and formation along the Antarctic margin. This means the model falls short in characterizing the ε_{Nd} composition of AABW and is a classical problem of coarse resolution OGCMs (Dutay et al., 2002).

Geographically speaking, the location of the core studied by Piotrowski et al. (2004) is situated in an area of rough topography, which is not accurately reproduced in this coarse model. In addition, in our model this region is also influenced by a variety of factors aside from the relative influence of AABW and GNAIW. For example, ACC strength and associated sediment transport with a Pacific radiogenic signature, variation in Indo-Pacific radiogenic waters entering the basin via the Agulhas current are crudely resolved in our model (Franzese et al., 2006). This might influence the reproduction of ε_{Nd} either in a radiogenic or non radiogenic way, but makes the contribution of each factor unclear.

5.3 Constraining ε_{Nd} north end-member evolution

The critical problem in evaluating the potential of ε_{Nd} as a water mass tracer is to constrain the time-evolution of the isotopic composition of the end-members. Resolving this would also provide complementary information if used together with other chemical and isotopic paleotracers. The present study clearly suggests a difference of at least +0.5 ε_{Nd} for the northern end-member as compared to present.

However, van de Flierdt et al. (2006) measured Nd variations in deep-sea corals from the New England Seamounts during Younger Dryas (short time period at 11.5–12.9 kyr B.P. which is suspected to display an oceanic circulation regime similar to the LGM, Keigwin and Schlegel, 2002; Keigwin, 2004) and found signatures in ε_{Nd} of surface (-14.5 ε_{Nd}) and deep (-13/-13.5 ε_{Nd}) waters that are similar to the present. They therefore concluded that there was probably no variation in the composition of end-members with time. Foster et al. (2007), using data in ferromanganese crusts over glacial/interglacial periods, also concluded that there was no significant change in the ε_{Nd} of north end-member, but the time resolution of their study (30 k.y. at least) may be too low to constrain such short-term variations as those which characterize the LGM.

These two results provide an indication that the ε_{Nd} signature of the northern end-member is invariant through time.

In contrast, recent Nd data obtained in the authigenic Fe-Mn oxyhydroxide fraction of sediments collected in the western boundary current shows that GNAIW at LGM displayed ε_{Nd} values that were 3.5 units greater, relative to the Holocene ones (Gutjahr et al., 2008). At the core location of Gutjahr et al. (2008), all three of our LGM simulations reproduce a northern end-member that is shifted to more radiogenic values at intermediate depths, with LGMa providing the most realistic results. These radiogenic values for LGMa are generated by strong overturning that transports surface radiogenic waters up to the formation site of the northern end-member.

Conversely, LGMc is the only simulation that succeeds in producing a correct tendency in ε_{Nd} LGM-Holocene variation for deep waters (i.e. a positive gradient, Table 1, Figs. 4 and 5). The glacial reduction in ε_{Nd} during this simulation is due to both the influence of waters of southern origin and to the shift in the northern end-member to more radiogenic values. These results and the comparison with local data in the area (Gutjahr et al., 2008) suggest that: 1) strong MOC is needed to bring radiogenic waters to formation site of northern end-member, 2) LGMc circulation with prominent AABW that fills the basin at bottom depths is the only plausible scenario to simulate the observed deep value.

Sediment focusing may be important in dictating the interpretation of Gutjahr et al. (2008) and these authors suggest that acquiring complementary data is essential. Our study also illustrates the necessity for additional depth profile measurements of ε_{Nd} at LGM in the western part of the Atlantic basin, where AABW preferentially flows. Such observations would allow a clear statement about the signature of the NADW/GNAIW change. Deep water measurements would also provide a information concerning the penetration of AABW into the basin, as it is expected to flow northward as far as 60° N (Curry and Oppo, 2005). Indeed, this area is more representative of the water mass influences in the basin, with a ε_{Nd} gradient directly dependent on the end-members contributions. The signature of bottom waters in LGMa is representative of the northern end-member ($\varepsilon_{\text{Nd}}=-9.8$), whereas southern component signature ($\varepsilon_{\text{Nd}}=-7.6$) can be observed in simulation LGMc (Table 1).

6 Conclusions

Using a simple parameterisation to model ε_{Nd} distribution in an OGCM, we have studied the impact of changes in the overturning cell and circulation patterns between LGM and Holocene on ε_{Nd} in the Atlantic basin.

The modernM simulation (LGM land-sea mask with modern forcing) shows that the presence of ice sheets, without significant variation in circulation, affects the ε_{Nd} of the Atlantic basin, and generates shifts in the composition of the end-members leading to a change in the mean ε_{Nd} of +0.4 units. In particular, the northern end member does

not acquire its modern negative signature, due to restricted exchange with highly negative margins that are protected by ice sheets at the LGM. On the other hand, the southern end-member is not significantly affected by the change in bathymetry.

Water mass structures in the Atlantic basin are qualitatively similar in terms of ε_{Nd} distribution for the three LGM simulations, even though the circulation changes drastically from one to another. However, qualitatively, we note important changes in the ε_{Nd} of bottom waters in the western basin, which are consistent with a stronger penetration of southern water mass and the relative influence of components. As for modernM, the mean ε_{Nd} is 0.5 more radiogenic than during the modern run, suggesting that although circulation changes do not play a key role in end-members ε_{Nd} acquisition, they are important in redistributing the characteristics of the basin.

Very few data concerning ε_{Nd} at LGM are presently available. The change in isotopic composition between present and LGM observed in the data provided by Piotrowski et al. (2004) is partially reproduced by the model in all the oceanic circulation configurations. However, the location of the core is not the most relevant place for a comparison appraisal of the model, since the very complex local bathymetry and ocean dynamics complicate any comparison with our coarse resolution model. On the other hand, the LGMc simulation yields the most conclusive model-data comparison for bottom water in the western part of the basin (Gutjahr et al., 2008), but requires a greater influence of southern radiogenic waters to the northern end-member formation area (associated with a stronger MOC, like in LGMa scenario). We propose here that the north of the western part of the basin, where the composition of the end-members can easily be constrained, and where the only factor controlling the distribution of ε_{Nd} is the relative influence of the northern and southern components, would be a relevant site for future model/data comparison. This would also confirm/infirm the interpretation of the data of Gutjahr et al. (2008).

Substantial progress must be made in:

1. Understanding the modern Nd oceanic cycle, so as to better reproduce the features that drive the temporal evolution in the ε_{Nd} .
2. Modeling of the LGM ocean circulation, since simulation LGMc was produced via the artificial addition of freshwater, and modeling of the other scenarios suggested by other studies (for example scenarios 2) and 3) mentioned in the introduction, which we have not tested because they have not yet been reproduced by OAGCMs).
3. Obtaining more data for Nd isotopes in order that Nd can be a consistent tool for intercomparison with other paleo proxies.

Acknowledgements. The authors would like to thank F. Peeters, M. Siddall, D. Vance and an anonymous referee for their comments that significantly improve the quality of the paper. A. Tagliabue is thanked for his linguistic advice. The LGM simulations have been obtained in the framework of the MOTIF (European Project EVK2-CT-2002-00153) and PMIP2 (<http://pmip2.lsce.ipsl.fr>) projects and in the ANR BLANC project IDEGLACE (ANR-05-BLAN-0310-01, 2006-2009).

Edited by: F. Peeters

References

- Abouchami, W., Galer, S. J. G., and Koschinsky, A.: Pb and Nd isotopes in NE Atlantic Fe-Mn crusts : Proxies for trace metal paleosources and paleocean circulation, *Geochim. Cosmochim. Ac.*, 63, 1489–1505, 1999.
- Albarede, F., Goldstein, S. L., and Dautel, D.: The neodymium isotopic composition in Mn nodules from the Southern and Indian Oceans, the global oceanic neodymium budget and their bearing on deep ocean circulation, *Geochim. Cosmochim. Ac.*, 61, 1277–1291, 1997.
- Alkama, R., Kageyama, M., and Ramstein, G.: Freshwater discharges in a simulation of the Last Glacial Maximum climate using improved river routing, *Geophys. Res. Lett.*, 33, L21709, doi:10.1029/2006GL027746, 2006.
- Alkama, R., Kageyama, M., Ramstein, G., and Marti, O.: Impact of a realistic river routing in coupled ocean-atmosphere simulations of the Last Glacial Maximum climate, *Clim. Dynam.*, 30, 855–869, 2008.
- Amakawa, H., Nozaki, Y., Alibo, D. S., Zhang, J., Fukugawa, K., and Nagai, H.: Neodymium isotopic variations in Northwest Pacific waters, *Geochim. Cosmochim. Ac.*, 68, 715–727, 2004.
- Arsouze, T., Dutay, J. C., Lacan, F., and Jeandel, C.: Modeling the neodymium isotopic composition with a global ocean circulation model, *Chem. Geol.*, 239, 165–177, 2007.
- Bayon, G., German, C. R., Boella, R. M., Milton, J. A., Taylor, R. N., and Nesbitt, R. W.: An improved method for extracting marine sediment fractions and its application to Sr and Nd isotopic analysis, *Chem. Geol.*, 187, 179–199, 2002.
- Broecker, W. S. and Denton, G. H.: The role of ocean-atmosphere reorganizations in glacial cycles, *Geochim. Cosmochim. Ac.*, 53, 2465–2501, 1989.
- Broecker, W. S.: Constraints on the glacial operation of the Atlantic Ocean's conveyor circulation, *Israel J. Chem.*, 42, 1–14, 2002.
- Charles, C. D. and Fairbanks, R. G.: Evidence from Southern Ocean sediments for the effect of North Atlantic deep-water flux on climate, *Nature*, 355, 416–419, 1992.
- Curry, W. B. and Lohmann, G. P.: Reduced advection into Atlantic Ocean deep eastern basins during last glaciation maximum, *Nature*, 306, 577–580, 1983.
- Curry, W. B. and Oppo, D. W.: Glacial water mass geometry and the distribution of delta C-13 of Sigma CO₂ in the western Atlantic Ocean, *Paleoceanography*, 20, PA1017, doi:10.1029/2004PA001021, 2005.
- Duplessy, J. C., Shackleton, N. J., Fairbanks, R. G., Labeyrie, L., Oppo, D., and Kallel, N.: Deep water source variations during the last climatic cycle and their impact on the global deep water circulation, *Paleoceanography*, 3, 343–360, 1988.

- Dutay, J. C., Bullister, J. L., Doney, S. C., Orr, J. C., Najjar, R., Caldeira, K., Campin, J. M., Drange, H., Follows, M., Gao, Y., Gruber, N., Hecht, M. W., Ishida, A., Joos, F., Lindsay, K., Madec, G., Maier-Reimer, E., Marshall, J. C., Matear, R. J., Monfray, P., Mouchet, A., Plattner, G.-K., Sarmiento, J., Schlitzer, R., Slater, R., Totterdell, I. J., Weirig, M.-F., Yamamoto, Y., and Yool, A.: Evaluation of ocean model ventilation with CFC-11: comparison of 13 global ocean models, *Ocean. model.*, 4, 89–120, 2002.
- Elderfield, H., Hawkesworth, C. J., Greaves, M. J., and Calvert, S. E.: Rare earth element geochemistry of oceanic ferromanganese nodules and associated sediments, *Geochim. Cosmochim. Ac.*, 29, 209–220, 1981.
- Fichefet, T. and Maqueda, M. A. M.: Sensitivity of a global sea ice model to the treatment of ice thermodynamics and dynamics, *J. Geophys. Res.-Oceans*, 102, 12 609–12 646, 1997.
- Foster, G. L., Vance, D., and Prytulak, J.: No change in the neodymium isotope composition of deep water exported from the North Atlantic on glacial-interglacial time scales, *Geology*, 35, 37–40, 2007.
- Franzese, A. M., Hemming, S. R., Goldstein, S. L., and Anderson, R. F.: Reduced Agulhas Leakage during the Last Glacial Maximum inferred from an integrated provenance and flux study, *Earth Planet. Sc. Lett.*, 250, 72–88, 2006.
- Ganopolski, A., Rahmstorf, S., Petoukhov, V., and Claussen, M.: Simulation of modern and glacial climates with a coupled global model of intermediate complexity, *Nature*, 391, 351–356, 1998.
- Gherardi, J. M., Labeyrie, L., McManus, J. F., Francois, R., Skinner, L. C., and Cortijo, E.: Evidence from the Northeastern Atlantic basin for variability in the rate of the meridional overturning circulation through the last deglaciation, *Earth Planet. Sc. Lett.*, 240, 710–723, 2005.
- Goldstein, S. L. and Hemming, S. R.: Long lived Isotopic Tracers in Oceanography, Paleoceanography, and Ice sheet dynamics, in: Treatise on Geochemistry, edited by: Elderfield, H., Elsevier Pergamon press, Amsterdam, chapter 6.17, 2003.
- Goosse, H. and Fichefet, T.: Importance of ice-ocean interactions for the global ocean circulation: A model study, *J. Geophys. Res.-Oceans*, 104, 23 337–23 355, 1999.
- Gutjahr, M., Frank, M., Stirling, C. H., Keigwin, L. D., and Halliday, A. N.: Tracing the Nd isotope evolution of North Atlantic deep and intermediate waters in the Western North Atlantic since the Last Glacial Maximum from Blake Ridge sediments, *Earth Planet. Sc. Lett.*, 266, 61–77, 2008.
- Henderson, G. M., Heinze, C., Anderson, R. F., and Winguth, A. M. E.: Global distribution of the Th-230 flux to ocean sediments constrained by GCM modelling, *Deep-Sea Res. Pt. I*, 46, 1861–1893, 1999.
- Hourdin, F., Musat, I., Bony, S., Braconnot, P., Codron, F., Dufresne, J. L., Fairhead, L., Filiberti, M. A., Friedlingstein, P., Grandpeix, J. Y., Krinner, G., Levan, P., Li, Z. X., and Lott, F.: The LMDZ4 general circulation model: climate performance and sensitivity to parametrized physics with emphasis on tropical convection, *Clim. Dynam.*, 27, 787–813, 2006.
- Jacobsen, S. B. and Wasserburg, G. J.: Sm-Nd isotopic evolution of chondrites, *Earth Planet. Sc. Lett.*, 50, 139–155, 1980.
- Jeandel, C.: Concentration and isotopic composition of Nd in the South Atlantic Ocean, *Earth Planet. Sc. Lett.*, 117, 581–591, 1993.
- Jeandel, C., Thouron, D., and Fieux, M.: Concentrations and Isotopic compositions of Nd in the Eastern Indian Ocean and Indonesian Straits, *Geochim. Cosmochim. Ac.*, 62, 2597–2607, 1998.
- Jeandel, C., Arsouze, T., Lacan, F., Techine, P., and Dutay, J. C.: Isotopic Nd compositions and concentrations of the lithogenic inputs into the ocean: A compilation, with an emphasis on the margins, *Chem. Geol.*, 239, 156–164, 2007.
- Keigwin, L. D. and Schlegel, M. A.: Ocean ventilation and sedimentation since the glacial maximum at 3 km in the western North Atlantic, *Geochem. Geophys. Geosy.*, 3, 1034, doi:10.1029/2001GC000283, 2002.
- Keigwin, L. D.: Radiocarbon and stable isotope constraints on Last Glacial Maximum and Younger Dryas ventilation in the western North Atlantic, *Paleoceanography*, 19, PA4012, doi:10.1029/2004PA001029, 2004.
- Krinner, G., Viovy, N., de Noblet-Ducoudre, N., Ogee, J., Polcher, J., Friedlingstein, P., Ciais, P., Sitch, S., and Prentice, I. C.: A dynamic global vegetation model for studies of the coupled atmosphere-biosphere system, *Global Biogeochem. Cy.*, 19, GB1015, doi:10.1029/2003GB002199, 2005.
- Lacan, F. and Jeandel, C.: Neodymium isotopic composition and rare earth element concentrations in the deep and intermediate Nordic Seas: constraints on the Iceland Scotland Overflow Water signature, *Geochem. Geophys. Geosy.*, 5, Q11006, doi:10.1029/2004GC000742, 2004.
- Lacan, F. and Jeandel, C.: Acquisition of the neodymium isotopic composition of the North Atlantic Deep Water, *Geochem. Geophys. Geosy.*, 6, Q12008, doi:10.1029/2005GC000956, 2005a.
- Lacan, F. and Jeandel, C.: Neodymium isotopes as a new tool for quantifying exchange fluxes at the continent – ocean interface, *Earth Planet. Sc. Lett.*, 232, 245–257, 2005b.
- Lévy, M., Aumont, O., Kremmer, A. S., Memery, L., and Ethé, C.: NEMO reference manual, tracer component: NEMO-TOP, Preliminary version, Note du Pole de modélisation, Institut Pierre-Simon Laplace (IPSL), 28, 2006.
- Lynch-Stieglitz, J., Curry, W. B. and Slowey, N.: Weaker Gulf Stream in the Florida straits during the last glacial maximum, *Nature*, 402, 644–648, 1999.
- Lynch-Stieglitz, J., Curry, W. B., Oppo, D. W., Ninneman, U. S., Charles, C. D., and Munson, J.: Meridional overturning circulation in the South Atlantic at the last glacial maximum, *Geochem. Geophys. Geosy.*, 7, Q10N03, doi:10.1029/2005GC001226, 2006.
- Lynch-Stieglitz, J., Adkins, J. F., Curry, W. B., Dokken, T., Hall, I. R., Herguera, J. C., Hirschi, J. J. M., Ivanova, E. V., Kissel, C., Marchal, O., Marchitto, T. M., McCave, I. N., McManus, J. F., Mulitza, S., Ninnemann, U., Peeters, F., Yu, E. F., and Zahn, R.: Atlantic meridional overturning circulation during the Last Glacial Maximum, *Science*, 316, 66–69, 2007.
- Madec, G.: NEMO reference manual, ocean dynamics component: NEMO-OPA. Preliminary version, Note du Pole de modélisation, Institut Pierre-Simon Laplace (IPSL), 27, 2006.
- Marchal, O., Francois, R., Stocker, F., and Fortunat, J.: Ocean thermohaline circulation and sedimentary $^{231}\text{Pa}/^{230}\text{Th}$ ratio, *Paleoceanography*, 15, 625–641, 2000.
- Marchitto, T. M. and Broecker, W. S.: Deep water mass geometry in the glacial Atlantic Ocean: A review of constraints from the paleonutrient proxy Cd/Ca, *Geochem. Geophys. Geosy.*, 7, Q12003, doi:10.1029/2006GC001323, 2006.

- Marti, O., Braconnot, P., Bellier, J., Benshila, R., Bony, S., Brockmann, P., Cadule, P., Caubel, A., Denvil, S., Dufresne, J.-L., Fairhead, L., Filiberti, M.-A., Foujols, M.-A., Fichefet, T., Friedlingstein, P., Goosse, H., Grandpeix, J.-Y., Hourdin, F., Krinner, G., Lévy, C., Madec, G., Musat, I., de Noblet, N., Polcher, J., and Talandier, C.: The new IPSL climate system model: IPSL-CM4, Note du Pôle de Modélisation 26, 2006.
- McManus, J. F., Francois, R., Gherardi, J.-M., Keigwin, L. D., and Brown-Leger, S.: Collapse and rapid resumption of Atlantic meridional circulation linked to deglacial climate changes, *Nature*, 428, 834–837, 2004.
- Oppo, D. and Fairbanks, R. G.: Variability in the Deep and Intermediate Water Circulation of the Atlantic Ocean During the Past 25,000 Years: Northern Hemisphere Modulation of the Southern Ocean, *Earth Planet. Sc. Lett.*, 86, 1–15, 1987.
- Oppo, D. and Rosenthal, Y.: Cd/Ca changes in a deep Cape Basin core over the past 730 000 years: Response of circumpolar deep-water variability to northern hemisphere ice sheet melting?, *Paleoceanography*, 9, 661–676, 1994.
- Peltier, W. R.: Global glacial isostasy and the surface of the ice-age earth: The ICE-5G (VM2) Model and GRACE, *Annu. Rev. Earth Pl. Sc.*, 32, 111–149, 2004.
- Piepgras, D. J. and Wasserburg, G. J.: Neodymium isotopic variations in seawater, *Earth Planet. Sc. Lett.*, 50, 128–138, 1980.
- Piepgras, D. J. and Wasserburg, G. J.: Isotopic composition of neodymium in waters from the Drake Passage, *Science*, 217, 207–217, 1982.
- Piepgras, D. J. and Wasserburg, G. J.: Influence of the Mediterranean outflow on the isotopic composition of neodymium in waters of the North Atlantic, *J. Geophys. Res.*, 88, 5997–6006, 1983.
- Piepgras, D. J. and Wasserburg, G. J.: Rare earth element transport in the western North Atlantic inferred from isotopic observations, *Geochim. Cosmochim. Ac.*, 51, 1257–1271, 1987.
- Piotrowski, A. M., Goldstein, S. L., Hemming, S. R., and Fairbanks, R. G.: Intensification and variability of ocean thermo-haline circulation through the last deglaciation, *Earth Planet. Sc. Lett.*, 225, 205–220, 2004.
- Rahmstorf, S.: Ocean circulation and climate during the past 120 000 years, *Nature*, 419, 207–214, 2002.
- Reynolds, B. C., Sherlock, S. C., Kelley, S. P., and Burton, K. W.: Radiogenic isotope records of Quaternary glaciations: Changes in the erosional source and weathering processes, *Geology*, 32, 861–864, 2004.
- Rutberg, R. L., Hemming, S. R., and Goldstein, S. L.: Reduced North Atlantic deep Water flux to the glacial Southern Ocean inferred from neodymium isotope ratios, *Nature*, 405, 935–938, 2000.
- Spivack, A. J. and Wasserburg, G. J.: Neodymium isotopic composition of the Mediterranean outflow and the eastern North Atlantic, *Geochim. Cosmochim. Ac.*; Vol/Issue: 52:12, Pages: 2767–2773, 1988.
- Swingedouw, D., Braconnot, P., Delecluse, P., Guilyardi, E., and Marti, O.: The impact of global freshwater forcing on the thermohaline circulation: adjustment of North Atlantic convection sites in a CGCM, *Clim. Dynam.*, 28, 291–305, 2007.
- Tachikawa, K., Athias, V., and Jeandel, C.: Neodymium budget in the ocean and paleoceanographic implications, *J. Geophys. Res.*, 108(C8), 3254, 2003.
- Valcke, S.: OASIS3 User Guide (prism_2–5), PRISM Support Initiative Report, 3, 64, 2006.
- Van De Flierdt, T., Frank, M., Lee, D. C., Halliday, A. N., Reynolds, B. C., and Hein, J. R.: New constraints on the sources and behavior of neodymium and hafnium in seawater from Pacific Ocean ferromanganese crusts, *Geochim. Cosmochim. Ac.*, 68, 3827–3843, 2004.
- van de Flierdt, T., Robinson, L. F., Adkins, J. F., Hemming, S. R., and Goldstein, S. L.: Temporal stability of the neodymium isotope signature of the Holocene to glacial North Atlantic, *Paleoceanography*, 21, PA4102, doi:10.1029/2006PA001294, 2006.
- Vance, D. and Burton, K.: Neodymium isotopes in planktonic foraminifera: A record of the response of continental weathering and ocean circulation rates to climate change, *Earth Planet. Sc. Lett.*, 173, 365–379, 1999.
- von Blanckenburg, F.: Perspectives: Paleoceanography – Tracing past ocean circulation?, *Science*, 286, 1862–1863, 1999.
- Yu, E.-F., Francois, R., and Bacon, M.: Similar rates of modern and last-glacial ocean thermohaline circulation inferred from radiochemical data, *Nature*, 379, 679–680, 1996.

Chapitre 5

Modélisation de la composition isotopique en Atlantique nord

Sommaire

5.1	Résumé	101
5.2	<i>Modeling the Nd isotopic composition in the North Atlantic basin using an eddy-permitting model</i>	101

5.1 Résumé

Les premiers tests sur la modélisation de ε_{Nd} dans un modèle de circulation océanique global 3 montrent une bonne reproduction de la distribution du ε_{Nd} océanique au premier ordre. Cependant, la reproduction de la signature du bassin Atlantique est trop radiogénique comparée aux données. Ce problème a été associé aux défauts classiques de reproduction de la dynamique dans la région avec ce type de modèle basse résolution, en particulier pour la plongée des eaux profondes et des courants de bord (Dutay et al., 2002).

Près de la moitié des données de ε_{Nd} dissous actuellement disponibles dans la littérature est située en Atlantique Nord, dans les Mers Nordiques ou encore dans le bassin du Labrador. La plupart de ces données provient du travail fourni par François Lacan au cours de sa thèse (Lacan, 2002). Cette zone d'étude s'est révélée particulièrement pertinente pour l'étude du traceur ε_{Nd} en mettant en évidence le processus de BE et confirmant les propriétés de traceur de masses d'eau Lacan et Jeandel (2005a, 2004a,b,c). De plus, les moyens d'acquisition de la signature isotopique des eaux profondes dans la région qui sont par la suite advectées le long de la "Conveyor Belt" est un problème dont les implications pour le proxy ε_{Nd} sont importantes. L'existence d'une configuration de modèle à résolution eddy-permitting ($1/4^\circ \times 1/4^\circ$) dans cette région, avec une dynamique réaliste, est une opportunité pour valider de façon satisfaisante le jeu de données existant et insister sur le rôle du BE pour le ε_{Nd} . Ainsi, on met en place dans la configuration NATL4 du modèle NEMO le terme de rappel à la marge continentale utilisé lors de la modélisation globale pour paramétriser le BE, et les apports fluviaux et atmosphériques sont négligés. Des tests de sensibilité sur le temps d'échange sont effectués afin de comparer avec les estimations obtenues avec ORCA2 afin de contraindre son fonctionnement.

Les résultats montrent que le seul BE permet de reproduire de manière tout à fait satisfaisante la distribution en ε_{Nd} dans la région. Le temps caractéristique d'échange entre la marge continentale et l'océan est évalué entre quelques jours et 2 mois, ce qui est significativement plus court que les précédentes estimations déduites de la modélisation à échelle globale, et en meilleur accord avec les observations. Cette étude met en avant la dépendance de la paramétrisation du BE au modèle utilisé et souligne l'importance d'une dynamique simulée correcte pour reproduire correctement la signature isotopique des masses d'eau et estimer le temps d'échange du BE.

5.2 *Modeling the Nd isotopic composition in the North Atlantic basin using an eddy-permitting model*

Modeling the Nd isotopic composition in the North Atlantic basin using an eddy-permitting model

ARSOUZE, T.^{1,2,3,*,-}, TREGUIER, A.M.¹, PERONNE, S.^{1,+}, DUTAY, J.-C.², LACAN, F.³, JEANDEL, C.³

¹: Laboratoire Physique des Océans (LPO), IFREMER/CNRS/UBO/IRD, Z.I. Pointe du Diable, B.P. 70, 29280 Plouzané, France.

²: Laboratoire des Sciences du Climat et de l'Environnement (LSCE), CEA/CNRS/UVSQ/IPSL, Orme des Merisiers, Gif-Sur-Yvette, Bat 712, 91191 Gif sur Yvette cedex, France.

³: Laboratoire d'Etudes en Géophysique et Océanographie Spatiale (LEGOS), CNES/CNRS/UPS/IRD, Observatoire Midi-Pyrénées, 14 av. E. Belin, 31400 Toulouse, France.

*: Corresponding author: arsouze@ldeo.columbia.edu
fax: +1 (845) 365-8157

-: Now at Lamont-Doherty Earth Observatory, Columbia University, P.O. Box 1000
61 Route 9W, Palisades, NY 10964-1000, USA

⁺: Now at Laboratoire de Morphodynamique Continentale et Cotière, UCB-N/CNRS/UR, 2-4, Rue des tilleuls, Université de Caen (Campus 1), 14000 Caen cedex, France

Abstract

Boundary Exchange (BE - exchange of elements between continental margins and the open ocean) has recently been emphasized as a key process in the oceanic cycle of Nd. We here use a regional eddy-permitting resolution OGCM ($1/4^\circ$) of the North Atlantic basin to simulate the distribution of Nd isotopic composition, considering BE as the only source. Results show good agreement with the data, thus confirming the major role of the BE process on the regional scale. Experiments with a characteristic exchange time (i.e. time needed for the continental margin to significantly imprint the chemical composition of the surrounding seawater) of 0.2 and 0.5 years yield the best results. A very short exchange time (a few days) is needed to reproduce the highly negative values in the Labrador Sea, and a longer one (up to 0.5 years) to simulate the radiogenic influence of basaltic margins. These exchange times are significantly lower than the previous evaluations using a low resolution model (6 months to 10 years), but however in agreement with the available seawater Nd isotope data, highlighting the importance of the model dynamics in simulating the BE process.

Index terms

Geochemical cycles, Radiogenic isotope geochemistry, Numerical modeling, Continental shelf and slope processes

Introduction

The seawater neodymium Isotopic Composition (Nd IC, or ϵ_{Nd}) varies in the ocean in close relation to the oceanic circulation. ϵ_{Nd} is the part per 10000 deviation of the observed $^{143}\text{Nd}/^{144}\text{Nd}$ ratio from that of the bulk earth (Jacobsen and Wasserburg, 1980). Relatively negative ϵ_{Nd} values are observed in the North Atlantic Ocean, increasing along the path of the global thermohaline circulation to more radiogenic values in the North Pacific (Piepgras and Wasserburg, 1980; Lacan and Jeandel, 2005a). Changes in Nd IC observed in the water column are related to vertical distribution of water masses. In the Atlantic basin, the North Atlantic Deep Water (NADW) is characterized by a relatively homogeneous ϵ_{Nd} value ranging from -13 to -14, whereas the Antarctic Intermediate Water (AAIW) and Antarctic Bottom Water (AABW) are characterized by more radiogenic end-member isotopic signatures of approximately -8 ϵ_{Nd} prior to any mixing with other Atlantic water masses (Piepgras and Wasserburg, 1987; Jeandel, 1993). ϵ_{Nd} is considered to be a “quasi-conservative” tracer (ϵ_{Nd} values are conserved for sites distant from source regions) and is used to tag water masses with distinct isotope compositions in order to constrain water mass mixing.

Nd sources to the ocean are lithogenic, and the mean Nd IC of a basin is representative of the surroundings continents (Albarede et al., 1997; Jeandel et al., 2007). However, the process leading to the transfer of Nd from the continents to the ocean is still an open debate. Nevertheless, it is generally admitted that the role of hydrothermal inputs is negligible because Nd, as well as all Rare Earth Elements, are effectively scavenged at hydrothermal sites (Michard et al., 1983). It has also been shown that atmospheric dusts and river discharge alone cannot account for both the distributions of Nd IC and Nd concentration, (Tachikawa et al., 2003; Van de Flierdt et al., 2004). Finally, Lacan and Jeandel (2005a) proposed the *Boundary Exchange* (BE, exchange of elements between water masses and sediments deposited along continental margins) as an important term in the budget of REE's in the ocean.

The identification of Nd sources in the North Atlantic basin has been particularly challenging. Lacan and Jeandel (2005b) confirmed the need to invoke terrigenous inputs originating from the particulate discharge along the Southern Greenland continental margin (distinguished by a highly unradiogenic composition), as well as water-mass mixing, to explain the characteristic unradiogenic signature of the NADW. This conclusion complements results from several other studies that also evidenced the influence of BE as a source to explain changes in isotopic signature of water masses in this basin (Lacan and Jeandel, 2004a; 2004b; 2005b; Rickli et al. 2009). Therefore, the North Atlantic basin is a relevant region to test the impact of BE on the ϵ_{Nd} oceanic distribution. The high density of observations available, and the importance of this region to the thermohaline circulation, which is of particular interest to study past variations of global circulation, also make this the ideal region to evaluate the role of BE on the regional scale.

A first attempt to model global Nd IC distribution using a coarse resolution model ($2^\circ \times 2^\circ \cos(\text{lat})$) suggested BE is an important process among the sources of Nd to the ocean (Arsouze et al., 2007). In these simulations, the global ϵ_{Nd} distribution of high ϵ_{Nd} in the Pacific and low ϵ_{Nd} in the Atlantic was reproduced, but discrepancies with data were observed in the North Atlantic Ocean where the simulated Nd isotopic signature was too radiogenic. Other sources not taken into account, such as dusts and dissolved river inputs, are characterized by radiogenic signatures and therefore cannot be considered to reproduce the observed negative signal (Lacan and Jeandel, 2005b). Other possibilities to explain the offset between the simulated distribution and data in the North Atlantic are an under-estimation of the exchange time, or an incorrect representation of the circulation's dynamics in the region. Indeed, even if the use of a global coarse resolution model was necessary for our first global modeling study,

the conclusions were likely influenced by model's representation of boundary currents, which were too slow and too diffusive, notably in the North West Atlantic.

Other global modeling studies recently improved our understanding of the behavior of the Nd oceanic cycle. Jones et al. (2008) showed that ϵ_{Nd} distribution in the Atlantic basin could be explained via water mass mixing, hence confirming the conservative property of the Nd IC tracer. Siddall et al. (2009), using a reversible scavenging model emphasized the role of vertical processes in the water column to reconcile both Nd concentration and IC distribution. However, these both studies prescribed surface Nd concentration and IC, determined by data compilation, and did not focus on the sources of Nd in the ocean, which is a prerequisite for the application of ϵ_{Nd} as a water mass tracer. More recently, Arsouze et al. (subm.), using a coupled global dynamical/biogeochemical model, confirmed that BE is the dominant Nd source to the ocean (more than 95% of the total input), but however emphasized the essential role played by river inputs and atmospheric dusts sources in surface waters.

In this study we simulate for the first time the distribution of ϵ_{Nd} values in the North Atlantic basin using an eddy-permitting model. Higher resolution and good representation of boundary currents at the ocean margins is an important feature for improving simulation of processes occurring at the sediment/water interface. Also, we aim to confirm the influence of BE on a regional scale as the main Nd source term, and to better constrain the exchange time between continental margins and the open ocean (a problem of particular interest to help in constraining the processes involved in this exchange). To achieve these goals, we use a similar configuration to that of the global modeling, i.e. considering BE as the only Nd source, parameterized via a relaxation term along the continental margin (Arsouze et al. 2007).

Description of the model and ϵ_{Nd} modeling

We use the NEMO numerical model (Madec 2008), in the regional eddy permitting configuration NATL4, extracted from the global $1/4^\circ$ configuration ORCA025 (The Drakkar Group, 2007; Le Sommer et al, 2009). The domain includes the North Atlantic basin and Nordic Seas, extending from 20°S to 80°N in latitude, and up to 23°E in Mediterranean. Buffer zones are prescribed on the open boundaries of the domain. The vertical resolution (46 levels) ranges from 6 meters in the upper layer, to 250 meters at depth. We use partial-steps to adjust the last numerical level with the bathymetry.

The dynamic simulation is integrated for 20 years (1980 to 2000) from a climatological initial condition (Levitus et al., 1998) and using the Drakkar interannual atmospheric forcing DFS3. All ϵ_{Nd} simulations were run « offline », using the passive tracer model (Ethé et al., 2006), using the last 10 years of the pre-calculated dynamical fields (output averaged every 5 days), providing a mean state of the ocean circulation. The tracer is then integrated until equilibrium is reached (i.e. 160 years).

Comparison of the dynamical features simulated by the model between global coarse and regional eddy-permitting resolution shows large differences. Indeed, the transports are comparable in both configurations but the currents are much more vigorous in the eddy-permitting configuration. Barnier et al. (2006), Penduff et al. (2007), and Le Sommer et al. (2009) show how the use of an energy- and enstrophy-conserving momentum advection scheme in NEMO at $1/4^\circ$ yielded a clear improvement in the simulation of current-eddy-topography interactions, and thus of along-topography circulations. Comparisons between a large current meter database (Holloway, 2008) and two DRAKKAR global ocean simulations (T. Penduff, 2009, personal communication) confirm that increasing NEMO's resolution from 2° to $1/4^\circ$ yields a large reduction of local model-observation mismatches, both in terms of mean current strengths (which increase toward observed levels) and directions (aligning with measured flows more nearly along isobaths), in particular along basin margins where many

current meters are located.

Arsouze et al. (2007), in the global configuration of the model, defined BE as a source/sink term, $S(\epsilon_{Nd})$, parameterized by a relaxation term between the continental margin and the ocean:

$$S(\epsilon_{Nd}) = \frac{1}{\tau} \cdot (\epsilon_{Nd_{mar}} - \epsilon_{Nd}) \cdot mask_{mar} \quad (1)$$

where τ is the characteristic relaxing time, $\epsilon_{Nd_{mar}}$ is the ϵ_{Nd} value of the material deposited along the continental margin, $mask_{mar}$ is the percentage, for each grid point, of margin surface in a numerical grid cell of the model (determined using the 1 minute resolution bathymetry Gebco) and ϵ_{Nd} is the Nd IC value of the ocean. In the following experiments, we use the same parameterization as equation (1), refining the scale of the interpolation of $\epsilon_{Nd_{mar}}$ value compared to the map used on global scale using data compilation by Jeandel et al. (2007), and with $mask_{mar}$ recalculated on the NATL4 grid. We thus only model Nd IC, and make the hypothesis of a constant Nd concentration.

Because this is not a global GCM we have model boundaries in the open ocean in the high North Atlantic and South Atlantic that must be prescribed. We prescribe ϵ_{Nd} values for these “open ocean boundaries” using literature data from Signature 29 and Signature 30 data in the North Atlantic (Lacan and Jeandel, 2004a; 2004c), and SATl 217, SATl 271 and SATl 302 data at the South Atlantic (Jeandel, 1993). Prescribing these open ocean boundary conditions is similar to applying a relaxing term with a short characteristic relaxing time, which tags waters entering the basin with a Nd IC consistent with observations.

Four tests on the characteristic relaxing time are performed: experiments EXP1, EXP2, EXP3 and EXP4 have $\tau = 1$ day, 0.2 year (2.4 months), 0.5 year (6 months), and 1 year, respectively. In a last experiment (EXP5), we explore the possibility that our BE parameterization might be dependant on the mineralogical maturity of margin sediments (e.g. granitic vs. basaltic). We tested this by scaling the characteristic exchange time (τ) to the Nd IC of the margin ($\epsilon_{Nd_{mar}}$), so that exchange occurs faster along basaltic margins. We included this test because basaltic sediments contain minerals that are unstable at the Earth’s surface and thus erode much faster than granitic sediments (Amiotte Suchet et al., 2003; Dessert et al., 2003). Hence, τ is set to vary linearly from 0.1 years for the most radiogenic Nd IC values ($\epsilon_{Nd_{mar}} = +8$ along the Iceland margin) to 0.5 years for the most non-radiogenic values ($\epsilon_{Nd_{mar}} = -38$ on the South-East Greenland). Finally, for comparison purpose with the present sensitivity tests, we present an extraction of the North Atlantic basin from a previous simulation (Arsouze et al., 2007) in the ORCA2 configuration with a relaxing time of 1 year.

Results

Although BE is considered as the only source, the model simulates ϵ_{Nd} distributions are largely consistent with the data (Fig. 1, 2, and 3, Tab. 1). In particular, experiments EXP2 and EXP3 (relaxing time of 0.2 years and 0.5 years respectively) simulate in both cases 76% of the observed ϵ_{Nd} values with ± 3 unit accuracy (and almost 40% with ± 1 ϵ_{Nd} , Fig. 1 and Tab. 1). Remaining large errors in simulated values correspond mainly to surface or sub-surface samples located close to radiogenic coastal shelves, in particular along the Greenland – Iceland – Scotland ridge (Fig. 2).

These results are in better agreement than in the previous global coarse resolution simulations (ORCA2), with a relaxing time of 1 year (68% and 32% within ± 3 and ± 1 units errors respectively), which generated geographical gradients in ϵ_{Nd} , particularly on the surface along continental margins (leading to « patch » effects), suggesting overestimated exchange (Figs. 3 and 4 in Arsouze et al., 2007). However, using the regional eddy-permitting resolution (NATL4), simulation with the same relaxing time (1 year) leads to a homogeneous

distribution in surface (Figs. 1 and 2, EXP4, Tab. 1). The extremely short relaxing time of 1 day (EXP1) leads to large disparity in simulated ε_{Nd} values, including non-realistic radiogenic extremes near Iceland-Scotland and Caribbean Sea. Our first experiment (EXP1) is the only experiment that successfully simulates the observed negative ε_{Nd} values in surface waters of Labrador Sea (Fig. 2).

At depth (Fig. 3), all simulations EXP2, EXP3 and EXP4 ($\tau = 0.2$ year, 0.5 year and 1 year respectively) display comparable features, in good agreement with the data. Experiment $\tau = 1$ day (EXP1) generates deep waters that are too negative.

In experiment five (EXP5), we assume a linear relationship between the ε_{Nd} value of the continental margin and the relaxing time to test for possible chemical affinity for BE with the sediment. This experiment generates seawater ε_{Nd} that is globally too radiogenic in the basin, both in surface and at depth (Figs. 1, 2 and 3), particularly along the Caribbean arc and the Iceland-Scotland ridge.

In accordance with the previous results obtained with the global scale simulations, we find that a long characteristic exchange time induces longer residence time, and finally more homogeneous ε_{Nd} values in the basin, at all depths.

Discussion

The results presented here confirm at a regional scale what has been previously suggested on a global scale: by assuming BE as the only Nd oceanic source term it is possible to reproduce the main features of the distribution of this tracer in the basin. This suggests that BE is an important process in the Nd oceanic cycle.

One striking difference between these results and our previous results (Arsouze et al. 2007) is that the ideal characteristic exchange time τ is much shorter for eddy-permitting resolution simulations (NATL4) than for coarse resolution ones (ORCA2). The coarse resolution configuration (ORCA2) yielded an ideal exchange time varying from 6 months in surface to 10 years at depth. While the most realistic reproduction of ε_{Nd} distribution for the eddy-permitting model uses a relaxing time of 0.2 or 0.5 years, or even of the order of few days in surface and subsurface to correctly reproduce the highly non radiogenic waters in the Labrador Sea. This very short relaxing time implies a very intense exchange with the margins in the studied region. The rapid exchange rates suspected here are consistent with recent ε_{Nd} data that suggest an input from continental margins within only few weeks the Kerguelen Islands, another region where high dynamical forcing is present (Zhang et al., 2008).

One could argue that this short relaxing time needed to accurately represent BE likely lies in the missing sources other than BE not represented here. Indeed, even if the source of the BE dominates the budget of Nd sources to the ocean (about 90%, (Tachikawa et al., 2003), or more, (Arsouze et al., subm)), surface waters Nd IC distribution, where our model displays the largest discrepancies, is for the most part derived by river and aerosols inputs (Piepgrass and Wasserburg, 1987; Arsouze et al., subm.). The isotopic imprint of these sources is reflected in the sediment deposited along the associated continental margins, hence in the $\varepsilon_{\text{Nd}_{\text{mar}}}$ of the BE source. However, with exception of the Saharian dusts that essentially dictates the Nd IC distribution in the whole basin at mid latitudes in surface and sub-surface waters (Grousset et al., 1988), the isotopic signature of water masses evolves either by mixing or by contact with the margins (Lacan, 2002). Lacan and Jeandel (2005b) showed that dissolved river input and atmospheric dusts can rarely account for missing source in the Nordic Seas or in the Labrador Sea because 1) their IC is not compatible with the shift observed along the water-mass path, and/or 2) the total input is much lower than the flux required to reproduce this isotopic gradient. For example, these authors estimated that dissolved rivers discharges and atmospheric dust inputs account for only 8% and 1% of the

observed isotopic signature change along the path of formation of the North West Atlantic Bottom Water (at 2 700m depth), respectively.

This difference in relaxing time estimation between global and regional modeling likely lies in the reproduction of boundary currents that are more realistic and vigorous in NATL4 than in ORCA2. Sluggish water masses and important diffusion generated in the ORCA2 configuration (Dutay et al., 2004) overestimate the residence time of water masses in contact with continental margins and the transport of the margin signature into the ocean. Thus, simulation with a relaxing time of 1 year in ORCA2 configuration leads to strong geographical gradients, whereas simulation using the same relaxing time in the NATL4 configuration leads to a nearly homogenized basin. This underscores the importance of *Boundary Currents* representation to simulate the *Boundary Exchange* and the resulting ϵ_{Nd} distribution.

Experiment EXP5 suggests that in the studied area, the BE process doesn't seem to be more sensitive to the basaltic rather than granitic sediment. However, several authors suggested that the margin-to-water input of Fe (Moore and Braucher, 2008) or Nd (Lacan and Jeandel, 2005a, Jeandel et al., subm.) could result from lithogenic silicate dissolution. Such process should be favored by the high solubility of basalts (Dessert et al., 2003), which is not confirmed by EXP5 results. Nevertheless, these results have to be taken cautiously because the parameterization used might be simplistic and due to the highly demanding computing time of the simulations, we were unable to run other sensitivity experiments.

In the present simulations, the very radiogenic Caribbean Islands significantly imprint the water masses in the southwestern part of the domain, despite the occurrence of unradiogenic continents surrounding the Caribbean Sea. However, there are no data to confirm this result. However, the collection of data from this region would help provide further information about a potential BE sensitivity to the mineralogical maturity of the margin sediment, which is thought to be important based on seawater data from the Greenland - Scotland (Lacan and Jeandel, 2004a, 2004b). The reproduction of non-realistic radiogenic values in this area is likely due to overestimated inputs from this basaltic ridge, due to the parameterization of the continental margin used. In order to reduce these artifacts, it might be useful to couple this BE parameterization to a geographical sediment inputs map, rather than to a topographic one.

Conclusion

In this study, we simulated ϵ_{Nd} distribution using the regional NEMO/NATL4 eddy-permitting model in the North Atlantic Ocean. Boundary Exchange (BE) parameterization was performed via a relaxing term, in a manner similar to a previous study made on the global scale using the coarse resolution NEMO/ORCA2 model (Arsouze et al., 2007).

Characteristic exchange time is re-estimated to be between a few days and 6 months in the NATL4 configuration, which is significantly shorter than previous estimations of 6 months to 10 years, estimated from the global low resolution ORCA2 simulations. The reduced exchange time and the inclusion of the eddy permitting model yielded results that are in better agreement with the available data. This work highlights the dependency of the parameterization of BE to the model and dynamics used. In particular, a better reproduction of *Boundary Currents* in the NATL4 configuration compared to ORCA2 configuration is a key factor to improve the simulation of marine Nd isotopes through *Boundary Exchange* processes, and to estimate the characteristic exchange time between the ocean and the continental margins.

However, this important model-dependency does not undermine the importance of the BE hypothesis. Instead, even if we cannot rule out the importance of any source of Nd in the basin, we found that considering the source of the BE as the only Nd oceanic input term leads

to a very satisfying Nd IC distribution that closely matches observations in the whole basin. Available data in the region (Lacan, 2002) and global modeling (Arsouze et al., subm) suggest that sediment remobilization, rather than hydrothermal inputs, atmospheric dusts or even dissolved river inputs, might be the dominant term in the ocean Nd sources associated with the BE. Determining its behavior and the parameters acting on this process requires further studies.

Hence, we confirm on regional scale what has been previously suggested on local scale (via field observations) and global scale (via global modeling): Boundary Exchange is an important process in the cycling of Nd in the ocean.

Bibliography

- Albarede F., Goldstein S.L., and Dautel D. (1997), The neodymium isotopic composition in Mn nodules from the Southern and Indian Oceans, the global oceanic neodymium budget and their bearing on deep ocean circulation. *Geochim et Cosmochim Ac* 61 (6), 1277-1291.
- Arsouze T., Dutay J.-C., Lacan F., and Jeandel C. (2007), Modeling the neodymium isotopic composition with a global ocean circulation model, *Chem Geol*, 239, 165-177.
- Arsouze, T., Dutay, J.-C., Lacan, F., and Jeandel, C. (subm), Reconstructing the Nd oceanic cycle using a coupled dynamical – biogeochemical model, *Biogeosc*.
- Amiotte Suchet P., Probst J.-L. and Ludwig W. (2003), Worldwide distribution of continental rock lithology: Implications for the atmospheric/soil CO₂ uptake by continental weathering and alkalinity river transport to the oceans. *Glob Biogeochem Cy*, 17, 1038, doi:10.1029/2002GB001891.
- Barnier B., Madec G., Penduff, T., Molines J.-M., Treguier A.-M., Le Sommer J., Beckmann A., Biastoch A., Boening C., Dengg J., Derval C., Durand E., Gulev S., Remy E., Talandier C., Theetten S., Maltrud M., McClean J. and De Cuevas B. (2006), Impact of partial steps and momentum advection schemes in a global ocean circulation model at eddy-permitting resolution. *Ocea Dyn*, 56, 543-567.
- Dessert C., Dupré B., Gaillardet J., François L. M. and Allègre C. J. (2003), Basalt weathering laws and the impact of basalt weathering on the global carbon cycle. *Chem. Geol.*, Volume 202, Issues 3-4, 30, Pages 257-273.
- Drakkar group. (2007), Definition of the interannual experiment ORCA025-G70, 1958-2004. LEGI report, LEGI-DRA-2-11-2006, update.
- Dutay J.-C., Jean-Baptiste P., Campin J.-M., Ishida A., Maier-Reimer E., Matear R.J., Mouchet A., Totterdell I.J., Yamanaka Y., Rodgers K., Madec G., Orr J.C. (2004), Evaluation of OCMIP-2 ocean models' deep circulation with mantle helium-3. *J Mar Sys*, 48, 1-4, 15-36.
- Grousset, F. E., Biscaye, P. E., Zindler, A., Prospero, J., and Chester, R. (1988), Neodymium isotopes as tracers in marine sediments and aerosols: North Atlantic, *Earth Planet Sc Lett*, 87, 367-378.
- Holloway G. (2008), Observing global ocean topostrophy, *J. Geophys. Res.*, 113, C07054, doi: 10.1029/2007JC004635.
- Jacobsen S. and Wasserburg G. (1980), Sm-Nd isotopic evolution of chondrites. *Earth Planet Sc Lett*, 50, 139-155.
- Jeandel C. (1993), Concentration and isotopic composition of Nd in the South Atlantic Ocean, *Earth Planet Sc Lett*, 117, 581-591.
- Jeandel C., Arsouze T., Lacan F., Techine P., and Dutay J. C. (2007), Isotopic Nd compositions and concentrations of the lithogenic inputs into the ocean: A compilation, with an emphasis on the margins, *Chem Geol*, 239, 156-164.
- Jeandel C., Peucker-Ehrenbrink B., Godderis Y., Lacan F. and Arsouze T. (Submitted), Impact of ocean margin processes on dissolved Si, Ca and Mg inputs to the ocean. Submitted to Nature.
- Lacan F. (2002) Nordic Sea and Subarctic Atlantic Water Masses Traced by neodymium Isotopes (Masses d'eau des Mers Nordiques et de l'Atlantique Subarctique tracées par les isotopes du néodyme) PhD Thesis. Toulouse III University, France.
- Lacan F. and Jeandel C. (2004a), Denmark Strait water circulation traced by heterogeneity in neodymium isotopic compositions. *Deep Sea Research I*, 51, 71-82.
- Lacan F. and Jeandel C. (2004b), Neodymium isotopic composition and rare earth element concentrations in the deep and intermediate Nordic Seas: constraints on the Iceland

- Scotland Overflow Water signature. *Geochem Geophys Geosys*, 5, Q11006, doi:10.1029/2004GC000742.
- Lacan F. and Jeandel C. (2004c), Subpolar Mode Water formation traced by neodymium isotopic composition. *Geophys Res Lett*, 31, doi: 10.1029/2004GL019747.
- Lacan F., and Jeandel C. (2005a), Neodymium isotopes as a new tool for quantifying exchange fluxes at the continent - ocean interface. *Earth Planet Sc Lett*, 232, 245-257.
- Lacan F. and Jeandel C. (2005b), Acquisition of the neodymium isotopic composition of the North Atlantic Deep Water. *Geochem Geophys Geosys*, 6, doi: 10.1029/2005GC000956.
- Levitus S., Boyer T.P., Conkright M.E., O'Brien T., Antonov J., Stephens C., Stathoplos L., Johnson D., and Gelfeld R., (1998), World Ocean Database 1998, vol. 1, Introduction. NOAA Atlas NESDIS 18 (U.S. Government Printing Office, Washington, DC, 1998).
- Le Sommer J., Penduff T., Theetten S., Madec G. and Barnier B. (2009), How momentum advection schemes influence current-topography interactions at eddy permitting resolution. *Ocea Model*, 29, 1 - 14.
- Michard A., Albarede F., Michard G., Minster J.F., and Charlou J.L. (1983), Rare-earth elements and uranium in high-temperature solutions from east pacific rise hydrothermal vent field (13-degrees-N). *Nature*, 303 (5920), 795-797.
- Penduff T., Le Sommer J., Barnier B., Treguier A. M., Molines J. M. and Madec G. (2007), Influence of numerical schemes on current-topography interactions in 1/4 degrees global ocean simulations. *Ocea Sci*, 3, 509-524.
- Piepras D. J., and Wasserburg G. J. (1980), Neodymium isotopic variations in seawater, *Earth Planet Sci Lett*, 50, 128-138.
- Piepras D. J., and Wasserburg G. J. (1987), Rare earth element transport in the western North Atlantic inferred from isotopic observations, *Geochim Cosmochim Acta*, 51, 1257-1271.
- Rickli, J., Frank, M., Halliday A.N. (2009), The hafnium-neodymium isotope composition of Atlantic seawater. *Earth Planet Sci Lett* 280, 118-127.
- Tachikawa K., Athias V., and Jeandel C. (2003), Neodymium budget in the ocean and paleoceanographic implications, *J Geophys Res.*, 108, 3254 doi: 3210.1029/1999JC000285.
- van De Flierdt T., Frank M., Lee D. C., Halliday A. N., Reynolds B. C., and Hein J. R. (2004), New constraints on the sources and behavior of neodymium and hafnium in seawater from Pacific Ocean ferromanganese crusts, *Geochim Cosmochim Ac*, 68, 3827-3843.
- Zhang Y., Lacan F., and Jeandel C. (2008), Dissolved rare earth elements tracing lithogenic inputs over the Kerguelen Plateau (Southern Ocean), *Deep-Sea Res. Part II*, 55, 638-652.

Tab 1

Experience	Relaxing time τ	Percentage of points that reproduce the data with a $\pm 3 \varepsilon_{Nd}$ accuracy.	Percentage of points that reproduce the data with a $\pm 1 \varepsilon_{Nd}$ accuracy.	Regression coefficient of data/model points
EXP1 (NATL4)	1 day	57.91	25.63	1.231
EXP2 (NATL4)	0.2 year	75.63	33.54	0.7227
EXP3 (NATL4)	0.5 year	74.68	38.92	0.5708
EXP4 (NATL4)	1 year	73.73	38.61	0.4553
EXP5 (NATL4)	0.1 year (max $\varepsilon_{Nd_{mar}}$) to 0.5 year (min $\varepsilon_{Nd_{mar}}$)	57.91	25.95	0.5564
ORCA2	1 year	68.04	32.28	0.6693

Tab 1: Summary of the main characteristics for each experiment.

Figures

Fig. 1: Model / data comparison as a function of depth (color code) for the 5 simulations performed with the model in NATL4 configuration. The extraction in the North Atlantic from a previous simulation using the global ORCA2 configuration, with a relaxing time of 1 year, is also shown. Red line is the linear regression of the points. Diagonal black lines are lines $\varepsilon_{\text{Nd}} \text{ (modeled)} = \varepsilon_{\text{Nd}} \text{ (data)}$, $\varepsilon_{\text{Nd}} \text{ (modeled)} = \varepsilon_{\text{Nd}} \text{ (data)} + 3\varepsilon_{\text{Nd}}$ and $\varepsilon_{\text{Nd}} \text{ (modeled)} = \varepsilon_{\text{Nd}} \text{ (data)} - 3\varepsilon_{\text{Nd}}$. In EXP5, relaxing time varies from $\tau = 0.1$ years for margins associated with a “high ε_{Nd} ” value ($= +8$), to a relaxing time of $\tau = 0.5$ years for margins associated with a “low ε_{Nd} ” value ($= -38$). A linear relationship is set between those two extrema values. Main statistical characteristics for each experiment are reported in Tab. 1.

Fig. 2: 100m-depth ε_{Nd} distribution map, for the 5 simulations performed using the model in NATL4 configuration. EXP1: A map of the ε_{Nd} distribution at the same depth, from a previous simulation using the global ORCA2 configuration, with a relaxing time of 1 year, is also shown. Superimposed circles represent the data between 50 and 300m depth. Color scale is the same for both simulation output and data, and is nonlinear. Data are issued from Piegras and Wasserburg (1980, 1983, 1987), Stordal and Wasserburg (1986), Spivack and Wasserburg (1988), Tachikawa et al. (1999), Lacan and Jeandel (2004a, b, c, 2005a, b), Dahlqvist and Andersson (2005) and Rickli et al. (2009) and compiled by Lacan and van de Flierdt (available here: http://www.legos.obs-mip.fr/fr/equipes/geomar/results/database_may06.xls).

Fig. 3: Same as figure 2, but at 3000m depth. Data plotted (circles) are from 2500 to 3500 m depth. Data are issued from Piegras and Wasserburg (1980, 1983, 1987), Stordal and Wasserburg (1986), Spivack and Wasserburg (1988), Tachikawa et al. (1999), Lacan and Jeandel (2004a, b, c, 2005a, b), Dahlqvist and Andersson (2005) and Rickli et al. (2009) and compiled by Lacan and van de Flierdt (available here: http://www.legos.obs-mip.fr/fr/equipes/geomar/results/database_may06.xls).

Fig. 1

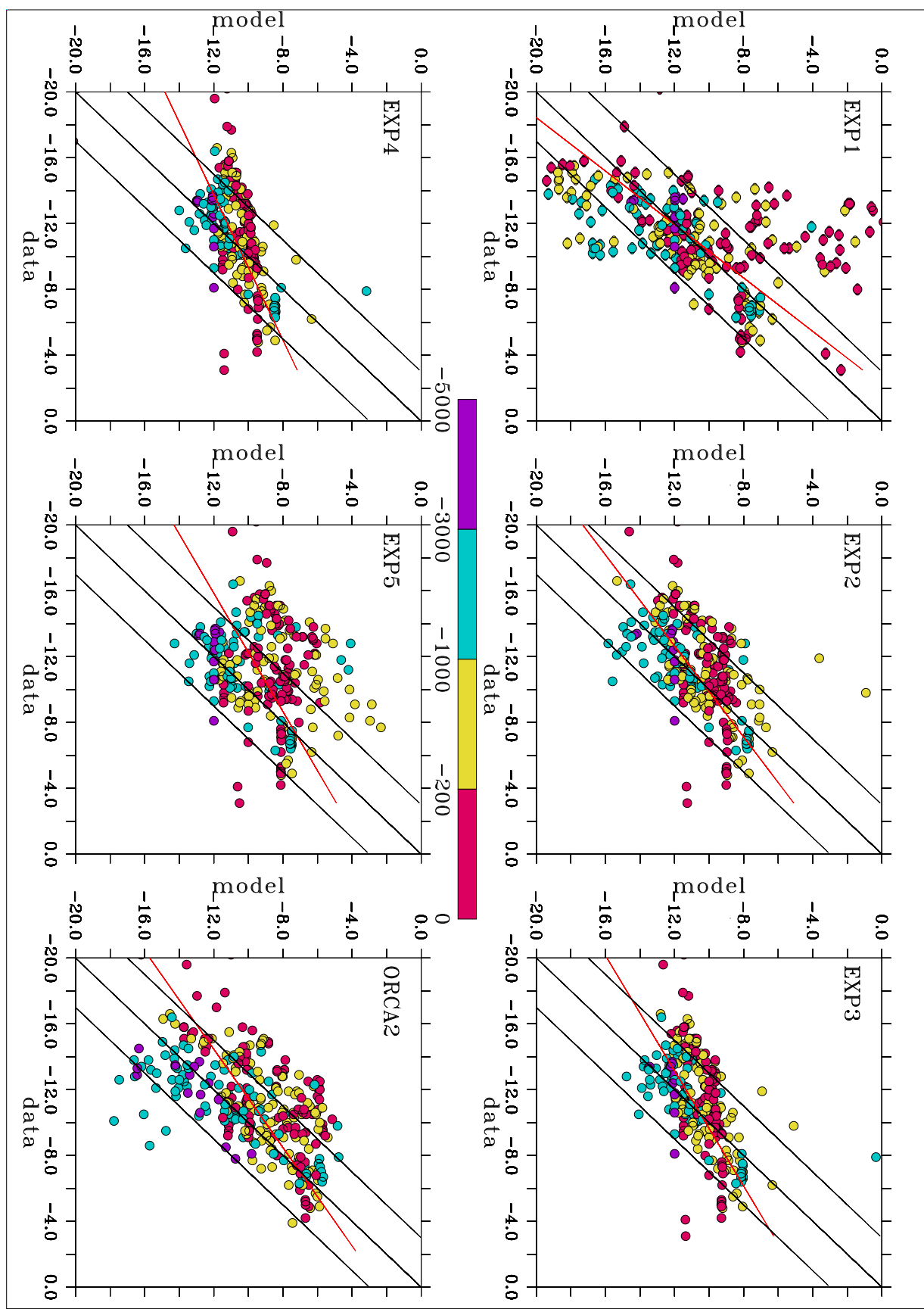


Fig. 2

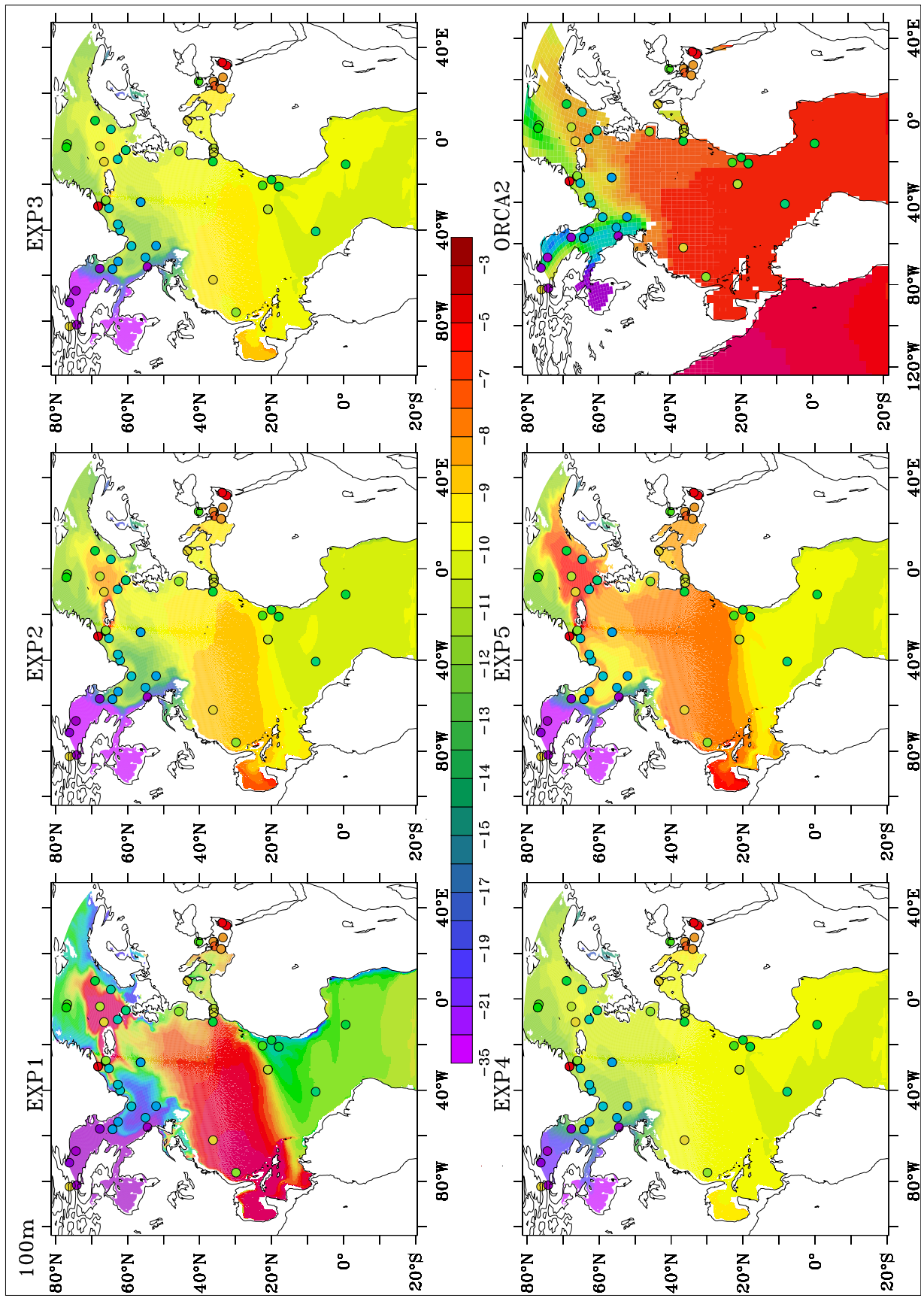
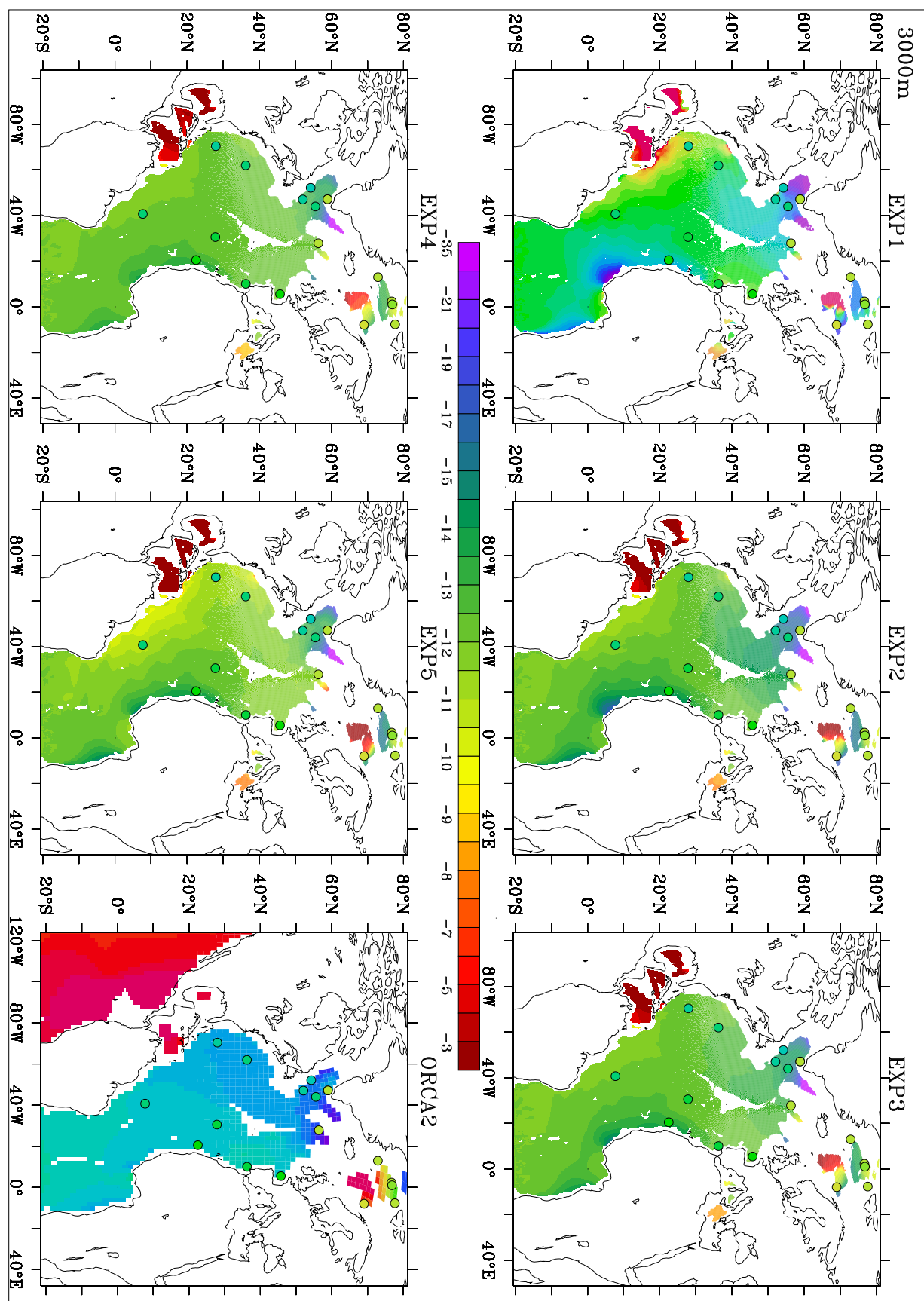


Fig. 3



Chapitre 6

Modélisation couplée de la concentration et de la composition isotopique du Nd

Sommaire

6.1	Résumé	119
6.2	<i>Reconstructing the Nd oceanic cycle using a coupled dynamical - biogeochemical model</i>	121
6.3	Compléments sur la description du modèle PISCES	140

6.1 Résumé

La première modélisation du ε_{Nd} effectuée avec le modèle dynamique NEMO-ORCA2 (cf. chapitre 3) a permis de déterminer que le processus de BE était probablement majeur pour le cycle océanique de l'élément. Or, comme on a pu le voir au cours de l'introduction (cf. section 1.2.3.1, p. 28), le paradoxe du Nd tient de l'observation du découplage entre le comportement de la CI (qui se comporte de façon conservative dans l'océan ouvert) et de la concentration en Nd (dont le profil montre une augmentation avec la profondeur). Cependant, l'hypothèse de conservativité de la CI émise jusqu'à maintenant ne prend en compte aucun processus au sein même de la colonne d'eau alors qu'il est démontré que dissolution, adsorption voire précipitation gouvernent la distribution de la concentration en Nd. Cette hypothèse devient donc trop restrictive pour appréhender le cycle océanique global du Nd et la résolution du paradoxe. Il est alors nécessaire de modéliser conjointement la CI et la concentration en Nd à l'aide d'un système de modélisation couplé entièrement pronostique qui prenne en compte à la fois le transport dynamique de Nd sous forme dissoute (modèle dynamique NEMO-ORCA2), mais aussi le transport au sein de la colonne d'eau par les particules (modèle biogéochimique PISCES, modèle d'écosystème et du cycle du carbone océanique, basé sur le Hamburg Model of Carbon Cycle version 5, HAMOCC5, (Aumont et al., 2003)). Les interactions entre les phases dissoutes et particulières sont simulées par un modèle de scavenging réversible qui établit un coefficient d'équilibre entre les deux phases en supposant un état d'équilibre de l'élément entre la phase dissoute et la phase particulaire lors de la chute des particules (Bacon et Anderson, 1982). Afin de s'astreindre de l'hypothèse de conservativité de la CI, on modélise explicitement les deux isotopes de ^{143}Nd et ^{144}Nd avant d'en recalculer le rapport pour exprimer la valeur de ε_{Nd} .

Cette approche de modélisation permet donc d'appréhender de façon beaucoup plus complète que les études précédentes le “Paradoxe du Nd” (cf. Fig. 1, p.124). Il permet à la fois de 1) **simuler le processus de scavenging réversible dans la colonne d'eau**, qui semble être nécessaire pour réconcilier les distributions de concentrations en Nd et de ε_{Nd} (Siddall et al., 2008), en cohérence avec ce qui était déjà le cas pour le *Pa* et *Th* (Siddall et al., 2005; Dutay et al., 2009), et 2) **confirmer l'hypothèse de BE** comme source océanique première de l'élément à l'océan. En effet, il est dorénavant possible de **quantifier les flux d'apport des différentes sources considérées** : BE (la source du BE est représenté par un flux d'appport de matériel à la marge, le puits - Boundary Scavenging - est pris en compte implicitement par la sédimentation), décharges fluviales dissoutes et dusts atmosphériques (cf. Fig. 2, p. 127). Dans ce modèle, l'apport de Nd particulaire en provenance des fleuves, dont le matériel échoue sur la marge continentale, est implicitement pris en compte par la source sédimentaire.

Dans un premier temps, le BE est considéré comme le “flux manquant” estimé par Tachikawa et al. (2003) lors de l'étude du cycle de Nd utilisant le modèle en boîtes Pan-dora, avec une valeur de 8.10^9 g(Nd)/an . Les apports de Nd dissous par décharge fluviale considérés sont ceux calculés à partir des valeurs de runoff du modèle NEMO (Milliman et Meade, 1983; Russell, 1990; van der Leeden et al., 1990; Weatherly et Walsh, 1996) en tenant compte d'une soustraction de 70% de Nd dans les estuaires, ce qui donne un flux

de $2.6 \cdot 10^8$ g(Nd)/an. Les apports par poussières atmosphériques ont été estimés à partir des cartes mensuelles de Tegen et Fung (1995) et un taux de dissolution de 2% (Greaves et al., 1994), soit un flux de $1.1 \cdot 10^8$ g(Nd)/an.

Une des particularités du modèle PISCES est qu'il génère deux classes de particules : les petites particules chutant à une vitesses de 3 m/jour, et les grosses particules chutant à une vitesse variant de 50 à 200 m/jour. Dutay et al. (2009) ont utilisé une configuration du modèle similaire pour la modélisation du ^{231}Pa et ^{230}Th , et ont pu mettre en évidence les difficultés liées à l'introduction des grosses particules simulées par PISCES, qui exagère le processus de scavenging dans la colonne d'eau. Ce sont les petites particules qui contrôlent le profil vertical de ^{231}Pa et ^{230}Th . Ainsi, dans le but de s'affranchir dans un premier temps de l'influence des grosses particules, les premiers tests effectués ne prenaient en compte que les particules fines. Des tests de sensibilité sur les flux de sources mais aussi sur l'influence du cycle vertical par rapport à l'advection dynamique (en augmentant les coefficients d'équilibre ou en ajoutant les grosses particules, ce qui permet d'accentuer le processus de scavenging réversible) ont été effectués.

Les résultats (Fig. 3, 4, 5, 6, p. 130, 131, 132 et 133 respectivement) montrent que pour reproduire correctement à la fois la distribution en ε_{Nd} et en concentration de Nd avec ce modèle pronostique, et ainsi résoudre le paradoxe du Nd, il est nécessaire 1) d'invoquer le processus de scavenging réversible et 2) de considérer l'apport par les sédiments sur la marge continentale comme principal terme source de Nd au réservoir océanique, avec un flux de $1.1 \cdot 10^{10}$ g(Nd)/an. Ce flux de source du BE ne représente que 3 à 5% des apports de matériel érodé par les continents et déposé sur les marges continentales par les décharges fluviales particulières. Il est en bon accord avec la première estimation par Tachikawa et al. (2003), et confirme que le BE représente entièrement les flux non considérés jusqu'alors. Associé à cette source, 65% du puit de Nd a lieu sur les marges continentales (Fig. 11, p. 135). Les autres flux considérés sont 20 fois inférieurs au flux de source sédimentaire ($4.0 \cdot 10^8$ g(Nd)/an). Cependant, malgré ces apports bien moindres, le Nd amené par ces sources est important pour reproduire les distributions de ε_{Nd} en surface et aux profondeurs intermédiaires. Le temps de résidence pour l'élément associé à ces flux d'apports est calculé entre 310 et 330 ans dans nos simulations, ce qui est sensiblement égal, voire légèrement inférieur, aux précédentes estimations disponibles (Piepgras et Wasserburg, 1983; Jeandel et al., 1995; Tachikawa et al., 1999, 2003; Siddall et al., 2008).

De la même façon que pour le ^{231}Pa et ^{230}Th , le cycle vertical du Nd est principalement contrôlé par le scavenging des petites particules. Cependant, la reproduction des champs de particules simulée en profondeur par le modèle PISCES sous-estime largement les observations, ce qui engendre une variabilité verticale des concentrations en Nd trop importante par rapport aux observations. Ce problème souligne le besoin d'améliorer les représentations des interactions dissout-particulaire, en particulier à l'aide d'autres traceurs géochimiques tels que le ^{231}Pa et ^{230}Th qui sont plus réactifs aux particules que le Nd, ou encore en insérant dans le modèle les principales phases particulières porteuses de Nd telles que les hydroxydes de fer ou de manganèse.

6.2 ***Reconstructing the Nd oceanic cycle using a coupled dynamical - biogeochemical model***

Article publié dans Biogeosciences, 6, 2829 - 2846, 2009.



Reconstructing the Nd oceanic cycle using a coupled dynamical – biogeochemical model

T. Arsouze^{1,2,*}, J.-C. Dutay¹, F. Lacan², and C. Jeandel²

¹Laboratoire des Sciences du Climat et de l'Environnement (LSCE), IPSL, CEA/UVSQ/CNRS, Orme des Merisiers, Gif-Sur-Yvette, Bat 712, 91191 Gif sur Yvette cedex, France

²Laboratoire d'Etudes en Géophysique et Océanographie Spatiale (LEGOS), UPS/CNES/CNRS/IRD, Observatoire Midi-Pyrénées, 14 av. E. Belin, 31400 Toulouse, France

* now at: Lamont-Doherty Earth Observatory (LDEO), P.O. Box 1000 61 Route 9W, Palisades, NY 10964-1000, USA

Received: 11 May 2009 – Published in Biogeosciences Discuss.: 10 June 2009

Revised: 9 November 2009 – Accepted: 24 November 2009 – Published: 4 December 2009

Abstract. The decoupled behaviour observed between Nd isotopic composition (Nd IC, also referred as ε_{Nd}) and Nd concentration cycles has led to the notion of a “Nd paradox”. While ε_{Nd} behaves in a quasi-conservative way in the open ocean, leading to its broad use as a water-mass tracer, Nd concentration displays vertical profiles that increase with depth, together with a deep-water enrichment along the global thermohaline circulation. This non-conservative behaviour is typical of nutrients affected by scavenging in surface waters and remineralisation at depth. In addition, recent studies suggest the only way to reconcile both concentration and Nd IC oceanic budgets, is to invoke a “Boundary Exchange” process (BE, defined as the co-occurrence of transfer of elements from the margin to the sea with removal of elements from the sea by Boundary Scavenging) as a source-sink term. However, these studies do not simulate the input/output fluxes of Nd to the ocean, and therefore prevents from crucial information that limits our understanding of Nd decoupling. To investigate this paradox on a global scale, this study uses for the first time a fully prognostic coupled dynamical/biogeochemical model with an explicit representation of Nd sources and sinks to simulate the Nd oceanic cycle. Sources considered include dissolved river fluxes, atmospheric dusts and margin sediment re-dissolution. Sinks are scavenging by settling particles. This model simulates the global features of the Nd oceanic cycle well, and produces a realistic distribution of Nd concentration (correct order of magnitude, increase with depth and along the conveyor belt, 65% of the simulated values fit in the $\pm 10 \text{ pmol/kg}$ envelop when compared to the data)

and isotopic composition (inter-basin gradient, characterization of the main water-masses, more than 70% of the simulated values fit in the $\pm 3 \varepsilon_{\text{Nd}}$ envelop when compared to the data), though a slight overestimation of Nd concentrations in the deep Pacific Ocean may reveal an underestimation of the particle fields by the biogeochemical model. Our results indicate 1) vertical cycling (scavenging/remineralisation) is absolutely necessary to simulate both concentration and ε_{Nd} , and 2) BE is the dominant Nd source to the ocean. The estimated BE flux ($1.1 \times 10^{10} \text{ g(Nd)/yr}$) is much higher than both dissolved river discharge ($2.6 \times 10^8 \text{ g(Nd)/yr}$) and atmospheric inputs ($1.0 \times 10^8 \text{ g(Nd)/yr}$) that both play negligible role in the water column but are necessary to reconcile Nd IC in surface and subsurface waters. This leads to a new calculated residence time of 360 yrs for Nd in the ocean. The BE flux requires the dissolution of 3 to 5% of the annual flux of continental weathering deposited via the solid river discharge to the continental margin.

1 Introduction

Variations in neodymium isotopic composition (hereafter referred as Nd IC¹) observed within the ocean reflect influences from both lithogenic inputs of the element (whose IC varies as a function of age and geological composition of

¹By convenience, we preferentially use the ε_{Nd} parameter defined as: $\varepsilon_{\text{Nd}} = \left(\left(^{143}\text{Nd} / ^{144}\text{Nd} \right)_{\text{sample}} / \left(^{143}\text{Nd} / ^{144}\text{Nd} \right)_{\text{CHUR}} - 1 \right) \cdot 10^4$, where $\left(^{143}\text{Nd} / ^{144}\text{Nd} \right)_{\text{CHUR}} = 0.512638$ is the present averaged earth value (Jacobsen and Wasserburg, 1980).



Correspondence to: T. Arsouze
(arsouze@ldeo.columbia.edu)

the continent, Jeandel et al., 2007) and the subsequent redistribution by oceanic circulation. ε_{Nd} data show that these variations are closely linked to water mass distribution at depth, and that far from any continental sources, Nd IC behaves quasi-conservatively (Piepgras and Wasserburg, 1982; Jeandel, 1993; von Blanckenburg, 1999; Goldstein and Hemming, 2003). Hence, the main water masses display characteristic ε_{Nd} values (e.g. NADW: $\varepsilon_{\text{Nd}} \approx -13.5$, AAIW and AABW: $\varepsilon_{\text{Nd}} \approx -8$). This water mass tracer property has been recently explored in the modern ocean, by measuring dissolved Nd IC and concentrations (Jeandel, 1993; Piepgras and Wasserburg, 1980; Piepgras and Wasserburg, 1982, 1987; Shimizu et al., 1994; Lacan 2004), but has also been used for reconstructing past ocean circulation from measurements in the authigenic fraction of sediments (Rutberg et al., 2000; Piotrowski et al., 2004, 2005; Gutjahr et al., 2008). The water mass tracer property of ε_{Nd} is commonly accepted, however our understanding of the complete Nd oceanic cycle is far from sufficient to allow a reliable use of this proxy as a paleocirculation tracer (Arsouze et al., 2008). In particular, the nature and the relative importance of the different Nd sources and sinks, and the dissolved/particulate interactions within the water column remain unconstrained.

Previous studies show a decoupling behaviour between Nd concentration and its IC in the open ocean (Bertram and Elderfield, 1993; Jeandel et al., 1995; Tachikawa et al., 1999, 2003; Lacan and Jeandel, 2001). This feature has been named the “Nd paradox” (Tachikawa et al., 2003; Goldstein and Hemming, 2003; Lacan and Jeandel, 2005), and results in different properties characterizing the Nd concentration and its IC distribution in the dissolved phase. Vertical profiles of Nd concentration are similar to that of all Rare Earth Elements (excluding Ce), showing low values in surface waters which increase with depth, suggesting the influence of vertical cycling (i.e. the element is scavenged at the surface, sinks with the particles, and is subsequently remineralized at depth). Furthermore, Nd concentrations increase along the thermohaline circulation, which is a typical distribution for nutrients like silicate (Elderfield, 1988), whose characteristic residence time is on the order of $\sim 2 \times 10^4$ years (Broecker and Peng, 1982). In contrast, pronounced ε_{Nd} variations between each oceanic basin indicate that the Nd residence time is shorter than the global oceanic mixing time estimated to $\sim 10^3$ years (Broecker and Peng, 1982). The conservativity of ε_{Nd} within the major oceanic water masses suggests at first sight that ε_{Nd} may vary in the open ocean only by water-mass mixing, excluding vertical cycling.

It has been demonstrated that Nd oceanic budgets that consider only dissolved river and atmospheric dust inputs fail to balance both concentration and Nd IC (Bertram and Elderfield, 1993; Tachikawa et al., 2003; van de Flierdt et al., 2004). Other sources have been suggested in order to reconcile the budget of both quantities, like submarine groundwaters (Johannesson and Burdige, 2007) or input from continental margin inputs (Tachikawa et al., 2003) subsequently

leading to the notion of “Boundary Exchange” (BE, strong interactions between continental margin and water masses by co-occurrence of sediment dissolution and Boundary Scavenging, Lacan and Jeandel, 2005). This last process has the advantage of including both a source (Boundary Source) and a sink (Boundary Scavenging) for the element, affecting the IC without changing the observed concentration when both fluxes are similar.

Resolving the “Nd Paradox” hence resides in 1) finding the vertical processes responsible for both Nd concentration increase with depth and the Nd IC conservative property in the water column, and 2) constraining the missing source which may explain the important observed Nd IC gradient observed along the thermohaline circulation together with the relatively moderated increase of Nd concentrations.

Recent modelling of oceanic ε_{Nd} , schematically presented in Fig. 1, has helped to improve our understanding of the Nd oceanic cycle. Arsouze et al. (2007, Fig. 1a), taking into account only BE as a source/sink term, simulated a realistic global ε_{Nd} distribution, suggesting that this process plays a major role in the oceanic cycle of the element. However, this first approach was based on the simulation of the Nd IC only (the Nd concentration being considered constant), using a simple relaxing term parameterization for the BE process. Given that no source flux is explicitly considered in this method, the authors could not address the “Nd paradox” and quantify the processes acting in the oceanic Nd cycle. Jones et al. (2008, Fig. 1b) considered no external sources, but prescribed surface Nd IC with observations, to conclude that ε_{Nd} behaves conservatively in the ocean (changing only by water mass mixing). However they needed to invoke an input to the deep North Pacific, which could represent an input directly to the deep ocean (e.g. by boundary exchange), or vertical cycling. We underline here that prescribing ε_{Nd} at the surface must be considered as an implicit source of Nd, in contradiction to the conclusion of these authors upon the role of mixing. Lastly, Siddall et al. (2008, Fig. 1c) have modelled explicitly both Nd concentration and IC using a reversible scavenging model to test the influence of vertical cycling in the oceanic distribution of this element. These authors suggest that both scavenging and remineralisation processes are important for explaining Nd concentration and IC profiles, consistent with the conclusions of Bertram and Elderfield (1993) and Tachikawa et al. (1999, 2003). If the results of Siddall et al. (2008) provide important implications for solving the “Nd paradox”, the authors can not in return estimate the different fluxes involved in the Nd cycle. Indeed, this study by Siddall et al. (2008) is prescribing Nd concentration and ε_{Nd} to observations in surface waters, and leaves the detailed simulation of Nd oceanic sources and sinks for further work. This parameterization, although appropriate to initiate studies using coupled dynamical/biogeochemical models, is insufficient for comprehending the full Nd oceanic cycle and investigating all parts of the “Nd paradox”. Also, prescribing Nd IC surface distribution (Jones et al., 2008; Siddall et

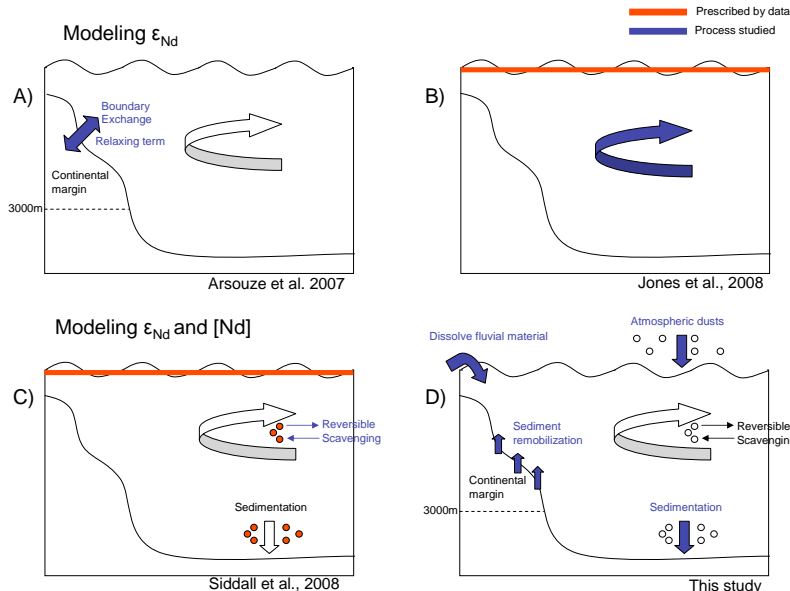


Fig. 1. Summary of the main published Nd oceanic modelling efforts using an OGCM. In each case, the different processes explicitly simulated are represented. Arrows and legends in blue underline the processes specifically studied, while red components refer to parameters prescribed by the data. **(A)** Arsouze et al. (2007), modelling only Nd IC, focused on the role of Boundary Exchange using a relaxing term and defined on the first 3000 m of the continental margin: this work highlighted the importance of this process in the element's global cycle. **(B)** Jones et al. (2008), prescribing a surface ε_{Nd} value estimated by the data suggested that Nd IC distribution can simply be explained by water mass mixing, except in the North Pacific region, where some external radiogenic inputs are required. **(C)** Using prescribed surface ε_{Nd} and Nd concentration, as well as particle fields determined by satellite observations and then interpolated within the water column, Siddall et al. (2008) showed the major role of vertical cycling (reversible scavenging process) to reproduce both ε_{Nd} and Nd concentration oceanic distribution. **(D)** In this study, besides confirming, as in Siddall et al. (2008), the role of vertical cycling in Nd oceanic distribution, we aimed to determine and quantify the different sources involved in the Nd oceanic cycle. The Boundary Exchange process is implicitly taken into account via sediment redissolution along the continental margins (source term) as well as by particle sedimentation (sink term).

al., 2008) and Nd concentration, as well as particle distribution (imposed by satellite data and then extrapolated into the water column, Siddall et al., 2008) limits any potential paleo-application.

This study continues the modelling work initiated by Tachikawa et al. (2003), Arsouze et al. (2007) and Siddall et al. (2008) using a coupled dynamical (Ocean Global Circulation Model, that generates dynamical fields)/biogeochemical (dedicated to carbon cycle and ecosystems studies, that simulates particle fields in the ocean) model. The vertical cycling is simulated using a reversible scavenging model developed for the simulation of trace elements with this coupled model (Dutay et al., 2009). Although these authors identified some limitations of this coupled model for geochemical tracer modelling, as we will see hereafter, our approach is dictated by the need for collaboration with carbon cycling modellers to initiate further studies aimed at developing the biogeochemical model. Such developments may lead to mutual advance for both carbon cycle and geochemical (Pa , Th , $\delta^{13}\text{C}$, Nd, etc...) modelling (Dutay et al., 2009), and also to a significant improvement on our understanding of the element oceanic cycles in the long term, mostly in the context of the increasing database that will result from the interna-

tional GEOTRACES effort (GEOTRACES, 2005). Also, this model is fully prognostic so that it can be easily used for paleo applications or even future climate scenarios.

We explicitly represent and quantify the different sources implied in the oceanic cycle of the element (Fig. 1d). This allows investigation from an independent approach 1) if the Boundary Source could globally represent the primordial flux of the tracer into the ocean, as suggested by Arsouze et al. (2007), and 2) if the Boundary Source and Boundary Scavenging fluxes of the BE process can be associated with the “missing flux” proposed by Tachikawa et al. (2003) in order to balance the Nd oceanic budget.

Besides being a potential component of primary importance for the Nd oceanic cycle, the determination of trace element sources is essential to better constrain the general lithogenic flux to the ocean. It is important to understand the effects of erosion fluxes on the ocean chemistry, and more particularly on primary production and sedimentation. Studying the BE process may provide substantial information on the general geochemical cycle of the elements, such as carbon and iron, which have a direct impact on climate change.

2 Modelling the Nd oceanic cycle

2.1 The dynamical model NEMO-OPA

The dynamical model used is the NEMO-OPA model (IPSL/LOCEAN, Madec, 2006). It includes the sea-ice model LIM (Louvain-La Neuve, Fichefet and Maqueda, 1997), in its low-resolution configuration ORCA2. The definition of the mesh is based on a $2^\circ \times 2^\circ \times \cos(\text{latitude})$ MERCATOR grid, with poles defined on the continents so as to get rid of singularities near the North Pole. Meridional resolution increases to 0.5° near the equator, in order to account for the specific local dynamics. Vertical resolution varies with depth, from 10 m at the surface (12 levels included in the first 125 m) to 500 m at the bottom (31 levels in total). The model is forced at the surface by heat and freshwater fluxes obtained from bulk formulae and ERS satellite data from the tropics, and NCEP/NCAR data from polar regions. Surface salinity is readjusted every 40 days to monthly WA01 data to prevent model drift (Timmermann et al., 2005). The Turbulent Kinetic Energy closure is applied to the mixing layer (Blanke and Delecluse, 1993), and subscale physics is parameterized using the Gent and McWilliams scheme (1990). The same model, in similar configurations, has previously been used for other geochemical tracer simulations (Dutay et al., 2002, 2004, 2009; Doney et al., 2004; Arsouze et al., 2007). Despite classical shortcomings of low resolution models (boundary currents too weak, crude representation of sinking of dense water during deep water masses formation), this model satisfactorily simulates the main structures of the global thermohaline circulation.

2.2 The biogeochemical model PISCES

The biogeochemical model PISCES developed for carbon cycle modelling was coupled to NEMO. It is a prognostic ecosystem and oceanic carbon cycle model, based on the Hamburg Model of Carbon Cycle version 5 (HAMOC5, Aumont et al., 2003), that represents the biogeochemical cycles of carbon, oxygen, and five nutrients of primary production (phosphates, nitrates, silicates, ammonium and iron). Redfield ratios are set constant, and are based on phytoplankton growth limited by nutrient availability (Monod, 1942).

The model features two classes of phytoplankton (nanophytoplankton and diatoms), and two classes of zooplankton (microzooplankton and mesozooplankton), as well as three non-living components, including Dissolved Organic Carbon (DOC), small and large particles. Small particles (particles between 2 and 100 μm in size) have a sinking velocity of 3 m/day (determined using the relationship between particle size and the sinking velocity established by Kriest, 2002), and consist of Particulate Organic Carbon (POCs). Large particles include Particulate Organic Carbon with a diameter larger than 100 μm (POCb), biogenic silica (BSi), calcite (CaCO_3) and lithogenic particles (atmospheric dust),

sinking with a velocity varying from 50 m/day at the surface to 300 m/day at depth. The two classes of POC interact via the processes of aggregation/disaggregation. Also a remineralization process depending on temperature (with a Q_{10} of about 1.9) is represented between POCb and POCs, and between POCs and DOC (Aumont and Bopp, 2006). The reference of 100 μm used to differentiate small and large carbonate particles (POCs and POCb, respectively) does not correspond to the definition used by experimentalists, who usually refer to large particles as particles collected in traps or by large volume filtration and has having a diameter larger than 50 μm . This being so, the size range of particles trapped remains unknown. In addition, the particles observed by the Underwater Video Profilers (UVP, Gorsky, 2000) have a diameter larger than 100 μm meaning the same limit as prescribed in the model.

A more detailed description of the model, as well as the equations used, are available as supplementary material of Aumont and Bopp (2006).

An evaluation of the particle fields generated by the PISCES model with available data collected by particle traps, satellite observations and estimations, was performed by Gehlen et al. (2006) and Dutay et al. (2009). The small particle pool represents the main particle stock at the surface (at least one order of magnitude higher than the large particle concentration). The simulated small particle concentrations in surface waters are in agreement with observations, mostly in regions of high productivity (coastal upwellings, Equatorial Pacific, Austral Ocean). In contrast, PISCES generates exaggerated vertical variations of the small particle distributions at depth in the water column leading to small particles concentrations that are too low, due to remineralization and aggregation processes. This POCs vertical gradient largely overestimates the available observations (only a factor of 50 between surface and depth, compared to a factor of 1000 for the model). In contrast, the few CaCO_3 and BSi vertical profiles observed in the water column are successfully replicated by the model (Dutay et al., 2009).

2.3 The reversible scavenging model

The increase in Nd concentration with depth suggests a reversible exchange between the dissolved and the particulate phases (Nozaki and Alibo, 2003). Nd is adsorbed onto sinking particles in the surface layers, and is redissolved at depth (we refer to this combined process as vertical cycling). In order to represent this process, we use the approach developed by Nozaki et al. (1981) and Bacon and Anderson (1982), and reformulated by Henderson et al. (1999), Siddall et al. (2005) and Dutay et al. (2009) for ^{231}Pa and ^{230}Th modelling, and Siddall et al. (2008) for Nd isotope modelling. This approach considers dissolved and particulate phases as in equilibrium within the ocean, and their relative contribution is set using an equilibrium partition coefficient K .

Considering Nd dissolved concentrations (Nd_d) and Nd particulate concentrations (concentration of Nd by unity of particle mass, Nd_p), the equilibrium partition coefficient K is defined as:

$$K = \frac{Nd_p}{Nd_d C_p} \quad (1)$$

where C_p is the mass of particles per mass of water. This coefficient K is defined for each type of particles represented in the model: small (POCs) and big (POCb) Particulate Organic Carbon, Biogenic Silica (BSi), calcite (CaCO_3) and lithogenic atmospheric dust (litho).

We model the two ^{143}Nd and ^{144}Nd isotopes independently and calculate ε_{Nd} and Nd concentration afterward. Observations do not suggest any fractionation between ^{143}Nd and ^{144}Nd dissolved, colloidal and particulate phases (Dahlqvist, 2005), as they are two isotopes of the same element, and their masses are quite similar. Partition coefficients (K) are thus assumed as being identical for the two isotopes for each particle type.

In the model, we transport for both ^{143}Nd and ^{144}Nd tracers the total concentration (Nd_T), defined as the sum of dissolved concentration (Nd_d), small (POCs: Nd_{ps}) and big (POCb, BSi, CaCO, litho: Nd_{pg}) particulate concentration:

$$Nd_T = Nd_{ps} + Nd_{pg} + Nd_d \quad (2)$$

Applying Eq. (1) to the particulate pools to express total concentration as a function of dissolved Nd concentration, we obtain:

$$Nd_T = (K_{\text{POCs}} * C_{\text{POCs}} + K_{\text{POCb}} * C_{\text{POCb}} + K_{\text{BSi}} * C_{\text{BSi}} + K_{\text{CaCO}_3} * C_{\text{CaCO}_3} + K_{\text{litho}} * C_{\text{litho}} + 1) * Nd_d \quad (3)$$

that leads to:

$$Nd_{ps} = \frac{K_{\text{POCs}} * C_{\text{POCs}}}{K_{\text{POCs}} * C_{\text{POCs}} + K_{\text{POCb}} * C_{\text{POCb}} + K_{\text{BSi}} * C_{\text{BSi}} + K_{\text{CaCO}_3} * C_{\text{CaCO}_3} + K_{\text{litho}} * C_{\text{litho}} + 1} * Nd_T \quad (4)$$

$$Nd_{pg} = \frac{K_{\text{POCb}} * C_{\text{POCb}} + K_{\text{BSi}} * C_{\text{BSi}} + K_{\text{CaCO}_3} * C_{\text{CaCO}_3} + K_{\text{litho}} * C_{\text{litho}}}{K_{\text{POCs}} * C_{\text{POCs}} + K_{\text{POCb}} * C_{\text{POCb}} + K_{\text{BSi}} * C_{\text{BSi}} + K_{\text{CaCO}_3} * C_{\text{CaCO}_3} + K_{\text{litho}} * C_{\text{litho}} + 1} * Nd_T \quad (5)$$

This allows Nd concentrations in small and big particles to be defined a posteriori as a function of partition coefficients and total Nd concentration. The main advantage of this method is that we simulate explicitly the total concentration of the two isotopes (two tracers $^{143}\text{Nd}_T$ and $^{144}\text{Nd}_T$) rather than concentration in every phase (dissolved, small particles and all big particles, meaning 12 tracers), which implies a substantial gain of computational cost.

The evolution of the total concentration of the tracer is equal to the sum of all sources (A), influence of vertical cycling (B) and physical transport by advection and diffusion (C). The conservation equation of the tracer can therefore be written:

$$\frac{\partial Nd_T}{\partial t} = \underbrace{S(Nd_T)}_{(A)} - \underbrace{\frac{\partial(w_s Nd_{ps})}{\partial z} - \frac{\partial(w_b Nd_{pg})}{\partial z}}_{(B)} - \underbrace{U \cdot \nabla Nd_T + \nabla \cdot (k \nabla Nd_T)}_{(C)} \quad (6)$$

where $S(Nd_T)$ is the Source term of the tracer (cf. Sect. 2.4). The vertical cycling represents the scavenging of Nd by the particles (w_s and w_b are the sinking velocities of small and big particles, respectively). The simulations are performed “off-line” using pre-calculated dynamical: velocity (U) and mixing coefficient (k), and particle (POCs, POCb, BSi, and CaCO_3) distributions in order to reduce computational costs, which allows us to perform some sensitivity tests.

2.4 Description of Nd sources and sink

One of our main objectives is to study the relative influence of the different sources of Nd to the ocean. We therefore explicitly represent the different source of Nd in the ocean in our simulations.

The source of the BE process (Boundary Source) is assumed to be the dissolution of a small percentage of the sediments deposited along the continental margin. We specify this source in the model by imposing an input flux on each continental margin grid point of the model between 0 and 3000 m (Boillot and Coulon, 1998). This Nd Boundary Source is written as:

$$S(Nd_T)_{\text{sed}} = \int_S F_{\text{sed}} * \text{mask}_{\text{mar}} * f(z) \quad (7)$$

where F_{sed} is the source flux of sedimentary Nd to the ocean (in g(Nd)/m²/yr). Sediment flux is assumed here as geographically constant. This hypothesis may be not verified in the ocean and disparities could play an important role on a global scale. However, considering the lack of knowledge of the processes acting on this source, it seems reasonable to set it as constant as a first approximation. F_{sed} is then determined for both ^{143}Nd and ^{144}Nd isotopes by multiplying this sediment flux to the concentration along the margin. This is set up via ε_{Nd} definition and Nd isotopes abundances, using Nd concentration and ε_{Nd} maps along the continental margins (Fig. 2a and b), both generated in a similar way by interpolation of a recent data compilation (Jeandel et al., 2007). We use the high-resolution ETOPO-2 bathymetry to calculate, for each grid cell of the model, the percentage of continental margin surface within the cell with respect to the surface of the cell (mask_{mar}). This determines, for a geographical point, the fraction of the flux that is applied at each

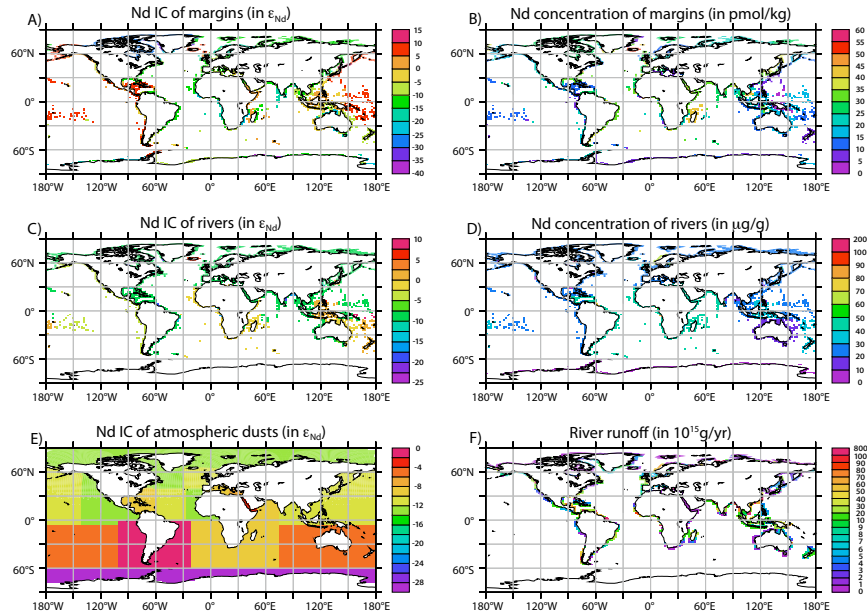


Fig. 2. Input maps applied to the model. (A) ε_{Nd} map along the continental margin determined by Jeandel et al. (2007). This input is applied to the sedimentary remobilization source F_{sed} . (B) Nd concentration map along continental margin (in $\mu\text{g/g}$) determined by Jeandel et al. (2007). This input is also applied to the sedimentary remobilization source F_{sed} . (C) ε_{Nd} map of river runoff given by Goldstein and Jacobsen (1987). (D) Nd concentration of river runoff (in ng/g) Goldstein and Jacobsen (1987); scale is non linear. (E) Interpolated ε_{Nd} map of atmospheric dust (Grousset et al., 1988; Grousset et al., 1998; Jeandel et al., 2007). Dust particle fields are provided by Tegen and Fung (1995), and Nd concentration is set constant to $20 \mu\text{g/g}$. (F) Runoff map prescribed by NEMO OGCM (in 10^{15} g/yr). Scale is non linear.

layer depth. Also, we multiply F_{sed} by a vertical function equal to 1 in the first 1000 m, then exponentially decreasing at depth ($f(z)$). This vertical variation has been applied in accordance with iron modelling (Aumont and Bopp, 2006) and previous ε_{Nd} modelling studies (Arsouze et al., 2007), because we suppose that the sediment dissolution is more important in surface waters than at depth (at the surface, dynamic activity is more vigorous, and biological processes are more important). The only available global estimation of the Nd Boundary Source flux is the “missing flux” calculated by Tachikawa et al. (2003). We therefore use their value of $8.0 \times 10^9 \text{ g(Nd)/yr}$ as a reference for our simulations.

In addition to Boundary Sources, dissolved river discharge (defined on continental margin points only) and atmospheric dust deposit are taken into account as Nd inputs in surface waters (first vertical level).

$$S(\text{Nd}_T)_{\text{surf}} = \int_S F_{\text{surf}} \quad (8)$$

where F_{surf} is the Nd flux of these two sources to the ocean (in $\text{g(Nd)/m}^2/\text{yr}$).

For dissolved river discharge we use the climatological runoff applied to the dynamical model (Fig. 2f). Nd IC (Fig. 2c) and concentrations (Fig. 2d) in river inputs are estimated using the compilation of data provided by Goldstein

and Jacobsen (1987). Using the runoff estimation provided by the NEMO model, and a subtraction of 70% of material in the estuaries (Sholkovitz, 1993; Elderfield et al., 1990; Nozaki and Zhang, 1995), we obtain a Nd dissolved flux from rivers of $2.6 \times 10^8 \text{ g(Nd)/yr}$ (Table 1). This value is lower, but the same order of magnitude, than the flux used by Tachikawa et al. (2003), equal to $5 \times 10^8 \text{ g(Nd)/yr}$.

Atmospheric dust flux is determined using monthly maps provided by Tegen and Fung (1995), in agreement with the method used for the PISCES model for nutrients (Aumont and Bopp, 2006). Nd IC of this source has been established using available data (Grousset et al., 1988, 1998). However, in the areas where no data were available, the ε_{Nd} of the dust is determined according to the ε_{Nd} value for the region of origin of the dusts (Fig. 2e). These data are available from Jeandel et al. (2007). Nd concentration in atmospheric dusts was set constant at $20 \mu\text{g/g}$ (Goldstein et al., 1984). We considered a 2% Nd dissolution rate (Greaves et al., 1994), as used by Tachikawa et al. (2003), i.e. 98% of the Nd brought by atmospheric dusts to the ocean sinks with the lithogenic particles to the sediment without interacting with the scavenging cycle. It is important to note that some uncertainty remains concerning dissolution rates of atmospheric dusts, as published data vary from 2 to 50% (Tachikawa et al., 1999; Greaves et al., 1994). However,

Table 1. Main characteristics of equilibrium partition coefficients and source fluxes for each experiment. Residence time of Nd in the ocean is calculated using the sum of flux (source or sink) and the total quantity of Nd simulated in the ocean: $\tau = Q_{\text{Nd}} / (S(\text{Nd}_T)_{\text{sed}} + S(\text{Nd}_T)_{\text{surf}})$. Also, for comparison purpose, values of equilibrium partition coefficient and residence time from Siddall et al. (2008) have been added.

Experience	Global flux Boundary Source ($S(\text{Nd}_T)_{\text{sed}}$) in g/(Nd)/yr	K_{POMs}	Equilibrium partition coefficient				Residence time (τ in years)	Total quantity of oceanic Nd (Q_{Nd} in g/(Nd))	Percentage of points where $\varepsilon_{\text{Nd}} \text{ (model)} = \varepsilon_{\text{Nd}} \text{ (data)} \pm 3 \varepsilon_{\text{Nd}}$	Percentage of points where $[\text{Nd}] \text{ (model)} = [\text{Nd}] \text{ (data)} \pm 10 \text{ pmol/kg}$
EXP1	0	1.4×10^7	0	0	0	2.3×10^6	760	4.1×10^{11}	64.76	12.21
EXP2	8×10^9	1.4×10^7	0	0	0	2.3×10^6	640	5.3×10^{12}	70.10	54.84
EXP3	8×10^9	7.7×10^7	0	0	0	2.3×10^6	150	1.3×10^{12}	63.24	21.43
EXP4	8×10^9	1.4×10^7	2.6×10^5	1.8×10^5	7.8×10^5	2.3×10^6	125	1.1×10^{12}	68.19	37.10
EXP5	1.1×10^9	1.4×10^7	5.2×10^4	3.6×10^4	1.6×10^5	4.6×10^5	360	4.2×10^{12}	71.05	64.52
Siddall et al., 2008	–	0	–	6.0×10^5	2.1×10^5	2.9×10^6	500	–	–	–
	–	0	–	6.0×10^6	2.1×10^6	2.9×10^7	100	–	–	–
	–	0	–	6.0×10^7	2.1×10^7	2.9×10^8	$10 \text{--} 30$	–	–	–
	–	0	–	0	4.9×10^5	3.8×10^6	360	–	–	–

Zhang et al. (2008) reconsidered all this data and estimated that this percentage does not exceed 10%. We finally obtain a flux of 1×10^8 g/(Nd)/yr (Table 1). Still, this value is lower than Tachikawa et al. (2003) who considered the earlier Duce et al. (1991) atmospheric dust deposit estimation, leading to a flux of 5×10^8 g/(Nd)/yr. Additional sensitivity tests on both dissolution rate ratios for atmospheric dusts and Nd dissolved river discharge (not shown here) do not significantly change the results and conclusions presented here.

The re-dissolution of solid material deposited by rivers at estuary mouths is potentially a source of great importance (Sholkovitz, 1993; von Blanckenburg et al., 1996). However, this source is implicitly taken into account via the Boundary Source (F_{sed}), as we consider that all material deposited along the continental margin is made available for sediment re-dissolution.

To balance the budget of Nd in the ocean, the only Nd sink considered is the burying of particles in the sediment at the bottom of the water column, i.e. scavenging. The particle-associated neodymium sinking at the deepest level thus leaves the model. Simulations are run until ^{143}Nd and ^{144}Nd oceanic concentrations reach an equilibrium state, which is when the sink balances global sources.

3 Simulation description

Currently the available observations of Nd concentrations in particulate phases, which allow constraint of the equilibrium partition coefficients (K) are scarce. In addition, the pool of particles generated by the PISCES model is biogenic, whereas data suggest that particulate Nd, is mainly adsorbed on the hydroxide phases coating the biogenic particles (Sholkovitz et al., 1994). Nd concentrations in iron or manganese hydroxides are at least an order of magnitude

higher than those observed for biogenic particles (Bayon et al., 2004). The fact that PISCES does not take into account these particles might be critical to simulate realistic Nd dissolved-particulate interactions. Nevertheless, observations in the Atlantic and Austral basins, give an estimation of Nd_p/Nd_d values between 0.05 and 0.1 (Jeandel et al., 1995; Tachikawa et al., 1997; Zhang et al., 2008).

Using the same model for their ^{231}Pa and ^{230}Th simulations, Dutay et al. (2009) have shown the necessity to impose a variation of the partition coefficient as a function of particle stock, in order to simulate realistic vertical profiles for both the dissolved and particulate phases. In addition, the scavenging of these tracers had to be controlled by the small particle pool, and thus the value of their partition coefficients with this pool had to be greater than those applied to the big particles. We adopt this approach for our Nd simulation and therefore set equilibrium partition coefficients for the big particle pools lower than those for the small particle pool.

Lastly, contrary to ^{231}Pa and ^{230}Th isotopes, for which scavenging coefficients can vary from several orders of magnitude depending on the particulate pool (Dutay et al., 2009), there is no current evidence from Nd data that preferential scavenging occurs when biogenic silica or carbonate dominate the particle pool. Thus we only differentiated small and big particles. The same equilibrium partition coefficient value is taken for each pool of big particles, considering their global averaged concentrations (POCb, BSi, CaCO₃ and litho). Characteristics of sensitivity tests performed on K values performed are summarized in Table 1 (EXP3, EXP4 and EXP5).

The first experiment (EXP1) takes into account only dissolved river discharge and atmospheric dust (surface sources), which are the classical sources generally considered in trace element budget studies. In addition only small

and lithogenic particles are taken into account to simulate the vertical cycle. We take $K_{\text{POMs}}=1.4\times10^7$ and $K_{\text{litho}}=2.3\times10^6$ that correspond to $\text{Nd}_P/\text{Nd}_d=0.001$ and 1×10^{-4} respectively, and $K=0$ for remaining particle pools (POMb, CaCO_3 , BSi, cf. Table 1). Although these values are much lower than the available data (Tachikawa et al., 1997), they are taken close to the same order of magnitude as in Siddall et al. (2008), and normalized to unit Nd_P/Nd_d value.

In a second experiment (EXP2), we consider the same configuration as the first simulation, but we added the sediment remobilization source (Boundary Source).

EXP3 and EXP4 test the sensitivity of the vertical cycling, considering the same sources of Nd as those considered in EXP2. For the third experiment (EXP3), we enhanced the small particle role relative to EXP2 by increasing the value of the equilibrium partition coefficient on small particles to $K_{\text{POMs}}=7.7\times10^7$ (which is equivalent to $\text{Nd}_P/\text{Nd}_d=0.005$). In the fourth experiment (EXP4) we have inserted the big particles (POMb, CaCO_3 , BSi) that were neglected in the first three experiments, the other equilibrium partition coefficients being identical to those of EXP2. The equilibrium partition coefficient value for big particles in EXP4 is set two orders of magnitude lower than for small particles, considering their respective concentrations in the PISCES model, i.e. $K_{\text{POCb}}=2.6\times10^4$, $K_{\text{BSi}}=1.8\times10^4$ and $K_{\text{CaCO}_3}=7.8\times10^4$ that correspond to $\text{Nd}_P/\text{Nd}_d=1\times10^{-5}$ (Table 1).

Finally, in the last experiment (EXP5) we optimized the characteristics of both our dynamical and biogeochemical models according to the information gained through the previous tests, in order to produce the most realistic simulation. BE flux is adjusted to $F(\text{Nd}_T)_{\text{sed}}=1.1\times10^{10} \text{ g(Nd)/yr}$ and equilibrium partition coefficients are slightly reduced compared to EXP4 for POMb, CaCO_3 , BSi and litho, and unchanged for the small particles (Table 1). Depending on the estimations, only between 3 and 5% (Milliman and Syvitski, 1992) dissolution of Nd material is required to explain our total Boundary Source flux $S(\text{Nd}_T)_{\text{sed}}=1.1\times10^{10} \text{ g(Nd)/yr}$.

4 Results

For each experiment, both Nd IC and concentration are shown along meridional sections in the Pacific Ocean (averaged zonally between 120°W and 160°W) and along the western boundary of the Atlantic Ocean (Figs. 3 and 5), where the water mass ε_{Nd} have been characterized. Figures 4 and 6 are scatter plots showing model and observations and Figs. 7, 8, 9 and 10 display horizontal maps of ε_{Nd} in surface (0–200 m) and at depth (2500–4000 m), and Nd concentration averaged over the same depth ranges, respectively.

The first experiment (EXP1) produces a satisfactory ε_{Nd} distribution in surface waters (Fig. 7), but is much too homogeneous in the deep ocean (Figs. 3, 5 and 8), particularly in the Atlantic basin, where the signature of the main water masses (NADW, AAIW, AABW) are not correctly sim-

ulated. Moreover, the Nd concentrations are at least an order of magnitude too low compared to the observations (average global value of [Nd] (model)=2.3 pmol(Nd)/kg, [Nd] (data)=21.5 pmol(Nd)/kg and only 12% of modelled Nd concentrations fit into the ±10 pmol/kg envelop when compared to the data, Fig. 5 and Table 1).

In the second experiment (EXP2, BE added), simulated ε_{Nd} values in surface waters are still in agreement with the observed data, and its distribution in the deep Atlantic Ocean is closer to the observed data. Indeed, the water masses in this basin are now simulated with very realistic ε_{Nd} values (Fig. 3): AABW (ε_{Nd} (model)) $\cong -10$, ε_{Nd} (data) $\cong -8$ but also AAIW (ε_{Nd} (model)) $\cong -8$, ε_{Nd} (data) $\cong -8$ and NADW (ε_{Nd} (model)) $\cong -13$, ε_{Nd} (data) $\cong -13$). Contrastingly, simulated ε_{Nd} values in the deep Pacific Ocean are still much too negative when compared with the observations (ε_{Nd} (model)) $\cong -10$, ε_{Nd} (data) = -4, Fig. 8), hence producing an ε_{Nd} inter-basin gradient which is much too homogeneous. As a consequence, the simulated Nd concentrations (Figs. 5 and 6) display values in the global ocean which are too high (average global value of [Nd] (model) = 35.7 pmol(Nd)/kg). The Nd vertical profiles are too pronounced, with realistic values at intermediate depth in both the Atlantic and Pacific basins, but concentrations are too low in surface waters, and too high at depth, particularly in the Pacific basin (Figs. 5 and 6). It should also be noted that this simulation produces a realistic increase of concentrations along the thermohaline circulation, in agreement with the observations.

Increasing the value of the equilibrium partition coefficient on small particles in the third experiment (EXP3) leads to a strengthening of the vertical cycling effect on simulated ε_{Nd} and Nd concentrations. It results in an undesirable vanishing of NADW isotopic signature along its pathway in the Atlantic Ocean (Fig. 3). However it improves the ε_{Nd} distribution in the deep Pacific Ocean where values becomes more radiogenic (Fig. 8), but also leads to unrealistic high values at intermediate depths. Increasing vertical cycling enhances the sedimentation process (sink of Nd), and excessively reduces the simulated Nd concentrations ([Nd] (model) = 6.8 pmol(Nd)/kg and only 21% fit into the [Nd] (model) = [Nd] (data) ±10 pmol/kg envelop, Fig. 5 and Table 1). The decrease of total Nd concentration with a constant source flux leads to a reduction of the residence time τ (defined as $\tau=(F(\text{Nd})_{\text{surf}}+F(\text{Nd})_{\text{sed}})/\text{Nd}_T$) from ~700 years in EXP1 and 2 to 150 years in EXP3 (Table 1).

Taking into account the influence of fast sinking biogenic big particles (POMb, CaCO_3 , BSi; EXP4) yields results close to those observed when increasing the equilibrium partition coefficient for small particles (EXP3): the oceanic residence time of the tracer decreases (125 years), and both Nd concentration and Nd IC in the water column are more homogeneous. Simulated Nd IC distribution in the deep Pacific Ocean is in better agreement with the observations than in EXP2, but Nd concentration becomes too low. Most of all,

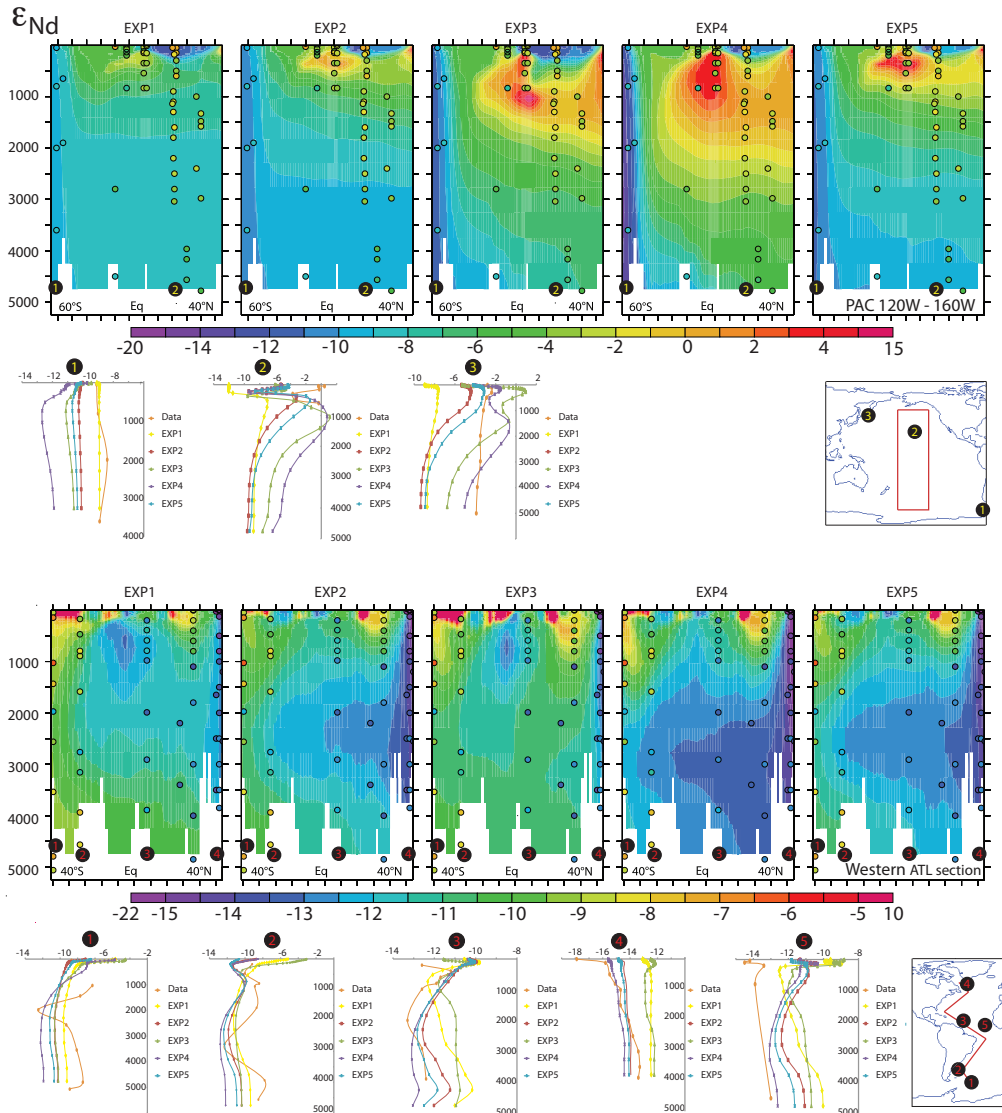


Fig. 3. Vertical ε_{Nd} sections for all simulations, in the Pacific basin averaged between 120°W and 160°W (upper panel), and along the western section of the Atlantic basin (lower panel). Superimposed circles are the data from the compilation by F. Lacan and T. van de Flierdt; http://www.legos.obs-mip.fr/fr/equipes/geomar/results/database_may06.xls (Piepgras et Wasserburg, 1982; Piepgras et Wasserburg, 1983; Stordal et Wasserburg, 1986; Piepgras et Wasserburg, 1987; Piepgras et Jacobsen, 1989; Jeandel, 1993; Jeandel et al., 1998; Lacan et Jeandel, 2001; Amakawa et al., 2004). Colour scales are the same for all simulations and data, but different for each section. For each basin, characteristic profiles are numbered and located on the associated map, and at the bottom of each transect, for each experiment. Main characteristics for each experiment are summarized in Table 1.

this simulation succeeds in keeping a realistic isotopic signature of AAIW and NADW in the Atlantic basin, although generating an AABW which is slightly too non-radiogenic (Fig. 3).

Finally in the last experiment (EXP5) in which intensity of the BE flux and values of partition coefficients of large particles have been adjusted, we simulate ε_{Nd} distribution in good agreement with the data (71% fit into the $\varepsilon_{\text{Nd}}(\text{model}) = \varepsilon_{\text{Nd}}$

(data) $\pm 3 \varepsilon_{\text{Nd}}$ envelop, Figs. 3, 4, 7 and 8). In particular, inter-basin ε_{Nd} gradients (Fig. 8) and isotopic signature of the main water masses (Fig. 3) are correctly reproduced, as well as surface isotopic signatures (Fig. 7). The increase of the Nd sink has been compensated by an increase of the sediment remobilization process (F_{sed}) to produce more coherent concentrations (Figs. 5, 6 and 10, average global value of $[\text{Nd}]$ (model)=24.6 pmol(Nd)/kg and 65% of modeled values

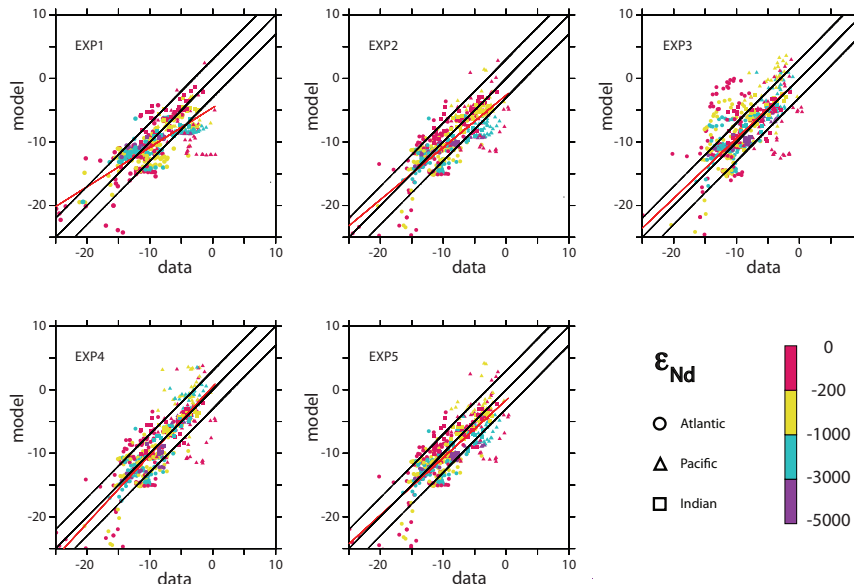


Fig. 4. ε_{Nd} model/data cross plot for each experiment as a function of depth (colour code). Circles represent the data located in the Atlantic basin; squares are data in the Indian basin and triangles are data in the Pacific basin. Red line is the linear interpolation line. Black lines represent the lines $\varepsilon_{\text{Nd}}(\text{model})=\varepsilon_{\text{Nd}}(\text{data})$ and $\varepsilon_{\text{Nd}}(\text{model})=\varepsilon_{\text{Nd}}(\text{data})\pm 3 \varepsilon_{\text{Nd}}$, which represents a characteristic value used to define a good agreement between the model and the data. Main characteristics for each experiment are summarized in Table 1. Data are from the compilation by F. Lacan and T. van de Flierdt; http://www.legos.obs-mip.fr/fr/equipes/geomar/results/database_may06.xls (see references therein).

in the $[\text{Nd}]$ (data) $\pm 10 \text{ pmol/kg}$ envelop). As observed in EXP4, the scavenging onto big particles leads to more coherent vertical gradients, even if concentrations in the surface layer remain systematically too low (Figs. 5 and 9) while concentrations generated at high northern latitudes are too high (Figs. 5, 6 and 9). Residence time is 360 years.

5 Discussion

5.1 Sensitivity of Nd oceanic cycle to sources

The above results provide valuable information about the role (or impact) of the different Nd sources on the oceanic Nd IC and concentration distributions. This information allows a better understanding of one important aspects of the Nd paradox: how can we explain the observed Nd IC gradient along the global thermohaline circulation despite a relatively small increase in Nd concentration?

In our first experiment, we first applied dissolved river discharge and atmospheric dust (F_{surf} – EXP1). This lead to simulated ε_{Nd} values that are close to the existing data at surface depths (0–200 m, Fig. 7), suggesting that these sources could control the isotopic Nd distribution in the upper ocean. However, it produces an ε_{Nd} distribution that is too homogeneous in the deep ocean, too negative in the deep Pacific, and provides a very poor simulation of water masses signature in

the Atlantic Ocean. A possible way to improve the results in the Pacific Ocean would be to enhance vertical cycling (either by increasing the equilibrium partition coefficient for the small particles or by inserting the big particles in the scavenging model), in order to export a radiogenic surface water-like signature at depth. However, this action yielded an increase in Nd sedimentation and subsequently a decrease in global Nd concentration. Since the simulated Nd concentrations in EXP1 are already an order of magnitude lower than the observed concentrations, increasing the vertical cycling does not help to reconcile both Nd IC and concentration distributions, as much as the sources are restricted to the surface only.

Another option for improving the simulated deep Pacific and Atlantic ε_{Nd} distributions was to consider an additional source of Nd to the oceanic reservoir. Sediment re-dissolution effects along the continental margin (Boundary Source) have been tested in the second experiment (EXP2). Sediment flux ($S(\text{Nd}_T)_{\text{sed}}$) intensity was estimated using first the “missing flux” proposed by Tachikawa et al. (2003) and then adjusted in EXP5. Taking into account this source largely improved our simulation of the Nd oceanic cycle, generating Nd concentrations closer to the observed data, though still an order of magnitude lower when compared to the data in surface and intermediate waters. It also greatly improved the simulation of the isotopic composition of the main water masses in the Atlantic Ocean.

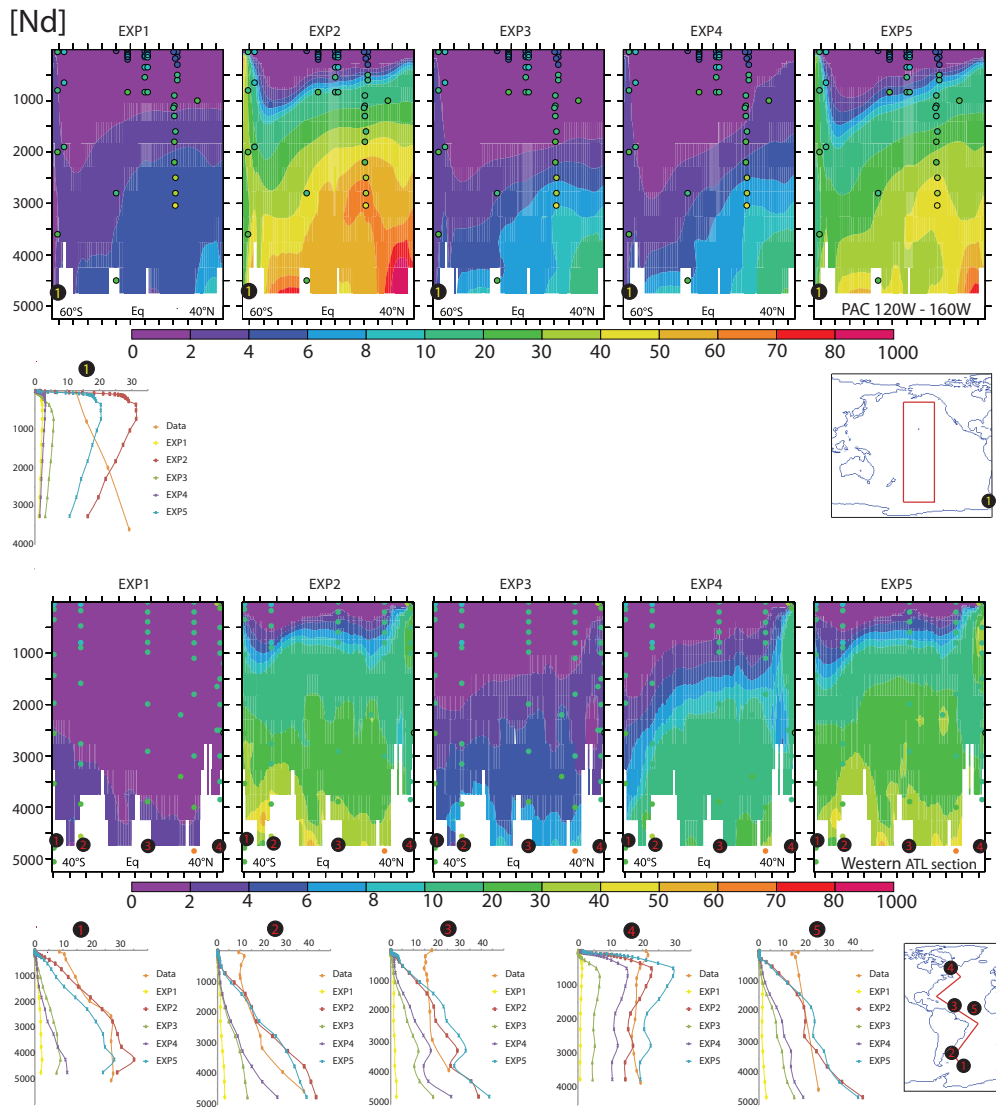


Fig. 5. Same figure as Fig. 3, for Nd concentration (in pmol/kg).

The Nd oceanic budget simulated here suggests a large predominance (about twenty times higher than cumulated other sources) of the role of the sediment re-dissolution source ($S(Nd_T)_{\text{sed}}$), meanwhile surface sources ($S(Nd_T)_{\text{surf}}$) appeared predominant for constraining surface water isotopic signatures. Other experiments, not reported here, showed that considering BE only, excluding dissolved river and dust inputs, have led to less realistic simulations of the surface ε_{Nd} distribution. As a source that influences Nd concentration and Nd IC at depth, we can preclude submarine groundwater as acting in the Boundary Sources, because their influence is mainly limited to the upper 200 m (Johannesson and Burdige, 2007).

Changing the solubility of atmospheric dust entering seawater or reducing the subtraction of dissolved material in the estuaries (which would contradict the field or experimental results) may change the $S(Nd_T)_{\text{surf}}$ value. However, this latter value still remains small compared to $S(Nd_T)_{\text{sed}}$ value, and the change does not significantly modify the Nd distribution (sensitivity tests not presented here). Boundary Source can therefore be considered as a major source of Nd in the ocean that is fundamental to simulate a realistic Nd oceanic cycle.

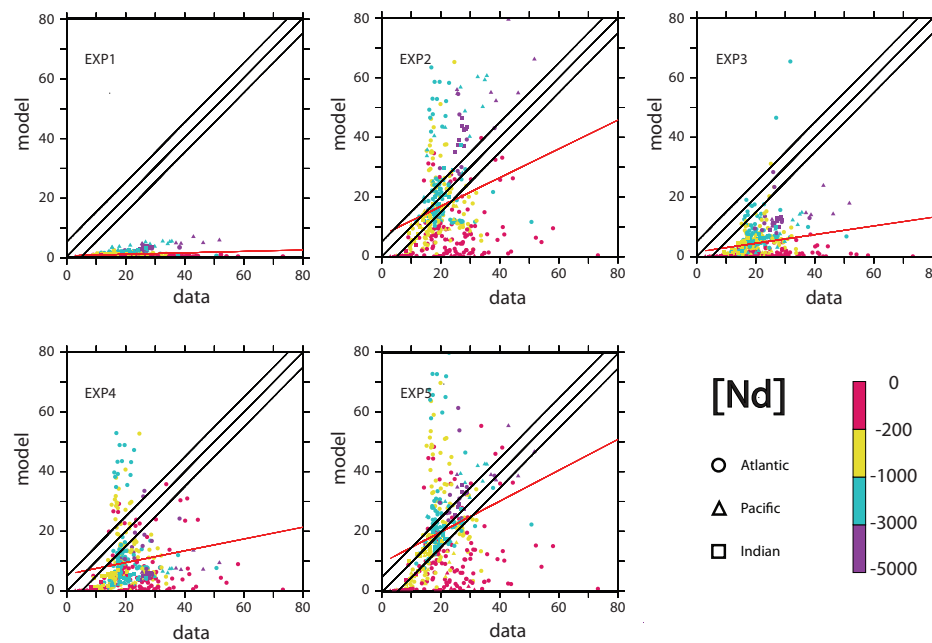


Fig. 6. Same figure as Fig. 4, for Nd concentration (in pmol/kg). Black lines represent the lines $[\text{Nd}]_{\text{model}} = [\text{Nd}]_{\text{data}}$ and $[\text{Nd}]_{\text{model}} = [\text{Nd}]_{\text{data}} \pm 10 \text{ pmol/kg}$, which represents a characteristic value used to define a good agreement between the model and the data.

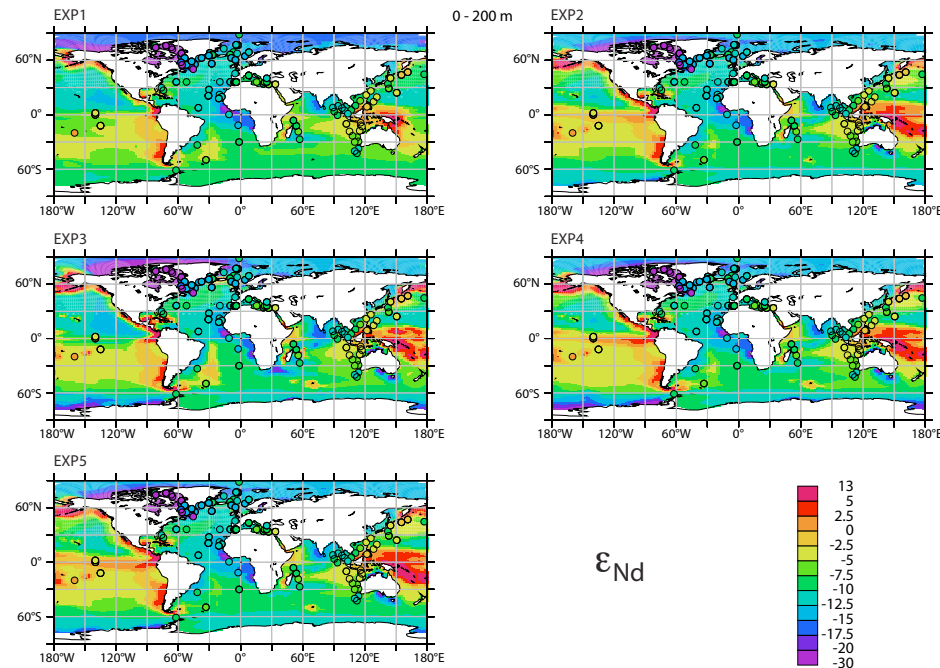


Fig. 7. Horizontal ε_{Nd} maps averaged between 0 and 200 m, for all the experiments. Superimposed circles represent the data at the same depth, from the compilation by F. Lacan and T. van de Flierdt; http://www.legos.obs-mip.fr/fr/equipes/geomar/results/database_may06.xls (see references therein) and Rickli et al. (2009). Colour scale is non linear. Main characteristics for each experiment are summarized in Table 1.

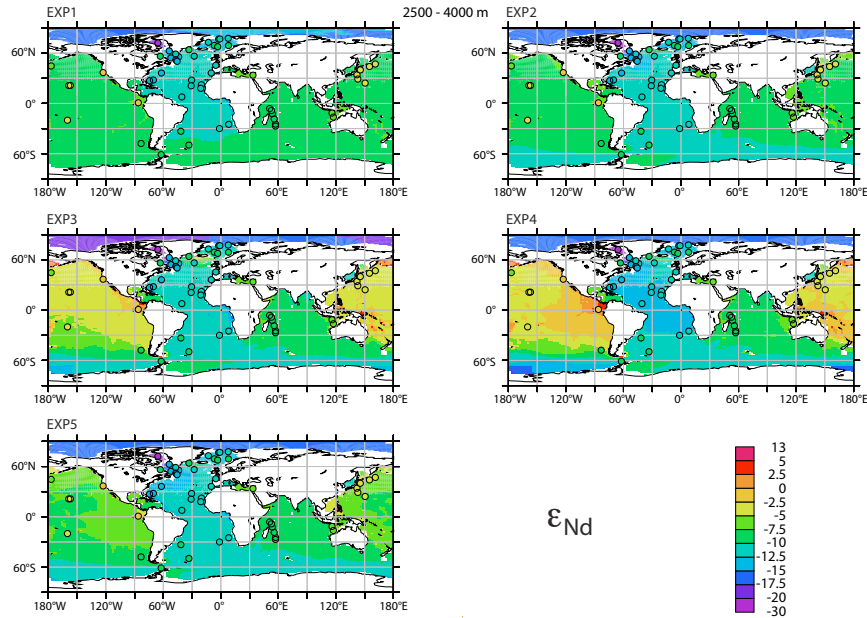


Fig. 8. Same figure as Fig. 7, with ϵ_{Nd} averaged between 2500 and 4000 m.

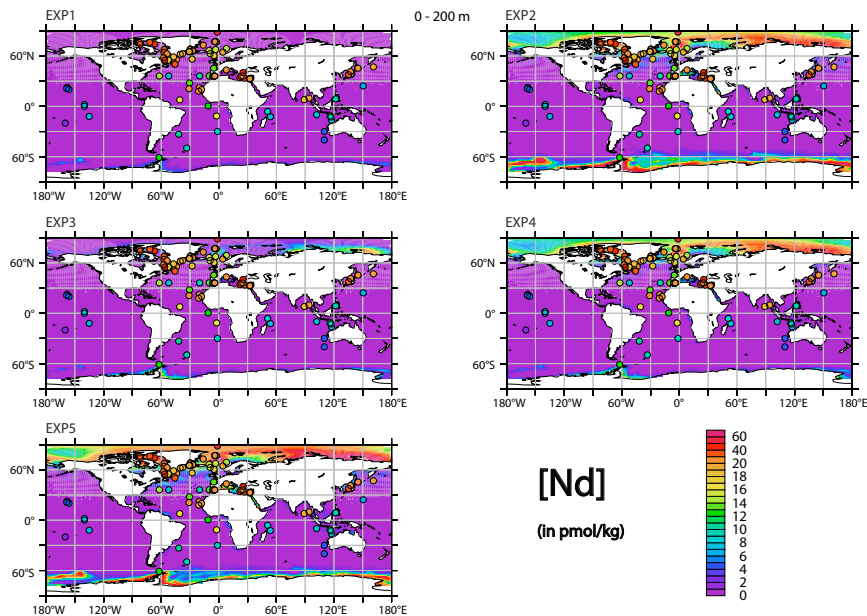


Fig. 9. Same figure as Fig. 7, for Nd concentration (in pmol/kg).

5.2 Sensitivity of Nd oceanic cycle to vertical cycling: small vs. big particles

The second experiment successfully simulated reasonable distributions of both Nd IC and concentrations. However, some discrepancies still remain, particularly in the deep Pacific where simulated deep waters had underestimated Nd IC and overestimated concentrations. Enhancing vertical cy-

cling in order to homogenize the vertical column in the Pacific is therefore pertinent, though it should maintain the outcome in the Atlantic Ocean. As the lateral isopycnal transport is more intense in the Atlantic than in the Pacific Ocean, vertical processes in this last basin might be more sensitive.

Basically, the equilibrium partition coefficient establishes the relative influence between dynamical lateral transport and vertical scavenging. Enhancing the influence of vertical

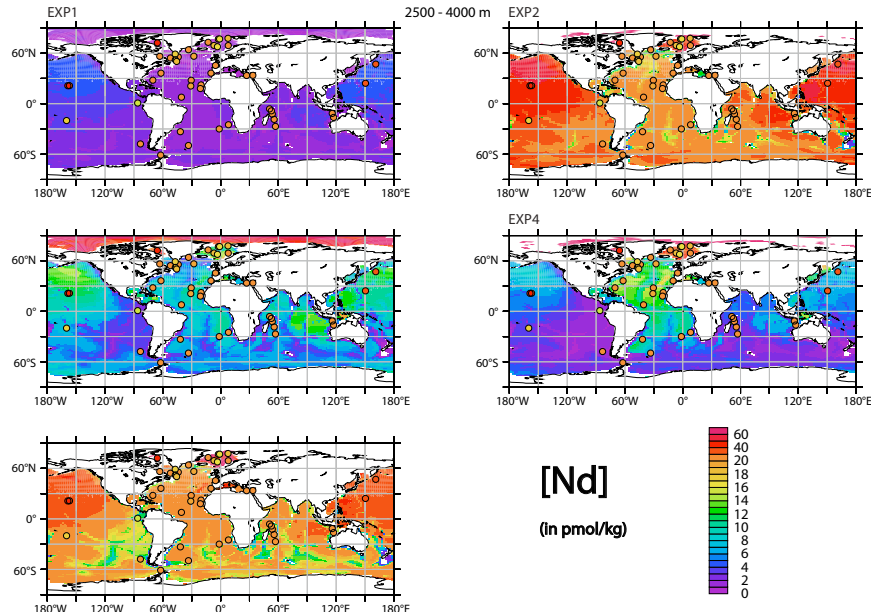


Fig. 10. Same figure as Fig. 8, for Nd concentration (in pmol/kg).

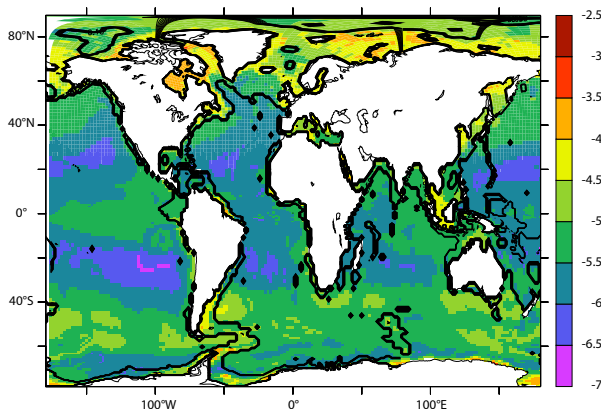


Fig. 11. Logarithmic map of Nd flux to the seafloor for experience EXP5, in $\text{g m}^{-2} \text{yr}^{-1}$. Black line delineates the continental margin area, where 64% of the Nd sink is located.

cycling, either by increasing the partition coefficient for small particles (EXP3) or by inserting big particles in the reversible scavenging model (EXP4), increases the removal of Nd from the water column and reduces our global Nd concentration to more unrealistic values (cf. Table 1, Figs. 5, 6, 9 and 10).

Both EXP3 and EXP4 successfully generated the required reduction of Nd concentration, and the formation of more radiogenic waters in the deep Pacific Ocean (Figs. 3, 4 and 8). However they differed in their performance in the Atlantic Ocean. EXP3 generated a significant degradation of simulated ε_{Nd} characteristics in the Atlantic Ocean, while EXP4

preserved and even improved agreement with the data in the Atlantic basin.

These results are consistent with those of Siddall et al. (2008), which demonstrated the importance of vertical cycling (reversible scavenging process) in reconciling Nd IC and concentration distributions, and therefore resolving the “Nd paradox”. Also, this highlights the importance of different pools of particles size in this model for setting the characteristics of the Nd isotopic distribution, and more precisely the potential role of fast sinking particles.

5.3 The “Nd paradox”

Based on information gained from previous sensitivity tests on sources and vertical cycling (EXP1 to EXP4), the configuration of our last experiment (EXP5) was adjusted to obtain the best agreement between simulations and data. We have considered the surface sources of EXP1 ($(\text{S(Nd}_T)_\text{surf}) = 2.6 \times 10^8 \text{ g(Nd)/yr}$) whereas the sediment remobilization has been slightly increased ($(\text{S(Nd}_T)_\text{sed}) = 1.1 \times 10^{10} \text{ g(Nd)/yr}$), in order to compensate for the decrease in Nd concentration caused by the insertion of big particles in the reversible scavenging model. Associated with this later source, the sink of Nd along the continental margin (corresponding to the Boundary Scavenging process), even if less important as the source, represents as much as 64% of the global Nd sink (Fig. 11), confirming that BE acts as both a major source and sink for oceanic Nd, as deduced from the observations (Lacan and Jeandel, 2005).

Due to the limited number of sensitivity experiments that could be conducted due to time constraints, this version is

not necessarily optimal, but it shows some improvements compared to the four other experiments. The resulting simulated Nd IC is in excellent agreement with the observed data (Figs. 3, 4, 7 and 8), though concentrations in the surface ocean are low (Figs. 5, 6 and 9). We attribute this bias to the particulate fields generated by the biogeochemical model PISCES. In this work, as in the ^{231}Pa and ^{230}Th simulations proposed by Dutay et al. (2009), and consistent with either experimental or field observations, the small particle pool drives the vertical cycling in the water column. It is characterized here with a higher equilibrium coefficient for small particles than for the big particle pool. However, small particle fields generated by PISCES are underestimated at depth (Dutay et al., 2009) leading to an overestimation of the Nd concentrations (as Nd is less scavenged). Improving the small particle concentration at depth in the PISCES model would likely help to smooth the vertical modelled gradient, recover deep Pacific radiogenic waters in our simulation (Figs. 3 and 8), and better simulate element cycles in the ocean, which is an important goal. Nevertheless, in our model, big particles also play an important role in reconciling deep ocean Nd concentration while keeping the Nd IC as a water-mass tracer property.

The residence time of Nd in the ocean in this last experiment is 360 years, which is in the lower range of previous estimations of ~ 300 to ~ 600 years (Pieprras and Wasserburg, 1983; Jeandel et al., 1995; Tachikawa et al., 1999, 2003; Siddall et al., 2008). This value is still consistent with the conservativity of ε_{Nd} within the major oceanic water masses. All together, these factors suggest that i) the Boundary Source is a major primordial source for Nd oceanic cycle ($\sim 95\%$ of the global sources), ii) Boundary Scavenging, resulting from vertical cycling in margin areas, is a major sink (64% of the global sink), and iii) vertical cycling in the open ocean is essential for the redistribution of Nd and its IC within the ocean interior. While the two first points provide an explanation for the BE observed in field data, the three points provide a means to reconcile the “Nd paradox”. The first estimation of the order of magnitude of the “missing flux” proposed by Tachikawa et al. (2003) is confirmed by our model results. The reversible scavenging is also essential to explain the Nd nutrient-like profile in the water column and the water mass tracer property of Nd IC, in agreement with recent REE modelling studies (Nozali and Alibo, 2003; Siddall et al., 2008; Oka et al., 2008).

However, if Boundary Sources are found to explain the large Nd IC variation observed along the global thermohaline circulation, without a large Nd concentration change (due to the associated Boundary Scavenging, Fig. 11), the question of why there is an apparent contradiction between conservative Nd IC and non conservative Nd concentrations remains to be solved. This critical point should be addressed in another dedicated study, so as to fully resolve the “Nd paradox”.

6 Conclusions

The objective of this study was to use an ocean model as a tool to better understand the Nd oceanic cycle and to work toward the resolution of the “Nd paradox”, (i.e. estimating the sources and sink of the element, and qualifying the processes acting on the element’s distribution within the reservoir). We simultaneously simulated both Nd isotopic composition and concentration using a prognostic coupled dynamical/biogeochemical model and used a reversible scavenging model to simulate the Nd transformation and sink into the ocean. We have also implemented for the first time a realistic calculation of the Nd sources, with an explicit representation of sedimentary remobilization along continental margins (source of the Boundary Exchange process) as well as dissolved river discharge and atmospheric dust sources (surface sources).

In accordance with previous results of Siddall et al. (2008) and Oka et al. (2008), vertical cycling needs to be invoked (surface removal combined with remineralisation at depth) to correctly simulate Nd isotopic composition and concentration distributions. As yet, we are unable to verify the validity of our partition coefficients because very little data are available. A strong recommendation deduced from this work is to improve our knowledge of the dissolved/particle distribution of the geochemical tracers, which the GEOTRACES program should make possible. Our performance in simulating Nd concentration is also still limited by our models. In particular, the low concentration in the small particles field simulated at depth by the PISCES model is very likely the cause for overestimated Nd concentration surface to depth gradients. This work also suggests that regarding the parameterization used and the particle distribution generated by the biogeochemical model, it is important to consider different kinds of particles, and especially their sinking velocity, in setting the characteristics of the Nd isotopic distribution. This study can therefore be used as a basis for improving the representation of the complexity of observed particle field distribution in the model, such as considering a whole continuous spectrum of particle size (Gehlen et al., 2006).

The simulations performed strongly suggest that sediment dissolution is the main Nd source to the oceanic reservoir, with a flux of $1.1 \times 10^{10} \text{ g(Nd)/yr}$ (95% of the total Nd source), whereas the associated Boundary Scavenging process represents up to 64% of the total Nd sink. Combination of these dominant source and sink at the margins are consistent with the concept of Boundary Exchange deduced from field observations. We suggest that the Boundary source is likely the “missing source term” mentioned by Tachikawa et al. (2003) that could reconcile both Nd isotopic composition and concentration oceanic budgets. The fact that this potential source has only been recently considered, despite the large amount of Nd available from solid material from river discharge deposited on the continental margin, may be explained by the very small amount of

dissolution (3–5%) required to obtain these fluxes. Dissolved river discharge (2.6×10^8 g(Nd)/yr), and atmospheric dusts (1.0×10^8 g(Nd)/yr) play a significant role only on surface ε_{Nd} distribution. The residence time of Nd in the ocean, calculated in this configuration, is estimated to be 360 years, which is in agreement with previous estimates.

The high computational cost for one simulation was a limiting factor for sensitivity tests on sources and equilibrium partition coefficients. Optimal values of parameters of the model may not be those used for experiment EXP5, but we are confident that our main results are robust. One easily envisaged improvement could be the use of the Transport Matrix Method (Katiwala et al., 2005) for this model, to better optimize these parameters.

This study highlights the predominant role of Boundary Exchange on Nd oceanic cycle, and suggests Nd isotopes as a powerful tool to quantify margin source to the ocean, which may have significance for the general ocean chemistry. However, we have no indication of chemical, biological or physical processes that act on this sediment re-dissolution. Particularly, one of the main shortcomings resides in the assumption that the input from the margin is set geographically constant, whereas some factors can act on the source (oxygen concentration, currents velocity, turbulence, temperature, organic matter deposition, etc...), leading to potentially large variations. It then appears to be quite important for the geochemical community to pay attention at continental margins/open ocean interfaces to determine if the “Boundary Scavenging” (observed for Be and Pa/Th, Anderson et al., 1990) is compensated by lithogenic inputs for other chemical tracers, and how this input is materialized (e.g. cold hydrothermalism on margins, remobilization and dissolution of sediments after resuspension, early diagenesis or both, water penetration in sediments, etc...).

This implies the need for a multi-tracer approach, in particular with highly reactive elements such as ^{231}Pa and ^{230}Th . Also, it seems inevitable to improve and adapt biogeochemical models to the simulation of trace elements, including iron manganese hydroxides and oxide crusts that are hypothesized to be main carriers of these tracers.

Acknowledgements. We thank B. O’Shea and K. Jones for the linguistic advice. We also thank F. Joos, M. Siddall and two anonymous reviewer for their careful reading of the manuscript and helpful remarks.

Edited by: F. Joos



The publication of this article is financed by CNRS-INSU.

References

- Amakawa, H., Nozaki, Y., Alibo, D. S., Zhang, J., Fukugawa, K., and Nagai, H.: Neodymium isotopic variations in Northwest Pacific waters, *Geochim. Cosmochim. Ac.*, 68, 715–727, 2004.
- Anderson, R. F., Lao, Y., Broecker, W. S., Trumbore, S. E., Hofmann, H. J., and Wolfli, W.: Boundary scavenging in the Pacific Ocean: a comparison of ^{10}Be and ^{231}Pa , *Earth Planet. Sci. Lett.*, 96, 287–304, 1990.
- Arsouze, T., Dutay, J. C., Lacan, F., and Jeandel, C.: Modeling the neodymium isotopic composition with a global ocean circulation model, *Chem. Geol.*, 239, 165–177, 2007.
- Arsouze, T., Dutay, J.-C., Kageyama, M., Lacan, F., Alkama, R., Marti, O., and Jeandel, C.: A modeling sensitivity study of the influence of the Atlantic meridional overturning circulation on neodymium isotopic composition at the Last Glacial Maximum, *Clim. Past*, 4, 191–203, 2008, <http://www.clim-past.net/4/191/2008/>.
- Aumont, O., Maier-Reimer, E., Blain, S., and Monfray, P.: An ecosystem model of the global ocean including Fe, Si, P colimitations, *Global Biogeochem. Cy.*, 17(2), 1060, doi:10.1029/2001GB001745, 2003.
- Aumont, O. and Bopp, L.: Globalizing results from ocean in situ iron fertilization studies, *Global Biogeochem. Cy.*, 20, GB2017, doi:10.1029/2005GB002591, 2006.
- Bacon, M. P. and Anderson, R. F.: Distribution of thorium isotopes between dissolved and particulate forms in the Deep-Sea., *J. Geophys. Res.*, 87, 2045–2056, 1982.
- Bayon, G., German, C. R., Burton, K. W., Nesbitt, R. W., and Rogers, N.: Sedimentary Fe-Mn oxyhydroxides as paleoceanographic archives and the role of aeolian flux in regulating oceanic dissolved REE, *Earth Planet. Sci. Lett.*, 224, 477–492, 2004.
- Bertram, C. J. and Elderfield, H.: The geochemical balance of the rare earth elements and Nd isotopes in the oceans, *Geochim. Cosmochim. Ac.*, 57, 1957–1986, 1993.
- Blanke, B. and Delecluse, P.: Variability Of The Tropical Atlantic-Ocean Simulated By A General-Circulation Model With 2 Different Mixed-Layer Physics, *J. Phys. Oceanogr.*, 23, 1363–1388, 1993.
- Boillot, G. and Coulon, C.: La déchirure continentale et l’ouverture océanique - Géologie des marges passives, Overseas Publishers Association eds., Gordon and Breach Science Publishers ed., 1998.
- Broecker, W. S. and Peng, T. H.: Tracers in the Sea, Eldigio Press, Palisades, NY, 690 pp., 1982.
- Dahlqvist, R., Andersson, P. S., and Ingri, J.: The concentration and isotopic composition of diffusible Nd in fresh and marine waters, *Earth Planet. Sci. Lett.*, 233, 9–16, 2005.
- Doney, S. C., Lindsay, K., Caldeira, K., Campin, J. M., Drange, H., Dutay, J. C., Follows, M., Gao, Y., Gnanadesikan, A., Gruber, N., Ishida, A., Joos, F., Madec, G., Maier-Reimer, E., Marshall, J. C., Matear, R. J., Monfray, P., Mouchet, A., Najjar, R., Orr, J. C., Plattner, G. K., Sarmiento, J., Schlitzer, R., Slater, R., Totterdell, I. J., Weirig, M. F., Yamanaka, Y., and Yool, A.: Evaluating global ocean carbon models: The importance of realistic physics, *Global Biogeochem. Cy.*, 18, GB3017, doi:10.1029/2003GB002150, 2004.
- Duce, R. A., Liss, P. S., Merrill, J. T., Atlas, E. L., Buat-Ménard, P., Hicks, B. B., Miller, J. M., Prospero, J. M., Arimoto, R., Church, T. M., Ellis, W., Galloway, J. N., Hansen, L., Jickells,

CHAPITRE 6 : Modélisation couplée de la concentration et de la composition isotopique du Nd

- T. D., Knap, A. H., Reinhardt, K. H., Schneider, B., Soudine, A., Tokos, J. J., Tsunogai, S., Wollast, R., and Zhou, M.: The atmospheric input of trace species to the world ocean, *Global Biogeochem. Cy.*, 5, 193–259, 1991.
- Dutay, J. C., Bullister, J. L., Doney, S. C., Orr, J. C., Najjar, R., Caldeira, K., Campin, J. M., Drange, H., Follows, M., Gao, Y., Gruber, N., Hecht, M. W., Ishida, A., Joos, F., Lindsay, K., Madec, G., Maier-Reimer, E., Marshall, J. C., Matear, R. J., Monfray, P., Mouchet, A., Plattner, G.-K., Sarmiento, J., Schlitzer, R., Slater, R., Totterdell, I. J., Weirig, M.-F., Yamamoto, Y., and Yool, A.: Evaluation of ocean model ventilation with CFC-11: comparison of 13 global ocean models, *Ocean Model.*, 42, 89–120, 2002.
- Dutay, J. C., Jean-Baptiste, P., Campin, J. M., Ishida, A., Maier-Reimer, E., Matear, R. J., Mouchet, A., Totterdell, I. J., Yamamoto, Y., Rodgers, K., Madec, G., and Orr, J. C.: Evaluation of OCMIP-2 ocean models' deep circulation with mantle helium-3, *J. Marine Syst.*, 48, 15–36, 2004.
- Dutay, J.-C., Lacan, F., Roy-Barman, M., and Bopp, L.: Influence of particle size and type on ^{231}Pa and ^{230}Th simulation with a global coupled biogeochemical-ocean general circulation model: A first approach, *Geochem. Geophys. Geosys.*, 10, Q01011, doi:10.1029/2008GC002291, 2009.
- Elderfield, H.: The oceanic chemistry of the Rare Earth Elements, *Philos. T. Roy. Soc. Lond.*, 325, 105–106, 1988.
- Elderfield, H., Upstill-Goddard, R., and Sholkovitz, E. R.: The rare earth elements in rivers, estuaries, and coastal seas and their significance to the composition of ocean waters, *Geochim. Cosmochim. Ac.*, 54, 971–991, 1990.
- Fichefet, T. and Maqueda, M. A. M.: Sensitivity of a global sea ice model to the treatment of ice thermodynamics and dynamics, *J. Geophys. Res.-Oceans*, 102, 12609–12646, 1997.
- Gehlen, M., Bopp, L., Empadin, N., Aumont, O., Heinze, C., and Ragueneau, O.: Reconciling surface ocean productivity, export fluxes and sediment composition in a global biogeochemical ocean model, *Biogeosciences*, 3, 521–537, 2006, <http://www.biogeosciences.net/3/521/2006/>.
- Gent, P. R. and McWilliams, J. C.: Isopycnal Mixing In Ocean Circulation Models, *J. Phys. Oceanogr.*, 20, 150–155, 1990.
- GEOTRACES: An international study of the marine biogeochemical cycles of trace elements and isotopes, online available at: <http://www.geotraces.org/>, 2005.
- Goldstein, S. L., O'Nions, R. K., and Hamilton, P. J.: A Sm-Nd study of atmospheric dusts and particulates from major river systems, *Earth Planet. Sci. Lett.*, 70, 221–236, 1984.
- Goldstein, S. L. and Jacobsen, S. B.: The Nd and Sr isotopic systematics of river-water dissolved material: implications for the sources of Nd and Sr in the seawater, *Chem. Geol. (Isotope Geosc. Section)*, 66, 245–272, 1987.
- Goldstein, S. L. and Hemming, S. R.: Long lived Isotopic Tracers in Oceanography, Paleoceanography, and Ice sheet dynamics, in: Treatise on Geochemistry, edited by: Elderfield, H., Elsevier Pergamon press, Amsterdam, chapter 6.17, 2003.
- Greaves, M. J., Statham, P. J., and Elderfield, H.: Rare earth element mobilization from marine atmospheric dust into seawater, *Mar. Chem.*, 46, 255–260, 1994.
- Grousset, F., Parra, M., Bory, A., Martinez, P., Bertrand, P., Shiembeld, G., and Ellam, R. M.: Saharan wind regimes traced by the Sr-Nd isotopic composition of subtropical Atlantic Sediments: last glacial maximum vs. today, *Quaternary Sci. Rev.*, 17, 395–409, 1998.
- Grousset, F. E., Biscaye, P. E., Zindler, A., Prospero, J., and Chester, R.: Neodymium isotopes as tracers in marine sediments and aerosols: North Atlantic, *Earth Planet. Sci. Lett.*, 87, 367–378, 1988.
- Gutjahr, M., Frank, M., Stirling, C. H., Keigwin, L. D., and Halliday, A. N.: Tracing the Nd isotope evolution of North Atlantic deep and intermediate waters in the Western North Atlantic since the Last Glacial Maximum from Blake Ridge sediments, *Earth Planet. Sci. Lett.*, 266, 61–77, 2008.
- Henderson, G. M., Heinze, C., Anderson, R. F., and Winguth, A. M. E.: Global distribution of the Th-230 flux to ocean sediments constrained by GCM modelling, *Deep-Sea Res. I*, 46, 1861–1893, 1999.
- Jeandel, C.: Concentration and isotopic composition of Nd in the South Atlantic Ocean, *Earth Planet. Sci. Lett.*, 117, 581–591, 1993.
- Jeandel, C., Bishop, J. K., and Zindler, A.: Exchange of Nd and its isotopes between seawater small and large particles in the Sargasso Sea, *Geochim. Cosmochim. Ac.*, 59, 535–547, 1995.
- Jeandel, C., Thouron, D., and Fieux, M.: Concentrations and Isotopic compositions of Nd in the Eastern Indian Ocean and Indonesian Straits, *Geochim. Cosmochim. Ac.*, 62, 2597–2607, 1998.
- Jeandel, C., Arsouze, T., Lacan, F., Techine, P., and Dutay, J. C.: Isotopic Nd compositions and concentrations of the lithogenic inputs into the ocean: A compilation, with an emphasis on the margins, *Chem. Geol.*, 239, 156–164, 2007.
- Johannesson, K. H. and Burdige, D. J.: Balancing the global oceanic neodymium budget: Evaluating the role of groundwater, *Earth Planet. Sci. Lett.*, 253, 129–142, 2007.
- Jones, K., Khatiwala, S., Goldstein, S. L., Hemming, S. R., and Van de Flierdt, T.: Modeling the distribution of Nd isotopes in the oceans using an offline Ocean General Circulation Model, *Earth Planet. Sci. Lett.*, 202(3–4), 610–619, 2008.
- Khatiwala, S., Visbeck, M., and Cane, M. A.: Accelerated simulation of passive tracers in ocean circulation models, *Ocean Model.*, 9, 51–69, 2005.
- Kriest, I.: Different parameterizations of marine snow in a 1D-model and their influence on representation of marine snow, nitrogen budget and sedimentation, *Deep-Sea Res. I*, 49, 2133–2162, 2002.
- Lacan, F. and Jeandel, C.: Tracing Papua New Guinea imprint on the central Equatorial Pacific Ocean using neodymium isotopic compositions and Rare Earth Element patterns, *Earth Planet. Sci. Lett.*, 186, 497–512, 2001.
- Lacan, F. and Jeandel, C.: Subpolar Mode Water formation traced by neodymium isotopic composition, *Geophys. Res. Lett.*, 31, L14306, doi:10.1029/2004GL019747, 2004.
- Lacan, F. and Jeandel, C.: Neodymium isotopes as a new tool for quantifying exchange fluxes at the continent – ocean interface, *Earth Planet. Sci. Lett.*, 232, 245–257, 2005.
- Madec, G.: NEMO reference manual, ocean dynamics component : NEMO-OPA. Preliminary version, Note du Pole de modélisation, Institut Pierre-Simon Laplace (IPSL), 27, 2006.
- Monod, J.: Recherches sur la croissance des cultures bactériennes, Hermann, Paris, 1942.
- Milliman, J. D. and Syvitski, J. P. M.: Geomorphic/tectonic con-

- trol of sediment discharge to the ocean: the importance of small mountain rivers, *J. Geol.*, 100, 325–344, 1992.
- Nozaki, Y., Horibe, Y., and Tsubota, H.: The water column distribution of thorium isotopes in the western North Pacific, *Earth Planet. Sci. Lett.*, 54, 203–216, 1981.
- Nozaki, Y. and Zhang, J.: The rare earth elements and yttrium in the coastal/offshore mixing zone of Tokyo Bay waters and Kuroshio, *Biogeochemical Processes and Ocean Flux in the Western Pacific*, edited by: Sakai, H. and Nozaki, Y., 171–184, 1995.
- Nozaki, Y. and Alibo, D.: Importance of vertical geochemical processes in controlling the oceanic profiles of dissolved rare earth elements in the northeastern Indian Ocean, *Earth Planet. Sci. Lett.*, 205, 155–172, 2003.
- Oka, A., Kato, S., and Hasumi, H.: Evaluating effect of ballast mineral on deep-ocean nutrient concentration by using an ocean general circulation model, *Global Biogeochem. Cy.*, 22, GB3004, doi:10.1029/2007GB003067, 2008.
- Piepgras, D. J., Wasserburg, G. J., and Dasch, E. G.: The isotopic composition of Nd in different ocean masses, *Earth Planet. Sci. Lett.*, 45, 223–236, 1979.
- Piepgras, D. J. and Wasserburg, G. J.: Neodymium isotopic variations in seawater, *Earth Planet. Sci. Lett.*, 50, 128–138, 1980.
- Piepgras, D. J. and Wasserburg, G. J.: Isotopic composition of neodymium in waters from the Drake Passage, *Science*, 217, 207–217, 1982.
- Piepgras, D. J. and Wasserburg, G. J.: Influence of the Mediterranean outflow on the isotopic composition of neodymium in waters of the North Atlantic, *J. Geophys. Res.*, 88, 5997–6006, 1983.
- Piepgras, D. J. and Wasserburg, G. J.: Rare earth element transport in the western North Atlantic inferred from isotopic observations, *Geochim. Cosmochim. Ac.*, 51, 1257–1271, 1987.
- Piotrowski, A. M., Goldstein, S. L., Hemming, S. R., and Fairbanks, R. G.: Intensification and variability of ocean thermohaline circulation through the last deglaciation, *Earth Planet. Sci. Lett.*, 225, 205–220, 2004.
- Rickli, J., Frank, M., and Haliday, A. N.: The Halfnium-neodymium isotopic composition of Atlantic seawater, *Earth Planet. Sci. Lett.*, 280, 118–127, 2009.
- Rutberg, R. L., Hemming, S. R., and Goldstein, S. L.: Reduced North Atlantic deep Water flux to the glacial Southern Ocean inferred from neodymium isotope ratios, *Nature*, 405, 935–938, 2000.
- Shimizu, H., Tachikawa, K., Masuda, A., and Nozaki, Y.: Cerium and neodymium ratios and REE patterns in seawater from the North Pacific Ocean, *Geochim. Cosmochim. Ac.*, 58, 323–333, 1994.
- Sholkovitz, E., Landing, W., and Lewis, B.: Ocean particle chemistry: The fractionation of Rare Earth Elements between suspended particles and seawater, *Geochim. Cosmochim. Ac.*, 58, 1567–1579, 1994.
- Sholkovitz, E. R.: The geochemistry of rare earth elements in the Amazon River estuary, *Geochim. Cosmochim. Ac.*, 57, 2181–2190, 1993.
- Siddall, M., Henderson, G. M., Edwards, N. R., Frank, M., Muller, S. A., Stocker, T. F., and Joos, F.: Pa-231/Th-210 fractionation by ocean transport, biogenic particle flux and particle type, *Earth Planet. Sci. Lett.*, 237, 135–155, 2005.
- Siddall, M., Khatiwala, S., Van de Flierdt, T., Jones, K., Goldstein, S. L., Hemming, S. R., and Anderson, R. F.: Towards explaining the Nd paradox using reversible scavenging and the Transport Matrix Method, *Earth Planet. Sci. Lett.*, 274, 448–461, 2008.
- Stordal, M. C. and Wasserburg, G. J.: Neodymium isotopic study of Baffin Bay water: sources of REE from very old terranes, *Earth Planet. Sci. Lett.*, 77, 259–272, 1986.
- Tachikawa, K., Jeandel, C., and Dupré, B.: Distribution of rare earth elements and neodymium isotopes in settling particulate material of the tropical Atlantic Ocean (EUMELI site), *Deep-Sea Res.*, 44, 1769–1792, 1997.
- Tachikawa, K., Jeandel, C., and Roy-Barman, M.: A new approach to Nd residence time in the ocean: the role of atmospheric inputs, *Earth Planet. Sci. Lett.*, 170, 433–446, 1999.
- Tachikawa, K., Athias, V., and Jeandel, C.: Neodymium budget in the ocean and paleoceanographic implications, *J. Geophys. Res.*, 108, 3254 doi:3210.1029/1999JC000285, 2003.
- Tegen, I. and Fung, I.: Contribution to the atmospheric mineral aerosol load from land surface modification, *J. Geophys. Res.*, 100, 18707–18726, 1995.
- Timmermann, R., Goosse, H., Madec, G., Fichefet, T., Ethe, C., and Duliere, V.: On the representation of high latitude processes in the ORCA-LIM global coupled sea ice-ocean model, *Ocean Model.*, 8, 175–201, 2005.
- Van De Flierdt, T., Frank, M., Lee, D. C., Halliday, A. N., Reynolds, B. C., and Hein, J. R.: New constraints on the sources and behavior of neodymium and hafnium in seawater from Pacific Ocean ferromanganese crusts, *Geochim. Cosmochim. Ac.*, 68, 3827–3843, 2004.
- von Blanckenburg, F., O’Nions, P. K., Belshaw, N. S., Gibb, A., and Hein, J. R.: Global distribution of beryllium isotopes in deep ocean water as derived from Fe-Mn crusts, *Earth Planet. Sci. Lett.*, 141, 213–226, 1996.
- von Blanckenburg, F.: Perspectives: Paleoceanography – Tracing past ocean circulation?, *Science*, 286, 1862–1863, 1999.
- Zhang, Y., Lacan, F., and Jeandel, C.: Dissolved rare earth elements tracing lithogenic inputs over the Kerguelen Plateau (Southern Ocean), *Deep-Sea Res. II*, 55, 638–652, 2008.

6.3 Compléments sur la description du modèle PISCES

Les principales caractéristiques du modèle biogéochimique PISCES sont décrites dans les articles de Aumont et al. (2003), Gehlen et al. (2006), Aumont et Bopp (2006) et Dutay et al. (2009). On s'attache ici à fournir les informations nécessaires à la compréhension de ce chapitre, en complément de la brève description fournie au chapitre 6.2, p. 121.

PISCES simule les cycles océaniques du carbone, de l'oxygène, ainsi que des cinq principaux nutriments limitant la croissance du phytoplancton : nitrates, ammonium, phosphates, silicates et fer. Il existe deux types de phytoplancton (nanophytoplancton et diatomés), et deux types de zooplancton (microzooplancton et mesozooplancton). Les rapports C/N/P sont supposés constants et les variables pronostiques sont le carbone, le fer, la chlorophylle et la silice pour le phytoplancton, et seulement le carbone pour le zooplancton. Il existe deux classes de particules de carbone organique (petites : POC_s et grosses POC_b), ainsi que des particules de silice biogénique (bSi) et de calcite ($CaCO_3$).

La figure 6.1 représente les 24 compartiments du modèle.

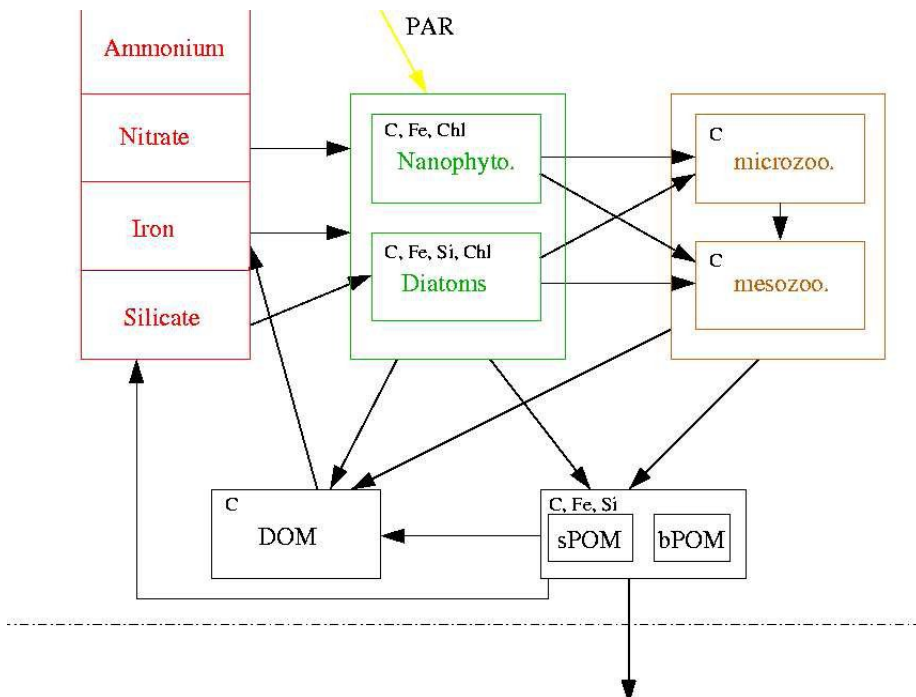


FIG. 6.1 – Schéma récapitulatif du fonctionnement du modèle biogéochimique PISCES. Les lettres dans le coin supérieur gauche de chaque réservoir représentent les éléments modélisés explicitement. Le carbone inorganique dissous, l'alcalinité et l'oxygène dissous ne sont pas représentés.

Les processus de production et consommation des particules sont établis selon Kriest et Evans (1999, 2000). Les détritus particulaires organiques sont produits par la mortalité, la production de pelotes fécales, le broutage et l'aggrégation de carbone entre les phases dissoutes et particulières. Au contraire, les processus de minéralisation ainsi que

d'excrétion contribuent au réservoir dissous.

La mortalité et le broutage des diatomés contribue au réservoir de *bSi* particulaire. La production de $CaCO_3$ est fonction de la mortalité des nanophytoplanctons, ainsi que du broutage des nanophytoplanctons par le zooplancton. 50% du carbone utilisé lors du broutage se transforme en particules, alors que le reste est consommé par le plancton. Les processus d'aggrégations sont simulés selon l'approche décrite par Kriest et Evans (1999, 2000) qui relie le nombre de particules à leur diamètre.

Le schéma 6.2, p. 141 représente les trois sources de nutriments au réservoir océanique (poussières atmosphériques, décharges fluviales et remobilisation sédimentaire), les différentes phases simulées dans le modèle, ainsi que les interactions entre chacune de ces phases.

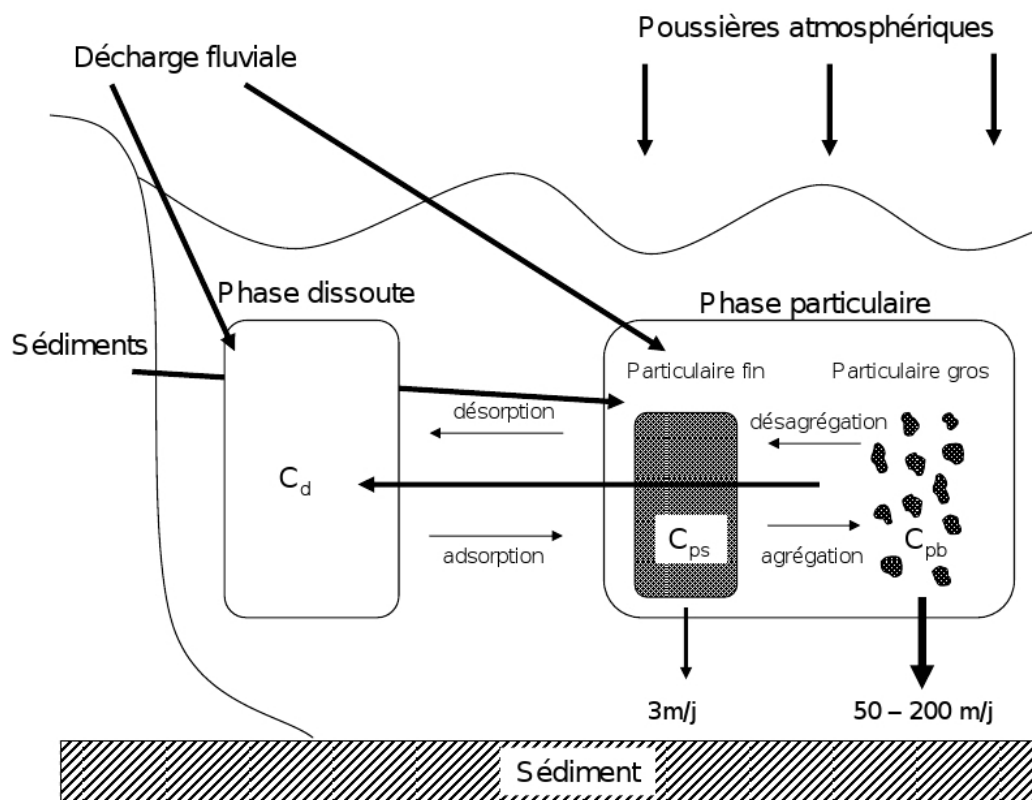


FIG. 6.2 – Schéma des sources de nutriments et des interactions entre les différentes phases dans le modèle PISCES. Schéma inspiré par Nozaki et Alibo (2003), actualisé pour PISCES

Les cartes 6.3, p. 142 et 6.4, p. 143 représentent respectivement les moyennes zonales globales et les cartes de distribution en surface pour chaque type de particules représenté dans le modèle, en g/l^{-1} .

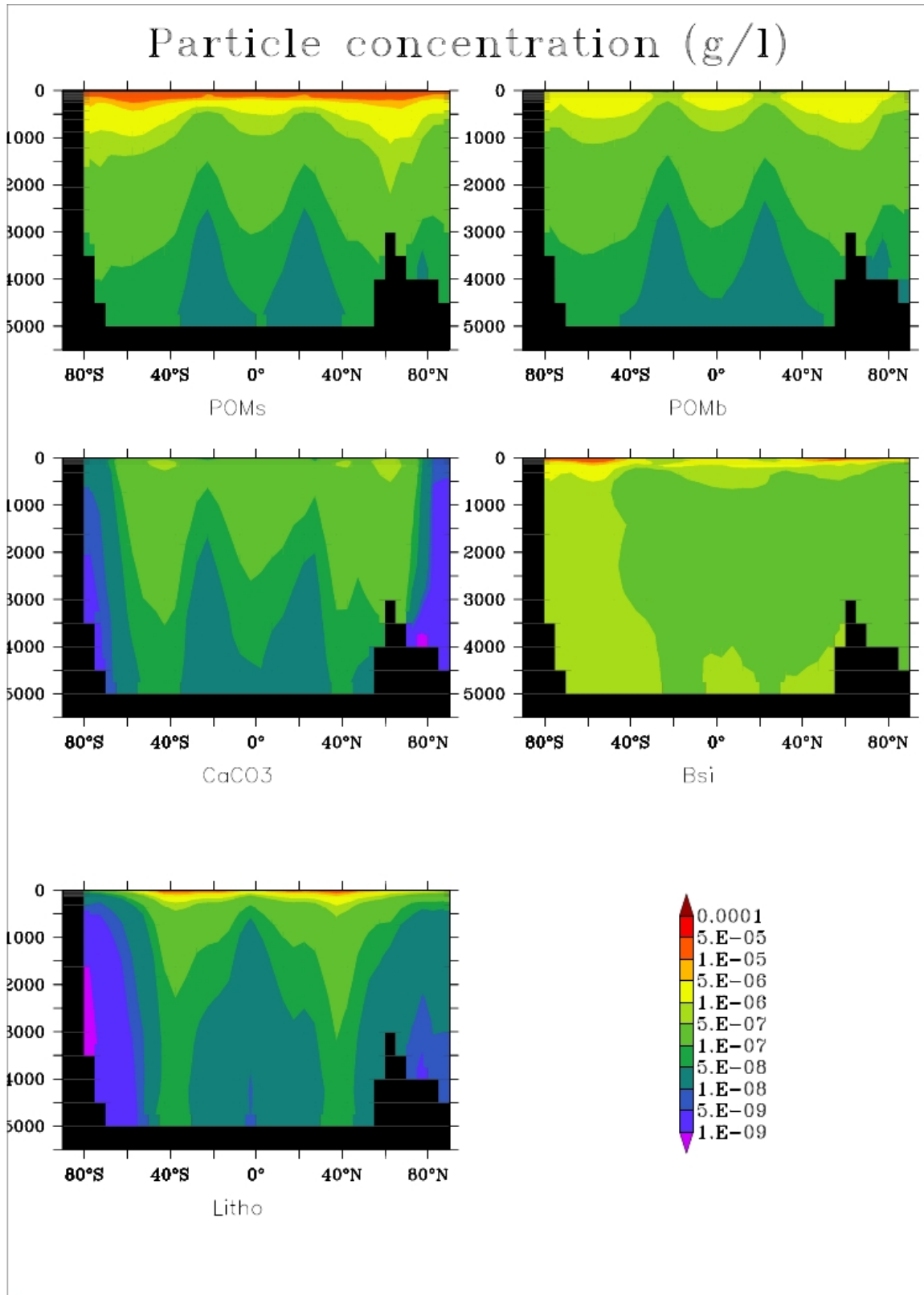


FIG. 6.3 – Concentration en particules zonale moyenne globale (en g/l), pour chaque type de particules modélisé.

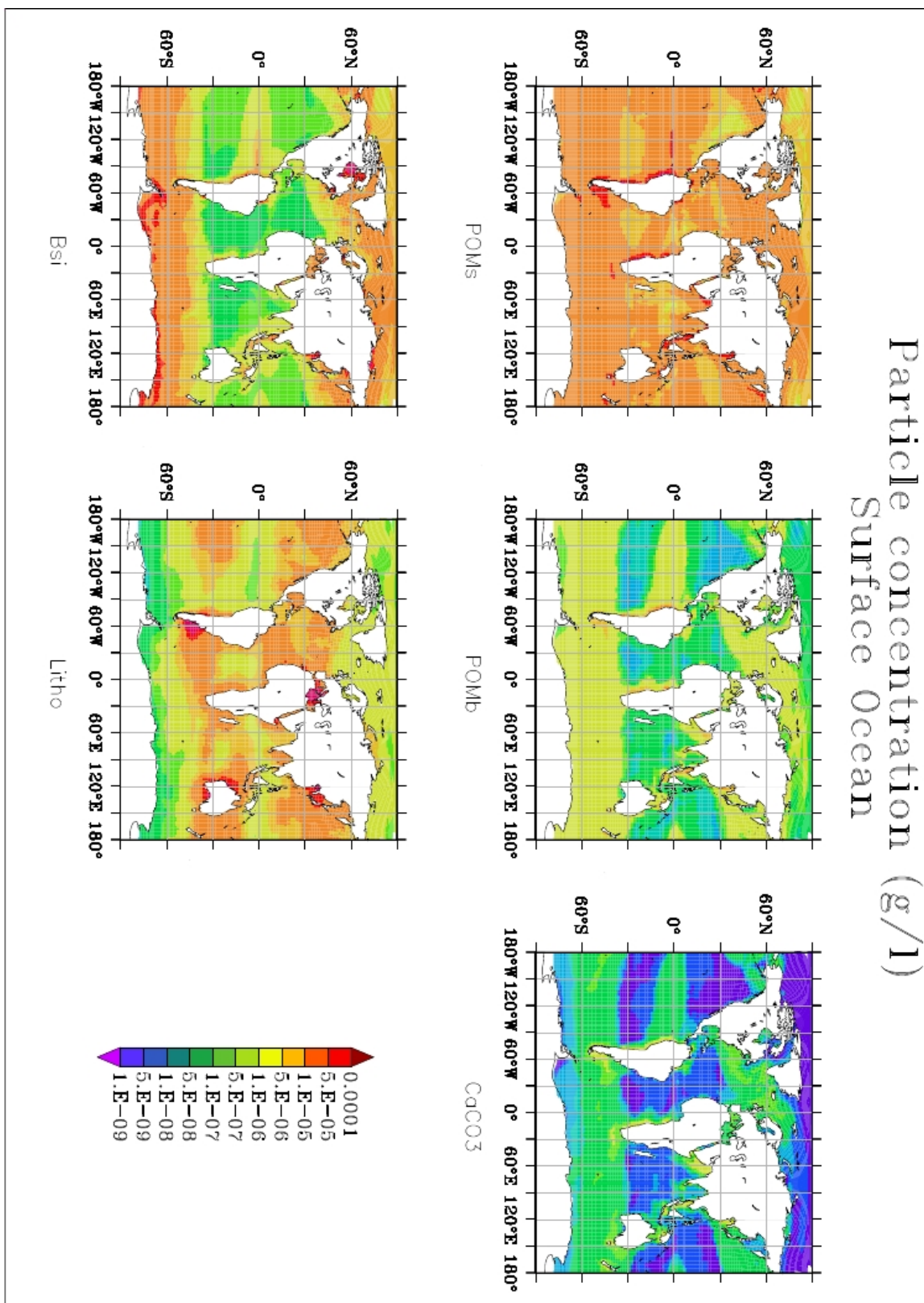


FIG. 6.4 – Carte en surface de concentration particulaire (en g/l), pour chaque type de particules modélisé.

Chapitre 7

Conclusion

Sommaire

7.1	Problématique	147
7.2	Principaux résultats	147
7.3	Perspectives	149

7.1 Problématique

L'objectif de cette thèse était d'améliorer la compréhension du cycle océanique des isotopes du Nd en insérant pour la première fois l'élément dans un modèle de circulation général océanique. Cette étude s'inscrit dans la continuité des travaux et campagnes de mesures réalisés au sein de l'équipe de géochimie marine au LEGOS. Les développements analytiques récents ont permis d'obtenir des jeux de données suffisamment conséquents pour être confrontés aux simulations numériques. Il s'inscrit aussi en continuité des travaux du LSCE sur la modélisation des traceurs géochimiques. Après l'étude des traceurs conservatifs, par exemple lors du projet OCMIP, nous avons initié la modélisation d'éléments traces non conservatifs. Plus précisément, les questions que nous nous sommes posées sont les suivantes :

1. Le “Boundary Exchange” (BE) est-il un terme source/puits important dans le cycle de ε_{Nd} ? Le cas échéant, quel est le temps d'échange entre la marge continentale et l'océan ouvert? Son influence est-elle équivalente au niveau régional et global?
2. Quelles informations sont enregistrées par ε_{Nd} dans les sédiments, et comment peuvent-elles être utilisées pour les études paléo? Peut-il être utilisé actuellement pour étudier les variations de circulation passées? Comment réagit-il sous différents forçages, différents scénarios de circulation?
3. Quelles importances relatives ont les différentes sources de Nd? Est-ce que le BE est à la fois la source et le puits qui permettent de réconcilier les bilans de concentration et de composition isotopique? Le cycle vertical de l'élément associé au transport horizontal peut-il résoudre le “paradoxe du Nd”?

Pour répondre à ces questions, nous avons utilisé différentes configurations du modèle OPA/NEMO. Dans un premier temps, nous avons modélisé la composition isotopique du Nd en paramétrisant le BE par un terme de relaxation, d'abord au niveau global, à l'Holocene et au Denier Maximum Glaciaire, puis au niveau régional dans l'Atlantique Nord. Aussi, nous avons mis en place un modèle couplé dynamique/biogéochimique entièrement pronostique pour modéliser de façon aussi complète que possible le cycle océanique de l'élément, et quantifier la contribution des flux des différents processus : sources, transport dissous (circulation) et particulaire (scavenging) et sédimentation.

7.2 Principaux résultats

Résultats sur les tests de l'influence du “Boundary Exchange” dans la distribution du ε_{Nd}

Nous avons dans un premier temps pu montrer par la modélisation que le BE joue un rôle essentiel dans la distribution océanique globale du ε_{Nd} (cf. Chapitre 3, p.49). Une paramétrisation simple du processus, par un terme de rappel entre l'océan et la marge continentale sur la valeur en ε_{Nd} , permet de reproduire de façon satisfaisante le gradient

inter-bassin (augmentation le long de la circulation thermohaline, allant de valeurs négatives en Atlantique Nord à des valeurs plus radiogéniques dans le Pacifique, en passant par des valeurs intermédiaires dans le bassin Indien) ainsi que les signatures isotopiques des principales masses d'eau. Le temps d'échange caractéristique de cet échange observé entre la marge continentale et l'océan ouvert est estimé à 6 mois en surface et variant jusqu'à 10 ans en profondeur. Toutefois, les simulations de ε_{Nd} dans le bassin Atlantique sont légèrement trop radiogéniques dans le modèle basse résolution.

Dans une étude localisée en Atlantique Nord (cf. Chapitre 5, p.101), avec un modèle régional à plus haute résolution et en utilisant la même paramétrisation du BE, nous avons pu confirmer l'importance de ce processus pour ε_{Nd} et montrer que le temps d'échange caractéristique est plus court que celui obtenu lors des premières estimations, de l'ordre de 2 mois à quelques jours, ce qui semble confirmer les variations importantes et rapides observées en mer Méditerranée (Tachikawa et al., 2004) ou encore aux îles Kerguelen (Zhang et al., 2008). Ces différences sont dues à une reproduction de la dynamique plus réaliste dans le modèle régional.

Résultats sur le proxy ε_{Nd}

La modélisation du ε_{Nd} au Dernier Maximum Glaciaire (DMG) (cf. Chapitre 4, p.79), en utilisant la configuration déjà validée précédemment avec une circulation moderne, nous a permis d'étudier les possibilités d'utilisation du ε_{Nd} en tant que traceur des variations climatiques passées, en se concentrant sur le bassin Atlantique. Deux phénomènes peuvent expliquer les variations observées dans les mesures de carottes sédimentaires : 1) une évolution des processus impliqués dans l'acquisition de la signature isotopique des masses d'eau, entraînant un changement de ε_{Nd} des "end-members" ; 2) un changement de circulation et des influences relatives des différentes masses d'eau. Les données disponibles actuellement sont encore peu nombreuses et contradictoires concernant l'évolution de la composition isotopique des "end-members" et de l'utilisation du traceur en tant que paléo-traceur de la circulation.

Nous avons pu montrer dans le cadre de cette thèse que les changements des forçages extérieurs seuls (abaissement du niveau de la mer, présence de calottes de glace à des latitudes moyennes) induisent des changements de signature isotopique des "end-members" (environ $+0.5 \varepsilon_{Nd}$). De plus, les changements de circulation océanique influent sur la distribution en ε_{Nd} (pouvant aller jusqu'à $\pm 3 \varepsilon_{Nd}$). Les résultats obtenus suggèrent une combinaison entre les changements de signature isotopique des end-members et de circulation pour expliquer certaines des variations observées entre le moderne et le DMG. Un scénario de circulation avec une prédominance de AABW dans le bassin, et une cellule de circulation méridienne vigoureuse en surface et jusqu'à 2000m est privilégié pour retrouver les données disponibles. En outre, nous faisons une recommandation de campagne de mesure dans la partie Ouest du bassin, là où les variations en ε_{Nd} sont les plus sensibles et les plus importantes aux différents scenarii de circulation.

Résultats sur la reproduction du cycle océanique du Nd

Le dernier point abordé au cours de cette thèse concerne l'étude du cycle océanique complet du Nd, et la résolution du "paradoxe du Nd" (cf. Chapitre 6, p.119). Les bilans de ε_{Nd} et de concentration en Nd effectués jusqu'alors ont montré l'impossibilité d'équilibrer conjointement les bilans des deux paramètres en considérant les sources classiques de Nd à l'océan (rivières et poussières atmosphériques). Nous nous sommes attachés à mettre en place un système de modélisation dynamique (transport dissous) et biogéochimique (transport particulaire et interactions dissous/particulaires - scavenging réversible) simulant à la fois la composition isotopique et la concentration en Nd. Un tel ensemble permet d'estimer les flux des sources en jeu dans le cycle océanique de l'élément. Nous avons ainsi pu montrer que la prise en compte du scavenging réversible permet de réconcilier les distributions en concentration et en composition isotopique, et ainsi d'améliorer notre compréhension du "paradoxe du Nd". Il reste néanmoins à comprendre pourquoi le transport vertical domine le cycle de la concentration en Nd, alors que le transport horizontal domine le cycle de ε_{Nd} . En d'autres termes, pourquoi l'augmentation de concentration en profondeur n'affecte-t-elle pas la conservativité du traceur ε_{Nd} ?

De plus, le flux d'apport de Nd par remobilisation sédimentaire calculé à 1.10^{10} g(Nd)/an est jusqu'à 25 fois plus important que les autres sources considérées (4.10^8 g(Nd)/an pour les poussières atmosphériques et les décharges fluviales dissoutes), ce qui, après les études préliminaires sur la modélisation du seul ε_{Nd} , confirme l'importance du BE comme terme source prépondérant dans le cycle océanique de l'élément. Ce flux représente entre 3 et 5 % de la matière apportée sur les marges continentales par l'érosion des continents sous forme de décharge fluviale particulaire. Néanmoins, malgré un flux très faible, les poussières atmosphériques ainsi que les décharges fluviales sous forme dissoute sont nécessaires pour réconcilier la distribution en ε_{Nd} en surface. Le temps de résidence de l'élément est calculé entre 310 ans et 330 ans, ce qui représente la valeur basse des précédentes estimations.

Enfin, cette dernière étude couplée a mis en évidence certains problèmes sur la distribution des particules marines par le modèle biogéochimique PISCES, qui sont pénalisants pour reproduire de façon plus réaliste le cycle du Nd.

7.3 Perspectives

Le programme international GEOTRACES (Geotrades, 2005) a été récemment mis en place afin de coordonner les efforts de la communauté des géochimistes à la fois sur les méthodes de mesure et sur la modélisation des traceurs. Le Nd fait partie intégrante des éléments qui vont être étudiés lors de ce programme, et les perspectives qui découlent de ce travail devraient connaître une avancée importante au cours de la prochaine décennie.

Les questions

Les résultats obtenus lors de cette thèse ont permis d'améliorer de façon appréciable les connaissances existantes sur le comportement de l'élément au sein du réservoir océanique.

Comme on a déjà pu le mentionner, le traceur ε_{Nd} est particulièrement intéressant car l'hétérogénéité géographique de ses sources permet d'identifier et de quantifier les apports de matière à l'océan, ainsi que de déterminer l'origine et l'histoire des masses d'eau. En particulier, le BE étant une source principale de l'élément au réservoir océanique, il permet d'estimer la proportion de matière déposée sur la marge continentale qui est par la suite apportée à l'océan. Ces questions sont particulièrement importantes car ces apports, qui affectent vraisemblablement de nombreux éléments autres que le Nd, peuvent influer la productivité biologique (notamment via le fer) et le cycle du carbone. Cette source sur la marge peut aussi être un outil essentiel pour considérer la dispersion des polluants anthropiques depuis les continents, ou encore pour les problématiques concernant le taux de dénudation des marges continentales et, de façon subséquente, des continents. Ce terme de BE pose donc des questions fondamentales sur les apports de matière à l'océan, via une source qui n'est pas jusqu'à présent considérée comme essentielle.

Cependant, pour mieux contraindre ce flux, il est nécessaire de comprendre quels sont les processus qui dirigent le BE. Si les résultats obtenus lors de cette thèse permettent de quantifier le flux d'échange à la marge, ils ne donnent aucune information sur les procédés qui en sont à l'origine. Cette étude soulève donc une problématique concernant les processus à l'origine de l'appport de matière de la marge continentale à l'océan. S'agit-il : des eaux souterraines, des sources hydrothermales (bien qu'identifiées en tant que puits pour les Terres Rares, ces sources sont encore peu documentées et concernent des études sur l'hydrothermalisme chaud seulement) ou de la remobilisation sédimentaire. Dans ce dernier cas, il est important de différencier si les sédiments sont déposés sur la marge continentale par la décharge particulaire des rivières, avant d'être redistribué le long de la marge par les courants marins, ou s'il s'agit d'un apport de sédiments direct des continents. Le cas échéant, quel est le processus chimique à l'origine de cet apport de matière : infiltration de l'eau au cœur des sédiments, diagénèse, dissolution de sédiments resuspendus, désorption ?

Enfin, la modélisation couplée a pu mettre en avant les lacunes affichées par le modèle biogéochimique PISCES pour reproduire des champs de particules en accord avec les données, ce qui semble pénalisant pour simuler correctement la distribution de la concentration en Nd. Cette étude a donc pointé la nécessité de mieux modéliser les champs de particules et les interactions dissous/particulaires, mais aussi de développer des outils propres à la modélisation de traceurs géochimiques.

Les propositions

Le ε_{Nd} possède des caractéristiques propres qui fournissent des renseignements non disponibles via d'autres traceurs géochimiques. Néanmoins, il est essentiel de recouper

ces informations avec celles apportées par d'autres traceurs, concernant les problèmes de circulation dynamique, de sources ou encore des interactions dissous/particulaire.

Ainsi, les isotopes $^{228}Ra/^{226}Ra$, $^{231}Pa/^{230}Th$ et les isotopes stables du Pb sont couramment utilisés en tant que traceurs de masses d'eau et il est important de pouvoir croiser les informations déduites de ces différentes données avec celles déduites de ε_{Nd} , et avec les traceurs classiques de la circulation tels que la température, la salinité, l'oxygène ou encore les nutriments.

De plus, les isotopes ^{231}Pa et ^{230}Th apportent des informations à la fois sur le taux de scavenging dans la colonne d'eau (et donc des interactions dissous/particulaires) et sur le temps de ventilation des masses d'eau. Ces indications sont complémentaires avec celles apportées par le Nd.

Il existe aussi différents traceurs de sources. Les concentrations en Terres Rares, dont les spectres sont différents selon l'origine des sources, peuvent en particulier permettre de déterminer le processus à l'origine du BE. Les isotopes ^{228}Ra et ^{226}Ra sont d'origine sédimentaire, et le rapport isotopique permet de déterminer le temps écoulé depuis le contact avec la source. Couplées avec le ε_{Nd} , ces données permettent d'obtenir le temps et le lieu du contact entre la masse d'eau et la marge, ce qui est une information primordiale pour étudier les processus, les chemins et les temps de transport vers l'océan. Enfin, le rapport $^{10}Be/^{9}Be$ ou encore les isotopes du Pb sont aussi des traceurs d'apports lithogéniques, principalement par les rivières et les poussières atmosphériques.

Ces approches multi-traceurs, semblent donc primordiales pour contraindre les flux, les temps caractéristiques d'échange et les processus des interactions entre les différentes biosphères. Il serait judicieux de focaliser ces études dans les régions interfaces entre les continents et l'océan, près des sources et là où l'activité biologique (et donc des interactions dissous/particulaires) est importante. Une modélisation multi-traceurs associée (la plupart de ces traceurs ont déjà fait l'objet d'une modélisation) dans ces études régionales serait particulièrement bénéfique pour appréhender de façon encore plus complète ces échanges.

Parmi les exemple d'études régionales, la Méditerranée est un cas particulièrement attrayant pour l'étude du Nd et des traceurs géochimiques en général. Il s'agit d'un bassin semi-fermé (ce qui permet de contraindre facilement les entrées et sorties), avec des apports considérables, en particulier dans la partie orientale du bassin, de poussières atmosphériques en provenance du Sahara et des fleuves avec des débits importants (Rhône, Po, Nil, Tarsus, etc...) dont les caractéristiques sont connues, et surtout une grande surface de marges continentales, propice à un apport sédimentaire.

On observe par exemple pour ε_{Nd} une variabilité remarquable au sein du bassin, avec des eaux entrantes à $\varepsilon_{Nd} \simeq -10, -12$ (Spivack et Wasserburg, 1988), des eaux sortantes à $\varepsilon_{Nd} \simeq -9.4$, en passant par des valeurs très radiogéniques $\varepsilon_{Nd} \simeq -4.8$ dans le bassin du Levantin (Tachikawa et al., 2004) et des sources comme le Nil à $\varepsilon_{Nd} \simeq -3$ et des aérosols à $\varepsilon_{Nd} \simeq -10$ (Frost et al., 1986).

Cette région apparaît donc comme adaptée à la mise en place une approche multi-traceurs portant spécifiquement sur la compréhension des processus dynamiques, chimiques et biologiques dirigeant les différentes sources. Il s'agit d'une étape essentielle

pour aller plus loin dans la compréhension des cycles géochimiques et du transport de matière en général. L'ordre de grandeur des flux en jeu dans le bassin méditerranéen offre la possibilité d'isoler les différentes sources. Une campagne de mesures ainsi qu'une modélisation à haute résolution près de la marge continentale pourrait permettre d'étudier les processus associés aux sources par les poussières atmosphériques (taux de dissolution, vitesse de chute des particules, reminéralisation), par les décharges fluviales, et surtout par la remobilisation sédimentaire (origine des sédiments déposés sur la marge, resuspension et dissolution à l'origine de la source, variables dynamiques favorisant la remobilisation).

Des expériences en laboratoire doivent être envisagées pour comprendre le mécanisme de cette source sédimentaire. Par exemple, il semble important d'étudier l'évolution de la CI et de la concentration en Nd d'une eau dont les caractéristiques sont connues initialement, en contact avec du matériel sédimentaire dont les propriétés sont différentes de celles de l'eau. La répétition de ce type d'expérience, avec différents types de sédiments (granitiques ou basaltiques ; boues, sables ou encore roches sédimentaires), sous différentes contraintes physiques, peut apporter des informations importantes sur la cinétique de dissolution des sédiments, et *in-fine* sur les conditions et temps d'échange entre l'eau et les sédiments.

Dans le cadre de l'étude du transport de matière des continents vers les océans, il est dans un premier temps essentiel de comprendre les processus à l'origine des apports sédimentaires à l'océan, afin de permettre une meilleure paramétrisation de cette source dans les modèles. Il serait ensuite intéressant de coupler le modèle océanique à un modèle de décharge sédimentaire des continents sur la marge continentale (que l'on a considéré homogène ici).

De plus, il semble nécessaire d'améliorer la représentation des interactions dissous/particulaires dans les modèles biogéochimiques pour espérer représenter de façon cohérente les cycles des éléments. Ainsi, une étude sur la modélisation des flux de scavenging grâce au rapport $^{231}Pa/^{230}Th$ semble importante. De même le développement de champs des phases particulières qui transportent préférentiellement les traceurs géochimiques, tels les alumino-silicates ou les hydroxydes de fer et manganèse pour le ε_{Nd} , le ^{231}Pa et ^{230}Th est une prochaine étape vers la reconstitution des cycles particulaires pour les traceurs géochimiques.

Enfin, Khatiwala et al. (2005) ont développé une méthode spécifique à la modélisation de traceurs passifs, permettant d'accélérer considérablement le temps de simulation. Une collaboration afin d'implémenter cette méthode au sein du modèle NEMO utilisé au cours de cette thèse faciliterait considérablement les travaux de modélisation, permettant une optimisation des paramètres ou encore la possibilité de d'effectuer de nombreux tests de sensibilité.

On a donc au cours de cette thèse pu vérifier la prédominance de l'influence du "Boundary Exchange" dans le cycle océanique du Nd, à la fois au niveau régional et global. Les flux de remobilisation sédimentaire calculés sont de 10 à 25 plus importants que ceux considérés par les décharges fluviales et les poussières atmosphériques. La modélisation au

Dernier Maximum Glaciaire a montré une variabilité de la distribution de la composition isotopique dans le bassin Atlantique, imputable à la fois au changement de signature des “end-members”, ainsi qu’aux variations de circulation océanique.

Afin d’améliorer notre connaissance du cycle du Nd en particulier, et des grands cycles bio-géochimiques en général, il est important de focaliser les efforts sur l’étude des processus, dans le cadre d’approches multi-traceurs à la fois pour les données et la modélisation. La Méditerranée, bien qu’étant un cas un peu particulier, semble un bassin adapté à ce type d’étude grâce aux flux importants des différentes sources qui affectent le bassin. Il serait aussi souhaitable de mettre en place des protocoles expérimentaux de laboratoire afin d’étudier le processus de BE. Concernant la modélisation, il est primordial d’améliorer la reproduction par les modèles de la distribution des champs de particules, et de se focaliser sur les phases porteuses des traceurs géochimiques. Enfin, la mise en place de méthodes adaptées aux traceurs passifs paraît inévitable pour simplifier les approches de modélisation.

Annexe A

Compilation de données

47	: Kiska Island (Al Is)	: 177.00	: 53.00	: 08.5	: 11.50	: (7)	: basalt rock n °54-452	: P
48	: At ocean (W Morocco)	: 352.99	: 34.20	: -11.7	: 35.30	: (8)	: core n° K23 (730m)	: At
49	: At ocean (W Morocco)	: 349.75	: 32.24	: -13.0	: 33.00	: (8)	: core n° K25 (3165m)	: At
50	: At ocean (W Morocco)	: 343.61	: 25.02	: -15.3	: 32.20	: (8)	: core n° K20b (1445m)	: At
51	: At ocean (W Morocco)	: 342.84	: 23.44	: -14.4	: 27.40	: (8)	: core n° K15 (1000m)	: At
52	: At ocean (W Mauritania)	: 341.85	: 21.20	: -14.8	: 24.50	: (8)	: core n° K09 (2002m)	: At
53	: At ocean (W Mauritania)	: 342.83	: 19.29	: -14.3	: 21.90	: (8)	: core n° K02 (1407m)	: At
53	: At ocean (W Senegal)	: 341.43	: 13.50	: -15.7	: 32.40	: (8)	: core n° VM22-196 (3728m)	: At
54	: At ocean (W Guinea)	: 338.93	: 04.55	: -18.6	: 40.00	: (8)	: core n° VM22-189 (2525m)	: At
55	: Canaries Island	: 346.00	: 28.00	: -12.8	: 34.60	: (8), (2)	: aerosols (average 2 samp.) ⁵⁵	: At
56	: off St Louis (Senegal)	: 341.70	: 17.00	: -14.6	: 13.90	: (8)	: aerosols n° SL	: At
57	: Cap Verde Basin	: 335.50	: 12.50	: -12.0	: 37.10	: (8)	: aerosols (average 2 samp.) ⁵⁷	: At
58	: Sierra Leone Basin	: 342.50	: 08.00	: -14.4	: 37.90	: (8)	: aerosols n° A18	: At
59	: Corsica	: 9.00	: 42.00	: -13.0	: 28.02	: (8)	: aerosols (average 5 samp.) ⁵⁹	: M
60	: Oujda (Morocco)	: 358.55	: 34.41	: -11.8	: 29.90	: (8)	: loess n°Ouj	: At
61	: Er Rachidia (Morocco)	: 355.75	: 31.58	: -13.6	: 32.70	: (8)	: loess n°Elra	: At
62	: Foum el Hassan (Morocco)	: 351.45	: 28.59	: -17.1	: 38.70	: (8)	: loess n°Foum	: At
63	: Zouerate (Mauritania)	: 347.79	: 22.44	: -17.8	: 39.00	: (8)	: loess n°Zouerat	: At
64	: Atar (Mauritania)	: 346.92	: 20.32	: -17.9	: 03.50	: (8)	: loess n°Atar	: At
65	: Nouakchott (Mauritania)	: 344.42	: 18.09	: -17.1	: 55.90	: (8)	: loess n°Nou	: At
66	: Dakar (Senegal)	: 342.73	: 14.38	: -16.2	: 03.20	: (8)	: loess n°Est	: At
67	: Foundiougne (Senegal)	: 343.70	: 14.08	: -14.3	: 28.40	: (8)	: loess n°Foun	: At
68	: Continental Shelf (Senegal)	: 342.00	: 14.00	: -14.5	: 41.90	: (8)	: loess n°Ro	: At
69	: Labe (Guinea)	: 347.65	: 11.43	: -12.1	: 22.00	: (8)	: loess n°Lab	: At
70	: N. Kurile (Alaid volcano)	: 155.39	: 50.51	: 07.6	: 18.18	: (9)	: basalt rock n° B-11-575	: P
71	: N. Kurile (Chirinkotan)	: 153.29	: 48.59	: 07.3	: 20.37	: (9)	: andesite rock n° B-11-527	: P
72	: N. Kurile (Beliankin)	: 154.08	: 49.56	: 07.7	: 17.18	: (9)	: basalt rock n° B-11-72/5	: P
73	: N. Kurile (Lovushki)	: 153.45	: 48.23	: 09.6	: 05.22	: (9)	: basalt andesite n° B-11-113/2	: P
74	: C. Kurile (Simushir)	: 152.00	: 47.00	: 10.1	: 10.76	: (9)	: basalt andesite n° 135-81	: P
75	: Wingham (Australia)	: 152.20	: -31.50	: -01.3	: 16.00	: (10)	: diss load river n° Manning	: P
76	: Murray Bridge (Australia)	: 139.17	: -35.10	: -06.0	: 15.20	: (10)	: diss load river n° Murray	: P
77	: Greenland	: 310.44	: 65.07	: -33.0	: 54.26	: (11)	: stream sediment n° 110528	: At
78	: Greenland	: 310.52	: 65.10	: -24.2	: 45.70	: (11)	: stream sediment n° 110326	: At
79	: Amazon Fan	: 312.00	: 07.50	: -10.2	: 42.00	: (12)	: river sed (average 6 samp.) ⁷⁹	: At
80	: Greenland	: 309.93	: 65.10	: -34.3	: 82.70	: (11)	: stream sediment n° 105862	: At
81	: Greenland	: 310.47	: 65.08	: -26.1	: 39.90	: (11)	: stream sediment n° 105894	: At
82	: Biscay abyssal plain	: 352.41	: 45.04	: -09.9	: 36.20	: (13)	: core n° TE1-M (4526m)	: At
83	: Newfoundland Basin	: 314.85	: 43.29	: -24.5	: 22.10	: (13)	: core n° TE2-S (4415m)	: At
84	: South Falkland Basin	: 299.72	: -52.55	: -04.4	: 13.70	: (13)	: core n° TE6-S (472m)	: At
85	: Angola Basin	: 12.36	: -12.12	: -24.9	: 09.10	: (13)	: core n° TE7-S (1760m)	: At
86	: West Mexico Basin	: 255.64	: 18.13	: 04.2	: 14.50	: (13)	: core n° CA24-S (680m)	: P
87	: Alaska Basin	: 214.41	: 54.37	: 01.6	: 17.30	: (13)	: core n° SS13-S (4111m)	: P
88	: Celebes Basin	: 121.32	: 02.42	: 04.2	: 19.20	: (13)	: core n° BA16-M (5336m)	: P
89	: Japan Basin	: 130.58	: 36.39	: -09.3	: 32.70	: (13)	: core n° BA23-M (2111m)	: P
90	: Middle America trench	: 254.70	: 19.06	: 01.3	: 26.00	: (13)	: core n° CA25-M (4912m)	: P
91	: Peru Chile trench	: 278.76	: -07.35	: -05.0	: 23.70	: (13)	: core n° CA29-M (5856m)	: P
92	: Java trench	: 103.07	: -07.21	: -13.8	: 35.00	: (13)	: core n° CA30-M (6454m)	: I
93	: Guatemala	: 269.00	: 13.00	: 02.0	: 19.00	: (14)	: core n° 495	: P

94	: W Indian	: 92.00	: 05.00	: -13.8	: 11.93	: (2)	: dust n° JL-13	: I
95	: W Pacific	: 110.00	: 07.00	: -10.6	: 16.42	: (2)	: dust n° JL-25	: P
96	: W Pacific	: 119.00	: 23.00	: -09.6	: 41.62	: (2)	: dust n° JL-17	: P
97	: Atlantic (Ivory Coast)	: 354.00	: 03.00	: -09.1	: 45.76	: (2)	: dust n° JL-42	: At
98	: Atlantic (Gambie)	: 342.00	: 14.00	: -13.6	: 30.67	: (2)	: dust n° JL-46	: At
99	: Gibraltar	: 350.00	: 36.00	: -08.5	: 21.35	: (2)	: dust n° JL-50	: At
100	: China (Lanzhou)	: 110.00	: 35.00	: -09.7	: 26.07	: (15),(2)	: loess (average 2 samp.) ¹⁰⁰	: P
101	: NE Pacific	: 228.30	: 46.30	: -06.1	: 18.50	: (15)	: core n° TT175-83P	: P
102	: SE Pacific	: 276.10	: -03.60	: -04.3	: 09.12	: (15)	: core n° V19-29	: P
103	: E Pacific	: 264.40	: 04.10	: -03.4	: 12.70	: (15)	: core n° DSDP 503B	: P
104	: N Pacific	: 161.40	: 46.30	: -00.5	: 12.30	: (15)	: core n° V20-122	: P
105	: Moses lake (E.U)	: 240.82	: 47.09	: -06.0	: 23.70	: (15)	: core n° Moses Lake	: P
106	: Rio de la plata	: 302.00	: -35.00	: -09.0	: 40.00	: (16)	: river sed.	: At
107	: Timor	: 130.13	: -09.06	: -09.3	: 17.33	: (17)	: core n° V28-341 (750m)	: I
108	: Sunda	: 107.11	: -08.25	: -03.1	: 16.98	: (17)	: core n° V33-75 (3396m)	: I
109	: Sunda	: 106.43	: -08.70	: -02.8	: 13.75	: (17)	: core n° V33-77 (3014m)	: I
110	: Sunda	: 88.57	: -06.02	: -07.7	: 08.27	: (17)	: core n° V34-55 (2996m)	: I
111	: Faeroe Island	: 353.00	: 62.00	: -06.5	: 07.00	: (4)	: core n° Rom1	: At
112	: S Iceland	: 341.50	: 63.40	: 07.6	: 54.00	: (4)	: stream sed.	: At
113	: Iceland basin	: 337.92	: 60.57	: 03.4	: 21.20	: (4)	: core n° SU-9033 (2400m)	: At
114	: Bay of Biscay	: 344.94	: 46.30	: -11.6	: 25.00	: (4)	: core (average 3 samp.) ¹¹⁴	: At
115	: Vizcaino peninsula, mex	: 246.40	: 27.00	: 07.6	: 15.00	: (18)	: adakite (average 5 samp.) ¹¹⁵	: P
116	: Peru Chile slope	: 286.27	: -16.92	: -03.2	: 19.70	: (13)	: core n° CA27-S (3603m)	: P
117	: Antilles	: 300.36	: 14.72	: -09.1	: 21.43	: (19)	: core n° GS7605-11 (2625m)	: At
118	: Antilles	: 299.65	: 13.03	: -09.6	: 26.80	: (19)	: core n° GS7605-48 (2430m)	: At
119	: Antilles	: 300.63	: 12.55	: -11.6	: 27.57	: (19)	: core n° GS7605-53 (1685m)	: At
120	: Antilles	: 300.42	: 11.03	: -13.3	: 29.30	: (19)	: core n° RC16-44 (1639m)	: At
121	: Antilles	: 311.60	: 03.40	: -10.7	: 22.60	: (19)	: core n° RC16-168 (836m)	: At
122	: E Greenland	: 332.00	: 69.00	: 04.0	: 07.80	: (20),(21)	: rocks (average 41 samp.) ¹²²	: At
123	: Iceland	: 338.00	: 65.00	: 08.0	: 17.00	: (22),(4)	: rocks (average 55 samp.) ¹²³	: At
124	: Iles Faroes	: 353.00	: 62.00	: 07.0	: 34.00	: (23)	: rocks (average 43 samp.) ¹²⁴	: At
125	: N-E Greenland	: 332.00	: 78.00	: -13.0	: 07.06	: (24)	: rocks (average 3 samp.) ¹²⁵	: At
126	: W Norway	: 5.25	: 60.50	: -14.0	: 16.75	: (25)	: rocks (average 2 samp.) ¹²⁶	: At
127	: Jan-Mayen	: 352.00	: 71.00	: 05.0	: 41.00	: (26)	: basalts (average 8 samp.) ¹²⁷	: At
128	: Norway	: 6.80	: 65.00	: -14.0	: 10.00	: (27)	: sandstones	: At
129	: N-E Greenland	: 346.01	: 72.90	: -13.7	: 26.99	: (28)	: core n° MD99-2308Hy (2520m)	: At
130	: S-E Greenland	: 326.00	: 67.00	: -38.0	: 15.00	: (29)	: granulites (average 11 samp.) ¹³⁰	: At
131	: N-E Greenland	: 333.00	: 72.30	: -29.8	: 32.02	: (30)	: rocks (average 5 samp.) ¹³¹	: At
132	: S Chile	: 284.00	: -46.20	: 05.6	: 21.00	: (31)	: basalts (average 10 samp.) ¹³²	: P
133	: Chile	: 288.00	: -38.00	: 02.5	: 18.60	: (32)	: rocks (average 26 samp.) ¹³³	: P
134	: Sunda	: 106.40	: -07.90	: -02.6	: 13.38	: (17)	: core n° V33-79 (3000m)	: I
135	: Antarctica	: 49.20	: -67.37	: -38.2	: 36.50	: (33)	: rocks (average 7 samp.) ¹³⁵	: P
136	: Lau basin	: 182.13	: -18.57	: 09.2	: 10.33	: (34)	: core n° 135-834B-33R-1 (2690m)	: P
137	: Lau basin	: 182.70	: -18.50	: 08.8	: 05.44	: (34)	: core n° 135-835B-3R2 (2905m)	: P
138	: Lau basin	: 183.18	: -20.13	: 07.5	: 05.10	: (34)	: core n° 135-836A-3HCC (2466m)	: P
139	: Costa Rica rift	: 277.00	: 03.00	: 09.8	: 05.44	: (35)	: core n° 143R-1 (3640m)	: P
140	: Maldives	: 73.30	: 00.40	: 06.4	: 07.50	: (36)	: core n° 115-713A-19R-2 (2266m)	: I
141	: Mascarene ridge	: 60.00	: -10.00	: 07.3	: 04.00	: (36)	: core n° 115-707C-27R-6 (1552m)	: I

142	: South Africa	: 28.00	: -32.00	: -09.2	: 30.13	: (37)	: rocks (average 3 samp.) ¹⁴²	: I
143	: South Africa	: 23.00	: -33.00	: -09.5	: 37.00	: (37)	: rocks (average 9 samp.) ¹⁴³	: I
144	: South australia	: 136.00	: -36.00	: -21.1	: 22.19	: (38)	: rocks (average 7 samp.) ¹⁴⁴	: I
145	: W Yemen	: 43.00	: 15.00	: 04.1	: 37.00	: (39)	: rocks (average 52 samp.) ¹⁴⁵	: I
146	: Indonesia	: 124.20	: -08.30	: -01.9	: 30.80	: (40)	: rocks (average 12 samp.) ¹⁴⁶	: I
147	: Barbados	: 309.50	: 13.25	: -12.0	: 42.63	: (41)	: aerosols (average 4 samp.) ¹⁴⁷	: At
148	: Andean Austral Zone	: 286.45	: -49.75	: -01.4	: 18.30	: (42)	: adakites (average 2 samp.) ¹⁴⁸	: P
149	: Andean Austral Zone	: 286.60	: -52.33	: 01.1	: 15.70	: (42)	: adakites (average 4 samp.) ¹⁴⁹	: P
150	: Andean Austral Zone	: 289.76	: -54.95	: 09.8	: 28.10	: (42)	: adakites n°Ck-3-198	: P
151	: N British Isles	: 358.00	: 58.00	: -10.6	: 40.00	: (4)	: rocks & riv. (average 18 samp.)	: At
152	: Papua New Guinea	: 132.65	: -01.20	: 04.1	: 03.55	: (43)	: rocks (average 4 samp.) ¹⁵²	: P
153	: SW Australia	: 115.63	: -33.32	: 01.7	: 14.40	: (44)	: rocks (average 3 samp.) ¹⁵³	: I
154	: SW Australia (id)	: 115.40	: -34.42	: -04.6	: 10.80	: (44)	: rocks (average 2 samp.) ¹⁵⁴	: I
155	: W Australia	: 119.00	: -20.00	: -15.1	: 19.67	: (40)	: river sed. (average 6 samp.) ¹⁵⁵	: I
156	: Manam volcano	: 145.05	: -04.08	: 07.1	: 18.03	: (45)	: rocks basalt	: I
157	: costa rica coast	: 275.00	: 10.00	: 07.3	: 09.30	: (46)	: rocks (average 46 samp.) ¹⁵⁷	: P
158	: C American arc	: 265.00	: 13.00	: 05.9	: 13.00	: (47)	: rocks (average 29 samp.) ¹⁵⁸	: P
159	: C American arc	: 262.66	: 19.83	: 01.5	: 21.00	: (48)	: rocks (average 18 samp.) ¹⁵⁹	: P
160	: Witu Islands	: 149.30	: -05.00	: 08.3	: 15.67	: (49)	: rocks (average 8 samp.) ¹⁶⁰	: I
161	: Comoros	: 44.00	: -12.00	: 03.4	: 41.90	: (50)	: rocks (average 19 samp.) ¹⁶¹	: I
162	: E Madagascar	: 49.00	: -19.00	: -22.1	: 23.73	: (51)	: rocks (average 7 samp.) ¹⁶²	: I
163	: Bismarck New Britain	: 150.00	: -05.00	: 08.3	: 04.10	: (49)	: rocks (average 20 samp.) ¹⁶³	: I
164	: Antarctic (Peninsula)	: 290.00	: -65.00	: 01.1	: 00.00	: (52)	: core n°1 ¹⁶⁴	: P
165	: Antarctic (Peninsula)	: 288.00	: -66.00	: -03.2	: 00.00	: (52)	: core n°2 ¹⁶⁵	: P
166	: New Hebrides Arc	: 168.00	: -15.00	: 07.4	: 14.40	: (53)	: rocks (average 28 samp.) ¹⁶⁶	: P
167	: NW USA	: 241.00	: 37.62	: -00.5	: 21.95	: (54)	: rocks (average 4 samp.) ¹⁶⁷	: P
168	: NE Pacific Ocean	: 226.00	: 53.00	: 09.6	: 12.80	: (55)	: rocks (average 6 samp.) ¹⁶⁸	: P
169	: Zimbabwe	: 34.50	: -20.00	: -14.5	: 14.82	: (56)	: rocks (average 12 samp.) ¹⁶⁹	: I
170	: Scotia arc	: 301.00	: -63.50	: 05.7	: 20.88	: (57)	: rocks (average 4 samp.) ¹⁷⁰	: At
171	: Central Chile	: 289.70	: -23.85	: 05.5	: 08.50	: (58)	: rocks (average 8 samp.) ¹⁷¹	: P
172	: Batan	: 121.90	: 20.25	: -02.8	: 05.66	: (59)	: rocks (average 13 samp.) ¹⁷²	: P
173	: Chile	: 288.00	: -42.00	: 02.1	: 18.60	: (32)	: rocks (average 26 samp.) ¹⁷³	: P
174	: S-E_Greenland	: 326.00	: 65.00	: -38.0	: 15.00	: (29)	: rocks (average 11 samp.) ¹⁷⁴	: At
175	: E_Greenland	: 332.00	: 70.50	: 04.0	: 07.80	: (20), (21)	: rocks (average 41 samp.) ¹⁷⁵	: At
176	: N-E_Greenland	: 333.00	: 71.00	: -29.8	: 32.02	: (30)	: rocks (average 5 samp.) ¹⁷⁶	: At
177	: Ontong_Java_Plateau	: 160.00	: -10.00	: 01.8	: 10.00	: (60)	: rocks (average)	: P
178	: Caribbean_Plateau	: 280.00	: 13.00	: 04.1	: 10.00	: (60)	: rocks (average)	: At
179	: Southern_Kerguelen	: 85.00	: -59.00	: -00.5	: 10.00	: (60)	: rocks (average)	: I
180	: Kaapvaal Craton	: 33.00	: -27.00	: -30.0	: 29.10	: (61)	: rocks (average 41 samp.) ¹⁸⁰	: I
185	: banda sea shelf	: 127.00	: -08.00	: -12.4	: 20.00	: (40)	: sediments	: I
186	: izu chain (japon)	: 140.00	: 35.00	: 07.7	: 12.00	: (62)	: basalts (average 3 samp.) ¹⁸⁶	: P
187	: aleutians	: 170.00	: 54.00	: 07.4	: 12.00	: (62)	: basalts (average 3 samp.) ¹⁸⁷	: P
188	: new britain	: 150.00	: 10.00	: 07.4	: 18.00	: (62)	: basalts (average 4 samp.) ¹⁸⁸	: P
189	: sunda	: 106.00	: -06.00	: 00.0	: 21.00	: (62)	: basalts (average 4 samp.) ¹⁸⁹	: I
190	: banda	: 122.00	: -10.00	: -03.3	: 11.50	: (62)	: basalts (average 2 samp.) ¹⁹⁰	: I
191	: antilles	: 298.00	: 16.00	: 05.5	: 10.00	: (62)	: basalts (average 10 samp.) ¹⁹¹	: At
192	: kerguelen	: 69.00	: -49.00	: 00.0	: 25.00	: (63), (64)	: basalts (average 25 samp.) ¹⁹²	: I
193	: antarctic (ross)	: 180.00	: -80.00	: -20.8	: 12.00	: (65)	: dolerites (average 6 samp.) ¹⁹³	: P

194	: tasmania	: 147.00	: -43.00	: -05.2	: 12.50	: (66)	: dolerites (average 12 samp.) ¹⁹⁴	: P
195	: djibouti	: 43.00	: 12.00	: 05.0	: 30.00	: (67)	: basalts (average 72 samp.) ¹⁹⁵	: I
196	: arabi seoudite	: 40.00	: 20.00	: 05.0	: 30.00	: (68)	: basalts (average 28 samp.) ¹⁹⁶	: I
197	: Bonin islands	: 140.00	: 27.00	: 02.3	: 01.50	: (43)	: rocks (average 4 samp.) ¹⁹⁷	: P
198	: Mariana	: 145.00	: 15.00	: 06.7	: 01.80	: (43)	: rocks (average 3 samp.) ¹⁹⁸	: P
199	: kerguelen	: 83.00	: -65.00	: -08.0	: 21.00	: (69)	: sediments (average 6 samp.) ¹⁹⁹	: I
200	: New Zealand	: 171.00	: -45.00	: -05.3	: 31.50	: (70)	: loess n° BP2 & BP4	: P
201	: Nanking	: 115.00	: 25.00	: -10.2	: 35.20	: (71)	: loess n° Nanking	: P
202	: Baltic Sea	: 25.00	: 67.00	: -19.4	: 13.00	: (72)	: sediments : At	
203	: Greenland SE	: 323.00	: 66.00	: -26.0	: 45.00	: (73)	: rocks (average 18 samp.) ²⁰³	: At
204	: La Reunion	: 55.50	: -21.00	: 04.0	: 24.40	: (74)	: volcanic (average 16 samp.) ²⁰⁴	: I
205	: Alboran Sea	: 356.80	: 36.10	: -10.1	: 30.30	: (41)	: core n° KS 8231 (855m)	: M
206	: South Andalousia	: 352.20	: 36.80	: -08.4	: 30.20	: (41)	: core n° KC 8221 (580m)	: M
207	: Gibraltar	: 351.30	: 35.80	: -11.8	: 22.10	: (41)	: core n° KS 8228 (2798m)	: M
208	: North West Spain	: 349.50	: 45.40	: -11.6	: 25.70	: (41)	: core n° Inter-B1 (2588m)	: At
209	: North West Ireland	: 346.25	: 56.50	: -11.1	: 25.50	: (41)	: core n° KS 73134 (2300m)	: At
210	: West Britain	: 351.50	: 47.50	: -11.6	: 25.90	: (41)	: core n° Flux-8 (2120m)	: At
211	: Red Sea	: 35.00	: 26.00	: -09.1	: 31.20	: (41)	: aerosols n° MR83	: I
212	: Rhone	: 5.00	: 43.00	: -09.7	: 25.77	: (75)	: river part	: M
213	: Po	: 12.00	: 45.00	: -10.8	: 26.85	: (75)	: river part	: M
214	: Seyhan	: 36.00	: 37.00	: -06.2	: 10.01	: (75)	: river part	: M
215	: Tarsus	: 36.20	: 37.00	: -06.3	: 10.81	: (75)	: river part	: M
216	: Eastern Ertrea	: 41.00	: 17.50	: -04.2	: 21.53	: (76)	: rocks (average 7 samp.) ²¹⁶	: I
217	: Gulf of Aden	: 42.50	: 11.60	: 06.2	: 24.50	: (77)	: rocks (average 3 samp.) ²¹⁷	: I
218	: Gulf of Aden	: 48.00	: 12.00	: 10.0	: 10.00	: (77)	: rocks (average 20 samp.) ²¹⁸	: I
219	: Gulf of Aden	: 43.15	: 11.60	: 06.3	: 29.60	: (77)	: core n° V-55 (900m)	: I
220	: Weddell Sea	: 314.58	: -60.95	: -06.2	: 23.98	: (78)	: core n° D-ORC-15 (290m)	: At
221	: Weddell Sea	: 304.68	: -66.05	: -05.7	: 21.20	: (78)	: core n° PS2805-1 (466m)	: At
222	: Waddell Sea	: 324.95	: -74.40	: -07.7	: 10.64	: (78)	: core n° PS1490-2 (497m)	: At
223	: Waddell Sea	: 319.50	: -77.15	: -10.4	: 18.56	: (78)	: core n° PS1016-1 (702m)	: At
224	: Baffin Bay	: 287.88	: 69.00	: -23.1	: 10.70	: (79)	: core n° HU77027-002TWC	: At
225	: Baffin Bay	: 300.00	: 66.50	: -25.8	: 10.70	: (79)	: core n° HU74026-557PC	: At
226	: East Greenland	: 8.00	: 68.00	: -15.1	: 40.00	: (79)	: core n° JM 98 624	: At
227	: East Seram	: 132.00	: -04.00	: -08.7	: 24.00	: (80)	: core (average 11 samp.) ²²⁷	: I
228	: East Serua	: 132.00	: -07.00	: -08.1	: 21.50	: (80)	: core (average 12 samp.) ²²⁸	: I
229	: East Timor	: 128.00	: -09.00	: -09.5	: 20.40	: (80)	: core (average 12 samp.) ²²⁹	: I
230	: Queensland	: 146.15	: -17.30	: -06.3	: 32.00	: (81)	: core n° BB 9979 W	: P
231	: New Zealand	: 172.40	: -41.00	: 01.2	: 05.00	: (82)	: rocks (average 8 samp.) ²³¹	: P
232	: Antarctic peninsula	: 289.10	: -69.50	: 05.5	: 37.65	: (57)	: rocks (average 6 samp.) ²³²	: At
233	: Agulhas current	: 38.85	: -23.37	: -15.5	: 33.30	: (83)	: core n° VM19-214 (3092m)	: I
234	: Agulhas current	: 32.60	: -31.50	: -13.4	: 23.60	: (83)	: core n° RC17-69 (3380m)	: I
235	: Agulhas current	: 32.87	: -29.63	: -15.3	: 21.60	: (83)	: core n° VM14-77 (1818m)	: I
236	: Agulhas current	: 18.45	: -35.78	: -11.2	: 21.90	: (83)	: core n° RC11-86 (2829m)	: I
237	: Cape Basin	: 13.28	: -30.58	: -11.6	: 21.80	: (83)	: core n° VM19-240 (3103m)	: At
238	: Cape Basin	: 11.30	: -25.50	: -11.6	: 16.20	: (83)	: core n° RC13-229 (4191m)	: At
239	: Antarctic Circum. Current	: 2.90	: -50.58	: -04.8	: 18.00	: (83)	: core n° RC13-255 (3332m)	: At
240	: Antarctic (Peninsula)	: 280.00	: -70.00	: -04.1	: 55.10	: (52)	: core n° ELT42-09 ²⁴⁰	: P
241	: Antarctic (West Antarctic)	: 240.00	: -70.00	: -03.7	: 52.90	: (52)	: core (average 5 samp.) ²⁴¹	: P

242	: Antarctic (Ross Sea)	:	170.00	:	-70.00	:	-06.8	:	46.10	:	(52)	:	core (average 3 samp.) ²⁴²	:	P
243	: Antarctic (Wilkes Land)	:	120.00	:	-65.00	:	-14.3	:	47.43	:	(52)	:	core (average 7 samp.) ²⁴³	:	I
244	: Antarctic (Pryzd Bay)	:	60.00	:	-65.00	:	-18.8	:	39.43	:	(52)	:	core (average 3 samp.) ²⁴⁴	:	I
245	: Antarctic (Dronning Maud)	:	20.00	:	-70.00	:	-14.0	:	59.93	:	(52)	:	core (average 3 samp.) ²⁴⁵	:	At
246	: Antarctic (Weddell Sea)	:	320.00	:	-75.00	:	-08.0	:	69.90	:	(52)	:	core (average 2 samp.) ²⁴⁶	:	At
247	: Indus shelf	:	37.00	:	25.00	:	-11.2	:	00.00	:	(84)	:	core n° ID-18 ²⁴⁷	:	I

33 : samples n° Ghw-4, HD, 422
 44 : samples n° AK4-EJ, AK4-15, AK4-33
 45 : samples n° MK-15, MK-17
 46 : samples n° B1796, B1927C
 55 : samples n° A17, JL-48
 57 : samples n° A9, A4
 59 : samples n° n 4, n 10, n 17, n 27, n 59
 79 : samples n° 155-931B-40X-2, 155-935A-32X-2, 155-938A-32X-5, 155-940A-27X-5
 100 : samples n° Lanzhou Loess, Malan Loess
 114 : samples n° SP3-33, Flux-7, Flux-8
 115 : samples n° 99-149, 99-131, 99-113, 99-122, 99-110
 122 : samples n° 416705 px, 416799 px, 416804 pl, 416812 pl, 416829 px, 416831 pl, 312326 pl, 312338 pl, 312383 pl,
 352144 pl, 352164 px, 1610 px, 312361 pl, 71068 pl, AP115 blk, P78a blk, P97 blk, KIMB12 px, 73599 px, 3609 px, PK504
 px, 3584 px, 75-323L, 75-322L, 75-305L, 75-303, 75-303L(1), 75-301L, 75-795, 75-795L, 75-770L, 75-755, 75-
 755L, 75-317L, 75-752L, 75-308L
 123 : samples n° A2, ATHO, K81, KK25, KK29, B1, H6650, NAL20, NAL36, NAL71, SAL56, SAL79, SAL9, TH15, TH29, VA1, HNL22,
 BL4, MIL10, MIL15, MIL25, MIL27, MIL51, MIL52, MIL54, MIL62, MIL83, H4T, Hek-18, Hek-8, SAL115, SAL55n VMG41, SNS14,
 SNS24, BTHO, D8B-1, HEN5, RSG19, RSG32, RSG35, RSG54
 124 : samples n° SV-12, Str-106, Va-17, Ey-129, Ku-32, Ey-156, B-15, Su-1, Str-112, Str-61, Su-36, B-8, Su-24, Ku-9,
 Ey-203, Ey-190, Str-188, Su-34, Va-34, Su-14, Ey-1, Ey-201, Str-47, Va-38, Str-74, Str-87, Str-209, Va-29, Str-67, Ey-
 56, Str-64, Str-216, Va-47, Va-20, Sa-2, Sa-5, 484.93, 439.78, 490.07, X14, 69A, XI6
 125 : samples n° 363183, 363020, 407542
 126 : sample n° BA39/92B
 127 : samples n° EN026 1D-1, EN026 2D-1, EN026 3D-2, EN026 4D-3, EN026 5D-1, EN026 6D-1, EN026 7D-1g, EN026 7D-2
 130 : samples n° 229605, 229606, 229617, 229632, 229636, 229642, 229645, 229661, 229673, 229700, 229501
 131 : samples n° 426008, 426018, 426034, 426019, 426009
 132 : samples n° CMU T18a, MVU T16d, BBO TA55, BBO TA65, BDS TA91, BDS TA103
 133 : samples n° C662, C663, C664, 060283-9, LM7, 511775, 511776, 511773, 511777, 1112761, 1212874, 289761, 279763,
 1112751, 279765, 1212759, 13826h, 272825, 2728246, 272821, 2728266, 138212, 272827, 220283-1, 120183-1, 2502913
 142 : samples n° WBF6, BF1, BF6
 143 : samples n° MM 3, MM 7, MM 4, BK 1, BK 2, BK 6b, WB 1, WB 3, WB 5
 144 : samples n° 87-129, 87-130, 87-131, 87-132, 87-133, 87-134, 87-135
 145 : samples n° JB51, JB2, JB5, JB7, JB59, JB11, JB14, JB62, JB63, JB64, JB65, JB66, JB68, JB73, JB74, JB76, JB77,
 JB78, jb79, JB80, JB87, JB82, JB84, JB85, JB284, JB283, JB282, JB255, JB280, JB256, JB279, JB259, JB260, JB261, JB262,
 JB328, JB330, JB335, JB225, JB231I, JB191, JB148, JB171, JB166, JB172, JB124, JB128, JB129, JB136, JB139, JB141
 146 : samples n° tr1.2.1, tr1.2.2, tr5.1.3, bual.2.3, bu1.2.1, bu1.2.3.2, pb2.2, me99a119, mea123, pk2.1, me99a16,
 me99a17
 147 : samples n° BBDS-1, BBDS-2, BBDS-3, BBDS-4
 148 : samples n° La-1, Vd-1
 149 : samples n° Ag-1, Re-4, MB-9, MB-21
 152 : samples n° 2984, 2985, 2986, 2987
 153 : samples n° 86694, 86697, 86712
 154 : samples n° 86723, 86724
 155 : samples n° ME1A, ME2, ME3, ME4, ME5, ME6
 157 : samples n° SE2, SE3, SE6, SE27, SE20, AN2, AN14, AN18, AN46, AN52, AN53, AN72, AN81, AN86, AN99, AN110, BN17,
 BN19, BN31, AH5, AH8, BH11, TG4, TG8, TG9, TG13, BC17, G01, G02, G04, BUR4, BUR11, BUR12, BUR13, BUR14, AQ8, AQ16,
 AQ19, AQ22, AQ28, BQ32, OS2, OS6, OS9, OS16

158 : samples n° TA-4C, AT-50, E1, T102, M4, SA22, IZ108, B-21, SM-7, ZA2, ZA4B, ZA7, COS9 A, TE1, TE114, CN1, MT101,
 MS4, GR101, C922, RV1, TE9, AR82, C502, C1004b, C1001, C112, C114, C118
 159 : samples n° HF15, HF239, HF238, HF76, HF2, CH52a, CH59, CH75, CH76, CH57, CH58, CH56, CH60, CH54, CH55b, HF117,
 CH51a, CH53, TZ02, TZ03
 160 : samples n° H1/1, H1/3, H2/3, H2/7, H3/3, H3/7, 69089, 69098, 69092
 161 : samples n° GC-1, GC-3, GC-5, RH-1b, RH-9, RH-15, RH-16, RH-17, RH-28, RH-26, RH-14, MA-29, MA-60, MA-55, MA-1,
 MA-3, MA-8, MA-11, MA-35, MA-33
 162 : samples n° Mad 50, Mad 62, Mad 64, Mad 68, Mad 73, Mad 74, Mad 76
 163 : samples n° O871E, 217E, 2651A, E2/1, 0217B, 2654A, 2649, 3039B, 3038G, 3028, 3035, 3038B, 3032A, E5/11, F5/2,
 F7/2, Gs2/1, Gs3/1, Gn1/4, Gn2/1
 164 : concentration not available
 165 : concentration not available
 166 : samples n° AYMAC20, TAC75, TAC82, UA10, UMAC4, MLMAC23, MLMAC43, MOMAC3, MOMAC4, VMAC5, VMAC6, AOW1,
 AOW115, AM039, AM27, AM39C, PAM20, TOW5, EA143, EA258, MLM6, MLM7, MLM10A, FMAC18, FMAC64, VGA1, VGA7
 167 : samples n° 92LV01, 92LV06, 92LV07, 93LV17
 168 : samples n° DR-302, GR-101, GR-104, OS-10-29, OS-208, OS-213
 169 : samples n° ZCH-1, ZCH-2, ZCH-3, ZD-16, ZD-17, ZD-18, ZH-4, ZH-7, ZD-13, ZS-1, ZS-2, ZS-4
 170 : samples n° R.3728.1, R.3731.4, R.3734.1, R.3742.3
 171 : samples n° CB19wr, CB42wr, CB46wr, CB51wr, CB70wr, CB74wr, CB76wr, KU5wr
 172 : samples n° 1b, 1a, 1aphl, 1acpx, 1c, 3f, 3n, 3cphl, 3c/1, 3c/2, 3c/3, 3c/6, 7a, 46b
 173 : cf. 133
 174 : cf. 130
 175 : cf. 122
 176 : cf. 131
 180 : samples n° C-90, C-130, C-169, D-72, D-79, D-84, CDV-1-2, CDV-1-4, CDV-1-5, D-31, MSF-2-1, MSF-2-8, CDV-1-28,
 MEE-20, MEE-35, C-196, D-56, D-111, JWS-8-9, JWS-8-11, JWS-8-12, MED-8, MEE-21, MEE-39, 730-5, MEE-24, SJ-3-5, AA0097,
 AA0099, C-75, MED-13, MED-14, MED-15, C-72, MED-10, MED-11, P-28, P-41, P-47, P-54, P-62, P-103
 186 : samples n° F-864, IZU-2, IZU3
 187 : samples n° 51-Sn-338, 51-Sn-340, 51-Sn-155
 188 : samples n° 343, 279B, 8015, 8042
 189 : samples n° 71-991, 71-980, 71-1142, 72-1076
 190 : samples n° T-7, T-8
 191 : samples n° KEJ100, GDA011, WIC020, STV79-70, V71008, TAB, STL207, GUAD504, MONT102, STK106
 192 : samples n° 81-18, 81-19, 85-12, 85-55, 78-77, K-47, 77-128, 77-211, 77-206, 77-180, 80-135, 80-71, 78-74, AG99-
 34, AG99-36, AG99-126, AG99-123, AG99-125, AG99-182, AG99-122, AG99-37, AG99-35, AG99-41, AG99-38, AG99-124
 193 : samples n° 87-87, 87-93, 87-104, 87-117, 87-122, 87-126
 194 : samples n° 84-108, 84-109, 84-129, 84-141, 84-144, 84-149, 84-169, 84-170, 84-203, 84-205, 84-221, 84-222
 195 : samples n° PP 706, PP 708, PP 711, PP 713, PP 714, PP 717, PP 718, PP 719, PP 727, PP 728, PP 730, PP 698, PV
 309, PP 664, PP 669, JV 240, PV 313, JV 244, JV 246, PP 670, PP 699, JV 231, PP 671, PP 672, PP 675, PP 685, PP 687,
 PP 695, PP 701, PP 726, PP 738, PP 739, PP 748, PP 749, PP 693, PV 231, PV 239, PV 243, PV 246, pG 55-AE2, pp 700, 29,
 30, 31, 32, PP 684, PP 683, PV 2, PV 7, PV 15, PV 353, PP 686-A, PP 688, pG 55-AA, pG 55-V, JA42, PP 515, JA 25, JA
 26, JV 37, JV 39, JV 73, JV 86, pG 55-W1, pG 55-W2, PP 689, PP 690, PP 691, PV 223, pG 55-Y1, pG 55-Y2, pG 55-Z
 196 : samples n° 165006, 165666, 165634, 175764, 175776, 165574, 165546, 165559, 165572, 165627, 165661, 165881,
 175780, 175834, 1655575, 175825, 165714, 165767, 165768, 165772, 175826, 165735, 165672, 165556, 165611, 165542,
 165008
 197 : samples n° 2981, 2982, 2983, 1129-4
 198 : samples n° 28-1, 29-1, 46-1
 199 : samples n° 33R-1-79-81, 33R-2-65-68, 33R-5-17-21, 34R-1-88-92, 34R-4-30-33, 35R-2-91-94

203 : samples n° 229501, 229531, 229661, 229673, 229700, 232884, 314015, 314332, 314377, 314506, 314537, 314545,
314606, 337067, 337068, 337165, 337172, 337192
204 : samples n° RE204, RE285, RE445, RE464, RE476, RE493, RE500, RE501, RE512, RE585, RE603, RE674, RE771
216 : samples n° 1-1, 3-1, 5-1, 8-1, 9-3, 9-2, 1307
217 : samples n° DJ-42, DJ-9, DJ-2
218 : samples n° V3307 47D-1, V3307 48D-2, V3307 49D-1, V3307 50D-1, V3307 51D-1, V3307 52D-1, V3307 53D-1, V3307 54D-
1, V3307 55D-1, V3307 56D-1, V3307 57D-1, V3307 58D-1, V3307 59D-1, V3307 60D-1, V3307 61D-1, V3307 62D-1, V3307 63D-
1, V3307 64D-1, V3307 65D-1
227 : samples n° G5-2-14, G5-2-19, G5-2-24, G5-2-34, G5-2-40, G5-2-45, G5-2-51, G5-2-56, G5-2-60, G5-2-63, G5-2-65
228 : samples n° G5-4-71, G5-4-75, G5-4-79, G5-4-83, G5-4-85, G5-4-88, G5-4-92, G5-4-99, G5-4-104, G5-4-106, G5-4-110,
G5-4-118
229 : samples n° G5-6-123, G5-6-129, G5-6-134, G5-6-136, G5-6-143, G5-6-145, G5-6-147, G5-6-149, G5-6-150, G5-6-153,
G5-6-157, G5-6-164
231 : samples n° NZ-227, NZ-311, NZ-029a, NZ-113b, NZ-011, NZ-013, NZ-053, NZ-019
232 : samples n° KG.3603.5, KG.3609.9, KG.3616.5, KG.3719.17, KG.3627.8, KG.3625.2
240 : cf. ¹⁶⁴
241 : samples n° ELT11-19, ELT11-18, ELT11-17, ELT33-12, ELT33-11
242 : samples n° ELT27-20, NBP9802-2H, NBP9802-4H
243 : samples n° ELT37-04, ELT37-06, ELT37-09, ELT37-10, ELT37-13, ELT37-18, ELT37-16
244 : samples n° ELT47-07, ELT47-14, RC17-51
245 : samples n° RC17-56, IO1277-25, IO1277-41
246 : samples n° IO1578-48, ELT07-11
247 : no concentration available

1. C. Colin, L. Turpin, J. Betaux, A. Desprairies, C. Kissel, *Earth and Planetary Science Letters* **171**, 647 (1999).
2. S. L. Goldstein, R. K. O'Nions, P. J. Hamilton, *Earth and Planetary Science Letters* **70**, 221 (1984).
3. G. Bayon, C. R. German, K. W. Burton, R. W. Nesbitt, N. Rogers, *Earth and Planetary Science Letters* **224**, 477 (Aug 15, 2004).
4. M. Revel, J. A. Sinko, F. E. Grousset, *Paleoceanography* **11-1**, 95 (1996).
5. C.-Y. Lan, T. Lee, X.-H. Zhou, S.-T. Kwon, *Geology* **23**, 249 (1995).
6. C. Innocent, N. Fagel, R. K. Stevensson, C. Hillaire-Marcel, *Earth and Planetary Science Letters* **146**, 607 (1981).
7. M. T. McCulloch, M. R. Perfit, *Earth and Planetary Science Letters* **56**, 167 (1981).
8. F. E. Grousset et al., *Earth and Planetary Science Letters* **17**, 395 (1998).
9. D. M. Zhuravlev, A. A. Tsvetkov, A. Z. Zhuravlev, N. G. Gladkov, I. V. Chernyshev, *Chemical Geology (Isotope Geoscience Section)* **66**, 227 (1987).
10. S. J. Goldstein, S. B. Jacobsen, *Chemical Geology (Isotope Geoscience Section)* **66**, 254 (1987).
11. F. VonBlanckenburg, T. F. Nagler, *Paleoceanography* **16-4**, 424 (2001).
12. D. K. McDaniel et al., *Proceedings of the Ocean Drilling Program, Scientific Results* (1997).
13. S. M. McLennan, S. R. Taylor, M. T. McCulloch, J. B. Maynard, *Geochimica et Cosmochimica Acta* **54**, 2015 (1990).
14. T. Plank, C. H. Langmuir, *Chemical Geology* **145**, 325 (1998).
15. S. Nakai, A. N. Halliday, D. K. Rea, *Earth and Planetary Science Letters* **119**, 143 (1993).
16. F. Henry, J.-L. Probst, D. Thouron, P. Depetris, V. Garcon, *Science Geologie* **49**, 89 (1996).
17. D. B. Othman, W. M. White, J. Patchett, *Earth and Planetary Science Letters* **94**, 1 (1989).
18. A. Aguillon-Robles et al., *Geology* **29-6**, 531 (2001).
19. W. M. White, B. Dupre, *Geochimica et Cosmochimica Acta* **49**, 1975 (1985).
20. S. Bernstein et al., *Earth and Planetary Science Letters* **160**, 845 (1998).
21. H. Hansen, T. F. D. Nielsen, *Chemical Geology* **157**, 89 (1999).
22. C. Hemond et al., *Journal of geophysical research* **98(B9)**, 15 (1993).
23. P. M. Holm, N. Hald, R. Waagstein, *Chemical Geology* **178**, 95 (2001).
24. H. K. Bruekner, J. A. Gilotti, A. P. Nutman, *Contribution to Mineralogy and Petrology* **130**, 103 (1998).
25. T. M. Boundy, K. Mezger, E. Essene, *Lithos* **39**, 159 (1997).
26. J.-G. Schilling, R. Kingsley, D. Fontignie, R. Poreda, S. Xue, *Journal of geophysical research* **104(B5)**, 10 (1999).
27. S. N. Ehrenberg, A. Dalland, P. H. Nadeau, E. W. Mearns, H. E. F. Amundesen, *Marine and Petroleum Geology* **15**, 403 (1998).
28. F. Lacan, Toulouse III University (2002).
29. P. N. Taylor, F. Kalsbeek, D. Bridgwater, *Chemical Geology* **94**, 281 (1992).
30. K. Thrane, *Precambrian Research* **113**, 19 (2002).
31. C. Guivel et al., *Tectonophysics* **311(1-4)**, 83 (1999).
32. R. L. Hickey, F. A. Frey, D. C. Gerlach, *Journal of geophysical research* **91-B6**, 5963 (1986).
33. D. J. DePaolo, W. I. Manton, E. S. Grew, M. Halpern, *Nature* **298**, 614 (1982).
34. J. M. Herget, C. J. Hawkesworth, *Proceedings of the Ocean Drilling Program, Scientific Results* **135**, 505 (1994).
35. H. Shimizu, K. Mori, A. Masuda, *Proceedings of the Ocean Drilling Program, Scientific Results* **111**, 77 (1989).
36. W. M. White, M. M. Cheatum, R. A. Duncan, *Proceedings of the Ocean Drilling Program, Scientific Results* **115**, 53 (1990).
37. A. Dia, C. J. Allegre, A. J. Erlank, *Earth Planetary Science Letters* **98**, 74 (1990).
38. J. M. Herget, D. W. Peate, C. J. Hawkesworth, *Earth Planetary Science Letters* **105**, 134 (1991).
39. J. A. Baker, M. F. Thirwall, M. A. Menzies, *Geochimica and Cosmochimica Acta* **60-14**, 2559 (1996).
40. M. A. Elburg et al., *Geochimica and Cosmochimica Acta* **66**, 2771 (2002).

41. F. E. Grousset, P. E. Biscaye, A. Zindler, J. Prospero, R. Chester, *Earth and Planetary Science Letters* **87**, 367 (1988).
42. C. R. Stern, R. Kilian, *Contribution Mineral Petrology* **123**, 263 (1996).
43. R. L. Hickey, F. A. Frey, *Geochimica and Cosmochimica Acta* **46**, 2099 (1982).
44. F. A. Frey, N. J. McNaughton, D. R. Nelson, J. R. D. Laeter, R. A. Duncan, *Earth Planetary Science Letters* **144**, 163 (1996).
45. J. B. Gill, J. D. Morris, R. W. Johnson, *Geochim. Cosmochim. Acta* **57**, 4269 (1993).
46. F. Hauff, K. A. Hoernle, P. V. D. Bogaard, G. E. Alvarado, C. D. Garbe-Schonberg, *Geochemistry and geophysics geosystems* **1** (2000).
47. L. C. Patino, M. J. Carr, M. D. Feigenson, *Contribution to Mineral Petrology* **138**, 265 (2000).
48. S. P. Verma, *Chemical Geology* **164**, 35 (2000).
49. J. D. Woodhead, S. M. Eggins, R. W. Johnson, *J. of Petrology* **39**, 1641 (1998).
50. A. Spaeth, A. P. L. Roex, A. R. Duncan, *Journal of Petrology* **37**, 961 (1996).
51. A. Kröner et al., *American Journal of Science* **300**, 251 (April, 2000).
52. M. Roy, T. Van de Flierdt, S. R. Hemming, S. L. Goldstein, *Chemical Geology* (submitted).
53. D. W. Peate, J. A. Pearce, C. J. Hawkesworth, C. M. H. Edwards, K. Hirose, *Journal of Petrology* **38**, 1331 (1997).
54. M. R. Reid, F. C. Ramos, *Earth Planetary Science Letters* **138**, 37 (1996).
55. B. L. Cousens, J. Dostal, T. S. Hamilton, *Can. Journal of Earth Science* **36**, 1021 (1999).
56. R. E. Harmer, C. A. Lee, B. M. Eglington, *Earth Planetary Science Letters* **158**, 131 (1998).
57. M. J. Hole, P. D. Kempton, I. L. Millar, *Chemical Geology* **109**, 51 (1993).
58. F. Lucassen, M. F. Thirlwall, *Geology Rundschau* **86**, 767 (1998).
59. P. Vidal, C. Dupuy, R. C. Maury, M. Richard, *Geology* **17**, 1115 (1989).
60. N. Arndt, D. Weis, *Joides Journal* **28**, 79 (2002).
61. B.-M. Jahn, K. C. Condie, *Geochimica and Cosmochimica Acta* **59-61**, 2239 (1995).
62. W. M. White, P. J. Patchett, *Earth Planetary Science Letters* **67**, 167 (1984).
63. D. Weis, F. A. Frey, A. Giret, J.-M. Cantagrel, *Journal of Petrology* **39**, 973 (1998).
64. S. Doucet, J. S. Scoates, D. Weis, A. Giret, *Geochemistry Geophysics Geosystems* **6** (Apr, 2005).
65. J. M. Hergt, B. W. Chappell, G. Faure, T. M. Mensing, *Contributions to Mineralogy and Petrology* **102**, 298 (1989).
66. J. M. Hergt, B. W. Chappell, M. T. McCulloch, I. McDougall, A. R. Chivas, *Journal of Petrology* **30**, 841 (1989).
67. C. Deniel, P. Vidal, C. Coulon, P.-J. Vellutini, P. Piguet, *Journal of geophysical research* **99**, 2853 (1994).
68. E. Hegner, J. S. Pallister, *Journal of geophysical research* **94**, 7749 (1989).
69. J. J. Mahoney et al., *Chemical Geology* **120**, 315 (1995).
70. S. R. Taylor, S. M. McLennan, M. T. McCulloch, *Geochimica et Cosmochimica Acta* **47**, 1897 (1983).
71. M. McCulloch, G. J. Wasserburg, *Science* **200**, 1003 (1978).
72. B. Ohlander, J. Ingri, M. Land, H. Schoeberg, *Geochimica et Cosmochimica Acta* **247**, 813 (2000).
73. F. Kalsbeek et al., *Precambrian Research* **62**, 239 (1993).
74. M. R. Fisk, B. G. J. Upton, C. E. Ford, W. M. White, *Journal of geophysical research* **B93**, 4933 (1988).
75. C. D. Frost, R. K. O'nions, S. L. Goldstein, *Chemical Geology* **55**, 45 (1986).
76. M. Beyth, R. J. Stern, A. Matthews, *Precambrian Research* (1997).
77. J. G. Schilling, R. H. Kingsley, B. B. Hanan, B. L. McCully, *Journal of geophysical research Solid earth* **97**, 10927 (1992).
78. H. J. Walter, E. Hegner, B. Diekman, G. Kuhn, M. M. R. V. D. Loeff, *Geochimica and Cosmochimica Acta* **64**, 3813 (2000).
79. G. L. Farmer, D. Barber, J. Andrews, *Earth Planetary Science Letters* **209**, 227 (2003).
80. P. Z. Vroon, M. J. V. Bergen, G. J. Klaver, W. M. White, *Geochimica and Cosmochimica Acta* **59**, 2573 (1995).
81. M. McCulloch, C. Pailles, P. Moody, C. E. Martin, *Earth Planetary Science Letters* (2003).
82. C. Munker, *Journal of Petrology* **41**, 759 (2000).

83. A. M. Franzese, S. R. Hemming, S. L. Goldstein, R. F. Anderson, *Earth and Planetary Science Letters* **in press** (2006).
84. P. D. Clift *et al.*, *Earth and Planetary Science Letters* **200**, 91 (2002).

Bibliographie

- Albarède, F. et Goldstein, S. (1992).** A world map of nd isotopes in seafloor ferromanganese deposits. *Geology*, 20 :761–763.
- Alkama, R., Kageyama, M., et Ramstein, G. (2006).** Freshwater discharges in a simulation of the last glacial maximum climate using improved river routing. *Geophys. Res. Lett.*, 33(L21709).
- Allègre, C. (2005).** *Géologie isotopique*. Belin Sup, Paris.
- Amakawa, H., Alibo, D. S., et Nozaki, Y. (2000).** Nd isotopic and ree pattern in the surface waters of the eastern indian ocean and its adjacent seas. *Geochim. Cosmochim. Acta*, 64 :1715–1727.
- Amakawa, H., Nozaki, Y., Alibo, D., Zhang, J., Fukugawa, K., et Nagai, H. (2004).** Neodymium isotopic variations in northwest pacific waters. *Geochimica et Cosmochimica Acta*, 68 :715–727.
- Arsouze, T., Dutay, J. C., Lacan, F., et Jeandel, C. (2007).** Modeling the neodymium isotopic composition with a global ocean circulation model. *Chemical Geology*, 239(1-2) :165–177.
- Aumont, O. et Bopp, L. (2006).** Globalizing results from ocean in situ iron fertilization studies. *Global Biogeochemical Cycles*, 20(2). GB2017.
- Aumont, O., Maier-Reimer, E., Blain, S., et Monfray, P. (2003).** An ecosystem model of the global ocean including fe, si, p colimitations. *Global Biogeochemical Cycles*, 17(2). 1060.
- Aumont, O., Orr, J. C., Jamous, D., Monfray, P., Marti, O., et Madec, G. (1998).** A degradation approach to accelerate simulations to steady-state in a 3-d tracer transport model of the global ocean. *Climate Dynamics*, 14(2) :101–116.
- Bacon, M. et Anderson, R. (1982).** Distribution of thorium isotopes between dissolved and particulate forms in the deep-sea. *Journal of Geophysical Research*, 87 :2045–2056.
- Bacon, M. P. (1988).** Tracers of chemical scavenging in the ocean : Boundary effects and large-scale chemical fractionation. *Royal Society of London Philosophical Transactions Series A*, 325 :147–160.

- Beckmann, A. et Scher, R. (1997).** A method for improved representation of dense water spreading over topography in geopotential-coordinate models. *Journal of Physical Oceanography*, 27(4) :581–591.
- Bertram, C. et Elderfield, H. (1992).** The geochemical balance of the rare earth elements and nd isotopes in the oceans. *Geochimica et Cosmochimica Acta*, 57 :1957–1986.
- Blanke, B. et Delecluse, P. (1993).** Variability of the tropical atlantic-ocean simulated by a general-circulation model with 2 different mixed-layer physics. *Journal Of Physical Oceanography*, 23(7) :1363–1388.
- Bopp, L., Kohfeld, K. E., Le Quere, C., et Aumont, O. (2003).** Dust impact on marine biota and atmospheric co₂ during glacial periods. *Paleoceanography*, 18(2). 1046.
- Broecker, W. (1991).** The great ocean conveyor. *Oceanography*, 4 :79–89.
- Broecker, W. et Peng, T. (1982).** *Tracers in the Sea*. Eldigio Press, Palisades, N.Y.
- Broecker, W. S. et Denton, G. H. (1989).** The role of ocean-atmosphere reorganizations in glacial cycles. *Geochimica et Cosmochimica Acta*, 53(10) :2465–2501.
- Burton, K. et Vance, D. (2000).** Glacial-interglacial variations in the neodymium isotope composition of seawater in the Bay of Bengal recorded by planktonic foraminifera. *EARTH AND PLANETARY SCIENCE LETTERS*, 176(3-4) :425–441.
- Courant, R., Friedrichs, K., et Lewy, H. (1928).** Āmber die partiellen differenzen-gleichungen der mathematischen physik. *Mathematische Annalen*, 100(1) :32–74.
- Duce, R., Liss, P., Merrill, J., Atlas, E., Buat-MĀ©nard, P., Hicks, B., Miller, J., Prospero, J., Arimoto, R., Church, T., Ellis, W., Galloway, J., Hansen, L., Jickells, T., Knap, A., Reinhardt, K., Schneider, B., Soudine, A., Tokos, J., Tsunogai, S., Wollast, R., et Zhou, M. (1991).** The atmospheric input of trace species to the world ocean. *Global Biogeochem. Cycles*, 5 :193–259.
- Duplessy, J.-C., Shackleton, N. J., Matthews, R. K., Prell, W., Ruddiman, W. F., Caralp, M., et Hendy, C. H. (1984).** 13c record of benthic foraminifera in the last interglacial ocean : Implications for the carbon cycle and the global deep water circulation. *Quaternary Research*, 21(2) :225–243.
- Dutay, J. C., Bullister, J. L., Doney, S. C., Orr, J. C., Najjar, R., Caldeira, K., Campin, J. M., Drange, H., Follows, M., Gao, Y., Gruber, N., Hecht, M. W., Ishida, A., Joos, F., Lindsay, K., Madec, G., Maier-Reimer, E., Marshall, J. C., Matear, R. J., Monfray, P., Mouchet, A., Plattner, G. K., Sarmiento, J., Schlitzer, R., Slater, R., Totterdell, I. J., Weirig, M. F., Yamanaka, Y., et Yool, A. (2002).** Evaluation of ocean model ventilation with cfc-11 : comparison of 13 global ocean models. *Ocea. model.*, - 4(- 2) :- 120.

- Dutay, J. C., Jean-Baptiste, P., Campin, J. M., Ishida, A., Maier-Reimer, E., Matear, R. J., Mouchet, A., Totterdell, I. J., Yamanaka, Y., Rodgers, K., Madec, G., et Orr, J. C. (2004). Evaluation of oc mip-2 ocean models' deep circulation with mantle helium-3. *Journal of Marine Systems*, 48(1-4) :15–36.
- Dutay, J.-C., Lacan, F., Roy Barman, M., et Bopp, L. (2009). Study of the influence of particle size and type on the simulation of ^{231}Pa and ^{230}Th with a global coupled biogeochemical-ocean general circulation model. *Geochemistry, Geophysics, and Geosystems*, 10, Q01011 :doi :10.1029/2008GC002291.
- Elderfield, H. (1988). The oceanic chemistry of the rare earth elements. *Phil. Trans. R. Soc. Lond.*, 325 :105–106.
- Elderfield, H. et Greaves, M. (1982). The rare earth elements in seawater. *Nature*, 296 :214–219.
- England, M. et Garçon, V. (1994). South atlantic ocean circulation in a ocean model. *An. Geophys.*, 12 :812–825.
- England, M. H. et Rahmstorf, S. (1999). Sensitivity of ventilation rates and radiocarbon uptake to subgrid-scale mixing in ocean models. *Journal of Physical Oceanography*, 29(11) :2802–2827.
- Ethé, C., Aumont, O., Foujols, M.-A., et L'Ecuyer, M. (2006). Nemo reference manual, tracer component : Nemo-top. preliminary version. *Note du Pole de modélisation, Institut Pierre-Simon Laplace (IPSL)*, France, 28.
- Fantle, M. et DePaolo, D. (2004). Iron isotopic fractionation during continental weathering. *EARTH AND PLANETARY SCIENCE LETTERS*, 228(3-4) :547–562.
- Foster, G. L., Vance, D., et Prytulak, J. (2007). No change in the neodymium isotope composition of deep water exported from the north atlantic on glacial-interglacial time scales. *Geology*, 35(1) :37–40.
- Frank, M. (2002). Radiogenic isotopes : Tracers of past ocean circulation and erosional input. *Review of Geophysics*, 40 :Art. No. 1001.
- Franzese, A. M., Hemming, S. R., Goldstein, S. L., et Anderson, R. F. (2006). Reduced agulhas leakage during the last glacial maximum inferred from an integrated provenance and flux study. *Earth and Planetary Science Letters*, 250(1-2) :72–88.
- Frost, C., O'Nions, R., et Goldstein, S. (1986). Mass balance for Nd in the mediterranean sea. *Chem. Geol.*, 55 :45–50.
- Ganachaud, A. et Wunsch, C. (2000). Improved estimates of global ocean circulation, heat transport and mixing from hydrographic data. *Nature*, 408(6811) :453–457.

- Gaspar, P., Grégoris, Y., et Lefevre, J.-M. (1990).** A simple eddy kinetic energy model for simulations of the oceanic vertical mixing : Tests at station papa and long-term upper ocean study site. *Journal of Geophysical Research-Oceans*, 95(C9) :16,179–16,193.
- Gehlen, M., Bopp, L., Emprin, N., Aumont, O., Heinze, C., et Ragueneau, O. (2006).** Reconciling surface ocean productivity, export fluxes and sediment composition in a global biogeochemical ocean model. *Biogeosciences*, 3 :521–537.
- Gent, P. R. et McWilliams, J. C. (1990).** Isopycnal mixing in ocean circulation models. *Journal Of Physical Oceanography*, 20(1) :150–155.
- Geotraces, g. (2005).** An international study of the marine biogeochemical cycles of trace elements and isotopes. <http://www.geotraces.org/>.
- Gherardi, J. M., Labeyrie, L., McManus, J. F., Francois, R., Skinner, L. C., et Cortijo, E. (2005).** Evidence from the northeastern atlantic basin for variability in the rate of the meridional overturning circulation through the last deglaciation. *Earth and Planetary Science Letters*, 240(3-4) :710–723.
- Gnanadesikan, A. (1999).** A Simple Predictive Model for the Structure of the Oceanic Pycnocline. *Science*, 283(5410) :2077–2079.
- Goldstein, S. et Hemming, S. (2003).** Long lived isotopic tracers in oceanography, paleoceanography, and ice sheet dynamics. In Elderfield, H., editor, *Treatise on Geochemistry*, volume volume 6, The oceans and marine Chemistry, page chapter 6.17. Elsevier Pergamon press, Amsterdam.
- Goldstein, S. et Jacobsen, S. (1987).** The nd and sr isotopic systematics of river-water dissolved material : implications for the sources of nd and sr in the seawater. *Chemical Geology (Isotope Geosc. Section)*, 66 :245–272.
- Goldstein, S., O'Nions, R., et Hamilton, P. (1984).** A sm-nd study of atmospheric dusts and particulates from major river systems. *Earth and Planetary Science Letters*, 70 :221–236.
- Goosse, H. et Fichefet, T. (1999).** Importance of ice-ocean interactions for the global ocean circulation : A model study. *Journal of Geophysical Research-Oceans*, 104(C10) :23337–23355.
- Gordon, A. (1986).** Intercean exchange of thermocline water. *J. Geophys. Res.*, 91 :5037–5046.
- Greaves, M., Statham, P., et Elderfield, H. (1994).** Rare earth element mobilization from marine atmospheric dust into seawater. *Mar. Chem.*, 46 :255–260.
- Grousset, F. E., Parra, M., Bory, A., Martinez, P., Bertrand, P., Shimmield, G., et Ellam, R. M. (1998).** Saharan wind regimes traced by the sr-nd isotopic composition of subtropical atlantic sediments : Last glacial maximum vs today. *Quaternary Science Reviews*, 17(4-5) :395–409.

- Gutjahr, M., Frank, M., Stirling, C. H., Keigwin, L. D., et Halliday, A. N. (2008).** Tracing the nd isotope evolution of north atlantic deep and intermediate waters in the western north atlantic since the last glacial maximum from blake ridge sediments. *Earth and Planetary Science Letters*, 266(1-2) :61–77.
- Henderson, G. M., Heinze, C., Anderson, R. F., et Winguth, A. M. E. (1999).** Global distribution of the th-230 flux to ocean sediments constrained by gcm modelling. *Deep-Sea Research Part I-Oceanographic Research Papers*, 46(11) :1861–1893.
- Henderson, G. M. et Maier-Reimer, E. (2002).** Advection and removal of 210pb and stable pb isotopes in the oceans : a general circulation model study. *Geochimica et Cosmochimica Acta*, 66(2) :257–272.
- Hourdin, F., Musat, I., Bony, S., Braconnot, P., Codron, F., Dufresne, J. L., Fairhead, L., Filiberti, M. A., Friedlingstein, P., Grandpeix, J. Y., Krinner, G., Levan, P., Li, Z. X., et Lott, F. (2006).** The lmdz4 general circulation model : climate performance and sensitivity to parametrized physics with emphasis on tropical convection. *Climate Dynamics*, 27(7-8) :787–813.
- Jeandel, C. (1993).** Concentration and isotopic composition of nd in the south atlantic ocean. *Earth and Planetary Science Letters*, 117(3-4) :581–591.
- Jeandel, C., Arsouze, T., Lacan, F., Techine, P., et Dutay, J. C. (2007).** Isotopic nd compositions and concentrations of the lithogenic inputs into the ocean : A compilation, with an emphasis on the margins. *Chemical Geology*, 239(1-2) :156–164.
- Jeandel, C., Bishop, J., et Zindler, A. (1995).** Exchange of nd and its isotopes between seawater small and large particles in the sargasso sea. *Geochimica et Cosmochimica Acta*, 59 :535–547.
- Jeandel, C., Thouron, D., et Fieux, M. (1998).** Concentrations and isotopic compositions of nd in the eastern indian ocean and indonesian straits. *Geochimica et Cosmochimica Acta*, 62 :2597–2607.
- Johannesson, K. H. et Burdige, D. J. (2007).** Balancing the global oceanic neodymium budget : Evaluating the role of groundwater. *EARTH AND PLANETARY SCIENCE LETTERS*, 253(1-2) :129–142.
- Khatiwala, S., Visbeck, M., et Cane, M. A. (2005).** Accelerated simulation of passive tracers in ocean circulation models. *Ocean Modelling*, 9(1) :51–69.
- Klevenz, V., Vance, D., Schmidt, D. N., et Mezger, K. (2008).** Neodymium isotopes in benthic foraminifera : Core-top systematics and a down-core record from the Neogene south Atlantic. *EARTH AND PLANETARY SCIENCE LETTERS*, 265(3-4) :571–587.
- Kriest, I. et Evans, G. (1999).** Representing phytoplankton aggregates in biogeochemical models. *DEEP-SEA RESEARCH PART I-OCEANOGRAPHIC RESEARCH PAPERS*, 46(11) :1841–1859.

- Kriest, I. et Evans, G. (2000).** A vertically resolved model for phytoplankton aggregation. *PROCEEDINGS OF THE INDIAN ACADEMY OF SCIENCES-EARTH AND PLANETARY SCIENCES*, 109(4) :453–469.
- Lacan, F. (2002).** *Masses d'eau des Mers Nordiques et de l'Atlantique Subarctique tracés par les isotopes du néodyme.* Phd thesis, Toulouse III University, France. Available at <http://francois.lacan.free.fr/job.htm>.
- Lacan, F. et Jeandel, C. (2001).** Tracing papua new guinea imprint on the central equatorial pacific ocean using neodymium isotopic compositions and rare earth element patterns. *Earth and Planetary Science Letters*, 186 :497–512.
- Lacan, F. et Jeandel, C. (2004a).** Denmark strait water circulation traced by heterogeneity in neodymium isotopic compositions. *Deep Sea Research I*, 51 :71–82.
- Lacan, F. et Jeandel, C. (2004b).** Neodymium isotopic composition and rare earth element concentrations in the deep and intermediate nordic seas : constraints on the iceland scotland overflow water signature. *Geochemistry Geophysics Geosystems*, 5 :Q11006, doi :10.1029/2004GC000742.
- Lacan, F. et Jeandel, C. (2004c).** Subpolar mode water formation traced by neodymium isotopic composition. *Geophysical Research Letters*, 31(L14306) :doi :10.1029/2004GL019747.
- Lacan, F. et Jeandel, C. (2005a).** Acquisition of the neodymium isotopic composition of the north atlantic deep water. *Geochemistry Geophysics Geosystems*, 6. Q12008.
- Lacan, F. et Jeandel, C. (2005b).** Neodymium isotopes as a new tool for quantifying exchange fluxes at the continent - ocean interface. *Earth and Planetary Science Letters*, 232(3-4) :245–257.
- Laes, A., Blain, S., Laan, P., Achterberg, E., Sarthou, G., et de Baar, H. (2003).** Deep dissolved iron profiles in the eastern north atlantic in relation to water masses. *Geophysical Research Letters*, 30.
- Madec, G. (2008).** Nemo reference manual, ocean dynamics component : Nemo-opa. preliminary version. *Note du Pole de modélisation, Institut Pierre-Simon Laplace (IPSL), France*, 27.
- Maier-Reimer, E. et Hasselmann, K. (1987).** Transport and storage of co₂ in the ocean, an inorganic ocean-circulation carbon cycle model. *Climate Dynamics*, 2(2) :63–90.
- Martin, E. E. et Scher, H. (2006).** A Nd isotopic study of southern sourced waters and Indonesian throughflow at intermediate depths in the Cenozoic Indian Ocean. *GEOCHEMISTRY GEOPHYSICS GEOSYSTEMS*, 7.
- Martin, J., Fitzwater, S., et Gordon, R. (1990).** Iron deficiencies limits plankton growth in antarctic waters. *Global Biogeochem. Cycles*, 4 :5–12.

- Matsumoto, K., Sarmiento, J. L., Key, R. M., Aumont, O., Bullister, J. L., Caldeira, K., Campin, J. M., Doney, S. C., Drange, H., Dutay, J. C., Follows, M., Gao, Y., Gnanadesikan, A., Gruber, N., Ishida, A., Joos, F., Lindsay, K., Maier-Reimer, E., Marshall, J. C., Matear, R. J., Monfray, P., Mouchet, A., Najjar, R., Plattner, G. K., Schlitzer, R., Slater, R., Swathi, P. S., Totterdell, I. J., Weirig, M. F., Yamanaka, Y., Yool, A., et Orr, J. C. (2004). Evaluation of ocean carbon cycle models with data-based metrics. *Geophysical Research Letters*, 31(7). L07303.
- McWilliams, J. C. (1996). Modeling the oceanic general circulation. *Annual Review of Fluid Mechanics*, 28(1) :215–248.
- Michard, A., Albarede, F., Michard, G., Minster, J. F., et Charlou, J. L. (1983). Rare-earth elements and uranium in high-temperature solutions from east pacific rise hydrothermal vent field (13-degrees-n). *Nature*, 303(5920) :795–797.
- Milliman, J. et Meade, R. (1983). World-wide delivery of river sediment to the oceans. *Journal of Geology*, 91 :1–21.
- Moorbath, S., Whitehouse, M. J., et Kamber, B. S. (1997). Extreme nd-isotope heterogeneity in the early archaean - fact or fiction ? case histories from northern canada and west greenland. *Chemical Geology*, 135(3-4) :213–231.
- Moore, W. (1996). Large groundwater inputs to coastal waters revealed by ^{226}Ra enrichments. *Nature*, 380 :612–614.
- Nakai, S., Halliday, A., et Rea, D. (1993). Provenance of dust in the pacific ocean. *Earth and Planetary Science Letters*, 119 :143–157.
- Nozaki, Y. et Alibo, D. (2003). Importance of vertical geochemical processes in controlling the oceanic profiles of dissolved rare earth elements in the northeastern indian ocean. *Earth and Planetary Science Letters*, 205 :155–172.
- O’Nions, R., Carter, S., Cohen, R., Evensen, N., et Hamilton, P. (1978). Pb, nd and sr isotopes in ferromanganese deposits and ocean floor basalts. *Nature*, 273 :435–438.
- Peng, T. H., Maier-Reimer, E., et Broecker, W. S. (1993). Distribution of $[^{32}\text{Si}]$ in the world ocean : Model compared to observation. *Global Biogeochemical Cycles* ; Vol/Issue : 7 :2; DOE Project, pages Pages : 463–474. (Oak Ridge National Lab., TN (United States)) (Max-Planck Institut fuer Meteorologie, Hamburg (Germany)) (Columbia Univ., Palisades, NY (United States)) ISSN0886-6236 ; CODEN : GBCYEP System Entry Date : 05/13/2001 Source : EDB-94-139290 Language : English.
- Petit, J. R., Jouzel, J., Raynaud, D., Barkov, N. I., Barnola, J. M., Basile, I., Bender, M., Chappellaz, J., Davis, M., Delaygue, G., Delmotte, M., Kotlyakov, V. M., Legrand, M., Lipenkov, V. Y., Lorius, C., Pepin, L., Ritz, C., Saltzman, E., et Stievenard, M. (1999). Climate and atmospheric history of the

- past 420,000 years from the vostok ice core, antarctica. *Nature*, 399(6735) :429–436. 0028-0836 10.1038/20859 10.1038/20859.
- Piepgras, D. et Jacobsen, S. (1988)**. The isotopic composition of neodymium in the north pacific. *Geochimica et Cosmochimica Acta*, 52 :1373–1381.
- Piepgras, D. et Wasserburg, G. (1982)**. Isotopic composition of neodymium in waters from the drake passage. *Science*, 217 :207–217.
- Piepgras, D. et Wasserburg, G. (1983)**. Influence of the mediterranean outflow on the isotopic composition of neodymium in waters of the north atlantic. *J. Geophys. Res.*, 88 :5997–6006.
- Piepgras, D. J. et Wasserburg, G. J. (1985)**. Strontium and neodymium isotopes in hot springs on the east pacific rise and guaymas basin. *Earth Planet. Sci. Lett.*, 72 :341–356.
- Piotrowski, A. M., Goldstein, S. L., Hemming, S. R., et Fairbanks, R. G. (2004)**. Intensification and variability of ocean thermohaline circulation through the last deglaciation. *Earth and Planetary Science Letters*, 225 :205–220.
- Pucéat, E., Lécuyer, C., et Reisberg, L. (2005)**. Neodymium isotope evolution of nw tethyan upper ocean waters throughout the cretaceous. *Earth and Planetary Science Letters*, 236 :705–720.
- Rahmstorf, S. (2002)**. Ocean circulation and climate during the past 120,000 years. *Nature*, 419(6903) :207–214.
- Rintoul, S. (1991)**. South atlantic interbasin exchange. *J. Geophys. Res.*, 96 :2675–2692.
- Robinson, A. et Stommel, H. (1959)**. The oceanic thermocline and the associated thermohaline circulation. *Tellus*, 11 :295–308.
- Russell, G. (1990)**. Global river runoff calculated from a global atmospheric general circulation model. *Journal of Hydrology*, 117 :241–254.
- Rutberg, R., Hemming, S., et Goldstein, S. (2000)**. Reduced north atlantic deep water flux to the glacial southern ocean inferred from neodymium isotope ratios. *Nature*, 405 :935–938.
- Sarmiento, J. (1983)**. A simulation of bomb tritium entry into the Atlantic-Ocean. *Journal of Physical Oceanography*, 13(10) :1924–1939.
- Sarmiento, J. L., Gruber, N., Brzezinski, M. A., et Dunne, J. P. (2004)**. High-latitude controls of thermocline nutrients and low latitude biological productivity. *Nature*, 427(6969) :56–60. 0028-0836 10.1038/nature02127 10.1038/nature02127.
- Scher, H. D. et Martin, E. E. (2008)**. Oligocene deep water export from the north atlantic and the development of the antarctic circumpolar current examined with neodymium isotopes. *Paleoceanography*, 23(26) :A261205+.

- Schlitzer, R. (2004).** Export production in the equatorial and north pacific derived from dissolved oxygen, nutrient and carbon data. *Journal of Oceanography*, 60(1) :53–62.
- Siddall, M., Henderson, G. M., Edwards, N. R., Frank, M., Muller, S. A., Stocker, T. F., et Joos, F. (2005).** Pa-231/th-210 fractionation by ocean transport, biogenic particle flux and particle type. *Earth And Planetary Science Letters*, 237(1-2) :135–155.
- Siddall, M., Khatiwala, S., van de Flierdt, T., Jones, K., Goldstein, S. L., Hemming, S., et Anderson, R. F. (2008).** Towards explaining the nd paradox using reversible scavenging and the transport matrix method. *Earth And Planetary Science Letters*, 274 :448–461.
- Sigman, D. M. et Boyle, E. A. (2000).** Glacial/interglacial variations in atmospheric carbon dioxide. *Nature*, 407(6806) :859–869.
- Speich, S., Blanke, B., de Vries, P., Drijfhout, S., Doos, K., Ganachaud, A., et Marsh, R. (2002).** Tasman leakage : A new route in the global ocean conveyor belt. *Geophysical Research Letters*, 29(10). 1416.
- Speich, S., Blanke, B., et Madec, G. (2001).** Warm and cold water routes of an ogcm thermohaline conveyor belt. *Geophysical Research Letters*, 28(2) :311–314.
- Spivack, A. et Wasserburg, G. (1988).** Neodymium isotopic composition of the mediterranean outflow and the eastern north atlantic. *Geochim. Cosmochim. Acta*, 52 :2762–2773.
- Tachikawa, K., Athias, V., et Jeandel, C. (2003).** Neodymium budget in the ocean and paleoceanographic implications. *Journ. Geophys.Res.*, 108 :3254 doi :10.1029/1999JC000285.
- Tachikawa, K., Jeandel, C., et Dupré, B. (1997).** Distribution of rare earth elements and neodymium isotopes in settling particulate material of the tropical atlantic ocean (eumeli site). *Deep-Sea Res.*, 44 :1769–1792.
- Tachikawa, K., Jeandel, C., et Roy-Barman, M. (1999).** A new approach to nd residence time in the ocean : the role of atmospheric inputs. *Earth and Planetary Science Letters*, 170 :433–446.
- Tachikawa, K., Roy-Barman, M., Michard, A., Thouron, D., Yeghicheyan, D., et Jeandel, C. (2004).** Neodymium isotopes in the mediterranean sea : Comparison between seawater and sediment signals. *Geochimica et Cosmochimica Acta*, 68(14) :3095–3106.
- Tagliabue, A. et Bopp, L. (2008).** Towards understanding global variability in ocean carbon-13. *Global Biogeochemical Cycles*, 22(1). GB1025.
- Tegen, I. et Fung, I. (1995).** Contribution to the atmospheric mineral aerosol load from land surface modification. *J. Geophys. Res.*, 100(D9) :18707–18726.

- Toggweiler, J. et Samuels, B. (1995).** Effect of drake passage on the global thermo-haline circulation. *Deep Sea Research Part I : Oceanographic Research*, 42 :477–500.
- Usbeck, R., Schlitzer, R., Fischer, G., et Wefer, G. (2003).** Particle fluxes in the ocean : comparison of sediment trap data with results from inverse modeling. *Journal of Marine Systems*, 39(3-4) :167–183.
- Valcke, S. (2006).** Oasis3 user guide (prism 2-5). *PRISM Support Initiative Report*, 3(CERFACS, Toulouse, France) :64.
- Van de Flierdt, T., Frank, M., Lee, D. C., Halliday, A. N., Reynolds, B. C., et Hein, J. R. (2004).** New constraints on the sources and behavior of neodymium and hafnium in seawater from pacific ocean ferromanganese crusts. *Geochimica Et Cosmochimica Acta*, 68(19) :3827–3843.
- Van de Flierdt, T., Robinson, L. F., Adkins, J. F., Hemming, S. R., et Goldstein, S. L. (2006).** Temporal stability of the neodymium isotope signature of the holocene to glacial north atlantic. *Paleoceanography*, 21(4). PA4102.
- van der Leeden, F., Troise, F., et Todd, D. (1990).** *Water Encyclopedia*. Lewis Publishers.
- Vance, D. et Burton, K. (1999).** Neodymium isotopes in planktonic foraminifera : A record of the response of continental weathering and ocean circulation rates to climate change. *Earth and Planetary Science Letters*, 173 :365–379.
- von Blanckenburg, F. (1999).** Perspectives : Paleoceanography - tracing past ocean circulation ? *Science*, 286(5446) :1862–1863.
- Watson, A. J., Bakker, D. C. E., Ridgwell, A. J., Boyd, P. W., et Law, C. S. (2000).** Effect of iron supply on southern ocean co₂ uptake and implications for glacial atmospheric co₂. *Nature*, 407(6805) :730–733.
- Weatherly, J. W. et Walsh, J. E. (1996).** The effects of precipitation and river runoff in a coupled ice-ocean model of the arctic. *Climate Dynamics*, 12 :785–798.
- Wells, M., Vallis, G., et Silver, E. (1999).** Tectonic processes in papua new guinea and past productivity in the eastern equatorial pacific ocean. *Nature*, 398 :601–604.
- Zhang, Y., Jeandel, C., et Lacan, F. (2008).** Boundary exchange processes on and along the kerguelen plateau. *GEOCHIMICA ET COSMOCHIMICA ACTA*, 72(12, Suppl. 1) :A1090.
- Zhuravlev, D., Tsvetkov, A., Zhuravlev, A., Gladkov, N., et Chernyshev, I. (1987).** 143nd/144nd and 87sr/86sr ratios in recent magmatic rocks of the kurile island arc. *Chemical Geology (Isotope Geoscience Section)*, 66 :227–243.

